Mircea ȘUȘCĂ

# Unified Robust Control Design for Digital Implementation

U.T.PRESS
Cluj-Napoca, 2026
ISBN 978-606-737-828-3

**Mircea ȘUȘCĂ**

# Unified Robust Control Design for Digital Implementation

**U.T.PRESS**
**Cluj - Napoca, 2026**
**ISBN 978-606-737-828-3**

Editura U.T.PRESS
Str. Observatorului nr. 34
400775 Cluj-Napoca
Tel.: 0264-401.999
e-mail: utpress@biblio.utcluj.ro
http://biblioteca.utcluj.ro/editura

Recenzia:

Prof.dr.ing. Lucian Buşoniu
Prof.dr.ing. Petru Dobra
Prof.dr.ing. Radu Precup
Prof.dr.ing. Cristian Oară
Prof.dr.ing. Octavian Păstrăvanu

Pregătire format electronic on-line: Gabriela Groza



**ISBN 978-606-737-828-3**

# PREFACE

This book is based on the author's 2023 doctoral thesis, updated with selected postdoctoral developments. It aims to present a unified perspective on modelling, synthesis, and implementation of robust control systems, with particular emphasis on practical deployment aspects. The material is organized such that each main chapter consolidates a core methodological contribution documented in a full journal article, while related refinements, variants, and a broader range of applications have been disseminated through conference publications. This structure allows the reader to follow a coherent end-to-end narrative while also identifying the publication trail associated with each contribution. Minor stylistic revisions have been performed for publication.

# ACKNOWLEDGEMENTS

*These acknowledgements reflect those expressed in the original PhD thesis on which this book is based.*

I would like to express my heartfelt gratitude to my beloved family, cherished friends, esteemed colleagues, fellow researchers, dedicated students, and accomplished graduates. Their unwavering support, engaging discussions, and invaluable exchange of ideas have profoundly shaped the development of this thesis, both directly and indirectly, bringing it to its current form. Their contributions have not only influenced the thesis but have also left an indelible mark on every aspect of my academic journey and existence.

I extend my deepest appreciation to the exceptional individuals who have played pivotal roles in this endeavor. In particular, I would like to convey my special thanks to my colleagues and friends Vlad Mihaly, Dora Morar, and Mihai Stănese for their remarkable guidance, encouragement, and invaluable insights throughout this transformative process. Additionally, I would like to express my sincere gratitude to Prof. Petru Dobra, who has been a remarkable role model and a source of inspiration since my first System Theory course during my second year of bachelor's studies. I thank him for his patience, brilliance, and kindness, which have been evident throughout our collaboration over the years. I would also like to acknowledge the significant impact of Prof. Paula Raica and Prof. Eva Dulf, whose collaborations and guidance have greatly influenced my academic journey. Their valuable contributions have been instrumental in fostering fruitful discussions in both didactic and research endeavors.

To each and every person who has been a part of this journey, I am eternally grateful. Without their support, the thesis, and indeed, the entirety of my endeavors, would have been vastly different. Their presence has been a constant source of inspiration and motivation, and I am profoundly indebted to them for their unwavering belief in my abilities. Thank you, from the depths of my heart, for contributing to the realization of this achievement and for enriching my life with your presence.

# TABLE OF CONTENTS

# ABBREVIATIONS AND NOTATIONS

**Abbreviations**

- 2D: two-dimensional;
- 3D: three-dimensional;
- ABC: artificial bee colony;
- ADC: analog-to-digital converter;
- ARE: algebraic Riccati equation;
- BMI: bilinear matrix inequality;
- CACSD: computer-aided control system design;
- CISC: complex instruction set computer;
- DAC: digital-to-analog converter;
- DAE: differential-algebraic equation;
- DCM: direct current motor;
- DFI: direct form I;
- DFII: direct form II;
- DFT: direct form transposed;
- DMA: direct memory access;
- DOF: degree-of-freedom;
- DSP: digital signal processor;
- FIR: finite impulse response;
- FO: fractional-order;
- GUI: graphical user interface;
- HiL: Hardware-in-the-loop;
- IIR: infinite impulse response;
- ISR: interrupt service routine;
- KPBC: Krasovskii passivity-based controller;
- LFT: linear fractional transformation;
- LHP: left half-plane;
- LLFT: lower linear fractional transformation;
- LMI: linear matrix inequality;
- LPV: linear parameter-varying;

- LSDP: loop-shaping design procedure;
- LTI: linear time invariant;
- LTV: linear time variant;
- MiL: Model-in-the-loop;
- MIMO: multiple-input and multiple-output;
- ODE: ordinary differential equation;
- OOP: object-oriented programming;
- PBC: passivity-based controller;
- PID: proportional-integral-derivative;
- PIDF: PID with filter;
- PSO: particle swarm optimization;
- RAM: random access machine;
- RCP: rapid control prototyping;
- RHP: right half-plane;
- RISC: reduced instruction set computer;
- RP: robust performance;
- RS: robust stability;
- SDP: semidefinite programming;
- SiL: Software-in-the-loop;
- SIMD: single instruction/multiple data;
- SIMP: single instruction stream/multiple instruction pipelining;
- SISO: single-input and single-output;
- SOS: second-order section;
- SSV: structured singular value;
- TDFI: transposed direct form I;
- TDFII: transposed direct form II;
- ULFT: upper linear fractional transformation;
- WCET: worst-case execution time.

**Notations and conventions**

- $\mathcal{G}$: continuous-time systems set;
- $\mathcal{G}_D$: discrete-time systems set;
- continuous-time systems: $G$, $K$, $P$ and so on;
- continuous-time signals: $x \equiv x(t)$, $u \equiv u(t)$ and so on;
- discrete-time systems: $\widetilde{G}$, $\widetilde{K}$, $\widetilde{P}$ and so on;

- process models will be considered with the conventional input/state/output interface $(u, x, y)$; their dimensionality will conventionally be denoted $(m, n, p)$ or $(n_u, n, n_y)$;
- regulator models will be considered either with the conventional input/state/output interface $(u, x, y)$, or the interface $(e \equiv r - y, x, u)$ when used in a closed-loop structure, to emphasize the interconnection with a plant model having $(u, x, y)$; their dimensionality will usually be denoted $(n_y, n_c, n_u)$;
- discrete-time signals: $x[k] \equiv x_k$, $e[k] \equiv e_k$ and so on;
- the circle having the center in $z \in \mathbb{C}$ and radius $r > 0$ is denoted $\mathcal{C}(z, r)$;
- $\mathcal{P}(G)$ and $\mathcal{Z}(G)$ denote the pole and zero sets of an LTI system $G$;
- $T_s = T = \tau > 0$: sampling period;
- $Q, q > 0$: quantization step;
- $\delta_e, \delta_x, \delta_u > 0$: quantizer resolutions;
- $L_e, L_x, L_u > 0$: word lengths for error, state, command input representations;
- $\lambda_i$: eigenvalues of a square matrix $A \in \mathbb{C}^{n \times n}$;
- $\sigma_i \geq 0$: singular values of a rectangular matrix $A \in \mathbb{C}^{m \times n}$; $\overline{\sigma}$ will denote its maximum singular value;
- $j\omega$, $e^{j\omega T}$: frequency response points for continuous-time and discrete-time systems, respectively.
- the negative feedback convention will be used throughout the thesis;
- vectors will be considered in column form.

# LIST OF FIGURES

# LIST OF TABLES

# INTRODUCTION

## 1.1 Context and motivation

The context of the current monograph is derived from practice, to provide better connections between fundamental research and practical applications. The end-to-end workflow in control system design is based on a collaboration of several subfields. It is usually seen starting from obtaining an abstract mathematical model of the physical process to be controlled, either through modelling or system identification techniques, followed by a preliminary analysis of the system properties and performances. Using the resulting performances as a baseline for the physical process, a set of specifications is proposed for the desired behaviour of the system, followed by a controller synthesis step with the goal of meeting these specifications. Furthermore, the controller dynamics are currently implemented on computer-based environments, which, in turn, requires the sampling and discretization of the regulator model. Further complications are induced due to the inherent quantization of the signals and coefficients involved, alongside other hardware and software constraints of the production environment. This leads to discrepancies between the expected performance metrics from continuous to discrete-time. Besides inherent problems in the controller implementation, the mathematical model of the process may appear inconsistent with reality after performing experimental tests. Such problems lead to an iterative process in control system practice. All previously-mentioned control system-based subfields are individually well-established, but the transitions between the output entities given by one study which represent the input and baseline for the application of another study are not treated in an unified manner and holistically with respect to the other subdomains.

The controller synthesis is usually performed in continuous-time domain, followed by a conversion of the resulting regulator to a discrete-time counterpart, of infinitely many possible variations. From the author's own findings, in many facets from the specialized literature, the analysis usually ends after the continuous-time design step and then, the implementation aspects are treated in an ad hoc manner for each particular use case. The relatively limited volume of studies focusing on the conversion from the continuous to discrete-time domains in control system design provides one of the main motivations of this book and its developments. Rather than considering control system design as a collection of independent subfields, such as system modelling, robust controller design, sampling, discretization, and quantization, it is important to ex-

plore how these areas can be integrated to address practical challenges in designing and deploying robust control systems. This requires identifying and addressing bottlenecks that arise when working with uncertainties, sensor noise, and implementation difficulties in microcontroller-based systems, among other issues. By taking a holistic approach to control system design, researchers and practitioners can develop effective solutions that account for the interdependencies and trade-offs between different design aspects.

While convex optimization has been a popular and effective tool in many optimization problems, there are many important problems that cannot be formulated as convex optimization problems or cannot be solved using convex optimization techniques. The growing demand for solving these nonconvex and nonsmooth optimization problems has motivated the development of new optimization techniques and algorithms that can provide efficient and effective solutions for these problems. This book aims to explore the use of techniques that can handle nonconvex and nonsmooth optimization problems, primarily with a focus on their possible applications in the system theory and control systems domain, with branches specified above.

## 1.2 Objectives and contributions

Starting from the context and motivations described above, this book will include two categories of objectives: research objectives and implementation-based objectives. These objectives are materialized through the contributions described throughout the book, which will also be individually stated in their corresponding chapters and sections, with specific references to the publications on which they are based upon.

### 1.2.1 Research objectives

The theoretical contributions are based on the general context of closed-loop control, viewed as a complete design process involving the modelling of the physical process, controller synthesis and controller implementation. A part of the contributions are focused around the particular field of robust control, by providing novel means to design, implement and validate control structures specific to this field, while some results are applicable to more general control design approaches. The main concepts studied and extended throughout this book are to:

(i) extend the classical series, parallel, upper and lower linear fractional transformations for general nonlinear and hybrid systems, to be used in Model-in-the-Loop simulation of physical processes and of the closed-loop system seen as a hybrid system with continuous dynamics (process) and discrete-time dynamics (numeric regulator);

(ii) compute equilibrium points with imposed specifications on families of nonlinear systems;

(iii) linearize families of analytical nonlinear system models starting from the set of equilibrium points as computed above;

(iv) fit reduced-order uncertainty models on frequency-response data using nonconvex optimization with stability, minimum phase and validity properties;

(v) correlate sampling rate parametrizations with control theory performance specifications, such as stability, steady-state and transient response performance metrics and implementation difficulty;

(vi) correlate regulator coefficient quantization effects with classical control theory performance specifications, such as the robust stability and robust performance metrics;

(vii) define a joint optimization encompassing the sampling rate and coefficient quantization step to allow the selection of the most faithful representation of the continuous-time controller or, alternatively, the easiest configuration for practical implementation on microcontroller devices such that the imposed performance metrics are still maintained;

(viii) analyze the execution time effects on classical linear time-invariant control solutions through state-space and infinite/finite impulse response filter topologies.

### 1.2.2 Implementation objectives

The proposed theoretical contributions will be implemented around a general-purpose software toolbox used to gather all aspects involved in the study, design, implementation and validation of closed-loop systems, with a focus on a rapid control prototyping paradigm. Many specified

design problems can be written as constrained nonlinear optimizations. The combination of the `fmincon` and `GlobalSearch` functions in the MATLAB environment is particularly well-suited for solving optimization problems in the context of control system design, such as sampling rate and quantization step selection, frequency-response data fitting, and other related use cases. These methods can efficiently handle nonconvex and nonlinear optimization problems, providing a powerful tool for engineers and researchers working in the field of control systems.

Proposed features, in conjunction to the theoretical aspects from Section 1.2.1, are to:

(i) implement an object-oriented programming (OOP) software framework to allow the definition and simulation of nonlinear, linearized, hybrid systems and their interconnections using the `ode` framework and the Hybrid Equations (HyEQ) toolbox from [SCN13], which allows the specification of arbitrary exogenous signals and time-dependent specifications;

(ii) define a Factory Method design pattern to generate a nominal plant model and an adjacent set of uncertain model variations, which can directly be used to fit transfer function envelopes useful in robust control synthesis;

(iii) automatically compute equilibrium points numerically, with the possibility to impose certain states, inputs, or outputs, while the remaining ones are deduced through numeric optimization based on a regression-type problem;

(iv) compute configurable uncertainty models (additive, inverse additive, multiplicative, inverse multiplicative etc.) through nonconvex optimization with a well-placed initialization point, as required for robust control synthesis, with the pole-zero structure suggested through a rook-type optimization using Log-Chebyshev fitting of frequency-response data;

(v) validate closed-loop performance metrics through Monte Carlo simulations based on the above OOP framework;

(vi) define Krasovskii passivity-based controllers and KPBC-based cascade control structures with robust control path-planning terms to guarantee local asymptotic stability and local performance metrics;

(vii) correlate sampling rates of 1DOF, 2DOF and cascade control structures with fidelity and implementability specifications through configurable functionals;

(viii) gather optimal sampling rates and coefficient quantization steps such that the equivalent discrete-time regulator maintains the robust stability and robust performance metrics imposed on the continuous regulator;

(ix) provide means to simulate quantized control systems, seen as a hybrid interconnection between a continuous-time process and numeric regulator, and then assert imposed performance metrics;

(x) design input/state/output signal balancing of discrete-time regulators to impose the least possible tracking error caused by quantization effects, without affecting the transient response of the initial regulator;

(xi) impose control law and hardware specifications in order to estimate the worst-case execution time of the numeric regulator or, the inverse problem of deciding the minimum microcontroller requirements to implement a given control law with a desired precision.

## 1.3 Book outline

The book is structured into four major parts. Part I gathers the introduction, context, motivation, objectives and summary; Part II holds the current stage of knowledge, being focused on describing the necessary concepts, results, establishing notations and hosts most of the literature studies performed in the work; Part III hosts the main chapters of the book, i.e. research contributions originating from the author's 2023 PhD thesis, classified in theoretical contributions in Chapters 5–10, followed by the extended Chapter 11 which gathers a wide variety of case studies and illustrations of the theoretical results shown beforehand; the remaining Part IV provides final discussions, the conclusions of the project and future research directions. Besides the previously-mentioned four parts, the book also provides a list of abbreviations and notations, figures, tables at the beginning, closing with a subject index and the references.

**Part I:** overlaps with the contents of **Chapter 1**, which hosts the scientific context of the monograph and its driving motivation, followed by a short list of specific objectives, and a summary of its contents, detailed by parts and corresponding chapters.

**Part II:** encompasses Chapters 2, 3, and 4, respectively. **Chapter 2** provides the definitions of the commonly-used continuous-time system models in the control system domain, as used throughout the book, such as nonlinear, input affine, linear time-invariant and hybrid systems, while also defining and describing the standard system interconnections: series, parallel, lower and upper linear fractional transformations. Then, **Chapter 3** is structured in three subsections, performing literature studies and mathematical descriptions of conventional control structures, such as one-degree-of-freedom, two-degrees-of-freedom and cascade configurations, followed by the generalized plant model used in robust control, encompassing uncertainties, abstract performance specifications and means of synthesizing regulators using the $\mathcal{H}_\infty$ and $\mu$-synthesis, concluding with a description on determining performance specifications and validation of the closed-loop system through simulation. **Chapter 4** gathers the theoretical foundations, literature reviews, and necessary notations used throughout the monograph referring to regulator implementation aspects: effects of sampling and discretization, signal and coefficient quantization, and execution time analysis necessary for the implementation of linear time-invariant regulators on microprocessor-based systems, with standard characterizations of numeric state-space realizations, infinite and finite impulse response filter transfer functions.

**Part III:** encompasses Chapters 5, 6, 7, which are linked by the overall scope of aiding in the design and validation of robust control systems, followed by Chapters 8, 9, and 10, which cover aspects regarding the implementation of linear and robust regulators, providing a comprehensive list and thorough description of theoretical contributions gathered from publications written throughout the years spent developing the monograph, with their applications gathered in Chapter 11. **Chapter 5** describes an `ode`-based toolbox which allows modelling and simulation for classes of systems their standard interconnections necessary in robust control: series, parallel, along with upper and lower linear fractional transformations, as described in Chapter 2. The toolbox also provides an extension of the Hybrid Equations (HyEQ) toolbox initially-presented in [SCN13]

to also account for exogenous inputs and direct specification of system interconnections through a unified software interface, used in multiple instances throughout the book. Besides modelling a nominal plant, the toolbox also allows the definition of factory-type class design patterns which can account for a wide range of structured and unstructured uncertainty types. Additionally, it provides a functionality to impose arbitrary input, state, and output signal values to force an operating point for such a family of uncertain plants and then compute, through numeric optimization, the remaining variables of the equilibrium point. Based on such forced equilibrium points, a set of LTI models of the initially nonlinear plant can be obtained and used to fit low-order uncertainty models. **Chapter 6** proposes a nonconvex optimization approach to fit SISO transfer function models on magnitude response data. The resulting transfer function will be, by design, stable, minimum phase and valid. Although there are convex optimum alternatives in the literature, the proposed method proves less conservative in an $\ell_1$-norm sense, while, to account for the NP-hardness of nonconvex approaches, a well placed starting solution is proposed based on the well-established Log-Chebyshev method. Chapters 5 and 6 can be used in conjunction as, starting from a nonlinear uncertain model with known analytic description, a set of LTI plant models can be computed around a forced equilibrium point, with the solutions of equilibrium points gathered also through numeric optimization, while an uncertainty model can then be fit based on the LTI descriptions to be directly used for robust synthesis. **Chapter 7** describes an approach to harvest the advantages of both passivity-based and robust control alike, by proposing a cascade control structure consisting of an inner nonlinear Krasovskii passivity-based controller which guarantees the stability of the nonlinear process along its entire operating domain, followed by a robust path-planning controller which imposes the steady-state response. **Chapter 8** proposes a unified approach to compute the sampling rate for a continuous-time control structure in an optimal manner, by taking into account both the fidelity of the response after discretization, regarding the open and closed-loop behaviour alike, and also the implementability of the regulator represented by an execution time penalization term and a coefficient quantization-based influence. This framework is then applied to one-degree-of-freedom, two-degrees-of-freedom and cascade control system architectures and validated using benchmark industrial processes. **Chapter 9** proposes a unified approach to analyze the quantization effects found in discrete-time regulator imple-

mentation, with separate studies performed for transient and steady-state response behaviour, which are found to be decoupled and independent from each other. Furthermore, to account for the transient response analysis, a joint constrained optimization problem is proposed involving both the sampling rate and coefficient quantization step in order to solve for the best possible solution while maintaining the robust stability and robust performance specifications. On the other hand, without affecting the transient response of the discrete regulator, an optimization regarding the state signal scaling is proposed to obtain a least possible tracking error due to quantization and, additionally, to frame this achievable value by a least conservative bound. This tracking error bound is analytically computed based only on the state-space matrices of the process, regulator, and hardware specifications made concrete by the resolutions of the input/output converters and state/output computation arithmetic. A hybrid model for the closed-loop system comprised of a continuous-time plant and discrete-time regulator is developed to account for Model-in-the-Loop simulation. **Chapter 10** presents a formal mathematical model to analyse the worst-case execution time of linear control structures represented by state-space realizations and filter topologies. It takes into account the formal mathematical operations found in the implementation of the control law, their low-level assembly counterparts and also various hardware-specific settings and metadata. Such an analysis can be used in rapid control prototyping applications to account for the possibility of implementation during a given sampling period. **Chapter 11** provides a practice oriented section to show recommended configurations, workflows and parameter setups for the developed theory through an extensive set of case studies. These examples illustrate the improvements achieved relative to classical benchmark systems. Examples include **(i)** fractional-order (FO) robust controller synthesis for a mass-spring-dashpot system, showing the flexibility of the Robust Control framework being transposed to fixed-structure regulators comprised of transfer functions with FO elements; **(ii)** nonconvex uncertainty model fitting on two mechanical systems, the first can be seen as an additive model for a resonant system, with an optimization performed to also suggest the optimal pole-zero configuration of the uncertainty envelope function, while the other is an inverted pendulum-type system with derivative behaviour, with an extended comparison to other uncertainty models, showing that the proposed solution is the least conservative, while still remaining valid with respect to the frequency-response data; **(iii)** multi-rate sampling period

selection for cascade control structures using the developed optimization framework, showing the advantages relative to classical bandwidth and Nyquist-Shannon theorem-based solutions, with intuitive 2D illustrations of contour plots for the nonconvex functionals; **(iv)** a joint sampling rate and coefficient quantization step is performed on an industrial overdamped system with non-minimum phase with a proposed optimal solution ensuring maximum response fidelity, compared to a different optimum which accounts for the easiest implementability of the regulator, while still maintaining the robust stability and performance indices; a thorough discussion is also performed relative to the numeric aspects involved in the optimization and resulting solutions, such as sensitivity and condition number; **(v)** a loop-shaping robust controller designed for a benchmark underdamped system is designed for minimum tracking error caused by fixed-point quantization effects, based on optimizing the developed analytical worst-case steady-state bound through an adequate signal scaling, with the illustration of the tightness of said bound; **(vi)** an extended analysis for the SEPIC converter is presented, involving the development of a hybrid state-space model, leading to an averaged uncertain state-space model to be used for robust control synthesis, followed by the development of a passivity-based controller in series with a robust path-planning component, and concluding with a quantization error analysis performed on said path-planning term; **(vii)** a DC motor two-degree-of-freedom PID with anti-windup controller is designed to ensure good a tracking and load disturbance rejection behaviour, with a further analysis of the worst-case anticipated execution time of the proposed regulator to anticipate the processor load and idle times, equivalent to deducing a minimum allowable sampling period.

**Part IV:** corresponds to the final chapter of the book, i.e. **Chapter 12**, which provides a series of discussions, conclusions and future research directions based on the concepts and results presented beforehand. It is then followed by the list of bibliographical references and the list of publications.

# CURRENT STAGE OF KNOWLEDGE

# 2. Continuous-time system modelling

For the purpose of this book, the focus will be on deterministic finite-dimensional nonlinear systems, and particular classes of system structures which arise in the proposed results, studied separately: linear time-invariant, input affine, and hybrid systems, alongside the classification of continuous-time systems and their discrete-time counterparts.

## 2.1 Nonlinear systems

The explicit or standard system form of a nonlinear dynamical system is obtained by writing the plant model in the following canonical form, using a set of differential equations and a set of output equations:

$$(\Sigma) : \begin{cases} \dot{x} = F\left(x, u, t\right); \\ y = h\left(x, u, t\right), \end{cases} \tag{2.1}$$

with vector maps $F$ and $h$ as Lipschitz functions. The input signal $u$ has dimension $m$, state signal $x$ with dimension $n$, and output signal $y$ with dimension $p$, with $t \geq 0$. The initial conditions are $x(0) = x_0 \in \mathbb{R}^n$.

The previous explicit structure presents a generalized canonical form, where besides the differential and output equations, it additionally contains an algebraic equation, described as:

$$(\Sigma_{\text{DAE}}) : \begin{cases} \dot{x} &= F(x, u, t); \\ 0 &= G(x, u, t); \\ y &= h(x, u, t), \end{cases} \tag{2.2}$$

with $F$, $G$, $h$ being Lipschitz functions of appropriate dimensions. Such systems are thus modelled by *differential-algebraic equations* (DAEs). Physically, they are comprised of subsystems described by differential equations and coupled by algebraic constraints, such as: models of chem-

ical processes (dynamic balance equations constrained by thermodynamic equilibrium relations, steady-state assumptions, empirical correlations), electric networks (components coupled through Kirchhoff's laws), mechanical systems (subsystems coupled by joints) [Mül00]. They also artificially arise in control system architectures, due to the control constraints imposed on the physical processes. Singular systems also typically arise as a limiting case or when redundant system modelling is used.

## 2.2 Control affine nonlinear systems

As utilized throughout the monographs [LaV06] and [Isi94], a relevant state-space structure used in practice in the field of robotics is described by the *control*, also known as *input*, *affine nonlinear system*:

$$(\Sigma^a) : \begin{cases} \dot{x} &= g_0(x) + \sum_{i=1}^{m} g_i(x) \cdot u; \\ y &= h(x), \end{cases} \tag{2.3}$$

described by the *drift term* $g_0(x)$ and *system vector fields* $g_i(x)$, $i \in \overline{1, m}$.

Such classes of systems can be directly employed and controlled using Lyapunov, Lyapunov-Krasovskii and passivity-based methods [Kha15].

## 2.3 Linear time-invariant systems

Of particular interest for the framework and for control systems in general are linear time-invariant (LTI) systems:

$$(G(s)) : \begin{cases} \dot{x} = Ax + Bu; \\ y = Cx + Du. \end{cases} \tag{2.4}$$

Separately, a nonlinear system can be linearized in the vicinity of an operating point, which is an equilibrium point for said system. The operating point $(u_0, x_0, y_0, t_0)$ can be provided by the user or can be computed via software tools. The linearized system will work with variations of the initial variables and have the following model:

$$(G(s)) : \begin{cases} \dot{\Delta x} = A \cdot \Delta x + B \cdot \Delta u; \\ \Delta y = C \cdot \Delta x + D \cdot \Delta u, \end{cases} \tag{2.5}$$

written in an expanded manner as:

$$(G(s)) : \begin{cases} \dot{x} &= A\,(x - x_0) + B\,(u - u_0)\,; \\ y &= C\,(x - x_0) + D\,(u - u_0) + y_0, \end{cases} \tag{2.6}$$

which allows simulation of such systems *in lieu* of the general interface provided by Equation (2.1).

Multiple approaches exist to obtain LTI models:

- linearization by numeric perturbation of the nonlinear model in an operating point; the perturbation step size should be selected to optimize the accuracy of the result by making a compromise between the rounding error and the slope of the tangent; higher-order differentiation methods could be used, resulting in higher precision with the trade-off of increased computational resources [GW08]. On the other hand, an exact linearization algorithm can be applied if the system model has a known analytical expression.
- exact linearization through feedback, via Lie derivatives [Isi95; Kha15; Son98], method which then adds the direct and inverse topological transformations in the controller implementation;
- using the Koopman spectral theory approach [Bru+22];
- describing function method [GV68], which additionally focuses on obtaining relevant information from the nonlinear dynamics.
- experimental identification at an operating point using time and frequency-domain methods [Lju99]; such methods could be applied in practice with the use of actuators, an acquisition system and identification algorithms, or through computer simulation.

## 2.4 Hybrid systems

An important extension of framework (2.1) for hybrid systems, to account for system discontinuities and switching behaviour, is described in [GST12], with state-space structure:

$$(\Sigma^h) : \begin{cases} \dot{x} &= F\,(x, u, t)\,, \ (x, u, t) \in \mathcal{C}; \\ x^+ &= G\,(x, u, t)\,, \ (x, u, t) \in \mathcal{D}; \\ y &= h\,(x, u, t)\,, \end{cases} \tag{2.7}$$

with $F$ as the *flow function*, $G$ the *jump function*, and $h$ the *output function*, while $\mathcal{C} \subset \mathbb{R}^{n+m+1}$ represents the *flow set* and $\mathcal{D} \subset \mathbb{R}^{n+m+1}$ is the *jump set*, respectively. When performing an `ode` simulation, a jump condition trigger is permanently verified and, based on the selected configuration, it allows prioritizing the flow logic, the jump logic, or a stochastic behavior which includes randomly selecting any of them. This jump condition will also be needed for hybrid system interconnections.

A MATLAB-based implementation of the above interface is provided in the book, starting from the Hybrid Equations (HyEQ) Toolbox from [SCN13], extended to support exogenous inputs and providing a unified interface for the system interconnections described in the next subsection, i.e. 2.5. The HyEQ Toolbox allows implementation and simulation of hybrid system models based on the `ode` suite from MATLAB/Simulink, with commutation logic implemented through the `events` functionality. Exogenous input signals must be known beforehand, such as reference signals and disturbance inputs, and it becomes useful for Model-in-the-Loop simulations.

## 2.5 System interconnections

After defining individual or *atomic* systems as in previous sections, the necessity for composing system interconnections readily appears. The classical interconnection operations are the series, parallel, lower and upper linear-fractional transformations (LLFT and ULFT), which are simplified cases of the Redheffer star product. The definitions are presented for nonlinear systems $\Sigma_1$ and $\Sigma_2$, with framework (2.1), alongside the generalization of hybrid systems $\Sigma_1^h$ and $\Sigma_2^h$ from (2.7). The first case is useful for linearization near an operating point, studying its system theoretical properties, and designing control techniques, while the latter becomes useful in a Model-in-the-Loop simulation context and for closed-loop system properties analysis. For hybrid system interconnections, the continuous and jump dynamics sets $\mathcal{C}$ and $\mathcal{D}$, respectively, are obtained using union and intersection set operations.

Moreover, the next discrete state for each subsystem is triggered by its own logic, defined by the jump function $G_i(x, u, t)$, $i \in \{1, 2\}$ and only when necessary, i.e. a jump condition is met; otherwise, it remains unchanged. For specifying the next discrete state $x^+$ logic, as in the

interface of the jump dynamics, assume the following notation:

$$\varphi(\beta, \xi_1, \xi_2) = \begin{cases} \xi_1, & \text{if } \beta = 1; \\ \xi_2, & \text{if } \beta = 0, \end{cases} \tag{2.8}$$

where, based on a logical variable $\beta \in \{0, 1\}$, the function $\varphi$ delegates to its output the second or third input argument, as in $\xi_1$ or $\xi_2$.

The scalar variables $\beta_1(t)$ for $\Sigma_1^h$, $\beta_2(t)$ for $\Sigma_2^h$ check the necessity of performing a jump at the current moment of time $t$.

### 2.5.1 Series connection

Given two subsystems $\Sigma_1$ and $\Sigma_2$ with dimensions $(m_1, n_1, p_1)$ and $(m_2, n_2, p_2)$, respectively, the resulting series connection system will have dimensions $(m{=}m_1, n{=}n_1{+}n_2, p{=}p_2)$. For a valid series connection, the precondition is that the number of outputs of the first subsystem must coincide with the number of inputs of the second subsystem, i.e. $m_2 = p_1$. An analytical expression for LTI components is provided in [IOW99].

$$(\Sigma_s) : \begin{cases} \begin{bmatrix} \dot{x}_1 \\ \dot{x}_2 \end{bmatrix} &= \begin{bmatrix} F_1(x_1, u, t) \\ F_2(x_2, h_1(x_1, u, t), t) \end{bmatrix}; \\ y &= h_2(x_2, h_1(x_1, u, t), t). \end{cases} \tag{2.9}$$

The equivalent series connection for hybrid models $\Sigma_1^h$ and $\Sigma_2^h$ has the state-space realization:

$$(\Sigma_s^h) : \begin{cases} \begin{bmatrix} \dot{x}_1 \\ \dot{x}_2 \end{bmatrix} &= \begin{bmatrix} F_1(x_1, u, t) \\ F_2(x_2, h_1(x_1, u, t), t) \end{bmatrix}; \\ \begin{bmatrix} x_1^+ \\ x_2^+ \end{bmatrix} &= \begin{bmatrix} \varphi(\beta_1, G_1(x_1, u, t), x_1) \\ \varphi(\beta_2, G_2(x_2, h_1(x_1, u, t), t), x_2) \end{bmatrix}; \\ \mathcal{C}(x, u, t) &= \mathcal{C}_1(x_1, u, t) \cap \mathcal{C}_2(x_2, h_1(x_1, u, t), t); \\ \mathcal{D}(x, u, t) &= \mathcal{D}_1(x_1, u, t) \cup \mathcal{D}_2(x_2, h_1(x_1, u, t), t); \\ y &= h_2(x_2, h_1(x_1, u, t), t). \end{cases} \tag{2.10}$$

### 2.5.2 Parallel connection

Given two initial subsystems $\Sigma_1$ and $\Sigma_2$ with dimensions $(m_1, n_1, p_1)$ and $(m_2, n_2, p_2)$, the resulting parallel connection system $\Sigma_p$ will have

dimensions ($m{=}m_1{=}m_2, n{=}n_1{+}n_2, p{=}p_1{=}p_2$). For a valid parallel connection, the required precondition is that the number of inputs of the two subsystems must coincide, alongside their number of outputs, i.e. $m_1 = m_2$ and $p_1 = p_2$.

The equivalent state-space representation is:

$$(\Sigma_p) : \begin{cases} \begin{bmatrix} \dot{x}_1 \\ \dot{x}_2 \end{bmatrix} & = \begin{bmatrix} F_1(x_1, u, t) \\ F_2(x_2, u, t) \end{bmatrix}; \\ y & = h_1(x_1, u, t) + h_2(x_2, u, t). \end{cases} \tag{2.11}$$

An analytical expression for LTI components is provided in [IOW99].

The equivalent parallel connection for hybrid models $\Sigma_1^h$ and $\Sigma_2^h$ has the state-space realization:

$$(\Sigma_p^h) : \begin{cases} \begin{bmatrix} \dot{x}_1 \\ \dot{x}_2 \end{bmatrix} & = \begin{bmatrix} F_1(x_1, u, t) \\ F_2(x_2, u, t) \end{bmatrix}; \\ \begin{bmatrix} x_1^+ \\ x_2^+ \end{bmatrix} & = \begin{bmatrix} \varphi(\beta_1, G_1(x_1, u, t), x_1) \\ \varphi(\beta_2, G_2(x_2, u, t), x_2) \end{bmatrix}; \\ \mathcal{C}(x, u, t) & = \mathcal{C}_1(x_1, u, t) \cap \mathcal{C}_2(x_2, u, t); \\ \mathcal{D}(x, u, t) & = \mathcal{D}_1(x_1, u, t) \cup \mathcal{D}_2(x_2, u, t); \\ y & = h_1(x_1, u, t) + h_2(x_2, u, t). \end{cases} \tag{2.12}$$

### 2.5.3 Lower LFT connection

Given two initial subsystems $\Sigma_1$ and $\Sigma_2$ with dimensions $(m_1, n_1, p_1)$ and $(m_2, n_2, p_2)$, respectively, the resulting LLFT connection system will have dimensions ($m{=}m_1{+}m_2, n{=}n_1{+}n_2, p{=}p_1{+}p_2$). The subsystem $\Sigma_1$ is usually seen as the augmented plant $P$, while $\Sigma_2$ is seen as the controller $K$. In order to ensure compatibility between the two, several assertions must be made: $n_{meas} = n_{y12} = n_{u21}$ and $n_{\text{con}} = n_{y21} = n_{u12}$.

$$(\Sigma_{\text{LLFT}}) : \begin{cases} \begin{bmatrix} \dot{x}_1 \\ \dot{x}_2 \end{bmatrix} & = \begin{bmatrix} F_1\left(x_1, u_1^{\text{LLFT}}, t\right) \\ F_2\left(x_2, u_2^{\text{LLFT}}, t\right) \end{bmatrix}; \\ y & = \begin{bmatrix} h_1\left(x_1, u_1^{\text{LLFT}}, t\right) \\ h_2\left(x_2, u_2^{\text{LLFT}}, t\right) \end{bmatrix}. \end{cases} \tag{2.13}$$

The equivalent LLFT connection for hybrid models $\Sigma_1^h$ and $\Sigma_2^h$ has

the state-space realization:

$$(\Sigma^{h}_{\text{LLFT}}) : \begin{cases} \begin{bmatrix} \dot{x}_1 \\ \dot{x}_2 \end{bmatrix} & = \begin{bmatrix} F_1\left(x_1, u_1^{\text{LLFT}}, t\right) \\ F_2\left(x_2, u_2^{\text{LLFT}}, t\right) \end{bmatrix}; \\ \begin{bmatrix} x_1^{+} \\ x_2^{+} \end{bmatrix} & = \begin{bmatrix} \varphi\left(\beta_1, G_1\left(x_1, u_1^{\text{LLFT}}, t\right), x_1\right) \\ \varphi\left(\beta_2, G_2\left(x_2, u_2^{\text{LLFT}}, t\right), x_2\right) \end{bmatrix}; \\ \mathcal{C}\left(x, u, t\right) & = \mathcal{C}_1\left(x_1, u_1^{\text{LLFT}}, t\right) \cap \mathcal{C}_2\left(x_2, u_2^{\text{LLFT}}, t\right); \\ \mathcal{D}\left(x, u, t\right) & = \mathcal{D}_1\left(x_1, u_1^{\text{LLFT}}, t\right) \cup \mathcal{D}_2\left(x_2, u_2^{\text{LLFT}}, t\right); \\ y & = \begin{bmatrix} h_1\left(x_1, u_1^{\text{LLFT}}, t\right) \\ h_2\left(x_2, u_2^{\text{LLFT}}, t\right) \end{bmatrix}. \end{cases} \tag{2.14}$$

The input-output interface used in the previous two definitions of (2.13) and (2.14) is given by the following relations:

$$u = \begin{bmatrix} u_1^{\top} & u_2^{\top} \end{bmatrix}^{\top} = \begin{bmatrix} u_{11}^{\top} & u_{12}^{ref,\top} & u_{21}^{ref,\top} & u_{22}^{\top} \end{bmatrix}^{\top}; \tag{2.15a}$$

$$u_1^{\text{LLFT}} = \begin{bmatrix} u_{11} \\ u_{12}^{ref} + y_{21}^{-} \end{bmatrix} \equiv \begin{bmatrix} u_{11} \\ u_{12} \end{bmatrix}, \tag{2.15b}$$

$$u_2^{\text{LLFT}} = \begin{bmatrix} u_{21}^{ref} + y_{12}^{-} \\ u_{22} \end{bmatrix} \equiv \begin{bmatrix} u_{21} \\ u_{22} \end{bmatrix}. \tag{2.15c}$$

The common convention in the literature is to consider the last $n_{\text{con}}$ values from the input vector $u_1$, i.e., $u_{12}$, as control input signals, while the last $n_{\text{meas}}$ values from the output vector $y_1$, i.e., $y_{12}$, as measurements signals. Only the vector $u$ will be an exogenous signal, as the feedback components $y_{12}^{-}$ and $y_{21}^{-}$ are local and private feedback components computed implicitly at the previous time step, dictated by the selected `ode` solver. The exogenous signals $u_{11}$ and $u_{22}$ are seen as disturbance signals, while the signals $u_{12}^{ref}$ and $u_{21}^{ref}$ are seen as references.

### 2.5.4 Upper LFT connection

Given two subsystems $\Sigma_1$ and $\Sigma_2$ with dimensions $(m_1, n_1, p_1)$ and $(m_2, n_2, p_2)$, respectively, the resulting ULFT connection system will have dimensions $(m{=}m_1{+}m_2, n{=}n_1{+}n_2, p{=}p_1{+}p_2)$. The subsystem $\Sigma_1$ is usually seen as the closed-loop plant with regulator $M$, while $\Sigma_2$ is seen as the

uncertainty block $\Delta$. In order to ensure compatibility between the two, several assertions must be made: $n_y = n_{y_{11}} = n_{u_2}$ and $n_u = n_{y_2} = n_{u_{11}}$.

$$(\Sigma_{\text{ULFT}}) : \begin{cases} \begin{bmatrix} \dot{x}_1 \\ \dot{x}_2 \end{bmatrix} &= \begin{bmatrix} F_1\left(x_1, u_1^{\text{ULFT}}, t\right) \\ F_2\left(x_2, u_2^{\text{ULFT}}, t\right) \end{bmatrix}; \\ y &= \begin{bmatrix} h_1\left(x_1, u_1^{\text{ULFT}}, t\right) \\ h_2\left(x_2, u_2^{\text{ULFT}}, t\right) \end{bmatrix}. \end{cases} \tag{2.16}$$

The equivalent ULFT connection for hybrid models $\Sigma_1^h$ and $\Sigma_2^h$ has the state-space realization:

$$(\Sigma_{\text{ULFT}}^h) : \begin{cases} \begin{bmatrix} \dot{x}_1 \\ \dot{x}_2 \end{bmatrix} &= \begin{bmatrix} F_1\left(x_1, u_1^{\text{ULFT}}, t\right) \\ F_2\left(x_2, u_2^{\text{ULFT}}, t\right) \end{bmatrix}; \\ \begin{bmatrix} x_1^+ \\ x_2^+ \end{bmatrix} &= \begin{bmatrix} \varphi\left(\beta_1, G_1\left(x_1, u_1^{\text{ULFT}}, t\right), x_1\right) \\ \varphi\left(\beta_2, G_2\left(x_2, u_2^{\text{ULFT}}, t\right), x_2\right) \end{bmatrix}; \\ \mathcal{C}\left(x, u, t\right) &= \mathcal{C}_1\left(x_1, u_1^{\text{ULFT}}, t\right) \cap \mathcal{C}_2\left(x_2, u_2^{\text{ULFT}}, t\right); \\ \mathcal{D}\left(x, u, t\right) &= \mathcal{D}_1\left(x_1, u_1^{\text{ULFT}}, t\right) \cup \mathcal{D}_2\left(x_2, u_2^{\text{ULFT}}, t\right); \\ y &= \begin{bmatrix} h_1\left(x_1, u_1^{\text{ULFT}}, t\right) \\ h_2\left(x_2, u_2^{\text{ULFT}}, t\right) \end{bmatrix}. \end{cases} \tag{2.17}$$

The input-output interface used in the previous two definitions of (2.16) and (2.17) is given by the following relations:

$$u = u_{12}, \quad u_1^{\text{ULFT}} = \begin{bmatrix} y_2^- \\ u_{12} \end{bmatrix}, \quad u_2^{\text{ULFT}} = y_{11}^-. \tag{2.18}$$

The common convention in the literature is to consider the first $n_u$ values from the input vector of the plant subsystem, i.e., $u_{11}$, as input uncertainty signals, while the first $n_y$ values from the output vector of the plant, i.e., $y_{11}$, as output uncertainty signals. Only the vector $u \equiv u_{12}$ will be an exogenous signal, as the feedback components $y_{11}^-$ and $y_2^-$ are local and private feedback components computed implicitly at the previous time step, dictated by the selected `ode` solver. The exogenous signal $u_{12}$ is seen as set of performance and control signals for the plant, without any reference signals recalled explicitly compared to the LLFT case.

# 3. Linear closed-loop control

## 3.1 Classical LTI control structures

### 3.1.1 Literature review

In the control systems domain, several classes of relevant problems can be gathered from literature:

(1) eigenvalue assignment via feedback, applicable to both singular [IOW99] and nonsingular systems [Ost11];
(2) minimization of quadratic cost criteria [ZDG96; Ost11; LXP08];
(3) disturbance rejection [ÅH06; SP05];
(4) asymptotic output regulation [SP05; Kha15];
(5) servo control [Mül00], leading to a DAE system formulation (2.2):

$$\dot{x} = F(x, u, t); \quad 0 = y_{\text{ref}} - h(x, u, t). \tag{3.1}$$

All previously-mentioned problems have their largest applicability in the framework of linear systems. Linear controller design techniques are available for both linear plants and nonlinear process models alike. Starting from the classical proportional-integral-derivative (PID) controller [ÅH06] towards the domain of robust controllers [ZDG96; SP05], these techniques can be extended to nonlinear systems via gain-scheduling methods [GA13], feedback linearization [Isi95; Isi94; Kha15], additional passivity-based components [Xia+15]. Moreover, with great advantage in also coping with disturbance rejection problems, alongside reference tracking specifications are the so-called two-degrees-of-freedom (2DOF) control schemes [ÅH06; AM22]. In [TA00], a 2DOF PID controller has been proposed, where the serial compensator is a classical PID controller, while the feedforward compensator is a PD controller, the integral effect being excluded due to the stability requirements. For the case of unstable plants with time delays, a discrete-time 2DOF control scheme has

been proposed in [Wan+16]. As such, for reference tracking, the serial controller was designed using the $\mathcal{H}_2$ optimal control framework, while the feedforward controller has been tuned by imposing the desired closed-loop transfer function. Also, in terms of software toolbox implementations, the robust advanced PID (RaPID) toolbox described in [OBO06] presents a set of possibilities to design a 2DOF PID control structure by minimizing a certain error criteria, like the integral of absolute error or integral of time multiplied by the absolute value of error.

There are multiple control design approaches available in the literature for linear and time-invariant systems, starting from classical PID [ÅH06], fractional-order (FO) PIDs [Pod99; DȘK18], root locus tuning [Oga10; ȘD16], linear quadratic regulator (LQR) and estimator-based (LQR) control techniques [ZDG96; LXP08], robust control techniques [ZDG96; SP05] or a combination of them, such as robust fractional-order PIDs [Mih+22a; Mih+22b]. Robust synthesis methods allow the design of both structured or unstructured regulators alike [AM22; BP20].

The cascade control structure is frequently-used in practice with good results, implying complex processes having decoupled faster and slower dynamics. There are cases which could support a faster sampling rate for the inner control loop, compared to the slower outer loop. Relevant examples are found in the domain of computer numeric control machines [Man14; Mor+22; Mor+23], electrical machines [Pet+21] and in temperature control systems [LZL17]. As particular cases of the multi-rate cascade control problem, there is the common one-degree-of-freedom (1DOF) control diagram, or a cascade connection where both controllers employ the same sampling period. In the case of multi-rate control systems, a proposed solution for cascade systems is found in [SAK18], a dual-rate switched observer-based predictive control structure has been proposed and implemented in [CZJ21], while in the case of multi-input and multi-output (MIMO) feedforward control is treated in [MOF20]. Of interest are also dual-rate systems and the difficulties arising in performing system identification on such structures, as illustrated in [YY17].

### 3.1.2 Numeric control systems

Modern control systems make use of numerically-implemented regulators to coordinate continuous-time processes. The classical configuration of a numeric regulator is presented in Figure 3.1. It uses sample and hold circuits as interfaces to the continuous-time adjacent compo-

nents and, as such, it imposes the zero-order hold discretization method for the plant $G$, assumed with the notations of Equation (2.4). In such cases, the physical implementation directly implies the plant discretization methodology as the mapping $(G(s), T) \mapsto G_T(z) \equiv G(z) \in \mathcal{G}_D$:

$$G_T(z) \equiv G(z) = \mathcal{Z}\left\{\mathcal{L}^{-1}\left\{G_{\text{zoh},T}(s) \cdot G(s)\right\}\right\} : \mathcal{G} \times \mathbb{R}_+ \to \mathcal{G}_D. \tag{3.2}$$

with digital-to-analog converter, i.e. zero-order hold, transfer function:

$$G_{\text{zoh},T}(s) = \frac{1 - e^{-sT}}{s}. \tag{3.3}$$

An equivalent state-spate formulation for the discretized plant is:

$$(G(z)) : \begin{cases} x_{k+1} & = \Phi x_k + \Gamma u_k; \\ y & = Cx_k + Du_k, \end{cases} \tag{3.4}$$

with the adaptations of the state and input matrices [Oga95]:

$$\Phi = e^{AT}, \quad \Gamma = \int_0^T e^{A\tau} B \; d\tau. \tag{3.5}$$

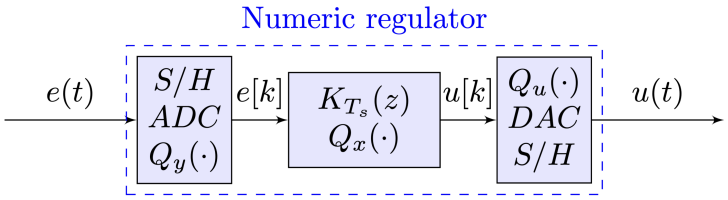


Figure 3.1: Numeric regulator and interfacing devices: sample and hold with analog-to-digital converter, along with the digital-to-analog converter followed by a sample and hold circuit.

Assuming an LTI framework, the resulting continuous-time and amplitude controllers have the state-space representation:

$$(K(s)) : \begin{cases} \dot{x}_c & = A_c x_c + B_c u_c; \\ y_c & = C_c x_c + D_c u_c, \end{cases} \tag{3.6}$$

where $u_c \leftarrow e$ and $y_c \leftarrow u$ are the connections in the closed-loop structure.

To implement a regulator $K(s)$ on a microcontroller, the selection

of the sampling period $T \in (0, \infty)$ becomes a critical step which will be later studied throughout the book. Using a fixed sampling period $T$ and an arbitrary discretization method, such as zero-order hold, forward or backward Euler, trapezoidal, also known as Tustin, least squares regression [FPW06], [ÅW02] and others, the discrete-time controller becomes:

$$(K(z)) : \begin{cases} x_{k+1} & = A_K x_k + B_K e_k; \\ u_k & = C_K x_k + D_K e_k, \end{cases} \tag{3.7}$$

where the transition and input matrices $\Phi$ and $\Gamma$ are obtained depending on the preferred discretization method. In some cases, the output equation matrix $C$ and instant transfer matrix $D$ may also be different than their continuous-time counterpart. The hardware interface is assumed as in Figure 3.1. As such, starting from the continuous-time transfer matrix $K(s) = (A_c, B_c, C_c, D_c)$, the equivalent discrete-time transfer matrix formulation can be viewed as a tuplet $(K(s), T) \mapsto K_T \equiv K(z)$:

$$K_T(z) = \mathcal{D}\left\{K(s), T\right\}, \tag{3.8}$$

having a discretization map with the structure $\mathcal{D} : \mathcal{G} \times \mathbb{R}_+ \to \mathcal{G}_D$.

### 3.1.3 One-degree-of-freedom (1DOF) structure

For the single-loop control system presented in Figure 3.2, the continuous-time MIMO closed-loop transfer matrix is given by:

$$G_0 = KG\left(I + KG\right)^{-1}. \tag{3.9}$$

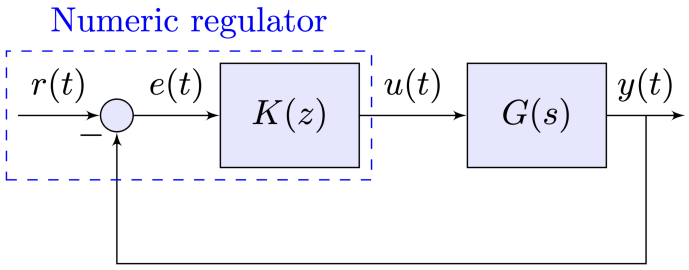


Figure 3.2: One-degree-of-freedom control structure having a continuous plant $G(s)$, numeric regulator $K(z)$, and standard signal notations.

With the discretization of the plant model $G(s)$ using the mecha-

nism from Equation (3.2), the discrete process becomes:

$$G_T(z) = \mathcal{Z}\left\{\mathcal{L}^{-1}\left\{G_{\text{zoh},T}(s)\cdot G(s)\right\}\right\}(z), \tag{3.10}$$

which, alongside a discrete-time regulator $K_T(z)$, with structure (3.7) obtained using (3.8), leads to the discrete closed-loop transfer matrix:

$$G_{0,T} = K_T G_T \left(I + K_T G_T\right)^{-1}. \tag{3.11}$$

### 3.1.4 Two-degrees-of-freedom (2DOF) structure

When describing two-degrees-of-freedom (2DOF) control structures, throughout the book, consider the canonical structure from Figure 3.3, which has an inner controller $K_{\text{in}}(z)$ usually designed for disturbance rejection, and a feedforward controller $K_{\text{ff}}(z)$ which provides the necessary compensation for the steady-state tracking behaviour, along with the process model with disturbance, described by $G(s)$ and $G_d(s)$. This structure can be encompassed into the more general R-S-T architecture [SP05]. As $K_{\text{ff}}$ does not influence the signal path from the disturbance $d(t)$ to the output $y(t)$, the usual design workflow is to synthesize $K_{\text{in}}$ and, then, to fine-tune the transient response from $r(t)$ to $y(t)$ through $K_{\text{ff}}$. Both initial continuous-time controllers $K_{\text{in}}(s)$ and $K_{\text{ff}}(s)$ are assumed to have the following linear and time-invariant state-space representations:

$$(K_x(s)): \begin{cases} \dot{x}_c &= A_{c,x}x_c + B_{c,x}u_c \\ y_c &= C_{c,x}x_c + D_{c,x}u_c \end{cases}, \quad x \in \{\text{in}, \text{ff}\}. \tag{3.12}$$

To implement $K_{\text{in}}(s)$ and $K_{\text{ff}}(s)$ microcontrollers, assume an appropriate sampling period $T \in (0, \infty)$. After that, the discrete-time form of the controllers $K_x(s)$, $x \in \{\text{in}, \text{ff}\}$, can be written using mappings (3.8) as:

$$(K_x(z)): \begin{cases} x_{k+1} &= A_{K,x}x_k + B_{K,x}u_k \\ y_k &= C_{K,x}x_k + D_{K,x}u_k \end{cases}, \quad x \in \{\text{in}, \text{ff}\}. \tag{3.13}$$

As such, starting from a tuple of a continuous-time transfer matrix $K_x(s) = (A_{c,x}, B_{c,x}, C_{c,x}, D_{c,x}) \in \mathcal{G}$ and sampling rate $T \in \mathbb{R}_+$ an equivalent discrete-time transfer matrix $(K_x(s), T)$ results, based on (3.8):

$$K_{x,T}(z) = \mathcal{D}\left\{K_x(s), T\right\} : \mathcal{G} \times \mathbb{R}_+ \to \mathcal{G}_D. \tag{3.14}$$

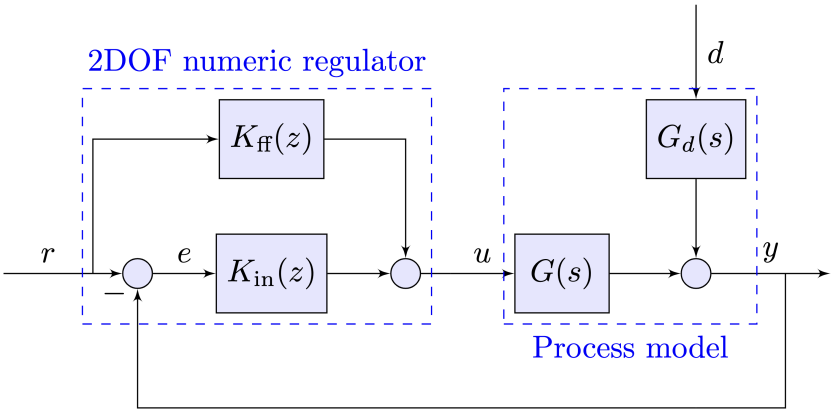


Figure 3.3: Two-degrees-of-freedom (2DOF) numeric control structure with component regulators $K_{\mathrm{in}}(z)$, $K_{\mathrm{ff}}(z)$ designed for the process model $G(s)$ with disturbance dynamics $G_d(s)$.

The open-loop process model has the input-output representation:

$$Y(s) = G_d(s) \cdot D(s) + G(s) \cdot U(s), \tag{3.15}$$

while the closed-loop system expression becomes:

$$Y(s) = \frac{G_d(s)}{1 + G(s)K_{\mathrm{in}}(s)} \cdot D(s) + \frac{G(s)(K_{\mathrm{in}}(s) + K_{\mathrm{ff}}(s))}{1 + G(s)K_{\mathrm{in}}(s)} \cdot R(s). \tag{3.16}$$

The discrete-time equivalent closed-loop model will thus be:

$$Y(z) = G_0^d(z) \cdot D(z) + G_0^r(z) \cdot R(z), \tag{3.17}$$

with components:

$$G_0^d(z) = \frac{G_d(z)}{1 + G(z)K_{\mathrm{in}}(z)}, \quad G_0^r(z) = \frac{G(z)(K_{\mathrm{in}}(z) + K_{\mathrm{ff}}(z))}{1 + G(z)K_{\mathrm{in}}(z)}, \tag{3.18}$$

which offer the starting point for various control design methodologies, such as pole placement and root locus.

### 3.1.5 Cascade structure

When the cascade control structure from Figure 3.4 is considered, the following assumption is used: the inner loop is faster than the outer

loop. As such, the sampling period $T_{\text{in}}$ used in the inner loop will be considered the base sampling time $T \equiv T_{\text{in}}$, while the sampling period $T_{out}$ used in the outer loop respects $T_{\text{out}} = k \times T_{\text{in}}$, where $k$ is a positive integer number. The controllers $K_{\text{in}}$ and $K_{\text{out}}$ will gather the same structures as (3.12) and (3.13), with indices $x \in \{\text{in}, \text{out}\}$, the discrete-time equivalent forms obtained through mappings:

$$K_{T,\text{in}}(z) = \mathcal{D}\left\{K_{\text{in}}(s), T\right\} : \mathcal{G} \times \mathbb{R}_+ \to \mathcal{G}_D; \tag{3.19}$$

$$K_{kT,\text{out}}(z) = \mathcal{D}\left\{K_{\text{out}}(s), kT\right\} : \mathcal{G} \times \mathbb{R}_+ \to \mathcal{G}_D. \tag{3.20}$$

In a similar manner to the single-loop structure mentioned above, the open-loop processes $G_{\text{in}}(s)$ and $G_{\text{out}}(s)$ have been discretized using the zero-order hold extrapolator:

$$G_{T,x}(z) = \mathcal{Z}\left\{\mathcal{L}^{-1}\left\{G_{\text{zoh},T}(s)G_x(s)\right\}\right\}(z), \ x \in \{\text{in}, \text{out}\}. \tag{3.21}$$

The resulting discrete-time inner closed-loop system is:

$$G_{0,T,\text{in}} = K_{T,\text{in}}G_{T,\text{in}}\left(I + K_{T,\text{in}}G_{T,\text{in}}\right)^{-1}. \tag{3.22}$$

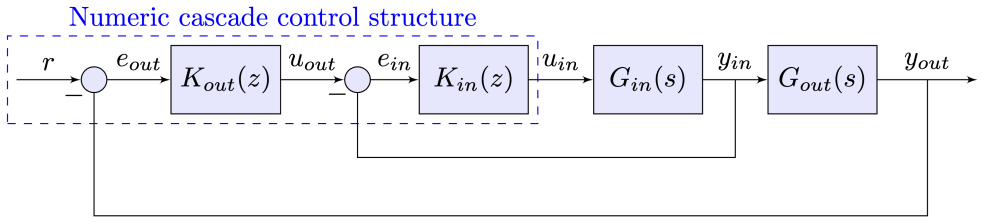


Figure 3.4: Numeric cascade control diagram with: inner plant $G_{\text{in}}$ and controller $K_{\text{in}}$ encompassing the faster loop, along with the outer plant $G_{\text{out}}$ and controller $K_{\text{out}}$ denoting the loop with slower dynamics.

To maintain the same sampling period for the full cascade discrete system, the outer controller is seen through the base period $T$ instead of $kT$, i.e.:

$$K_{kT,\text{out}}(z) = K_{T,\text{out}}(z^k) \equiv K_{T,k,\text{out}}, \tag{3.23}$$

resulting a closed-loop system:

$$G_{0,T,\text{out}} = G_{\text{op},T,k}\left(I + G_{\text{op},T,k}\right)^{-1}, \tag{3.24}$$

where $G_{\text{op},T,k}$ is the outer open-loop system, described by:

$$G_{\text{op},T,k} = K_{T,k,\text{out}} G_{0,T,\text{in}} G_{T,\text{out}}. \tag{3.25}$$

## 3.2 Generalized LTI structure. Robust control synthesis

### 3.2.1 Literature review

Beyond the classical paradigm of imposing a certain control structure, selecting a controller architecture, followed by tuning said controller's parameters through various possible methods or their combinations, by imposing ad hoc performance indices, and to possibly neglect certain aspects of the system model to account for the limitations of each design method, a relatively new approach, originating from the seminal paper of [Zam81], is based on using a generalized plant model for which the controller is then synthesized through optimization techniques. The concept introduced there is to quantify the worst-case influence of an arbitrary input channel configuration towards the outputs of the system, by employing the so-called Hardy space norms. Such a worst-case scenario based approach, by defining a comprehensive general plant model to also encompass the imposed performances, leads to a flexible and general-purpose framework which has been thoroughly used in the past three decades, in several particular variations.

Robust control is a branch of control theory focusing on the design and analysis of controllers which ensure stability and desired performance for the nominal case, as well as for uncertain plant variations, by using optimization techniques [ZDG96]. The functional cost considered for optimization is usually the $\mathcal{H}_\infty$ norm.

Continuous-time robust control synthesis has been employed in a wide range of practical applications, with great flexibility. It provides a general framework to model the nominal industrial process in transfer matrix form or state-space representations, extend it with several approaches to model uncertainties [ZDG96], specify performance indices through open [MG92] and closed-loop shaping [SP05], to synthesize unstructured regulators with the aid of algebraic Riccati equations and linear matrix inequalities [LY16], or to consider fixed-structure controller forms computed through nonsmooth optimization techniques [Apk11; AN17]. The $\mathcal{H}_2$ and $\mathcal{H}_\infty$ norms are commonly-used to quantify the performance of a system, for continuous and discrete cases alike, such as

in [KH22] and [TO15]. The approach of using the $\mathcal{H}_2/\mathcal{H}_\infty$ norms was further extended by the structured singular value (SSV) $\mu$ which adequately accounts for uncertainty in the plant dynamics [PDB93; Apk11]. This framework allows an intuitive application of the main loop theorem [LY16] in order to guarantee robust stability (RS) and robust performance (RP) of the closed-loop system [SP05]. Robustness analysis methods in presence of parametric and switching uncertainties have also been introduced in [PE14].

There are two classical solutions for solving such control problems for the nominal plant: algebraic Riccati equations (AREs) [ZDG96] and linear matrix inequalities (LMIs) [LY16]. Classical solutions to the $\mathcal{H}_2/\mathcal{H}_\infty$ problems are presented in [Doy+89; GA94; IOW99; ZDG96] and others. The solution of the $\mu$-synthesis procedure is usually performed using the well-known D-K iteration algorithm, described in [SP05] and with a reference implementation in MATLAB's Robust Control Toolbox [Bal+22]. Along with the LMI Lab utility, they allow modelling of uncertain systems, closed-loop mixed-sensitivity loop-shaping design, with also the Glover-McFarlane [MG92] loop shaping design procedure (LSDP), tune control loops, compute disk margins, perform $\mathcal{H}_2$, $\mathcal{H}_\infty$ and $\mu$-synthesis solutioned using the dual-Riccati or LMI method, unstructured or fixed-structure synthesis and order reduction functionalities. Various numeric methods targeted for linear systems, control theory and robust synthesis are described in [Dat04; IOW99].

Generalizations of robust control techniques in the context of LTI systems for singular and differential-algebraic equations (DAEs), and also for classes of nonlinear system can be found in [Col04], [FY17], [HJ99], [Isi94], [Spe+20], and others.

Plant modelling is one of the key studied aspects as the mathematical model needs to be simple enough to be used in the optimization problem without further difficulties, and sufficiently complex to reproduce the relevant behaviour of the real process. In order to mediate these aspects, a nominal plant is denoted along with its uncertainties. A major problem in robust control synthesis is to model uncertainties, classified as lumped, i.e. parametric and unstructured [ÅH00].

The study of parametric uncertainties is performed in the monograph [BCK95], based on polynomial models. An overview with focus on recent results is further presented in the survey paper [Bha17]. A graphical method to deal with parametric uncertainties based on a combination of the zero exclusion condition and the value set concept is presented in

[MP11]. However, as stated in [SP05], the use of parametric uncertainties only is generally not useful, because the exact model structure is required, which means that the neglected or unmodelled dynamics cannot be accounted for. A way to construct an uncertain model based on the appropriate selection of a nominal system, along with a suitable weighting function for RS analysis is presented in [MŞY17]. All these methods are based on magnitude information. In [TBL99], constraints on the phase of the uncertainties are also considered besides the classical idea of boundedness. As such, the notion of phase-sensitive structured singular value (PS-SSV) of a matrix was introduced along with sufficient conditions for RS. In [LS09], the authors proposed an extension of the classical robust control theory, called neo-robust control, which utilizes, besides the gain information of the uncertainty, the phase information as well, to factorize uncertainties in the robust control synthesis, which continues with aspects regarding uncertainty modelling and RS analysis presented in [LK09b], while the second part [LK09a] deals with the analysis of the robust sensitivity and the robust bandwidth.

Uncertainty bounds on frequency response data have been considered in the past with the works of [HSB02], later extended in [BV04], which cover convex bounds using the Log-Chebyshev magnitude fitting approach and return valid models in the sense of [Poo+94]. Extensions have been provided in [BPS09], [Som+22], which also cover relevant practical case studies. Robust controllers have been calibrated based on frequency response data for input-affine nonlinear systems in [Mih+22d]. The journal paper [Pat+23] proposes an analysis and computation of the worst-case attainable gain given the uncertainty family of processes.

In addition to the procedures described above, to implement continuous regulators on a numeric device, two other procedures must be applied: a sampling operation, leading to a discrete-time model, along with a quantization operation, which applies to both the regulator signals and its coefficients, while the latter problem is maintained even for regulators directly designed in the discrete-time domain.

The sampling period leads to the compromise of selecting a low value which leads to better fidelity [TJ19; MG90], with the cost of high microprocessor loads in order to be successfully implemented, and a higher value which becomes desirable with respect to implementation aspects, buy may lead to unsatisfactory performance degradation [Șuș+22b]. The sampling rate yields strong limitations on the $\mu$-synthesis procedure due to arising numeric issues, as specified in [Bal+22]. With

the recommendation that the sampling times must be selected such that the significant dynamics of the system and weighting functions should not be more than a decade or two below the theoretical Nyquist frequency, the proposed alternative is to design the regulator in continuous-time. This approach would prove to be feasible given that an adequate method to ascertain the quality of the discretized regulator is also available, which is one of the scopes of the book. In addition, the quantization effects bring nonlinear behaviour which perturbs the asymptotic stability of the closed-loop system with the appearance of limit cycles in the steady-state response [ȘMD22], alongside the degradation of the transient response, as presented in [XOG20], and reachability limitations [BMP02].

### 3.2.2 Numeric tools

Even though there is a large variety of CACSD toolboxes in the field, their number is still expanding due to the necessity of overcoming drawbacks or shortcomings that the already existing ones have. At this point, the purpose of new toolboxes is not only to determine robust controllers for a specific process class, but to use a unified approach that would make them work for more types of systems, even multiple interconnected systems, in various configurations. User experience is also more accentuated, which is why some incorporate graphical user interfaces (GUIs), for improved usability.

An example is Multivar, which is a MATLAB-based application used for MIMO control design, presented in [BS16]. This toolbox supports two working modes. It allows the user to work both in function and GUI mode (which represents a configuration wizard for determining the controller). Multivar can be used for LTI systems with or without time delay and it allows creating a model, converting, approximating, and analyzing it; input-output pairing and decoupling; and controller design and evaluation. Besides this, the user is able to export the control design and compare it with other saved designs. Another GUI-based robust controller design tool, which was created in LabVIEW, is presented in [ZK17], based on the $\mathcal{H}_\infty$ loop-shaping method. However, the goal was to provide a simple, user-friendly interface for easier use, especially for educational purposes. Therefore, as mentioned by the authors, it does not provide the same flexibility as other design tools on the market.

The Linear Control (LC) Toolbox [Jac+18; Swe+22] is a MATLAB-based wrapper for different software tools and supports modules for sys-

tem theory, using system, model and signal software entities, for LTI and also supporting linear parameter-varying (LPV) systems, system identification, by using regularized state-space model interpolation of local estimates, $\mathcal{H}_2/\mathcal{H}_\infty$ controller design, and simulation. One of the advantages of using this toolbox instead of classic MATLAB routines is the fact that it gathers all necessary steps for controller design in one place, while cutting the need of preprocessing steps such as separate construction of the plant, and postprocessing steps, such as closed-loop simulation.

Other $\mathcal{H}_\infty$-based CACSD toolboxes have been presented over the past years. One example is represented in [SOK12], which is based on linearizing or convexifying the conventional non-convex constraints on the classical robustness margins of $\mathcal{H}_\infty$ constraints. The controller parameters are then computed by using an optimization solver. This toolbox was created for MATLAB, and some of its main features are represented by the large variety of control problems in which it could be used, such as multi-model systems; the toolbox is designed to work with the output data of MATLAB's System Identification Toolbox [Lju20]. The output of the toolbox is represented by a PID controller, which can be easily implemented. Another example of a $\mathcal{H}_\infty$-based frequency-domain CACSD robust control toolbox is shown in [Kar13], in which the main advantage is the reduced conservatism of almost all types of model uncertainties which are defined. Another example is the HIFOO toolbox, initially presented in [Bur+06], designed for fixed order nonconvex and nonsmooth optimization, with several extensions in the forthcoming years and cited in the literature for various applications, such as in [GMO08; Gum+09].

Controller order is an important factor when implementing it on real systems. Therefore, may become an important issue in certain cases. However, methods that are determining a fixed structure controller are already presented, such as in [SK14], which is based on the $\mathcal{H}_2$ controller design method, but can be cumbersome to compute. To deal with the high order controller problem, other toolboxes include controller simplification steps to avoid the necessity of postprocessing, as in [VSP16].

Currently acknowledged problems in this domain regard closed-loop simulation, where performance validation is generally treated ad hoc, i.e. separately studied from one control problem to another. Another difficulty encountered is when the test cases were done only on the linearized system for which the controller is designed, without checking if the initially proposed performance indices are still valid for the nonlinear plant model. The purpose of the paper is to provide means for treating

the previously stated problems in a unified manner, such as implementing automated testing, performance validation, and report generation.

An open-source implementation for ARE-based approach using Popov triplets is presented in thesis [Șuș19], based on the monograph [IOW99], with an iterative refinement procedure shown in [Şuş+20], while an open-source implementation for LMI-based approach is described in thesis [Mih20], based on the approach from [LY16].

A general-purpose software tool for solving convex optimization problems is YALMIP, initially proposed in [Löf04]. It allows the user to define and solve LMI, linear, quadratic and semidefinite programming (SDP) problems, classes of non-convex optimization problems such as bilinear matrix inequalities (BMIs) or mixed integer problems. It is highly configurable and allows the extension with third party solvers, such as MOSEK, SEDUMI, SDPT3, GUROBI, PENBMI, CPLEX and so on.

### 3.2.3 $\mathcal{H}_\infty$ synthesis

**Definition 1.** *A continuous-time augmented plant $P$ is obtained by extending the physical process model with a set of mathematical signals which aid the optimization procedure and has the following structure:*

$$(P): \begin{pmatrix} z \\ y \end{pmatrix} = \begin{pmatrix} P_{zw} & P_{zu} \\ P_{yw} & P_{yu} \end{pmatrix} \begin{pmatrix} w \\ u \end{pmatrix};$$
$$P = \begin{pmatrix} P_{zw} & P_{zu} \\ P_{yw} & P_{yu} \end{pmatrix} = \left(\begin{array}{c|cc} A & B_w & B_u \\ \hline C_z & D_{zw} & D_{zu} \\ C_y & D_{yw} & D_{yu} \end{array}\right), \tag{3.26}$$

*where $w(t) \in \mathbb{R}^{n_w}$ is the exogenous input vector, $u(t) \in \mathbb{R}^{n_u}$ is the control input vector, $z(t) \in \mathbb{R}^{n_z}$ is the error, also known as output or performance vector, and $y(t) \in \mathbb{R}^{n_y}$ is the measurement vector.*

The closed-loop system is given by the LLFT connection of $P$ and $K$, illustrated in Figure 3.5–a) in the continuous-time case, and Figure 3.5–b) for the discrete-time case, with its expression obtained by particularizing Equation (2.13) for LTI components:

$$P_{0,zw} = \mathrm{LLFT}(P, K) = P_{zw} + P_{zu} K \left(I - P_{yu} K\right)^{-1} P_{yw}. \tag{3.27}$$

The connection is well-posed if $(I - P_{yu}K)$ is invertible.

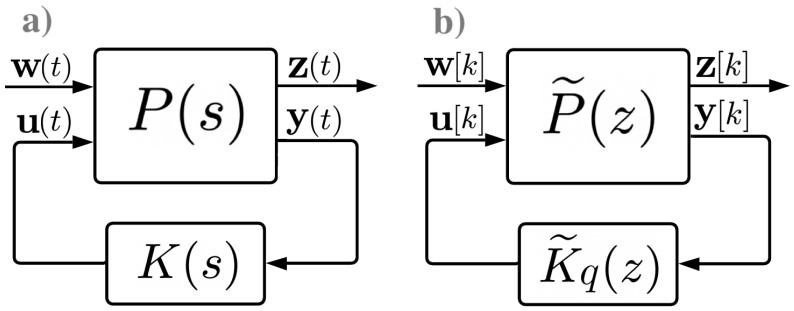


Figure 3.5: Plant with controller LLFT connection in continuous-time case *a*) and discrete-time case *b*), linking the nominal augmented plant $P$ and controller system $K$ as in relation (3.27).

For the nominal case, the target of the robust control problem is to minimize the $\mathcal{H}_\infty$ norm using a stabilizing controller $K$.

**Problem 1.** *Given a continuous-time augmented plant $P$, partitioned as in (3.26), the $\mathcal{H}_\infty$ norm minimization problem is defined as:*

$$\min_{K \text{ stab.}} \|P_{0,zw}\|_\infty = \min_{K \text{ stab.}} \sup_{\omega \in \mathbb{R}^+} \overline{\sigma}\left(P_{0,zw}(j\omega)\right) = \gamma > 0, \tag{3.28}$$

*obtaining a (sub)optimal value $\gamma$ by iteration, which minimizes the effects of the input vector $w$ as seen through the performance output vector $z$.*

However, the classical $\mathcal{H}_2/\mathcal{H}_\infty$ problem ensures only nominal stability and nominal performance.

### 3.2.4 Uncertainty modelling

In practice, the plant is a model of a physical process having uncertainties. There are two types of uncertainties: unstructured, which illustrates neglected and unmodelled dynamics and which are represented by a full block $\Delta \in \mathbb{R}^{m \times m}$, and parametric, which are represented by $\delta I$, where $\delta \in \mathbb{R}_+$ is the maximum bound of the variable parameter. In a mixed-scenario, the following set encompasses all possible combinations:

$$\begin{aligned} \mathbf{\Delta} = \{\Delta = \operatorname{diag}\left(\delta_1 I_{n_1}, \ldots, \delta_s I_{n_s}, \Delta_1, \ldots, \Delta_f\right) | \\ \delta_k \in \mathbb{R},\ \Delta_j \in \mathbb{R}^{m_j \times m_j},\ k = \overline{1,s},\ j = \overline{1,f}\}. \end{aligned} \tag{3.29}$$

**Definition 2.** *A continuous-time uncertain plant $G$ is obtained by extending the process model with a set of mathematical signals which account for the uncertain dynamics and has the following structure:*

$$
\begin{aligned}
(G): \begin{pmatrix} v \\ y \end{pmatrix} &= \begin{pmatrix} P_{vd} & P_{vu} \\ P_{yd} & P_{yu} \end{pmatrix} \begin{pmatrix} d \\ u \end{pmatrix}; \\
G = \begin{pmatrix} P_{vd} & P_{vu} \\ P_{yd} & P_{yu} \end{pmatrix} &= \left(\begin{array}{c|cc} A & B_d & B_u \\ \hline C_v & D_{vd} & D_{vu} \\ C_y & D_{yd} & D_{yu} \end{array}\right),
\end{aligned} \tag{3.30}
$$

*where $d(t) \in \mathbb{R}^{n_d}$ is the disturbance input, $u(t) \in \mathbb{R}^{n_u}$ is the control input, $v(t) \in \mathbb{R}^{n_v}$ is the disturbance output, and $y(t) \in \mathbb{R}^{n_y}$ is the measurement.*

To distinguish an uncertain plant $G$ from its nominal counterpart, where $\Delta \equiv 0$, denote the nominal subsystem used in classical control theory as the state-space model:

$$
G_n = \left(\begin{array}{c|c} A & B_u \\ \hline C_y & D_{yu} \end{array}\right). \tag{3.31}
$$

The closed-loop system is given by the ULFT connection of $G$ and $\Delta$, illustrated in Figure 3.6–a) in the continuous-time case, and Figure 3.6–b) for the discrete-time case, with its expression obtained by particularizing Equation (2.16) for LTI components:

$$
G_{0,yu} = \mathrm{ULFT}(G, \Delta) = G_{yu} + G_{yd}\Delta \left(I - G_{vd}\Delta\right)^{-1} G_{vu}. \tag{3.32}
$$

The connection is well-posed if $(I - G_{vd}\Delta)$ is invertible.

### 3.2.5 $\mu$-synthesis

One way to extend the traditional performance indices to the entire uncertainty set of the plant model is to use robust control techniques, such as $\mu$-synthesis, to design controllers that can guarantee stability and performance under various uncertainties. This approach is essential in practical control system design, where uncertainties are inevitable and can significantly affect the performance of the control system. By gathering the two structures from Definitions 1 and 2, a generalized plant

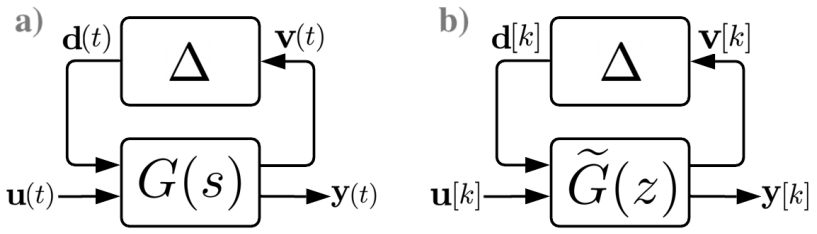


Figure 3.6: Uncertain plant model ULFT connection in the continuous-time case $a$) and discrete-time case $b$), linking the plant $G$ and uncertainty block $\Delta$ as in relation (3.32).

model which accounts for both uncertainty dynamics and augmented signals can be defined.

**Definition 3.** *A continuous-time generalized plant $P$ is obtained by augmenting the physical process model with a set of performance and uncertainty signals, and has the following structure:*

$$(P): \begin{pmatrix} v \\ z \\ y \end{pmatrix} = \begin{pmatrix} P_{vd} & P_{vw} & P_{vu} \\ P_{zd} & P_{zw} & P_{zu} \\ P_{yd} & P_{yw} & P_{yu} \end{pmatrix} \begin{pmatrix} d \\ w \\ u \end{pmatrix};$$

$$P = \begin{pmatrix} P_{vd} & P_{vw} & P_{vu} \\ P_{zd} & P_{zw} & P_{zu} \\ P_{yd} & P_{yw} & P_{yu} \end{pmatrix} = \left(\begin{array}{c|ccc} A & B_d & B_w & B_u \\ \hline C_v & D_{vd} & D_{vw} & D_{vu} \\ C_z & D_{zd} & D_{zw} & D_{zu} \\ C_y & D_{yd} & D_{yw} & D_{yu} \end{array}\right), \tag{3.33}$$

*where $d(t) \in \mathbb{R}^{n_d}$ is the disturbance, $w(t) \in \mathbb{R}^{n_w}$ is the exogenous input, $u(t) \in \mathbb{R}^{n_u}$ is the control input, $v(t) \in \mathbb{R}^{n_v}$ is the disturbance output, $z(t) \in \mathbb{R}^{n_z}$ is the performance output, and $y(t) \in \mathbb{R}^{n_y}$ is the measurement.*

Consider the following mappings which show the relationships between the previously-discussed nominal, uncertain, and augmented plants. The uncertain plant $G_{\mathbf{\Delta}} \equiv G$, Figure 3.6–a), can be written as a function of the structured normalized uncertainty block $\mathbf{\Delta}$ of corresponding dimension with an adequate mapping:

$$\mathcal{T}: \mathcal{G}^2 \to \mathcal{G},\ G = \mathcal{T}(G_n, U),\ \Delta \in \mathbf{\Delta},\ \|\Delta\|_\infty \leq 1, \tag{3.34}$$

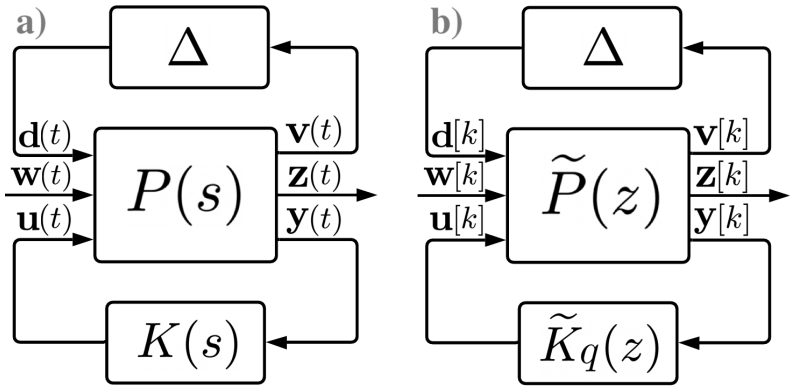


Figure 3.7: a) Continuous-time augmented plant $P$ in a ULFT connection with the uncertainty block $\Delta$ and LLFT connection with the regulator $K$; b) Discrete-time equivalents with sampled and discretized blocks $\widetilde{P}$, $\widetilde{K}$, and quantized regulator coefficients, further symbolized by $\widetilde{K}_q$.

having the transfer matrix $U$ partitioned as (3.29). As such, the nominal plant model becomes $G_n = G_{\mathbf{\Delta}}|_{\Delta=O}$. Additionally, the augmented plant $P$ is assumed to be written based on the uncertain plant $G$ through an adequate mapping $\mathcal{A}$ as:

$$\mathcal{A} : \mathcal{G} \times \mathcal{G} \to \mathcal{G}, \;\; P = \mathcal{A}\,(G, W)\,, \tag{3.35}$$

with a transfer matrix $W$ hosting the performance filters. As such, $G_n$ has the interface $u \mapsto y$, $G$ extends it with $d \mapsto v$, while $P$ adds the final components $w \mapsto z$ as in (3.33).

**Example 1.** *To illustrate the above notations, consider an example with a SISO nominal plant* $G_n = G_{n_1} G_{n_2}$, *with multiplicative and additive uncertainties,* $U = \begin{bmatrix} U_1 & U_2 \end{bmatrix}$, *i.e.* $G = G_{n_1}\,(1 + U_1\Delta_1)\,(G_{n_2} + U_2\Delta_2)$, $\Delta = diag\left(\begin{bmatrix} \Delta_1 & \Delta_2 \end{bmatrix}\right)$, $\|\Delta\|_\infty \leq 1$, *and its augmented plant model using the closed-loop sensitivity weight* $W{=}W_S$ *as* $P = \begin{bmatrix} -W_S G & W_S \end{bmatrix}$. □

In order to obtain the uncertainty measurements $\ell(j\omega) = U(j\omega)\Delta(j\omega)$, the inverse operator $\mathcal{T}^{-1}$ should be used, as in Table 3.1, leading to:

$$\ell(j\omega) = \mathcal{T}^{-1}(G, G_n). \tag{3.36}$$

A well-established approach in the literature to obtain a proper

Table 3.1: Common classes of uncertainty models.

| $G = \mathcal{T}(G_n, U),\ \|\Delta\|_\infty \leq 1$ | $U = \mathcal{T}^{-1}(G, G_n)$ |
|---|---|
| $G = G_n + \Delta U$ | $\Delta U = G - G_n$ |
| $G^{-1} = G_n^{-1} + \Delta U$ | $\Delta U = G^{-1} - G_n^{-1}$ |
| $G = G_n(I + \Delta U)$ | $\Delta U = G_n^{-1}(G - G_n)$ |
| $G = (I + \Delta U) G_n$ | $\Delta U = (G - G_n) G_n^{-1}$ |
| $G^{-1} = (I + \Delta U) G_n^{-1}$ | $\Delta U = G^{-1} G_n - I$ |
| $G^{-1} = G_n^{-1}(I + \Delta U)$ | $\Delta U = G_n G^{-1} - I$ |
| $G = (M + \Delta_M U_1)^{-1}(N + \Delta_N U_2)$ | $\Delta_M U_1 = (N + \Delta_N U_2) G^{-1}$ |
| $G = (N + \Delta_N U_2)(M + \Delta_M U_1)^{-1}$ | $\Delta_M U_1 = G^{-1}(N + \Delta_N U_2)$ |

weighting function $U(s)$ is presented, which minimizes the gap between itself and the measurements $\ell(j\omega)$, with the additional constraint that the magnitude of $U(j\omega)$ must lie above $|\ell(j\omega)|$ for all frequencies $\omega \in \Omega$. The optimization problem can be formulated as a semidefinite programming (SDP) one, as in [BV04]:

$$\mathcal{S}_\gamma(\theta): \min_\theta t \quad \text{s.t.} \quad \frac{1}{1+\frac{t}{\gamma}} < \frac{|U_\theta(j\omega)|^2}{|\ell(j\omega)|^2} < 1+\frac{t}{\gamma},\ \forall \omega \in \Omega, \tag{3.37}$$

considering a transfer function model $U_\theta$ parameterized by a variable $\theta$, with an additional hyperparameter $\gamma(\omega) > 0$ which can be used to weight certain frequencies in the optimization. In a similar manner, an LMI-based problem can be formulated to integrate additional constraints, as in [HSB02]. The solution to this problem is used as an initial point to our proposed method.

A mathematical tool used for studying the robustness with respect to uncertainties is the so-called structured singular value.

**Definition 4.** *The structured singular value (SSV) of a square matrix $M \in \mathbb{C}^{N\times N}$ with respect to the set $\mathbf{\Delta}$, is defined as:*

$$\mu_{\mathbf{\Delta}}(M) = \frac{1}{\min_{\Delta\in\mathbf{\Delta}}\{\overline{\sigma}(\Delta) | \det(I - M\Delta) = 0\}}, \tag{3.38}$$

*if there exists $\Delta \in \mathbf{\Delta}$ such that the matrix $(I - M\Delta)$ is rank deficient;*

*otherwise,* $\mu_{\mathbf{\Delta}}(M) = 0$.

For the system presented in Figure 3.7–a), the structured singular value of $\mathrm{LLFT}(P, K)$, according to the block $\Delta$ as in (3.29), can be defined as:

$$\mu_{\mathbf{\Delta}}(\mathrm{LLFT}(P, K)(s)) = \sup_{\omega \in \mathbb{R}_+} \mu_{\mathbf{\Delta}}(\mathrm{LLFT}(P, K)(j\omega)). \tag{3.39}$$

Besides the classical $\mathcal{H}_2/\mathcal{H}_\infty$ techniques, the $\mu$-synthesis framework manages to design a controller that meets the robust stability and robust performance specifications. The robust stability (RS) implies that a certain controller manages to stabilize all processes described by the ULFT between plant and uncertainty block, while the robust performance (RP) means that the controller is able to impose the desired closed-loop performance in the worst-case scenario [SP05]. Based on the main loop theorem [LY16], a controller $K$ meets the RS and RP properties if and only if the SSV of the LLFT with respect to $\mathbf{\Delta}$ is less than 1. Therefore, the minimization problem can be written as:

**Problem 2.** *The classical $\mu$-synthesis optimization problem is defined by the minimization over the stabilizing controllers $K$:*

$$\inf_{K \ stab.} \sup_{\omega \in \mathbb{R}_+} \mu_{\mathbf{\Delta}}(LLFT(P, K)(j\omega)). \tag{3.40}$$

Unfortunately, Problem 2 is not convex. Additionally, the structured singular values are difficult to be explicitly computed. In order to solve this problem, the following upper bound is used [PDB93]:

$$\mu_{\mathbf{\Delta}}(\mathrm{LLFT}(P, K)(j\omega)) \leq \inf_{D \in \boldsymbol{D}} \overline{\sigma}(D \cdot \mathrm{LLFT}(P, K)(j\omega) \cdot D^{-1}), \tag{3.41}$$

where the set $\boldsymbol{D}$ is defined in relation to the uncertainty set $\mathbf{\Delta}$ as:

$$\begin{aligned} \boldsymbol{D} = \Big\{ & \mathrm{diag}\left(D_1, \ldots, D_s, d_1 I_{m_1}, \ldots, d_f I_{m_f}\right) \Big| \\ & D_k = D_k^\top \in \mathbb{R}^{n_k \times n_k},\ d_j > 0,\ k = \overline{1, s},\ j = \overline{1, f} \Big\}. \end{aligned} \tag{3.42}$$

Now, with this bound, the solution of the initial non-convex problem can be practically approximated by solving the quasi-convex problem:

$$\inf_{K \text{ stab.}} \sup_{\omega \in \mathbb{R}_+} \inf_{D \in \boldsymbol{D}} \overline{\sigma}\left(D(j\omega) \cdot \mathrm{LLFT}(P, K)(j\omega) \cdot (D(j\omega))^{-1}\right). \tag{3.43}$$

Finally, if the system $D$ is fixed, the problem (3.43) becomes a

$\mathcal{H}_\infty$ control problem, in this case called the $K$ step. Furthermore, for a fixed controller $K$, the $D$ scale step can be obtained by solving a Parrot problem for a desired set of frequencies $\Omega = \{\omega_1, \ldots, \omega_N\}$ using a LMI and then by fitting a minimum phase system after performing an identification step. Gathering pairs of such steps, an iterative algorithm, based on alternative $D$-$K$ iterations, manages to solve the $\mu$-synthesis problem in many practical contexts. This procedure starts with $D = I$ and successively applies a $K$ step and a $D$ scaling step until a stopping criterion is reached.

The regulator $K$ can be synthesized in either an unstructured state-space form, as in [ZDG96], or using a fixed-structure form, through the nonsmooth optimization approach of [AN17].

## 3.3 Performance metrics. Testing and validation

To measure the quality of a control system, general means to quantify performance metrics must be defined and they should be correlated to the steady-state and transient response performances one expects from assessing a control system.

Traditional indicators of system performance can be classified into:

(i) *stability margins*: phase margin $\gamma_k$, corresponding to the gain crossover frequency $\omega_{cg}$, gain margin $m_k$, corresponding to the $-180^\circ$ phase crossing frequency $\omega_{cp}$, generalized disk margins.

(ii) *transient response* performances: rise time $t_r$, settling time $t_s$, overshoot $\sigma$, directly correlated to the maximum peak $M_p$, oscillation frequency $\omega_{osc}$, bandwidth $\omega_B$, high frequency roll-off slope etc.;

(iii) *steady-state response* performances, where the relevant indices are the final value of the system output signal and steady-state errors with respect to step, ramp or sine wave references, if stable.

The transition from specific performance indices, such as the damping ratio in second-order systems, to more general ones suitable for higher-order or MIMO systems, can be achieved by identifying common underlying principles. For example, the phase margin, which is related to the damping ratio in second-order systems, can be enforced through loop shaping by constraining the maximum sensitivity function magnitude. By identifying and utilizing such general principles, it is possible to develop performance indices that are applicable to a wider range of systems

and control problems. The performance input/output vectors $w$ and $z$ allow for a more generalized approach to evaluating the performance of control systems beyond the physical input/output interface described by vectors $u$ and $y$. By considering the effects of stability margins, transient response, and steady-state response on the overall system performance, the performance indices (i)–(iii) can be quantified and integrated into a unified cost function. The $\mathcal{H}_\infty$ norm of the closed-loop system based on the augmented plant models from (3.26)–(3.33) can then be used to minimize this cost function and optimize the control system performance. The traditional performance are well-defined for a nominal plant model. However, to ensure robust stability and performance, it is essential to extend these concepts to the entire uncertainty set of the plant model, as described in Section 3.2.5.

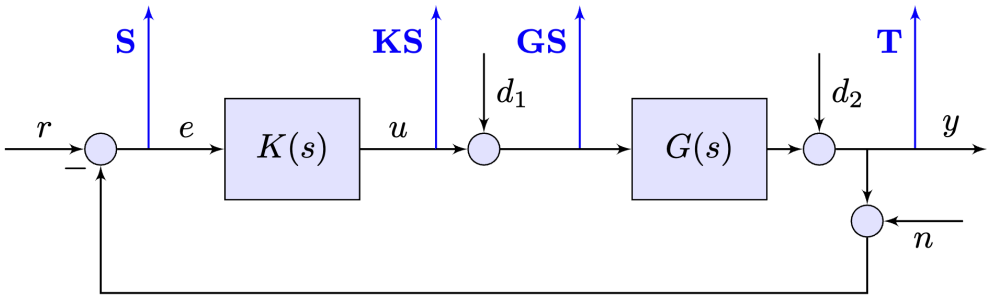


Figure 3.8: Conventional negative feedback control system with emphasized closed-loop sensitivity functions: $S$, $T$, $K \cdot S$, $G \cdot S$.

One approach to encompass such traditional performance metrics into a more general formulation is through the so-called closed-loop shaping method [ZDG96]. The relevant performance outputs are marked in Figure 3.8, showing the classical signals involved in a conventional 1DOF control diagram. An alternative would be to consider open-loop shaping presented in [MG92]. The open-loop shaping approach is an alternative to the closed-loop shaping approach, which uses sensitivity functions and complementary sensitivity functions to shape the loop transfer function. The open-loop shaping approach, on the other hand, uses an augmented plant model to shape the open-loop transfer function directly. Both approaches have their own advantages and limitations, and the choice between them often depends on the specific design requirements and constraints.

The closed-loop sensitivity functions from inputs $(r, d_1, d_2, n)^\top$ to

outputs $(e, u, y)^\top$ can be derived as:

$$\begin{pmatrix} e \\ u \\ y \end{pmatrix} = \begin{pmatrix} \frac{1}{1+GK} & -\frac{G}{1+GK} & -\frac{1}{1+GK} & -\frac{1}{1+GK} \\ \frac{K}{1+KG} & -\frac{KG}{1+KG} & -\frac{K}{1+KG} & -\frac{K}{1+KG} \\ \frac{GK}{1+GK} & \frac{G}{1+GK} & \frac{1}{1+GK} & -\frac{GK}{1+GK} \end{pmatrix} \cdot \begin{pmatrix} r \\ d_1 \\ d_2 \\ n \end{pmatrix}, \tag{3.44}$$

and, by weighting the frequency responses from each input to each output, one can impose a single design problem to encompass the desired response, depending on the application [SP05], with the advantage that, although the functions are contradictory, the ranges of frequencies where one must have a high gain usually is compensated by the necessity for low gains on the complementary term.

One such example to extend the $\mu$-synthesis problem (3.43) to account for standard sensitivity functions can be formulated as:

$$\inf_{K \text{ stab.}} \sup_{\omega \in \mathbb{R}_+} \inf_{D \in \boldsymbol{D}} \overline{\sigma} \left( D(j\omega) \cdot \text{LLFT}(P, K)(j\omega) \cdot (D(j\omega))^{-1} \right), \tag{3.45a}$$

$$\text{s.t.} \left\| \begin{pmatrix} W_S S & W_T T & W_{KS} K S \end{pmatrix}^\top \right\|_\infty < 1, \tag{3.45b}$$

also known in the literature as the mixed-sensitivity closed-loop shaping $\mu$-synthesis method, which uses frequency response weigthing functions $W$ to penalize or enhance certain frequencies in the closed-loop system, as desired according to the design specifications. Using [SP05] as a starting point, different frequency response specifications, directly correlated to desired time-response performances, can be imposed in the weighting functions. The sensitivity weighting function $W_S$ can be written as:

$$W_S(s) = \left( \frac{\frac{1}{M^{1/n}} s + \omega_B}{s + \omega_B A^{1/n}} \right)^n, \tag{3.46}$$

where $\omega_B$ represents the imposed bandwidth of the system, $M$ imposes the $\mathcal{H}_\infty$ norm of the sensitivity function, in order to limit the overshoot of the system, $n$ imposes the slope of the sensitivity function for low frequencies, and $A$ imposes the maximum allowed steady-state error.

On the other hand, the complementary sensitivity weighting function $W_T$ can be generally defined by the following structure, in a sym-

metrical manner compared to $W_S$:

$$W_T(s) = \left( \frac{s + \omega_{BT}}{A_T^{1/n} s + \omega_{BT} M_T^{1/n}} \right)^n, \tag{3.47}$$

with $\omega_{BT}$ being the imposed bandwidth of the system, $M_T$ imposes the $\mathcal{H}_\infty$ norm of $T(s)$, $n$ imposes the roll-off slope of the closed loop system, which should be directly coupled with sensor noise characteristics, and $A_T$ imposes the least required attenuation for high frequencies. In practice, the complementary sensitivity bandwidth $\omega_{BT}$ can be adapted to the characteristics of the sensor in order to account for high-frequency noise.

Furthermore, the control effort weighting function with specifications $M_0 = |W_{KS}(0)|$, $M_\infty = |W_{KS}(\infty)|$ and $|W_{KS}(j \cdot \omega_d)| = M_d$, $M_0 < M_d < M_\infty$, and order $n$ of its representation, which contributes to the steepness of the transitioning slope, can be synthesized by the following formula:

$$W_{KS}(s) = \frac{M_\infty s^n + M_0 \omega_d^n \sqrt{\frac{M_\infty^2 - M_d^2}{M_d^2 - M_0^2}}}{s^n + \omega_d^n \sqrt{\frac{M_\infty^2 - M_d^2}{M_d^2 - M_0^2}}}. \tag{3.48}$$

For the weighting function expressions (3.46), (3.47), (3.48), the order $n$ depends on the desired performance specifications and the complexity of the control problem. In practice, the order of the transfer function is often selected based on a trade-off between performance and complexity, as higher order transfer functions can be more difficult to implement, due to directly leading to a correspondingly-higher order regulator, and may also result in unwanted behavior.

Although the closed-loop shaping method provides a general-purpose approach to design regulators for MIMO LTI processes, like any control method, it has its limitations inherent to the dynamics of the process, as it is affected by: right half-plane (RHP) zeros, which can create instability in the closed-loop system and lead to a non-minimum phase behavior, dead times which reduce the effective phase margin of the system, making it more difficult to stabilize, limitations imposed by the Bode sensitivity integrals (the phenomenon also known as the waterbed effect), process nonlinearities and uncertainties, as discussed throughout the chapter.

With such difficulties and limitations, it is difficult to firmly guarantee that the performances resulting after the design phase can be ful-

filled in practice on the entire family of processes which can be encountered. As such, an automated software toolbox can be utilized to perform the aforementioned control design steps, simulate multiple closed-loop instances, and subsequently, generate a report by comparing the obtained controller's performance against the provided specifications. Simulation allows for testing the controller under different scenarios and disturbances to ensure that the controller meets the desired performance specifications. When validating the synthesized controller by simulation, there are several steps that can be followed, which are improved upon in the book through certain contributed innovations:

1. develop a simulation model of the closed-loop system that includes the controller and the plant model, in continuous or discrete-time formulations, with contributions brought in Chapters 5, 6, 7, 9;

2. choose appropriate initial conditions and disturbances to simulate the closed-loop system response;

3. run the simulation and record the closed-loop system response; of great use are the Model-in-the-Loop and Software-in-the-Loop simulation paradigms, with contributions to electrical machine and computer numerical control path-planning presented in [Șuș+18; ȘȘD18];

4. analyze the closed-loop system response to ensure that the performance specifications are met; this can include analyzing the stability, steady-state error, rise time, settling time, and overshoot, with theoretical contributions in Chapters 5, 8 and 9;

5. adjust the controller parameters if necessary and repeat the simulation until the performance specifications are met; this step can be performed in an automated manner in an optimization context with several approaches developed in the book;

6. verify the performance of the controller under different scenarios and disturbances to ensure that it is robust and meets the desired performance specifications, with several use cases studied in Chapter 11.

By following these steps in an organized manner, simulation can be a powerful tool to validate the synthesized controller before implementing it on the real system.

# 4. Controller implementation

## 4.1 Sampling and discretization

### 4.1.1 Literature review

In the current literature, sampling rate selection targeted for control engineering contexts is relatively sparse. The choice of sampling period usually depends on the purpose and particular structure of the control system. To illustrate this point, in [DR00], the overshoot and the rise time are used to choose the sampling period of a $P$ regulator. An approach to impose the Harris closed-loop performance index by accounting for the sampling rate is presented in [HI01]. An optimization criterion for finding the optimal or sub-optimal sampling period used for a proportional-integral-derivative (PID) controller is presented in [TG07]. A metaheuristic procedure for selecting the sampling period for parameter estimation of an induction machine is presented in [Ben+20]. The proposed model is used for the nonlinear model and reduces the necessary amount of data for the estimation step. In [JU21] it is demonstrated that the stability and the performance of the closed-loop system depend on the sampling period choice in the particular case of pressure control. Further extensions on the study of stability for systems governed by nonlinearities and delays using sampled-data control have been considered particularly for stochastic functional differential equation models, as in the paper [YY17], along with stochastic nonlinear delay systems affected by exogenous disturbances using a proposed event-based triggering method as in the work [Zhu19]. Such methods are based on the Lyapunov-Krasovskii framework to ensure the dissipative property of the closed-loop systems. Sampling rate selection in network control systems has been studied in [TC17] while a study for systems with piecewise affine components is presented in [Wan+19]. A study on the influence of the sampling rate which also emphasizes the disadvantages of increasing the

sampling frequency is found in [Gu+19]. In the context of robust control systems, paper [PZ15] presents an event-triggered $\mathcal{H}_\infty$-based approach, while [ER20] shows an event-based sampling strategy for PID regulators. The sampling rate yields thorough limitations in $\mu$-synthesis, as justified in [Bal+22]. Besides the shift operator approach to numeric systems, the difference operator approach has also been considered throughout the years, with improved quantization sensitivity, as demonstrated for $\mathcal{H}_\infty$ synthesis in [Col99], for high-precision switching converters in [Che+18], and ladder filter topologies [KRM22].

Additionally, in the context of waveform generators with variable clock, with the broad available sampling rate range, several approaches have been proposed to select an adequate sampling rate in order to guarantee anti-aliasing along with a low computation cost: paper [Xia+22] accounts to floating-point errors also, while the approach in [Xia+19] restricted the searching domain to safe regions exclusively. Such approaches could also be adapted for linear parameter-varying systems (LPV) and linear time-variant systems (LTV) to offer online sampling time computations for the proposed regulators.

### 4.1.2 Theoretical background

**Remark 1.** *Denote by $\mathcal{C}(z, r)$ the circle having the center in $z \in \mathbb{C}$ and radius $r > 0$. Additionally, $\mathcal{P}(G)$ and $\mathcal{Z}(G)$ denote the pole and zero sets of an LTI system $G$, respectively. An arbitrary sampling period will be denoted $T_s \equiv T \equiv \tau > 0$ in the book, unless stated otherwise.*

The classical Shannon theorem shows that in order to sample a band-limited signal with no information loss, it is necessary to sample it with a frequency greater than double the original signal's maximum frequency:

$$f_s > 2 \cdot f_{max} \quad \Leftrightarrow \quad T_s < \frac{T_{min}}{2}, \tag{4.1}$$

having the convention for $1/f_{max} = T_{min}$.

**Definition 5.** *The Nyquist frequency $\omega_N$ is defined based on the sampling frequency $f_s$ at:*

$$\omega_N = \frac{\omega_s}{2} = \pi \cdot f_s, \tag{4.2}$$

*whereupon $\forall\ \omega \geq \omega_N$, the aliasing phenomenon occurs.*

The Nyquist-Shannon theorem thus establishes a connection between a continuous and an equivalent discrete LTI system, stating that if the sample rate is sufficiently high, than the discrete representation will maintain all relevant system dynamics, which are fundamentally determined by its poles. As such, the sampling time should be at least two times less than the minimum system time constant. However, for practical considerations, due to the signal spectrum not being bounded by a well-established maximum frequency $f_{max}$, and the additional input lowpass filter employed in the sampled-data system, it becomes highly recommended not to work near the Nyquist frequency bound $\omega_N$, but to use a sampling period at least five-ten times less than the time constant.

The analytical relationship between the $s$-plane, specific to the Laplace transform of a continuous-time signal $x(t) \in \mathcal{L}_2$, and the $z$-plane, specific to the $\mathcal{Z}$ transform of a discrete-time signal $x[n] \in \ell_2$, is illustrated by the relation:

$$z = e^{s \cdot T_s}. \tag{4.3}$$

Denote $s = \sigma + j\omega$, with $\sigma, \omega \in \mathbb{R}$. Then, $z = e^{(\sigma + j\omega)T_s}$, with $|z| = e^{\sigma T_s}$ and $\angle z = \omega T_s$. It is assumed that the left half of the $s$-plane can be divided into an infinite number of strips, due to the periodicity at multiples of $\omega_N$ of trigonometric functions involved. The primary strip is described by $\angle z = \omega T_s \in [-\pi, \pi]$, symmetrically delimited by the Nyquist frequency $\pm\omega_N = \pm\frac{\pi}{T_s}$. The $s$-plane to $z$-plane mapping causes the topologies:

- the imaginary axis in $s$ is mapped to the $z$-plane unit circle $\mathcal{C}(0, 1)$;
- the $s$-plane edge of the primary strip is mapped to the negative axis inside the unit circle;
- the $s$-plane negative real axis is mapped to the positive axis inside the unit circle, i.e. $z \in (0, 1]$.
- the interior of the $s$-plane primary strip is mapped into the unit disk, denoting the discrete stability region.

A summary of the previous mappings can be seen in Figure 4.1.

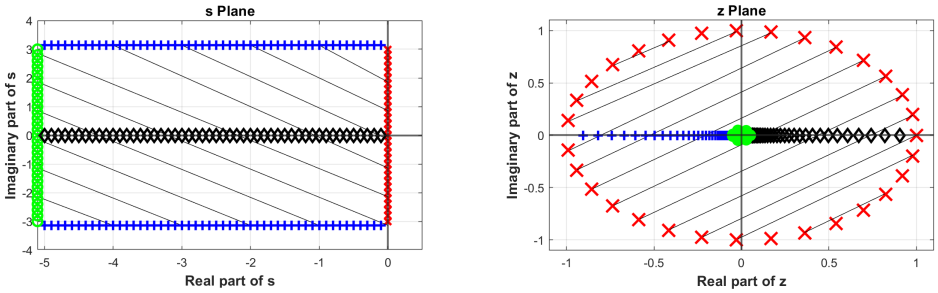


(a) $s$ plane (b) $z$ plane

Figure 4.1: Biunivocal correspondence between the unaliased $s$ plane and corresponding $z$ plane region through the mapping $z = e^{s \cdot T_s}$.

## 4.2 Quantization effects

### 4.2.1 Literature review

The implementation of a discrete-time regulator on a numeric device without compromising the control performance specifications is as important as the actual controller synthesis step. The first step comprises of selecting an adequate sampling period $T_s \in (0, \infty)$, followed by the selection of interfacing circuits with sufficiently-high quantizer precision to implement the control law with an acceptable performance degradation. Numeric implementation of regulator models involves several key steps which require an analysis regarding sampling, discretization, quantization of system coefficients and quantization of involved signals. The previously-mentioned phenomena can affect both the transient and steady-state responses of the desired continuous-time regulator dynamics.

The degradation of passivity indices during sampling and input-output controller quantization is analyzed in [XOG20], to ensure bounds for the closed-loop system. A different approach, proposed in [Xia+20], consists in defining the $R$-index which allows to impose passivity requirements using the robust control framework, and offers a possibility for the analysis and design of stable closed-loop systems driven by logarithmic quantizers. In [LL09] a hybrid system approach to the quantization effect and conditions for stabilizing such systems are presented. A stochastic approach for analysing closed-loop quantized systems in presented in [WK08], and stochastic stabilization treated in [Yuk10; Kos+21]. A solution for the feedback stabilization problem for LTI systems with quantized feedback measurements using a quantizer with dynamic sensitivity

is described in [BL00]. A quantized $\mathcal{H}_\infty$ controller design procedure for Itô stochastic systems is proposed in [Hu+17]. A set of stabilizing bit rate conditions for continuous-time scalar linear systems is presented in [Lin17]. In the thesis [Fer15], several results have been presented to provide stability conditions and to design observers in the context of sporadic measurements affected by quantization effects. An operator-based approach for discrete-time controller synthesis is described in [CF11].

The effects of a fixed sampling rate selection on the transient response has been studied in a unified manner for single- and multi-loop linear control systems in [ȘMD23c], while a time-variable sampling strategy for networked PID-based control systems is studied in [ER20]. The effects of discretization method selection on the transient performance of resonant controllers are described in paper [Yep+10], while in the context of robust control systems, a joint optimization problem for the regulator sampling rate and coefficients quantization step in order to maintain robust stability and performance is proposed in [ȘMD23a].

There are several types of quantizer circuits, such as fixed-point, floating-point, logarithmic, or delta-sigma, to name a few. Fixed-point quantization is widely used as it is fast, can be implemented with low energy consumption, or it can be harvested to increase the parallel processing capabilities of high-performance graphics processing units. Apart from the field of embedded systems, a newly-established use-case for fixed-point quantization, static or with dynamic scaling, is in deep neural network training and deployment. Using the framework proposed in [Wan+21], the main advantage is that the desired network performance is maintained with minimal degradation, without supervised retraining on the labeled data. The fundamental difference encountered in control is given by the feedback connection which, due to quantized subsystems, leads to highly-nonlinear behaviour, such as limit cycles [FX05].

Quantization effects are studied in digital signal processing and control applications such as in the monograph [WK08], providing a probabilistic approach, and for embedded robust control system design in [PSK18], where the authors present the phenomena which occur in practice, but exemplified through ad hoc studies for individual use cases. Steady-state deviations with tight bounds in the context of DC-to-DC converters are modelled in [Pen+07], followed by means to combat limit cycles in the particular case of boost converters in [AMC23], and an analytical bound provided for closed-loop linear control systems in [ȘMD22].

Recent applications involving quantization analysis can be found

for the practical implementation of control barrier functions in [MLY22] or robust model predictive control to maintain system stability during fixed-point encoding in [DRQ18]. By modelling output quantization and saturation, the paper [Zha+22] uses model reference control to provide convergence guarantees on the output tracking error without relying on polynomial coprimeness or initial condition assumptions. Similarly, using finite-and-quantized output feedback, the authors of [XZZ22] provide a pole-placement-based control law which guarantees that the tracking error converges to an arbitrarily-small residual set. The distributed consensus problem involving both uniform and logarithmic quantizers has been solved in a unified manner for the control of networked general linear systems in [Xu+22].

### 4.2.2 Theoretical background

Assume a numeric regulator $K(z)$ as in Equation (3.7). At the design and simulation stage, the controller $K(z)$ usually uses the IEEE-754 arithmetic, considered as the practically-ideal baseline for the expected performance of the closed-loop system. The majority of microcontroller systems do not have hardware support for floating-point operations and, in such cases, they either use software-based floating-point operations, which may take too long to be feasible, or use a fixed-point approximation for the coefficients and computed variables. Additionally, the ADC and DAC interface circuits have limited resolutions, as they become unjustifiably expensive for increased precision. The previous constraints are modelled by quantizer functions, with the two common quantizer types found in practice illustrated through Figures 4.2 and 4.3, defined as:

- rounding, formally known as the midtread quantizer:

$$Q_\delta^{mt}(x) = \delta \cdot \left\lfloor \frac{x}{\delta} + \frac{1}{2} \right\rfloor, \ \delta > 0, \ x \in \mathbb{R}; \tag{4.4}$$

- truncation, formally known as the midriser quantizer:

$$Q_\delta^{mr}(x) = \delta \cdot \left( \left\lfloor \frac{x}{\delta} \right\rfloor + \frac{1}{2} \right), \ \delta > 0, \ x \in \mathbb{R}. \tag{4.5}$$

Based on these two standard quantizer functions, several variations can be defined by adding noise, saturation, drifting coefficients causing non-

unit slopes, as in [WK08]. To link the mathematical formalism used for the analysis with practical hardware specifications, some auxiliary mathematical entities will be defined.

**Definition 6.** *A quantizer structure $\mathcal{S}$ is a triplet:*

$$\mathcal{S} = (\mathcal{D}, L, T)\,, \tag{4.6}$$

*where the quantizer assumes a fixed-point two's complement encoding, uniform quantizer of word length $L \in \mathbb{N}_+$ bits, type $T \in \{$`midriser`, `midtread`$\}$, and a domain described by the set $\mathcal{D} = [-R, R]^n$, $R > 0$.*

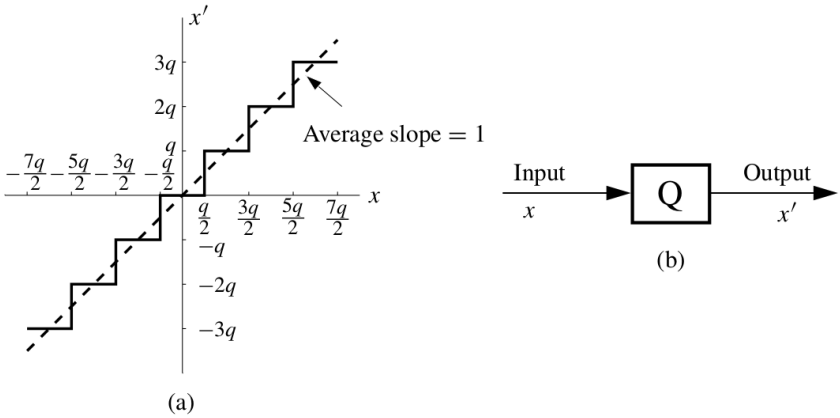


Figure 4.2: Midtread (rounding) quantizer [WK08] (a) input-output characteristic; (b) default block model.

**Definition 7.** *The resolution $q$ of the unequivocal map $Q_q^T(x) : \mathcal{S} \mapsto Q(x)$ which describes a quantizer function like (4.4) or (4.5) with signal saturation applied for absolute values above $R$ is given by:*

$$q = \frac{R - (-R)}{2^L} = \frac{R}{2^{L-1}}. \tag{4.7}$$

The computations executed throughout the microcontroller software are made with the equivalent two's complement encodings and, as such, the numbers in $\mathcal{D}$ representing the input to a set of $n_u$ ADC circuits will be mapped to a surjective fixed-point domain $\mathcal{D}^{\mathcal{F}}$:

$$\mathcal{D}^{\mathcal{F}}(L) = \left\{-2^{L-1}, -2^{L-1}+1, \ldots, 2^{L-1}-2, 2^{L-1}-1\right\}^n, \tag{4.8}$$

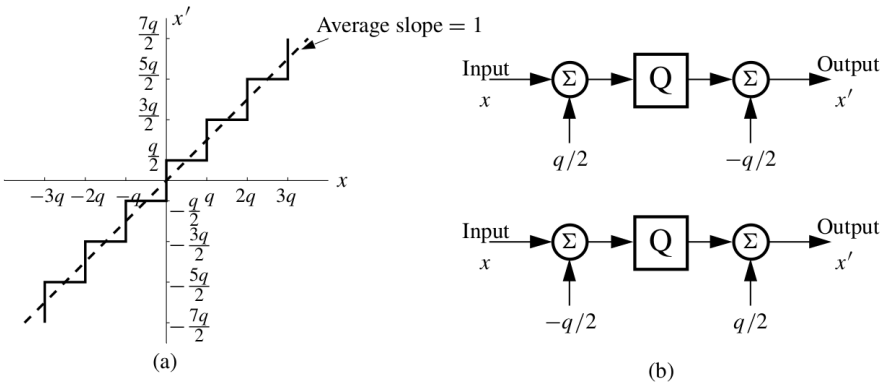


Figure 4.3: Midriser (truncation) quantizer [WK08] (a) input-output characteristic; (b) block model based on a midtread circuit.

followed by a reverse injective mapping when switching back from the internal computations to the set of $n_y$ DAC blocks.

## 4.3 LTI system execution time analysis

### 4.3.1 Literature review

After the first step of deciding on a sampling period value, an analysis regarding the practical implementation of the proposed control structure on a microprocessor-based system should be performed. This analysis needs to encompass several aspects which are not explicitly modelled in the control law, such as the register word lengths of the coefficients which directly influence the number of necessary assembly instructions, and saturation, overflow, underflow verifications on the computed command signals. In the specific context of rapid control prototyping (RCP), one key step before the proper code generation is to certify if its execution abides by the time span given by the sampling period. Moreover, other important verifications for phenomena like underflow and overflow, or saturation and anti-windup techniques should be also performed before the code generation step. As such, one important goal consists in approximating the number of software operations necessary to implement the designed control law, mandatory in the context of hard real-time systems. A survey of worst-case execution time computa-

tional methods is presented in the seminal paper [Wil+08]. A simplified study applied for control system-related interrupt service routines for state-space controller representations is presented in [Șuș+22c]. Another option for computational error analysis is presented in [Ngh+12].

Mathematical models for such studies assume the definition and behaviour general-purpose machines. A useful such model is the Random Access Machine (RAM) defined in [Cor+09], which have practical counterparts, materialized through reduced instruction set computer (RISC) machines. Reconfigurable RISC-machines specialized on certain problems have been proposed in [SVK16]. Additionally, there is the approach of multiply and accumulate (MAC) instructions supported in digital signal processors (DSP) [Sal+12]. Depending on the supported computer architectures of the RCP framework, relevant are also Single Instruction stream/Multiple instruction Pipelining (SIMP) [Mur+89] constructions with respect to single-processor architectures, or Single Instruction/Multiple Data (SIMD) features, which allow the practical parallelization of addition and multiplication operations for several sets of operands. For faster memory load and store instructions, due to bypassing the main signal bus of the microprocessor, Direct Memory Access (DMA) modules are desirable.

Of interest for control systems are the expressions of regulator dynamical systems, which are usually implemented as state-space representations or infinite and finite impulse response filters. A particular case of FIR topology is also the static feedback control law.

Infinite impulse response (IIR) filters are usually split into series connection of second-order subsystems, known as biquads. There are multiple approaches of implementing digital biquadratic filters, a good example being the description from the monograph [PM22]. The four usual topologies principally implement the same input-output transfer function, but with important differences regarding numeric stability when selecting fixed-point or floating-point implementations, are referred to as the canonical forms: direct form I (DFI), direct form II (DFII), transposed form I (TDFI), transposed form II (TDFII), which differ by the numeric properties of their implementations and by the number of necessary delay elements. Such implementation details are relevant when studying particularized structures, such as in the situations treated in [Ess20] and [Mar18].

Similarly, for finite impulse response (FIR) filters, four typical canonical forms are distinguished, namely the direct form (DF), direct

form transposed (DFT), symmetric and anti-symmetric [PM22], respectively. The main difference between DF and DFT is that for the former, the delay word lengths are that of the input signals $u[k-i]$, while for the latter, the delays have the word length of the accumulator variable. The Symmetric and Anti-symmetric cases make use of the linear phase of the filter through the regularity of the first $\lfloor \frac{N}{2} \rfloor$ coefficients as the symmetrical or anti-symmetrical equivalents of the latter half of the coefficients.

### 4.3.2 Theoretical background

To analyze the execution time of a numeric algorithm, the standard growth functions and their notations according to the monograph [Cor+09] are defined as:

$$\mathcal{O}(g(n)) = \{f(n) \mid \exists\, c, n_0 > 0 \text{ s.t. } 0 \leq f(n) \leq cg(n),\ \forall\, n \geq n_0\}\,; \tag{4.9}$$

$$\Omega(g(n)) = \{f(n) \mid \exists\, c, n_0 > 0 \text{ s.t. } 0 \leq cg(n) \leq f(n),\ \forall\, n \geq n_0\}\,; \tag{4.10}$$

$$\Theta(g(n)) = \{f(n) \mid \exists\, c_1, c_2, n_0 > 0 \text{ s.t. } 0 \leq c_1 g(n) \leq f(n) \leq c_2 g(n),\ \forall n \geq n_0\}\,. \tag{4.11}$$

Chapter 10 of the book will focus on execution time analysis aspects on the implementations of LTI-based control laws, which can be described by state-space realizations, IIR or FIR filters.

Discrete-time state-space realizations are described by the equivalent of Equation (2.4), namely systems of difference equations, with a corresponding output equation, as described in (3.7).

The difference equation of an IIR filter can be written in the form:

$$y[k] = -\sum_{i=0}^{n-1} a_i \cdot y[k-i] + \sum_{j=0}^{m-1} b_j \cdot u[k-n_d-j], \tag{4.12}$$

with $n_d \geq 0$ input delay ticks, common in control contexts. By applying the $\mathcal{Z}$ transform to the previous difference equation, an equivalent discrete-time transfer function can be obtained:

$$K_{IIR}(z) = \frac{U(z)}{E(z)} = z^{-n_d} \cdot \frac{b_0 + b_1 z^{-1} + \cdots + b_m z^{-m}}{1 + a_1 z^{-1} + a_2 z^{-2} + \cdots + a_n z^{-n}}. \tag{4.13}$$

For an arbitrary discrete-time IIR transfer function as written above,

with assumed order $n \in \mathbb{N}$, define $\mathcal{N}(K_{\text{IIR}})$ as the pair:

$$\mathcal{N}(K_{\text{IIR}}) = (n_2, n_1) = \begin{cases} \left(\left\lfloor \frac{n}{2} \right\rfloor, 1\right), & \text{if } n \text{ is odd;} \\ \left(\frac{n}{2}, \quad 0\right), & \text{if } n \text{ is even.} \end{cases} \tag{4.14}$$

Using this notation, the transfer function $K_{\text{IIR}}$ can be rewritten as:

$$\begin{aligned} K_{\text{IIR}}(z) &= \left(\frac{b_{0,1}z + b_{0,0}}{z + a_{0,0}}\right)^{n_1} \cdot \prod_{i=1}^{n_2} \left(\frac{b_{i,2}z^2 + b_{i,1}z + b_{i,0}}{z^2 + a_{i,1}z + a_{i,0}}\right) \\ &= ((K_1(z))^{n_1} \cdot \prod_{i=1}^{n_2} K_{2,i}(z), \end{aligned} \tag{4.15}$$

with the terms from each triplet $(b_{i,2}, b_{i,1}, b_{i,0})$ not all zero. $K_1$ is known as a *first-order section*, and each $K_{2,i}$, with $i = \overline{1, n_2}$ denoted in the literature as a *second-order section* (SOS).

Table 4.1 gathers all four canonical forms mentioned in Section 4.3.1. All difference equations implement the same input-output second-order transfer function, but differ by the definitions and interpretations of the state signals.

Table 4.1: Digital IIR biquadratic topologies.

| *IIR SOS topology* | *Difference equation* |
|---|---|
| Direct Form I (DFI) | $y[k] = g \cdot \left(\sum_0^2 b_i u[k-i] - \sum_1^2 a_i y[k-i]\right).$ |
| Direct Form II (DFII) | $\begin{cases} y[k] = g \cdot \sum_0^2 (b_i \cdot x[k-i]); \\ x[k] = u[k] - \sum_1^2 (a_i \cdot x[k-i]). \end{cases}$ |
| Transposed Direct Form I (TDFI) | $\begin{cases} y[k] = g \cdot \sum_0^2 (b_i \cdot x)[k-i]; \\ x[k] = u[k] - \sum_1^2 (a_i \cdot x)[k-i]. \end{cases}$ |
| Transposed Direct Form II (TDFII) | $\begin{cases} y[k] = g \cdot (b_0 u[k] + x_1[k-1]); \\ x_1[k] = b_1 u[k] - a_1 y[k] + x_2[k-1]; \\ x_2[k] = b_2 u[k] - a_2 y[k]. \end{cases}$ |

A further particularization on the structure of $K_{\text{IIR}}(z)$ is to consider the the expression of a FIR filter topology, which, by design, discards the previous output delays and can be viewed as a finite-order

approximation of an IIR filter:

$$K_{IIR}(z) = h_{n_d} z^{-n_d} + h_{n_d+1} z^{-n_d-1} + \cdots = h_0 + h_1 z^{-1} + h_2 z^{-2} + \cdots$$
$$= \sum_{k=0}^{\infty} h_k z^{-k} \approx \sum_{k=0}^{N-1} h_k z^{-k}, \tag{4.16}$$

which leads to the difference equation:

$$y[k] = \sum_{i=0}^{\infty} h_i u[k-i] \approx \sum_{i=0}^{N-1} h_i u[k-i]. \tag{4.17}$$

The present command signal $y[k]$ will, as such, depend only on an array of delays, i.e. delay tap of inputs $u[k-i]$, modelled as:

$$K_{FIR}(z) = g \cdot z^{-n_d} \cdot \sum_{i=0}^{m} b_i \cdot z^{-i} \equiv g \cdot \sum_{k=0}^{N-1} h_k \cdot z^{-k}, \ g \neq 0. \tag{4.18}$$

As noticeable from its definition, a FIR filter has poles only in $z = 0$. As such, it is an inherently stable dynamical system, irrespective of its coefficients.

In the case of FIR filters, Table 4.2 provides the four canonical forms mentioned in Section 4.3.1. All difference equations implement the same input-output $N$th order transfer function, but vary through the configuration of the accumulator arithmetic.

Table 4.2: Digital FIR filter topologies.

| *FIR topology* | *Difference equation* |
|---|---|
| Direct Form (DF) | $y[k] = g \cdot \sum_0^{N-1} \left(h[i]u[k-i]\right).$ |
| Direct Form Transposed (DFT) | $y[k] = g \cdot \sum_0^{N-1} \left(h[i] \cdot u\right)[k-i].$ |
| Symmetric | $\begin{cases} y[k] = g \cdot \sum_0^{\lfloor N/2 \rfloor} h[i] \left(u[i]+u[N-1-i]\right); \\ h[i] = h[N-1-i], \ i = \overline{0, \lfloor N/2 \rfloor}. \end{cases}$ |
| Anti-symmetric | $\begin{cases} y[k] = g \cdot \sum_0^{\lfloor N/2 \rfloor} h[i] \left(u[i]-u[N-1-i]\right); \\ h[i] = -h[N-1-i], \ i = \overline{0, \lfloor N/2 \rfloor}. \end{cases}$ |

# PERSONAL CONTRIBUTION

# 5. Modelling and simulation aspects

## 5.1 Motivation and contributions

The motivation for the results briefly presented in this section is fully presented in paper [Șuș+21], which represents the starting point for a computer-aided control system design (CACSD) toolbox, with building blocks formed using the theoretical contributions described in the chapters of this personal contribution part of the book. This section explicitly provides the means to bring all dynamical system models described in Chapter 2 under the same software framework for simulation and analysis, for an integrated development environment, using the object-oriented design paradigm available in current versions of the MATLAB programming language, and using its general-purpose `ode`-framework for integrating systems of differential equations in a unified manner.

## 5.2 Model-in-the-loop simulation of interconnected systems

The scope of software classes implemented and described in this section aims to provide a flexible framework for simulation by using the ordinary-differential equation `ode` solver exclusively, with the low-level requirement of integrating a differential state equation. As such, exogenous signals would be reference signals and disturbances, known a priori in a simulation context. The intrinsic signals, i.e. commands and corresponding measurements, are passed to their corresponding subsystems by means of MATLAB's `ode` framework. Figure 5.1 encompasses an overview of the toolbox classes described in this section. When the relationship between two classes is of type *inheritance*, the inherited class will not redundantly recall all previous properties and methods from the base class in the illustrated diagrams, unless they overload the methods and will be explicitly noted.

Dynamical systems of form (2.1) are implemented in class `System`.

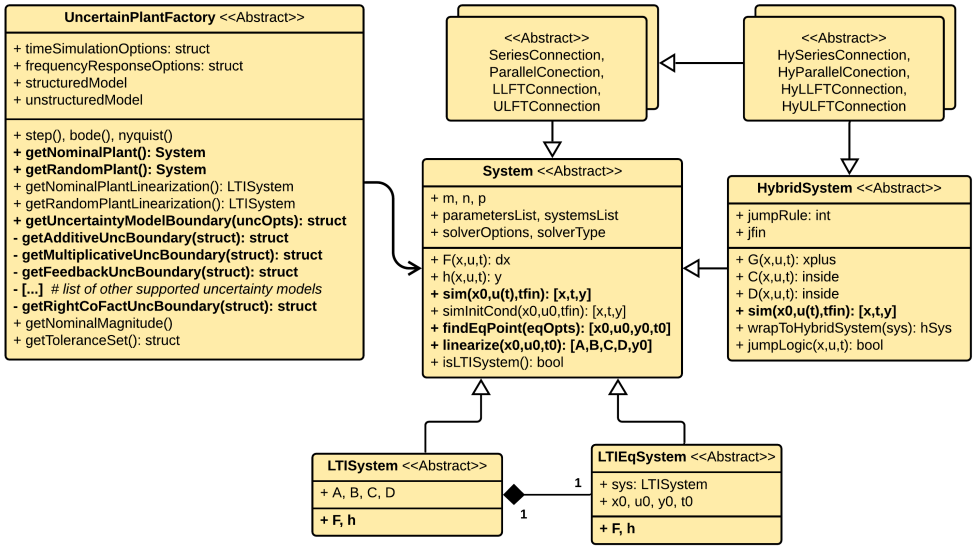


Figure 5.1: Class diagram for general-purpose nonlinear, LTI, linearized, and hybrid system implementations, along with the uncertain plant factory class, interconnections, and main functionalities.

This will be the baseline interface for all systems the toolbox works with. Its most important methods are `sim`, `findEqPoint`, and `linearize`. The method `sim` simulates the dynamical system described by the flow map $F$ from the initial condition $x_0$, using the exogenous signal $u(t)$, which is a predetermined anonymous function with at least the input argument time. $t_{fin}$ can be a scalar time value representing the final simulation time, a simulation interval, or a vector of predetermined time values. The solver options and type are based on MATLAB's `ode` framework options and are sent directly to it. The solver type can be selected from any of the supported functions: `ode113`, `ode15s`, `ode15i`, `ode23`, `ode23t`, `ode23s`, `ode23tb`, `ode45`. After integrating the state equation, the output signal $y(t)$ can be directly computed using the memoryless output function $h(t)$. A useful particularization is also the method `simInitCond`, with the only difference being that it replaces the time-varying input signal $u(t)$ with a constant value $u_0$, thus obtaining an impulse response. The method `findEqPoint` deduces an equilibrium point for the system given a set of specifications on the input, state, or output vectors and is described in detail in Section 5.3. After obtaining a valid equilibrium point, a linearized system can be obtained using the method `linearize`.

Auxiliary structures are also provided, such as for LTI systems, implemented in class `LTISystem`, and LTI systems simulated around a provided equilibrium point $(u_0, x_0, y_0, t_0)$, useful for MiL simulations, implemented through class `LTIEqSystem`, seen as an affine nonlinear system. The advantage of having such a model readily available is that it is interchangeable with the initial nonlinear interface in a closed loop context without making further adaptations in the source code and can be used to study the performance degradation obtained by replacing the controller from the linearized system to the nonlinear plant. An additional provided base class is called `HybridSystem`, inheriting `System`. It includes the `ode` event-based mechanism from the HyEQ Toolbox [SCN13], and is extended to support time-varying differential equation systems and exogenous input signals. Besides the base interface, it also provides methods for the jump function $G$, along with definitions for the continuous and discrete logic domains, $\mathcal{C}$ and $\mathcal{D}$, respectively. It also provides a wrapper function to promote any `System` object to the type `HybridSystem`, by adding placeholder $G$, $\mathcal{C}$, and $\mathcal{D}$ methods, in order to be compatible for use in hybrid system interconnections. The flexibility added by the `HybridSystem` class in the toolbox allows model-in-the-Loop simulations using physical processes with hybrid dynamics, such as switching systems, i.e., electrical machines and power converters, or simulations of the closed loop control system, seen as hybrid system through the interconnection of a continuous-time process and a discrete-time controller, allowing the user to assess several performance analysis steps.

The last class shown in Figure 5.1 is called `UncertainPlantFactory`, which acts as a Factory design pattern to provide means to implement a family of uncertain plant models, with essential functionalities gathered in the `getNominalPlant` and `getRandomPlant` methods. Using a set of specification and corresponding tolerance values, the class allows the generation of both parametric and unstructured uncertainty samples, which can be further bounded in magnitude using an arbitrary model type as supported by the classical structures detailed in Chapter 6. Using the procedure from Section 5.3, starting from nonlinear models, a set of linearized models can be fitted through optimization in order to directly obtain uncertainty models as required for robust synthesis.

The classical generalized nonlinear and hybrid system interconnections presented in Section 2.5 are implemented in classes which inherit the base class `System`. They extend the `series`, `parallel`, `feedback`, and `lft` functions from MATLAB. Figures 5.2 and 5.3 present the resulting

interfaces and their internal behaviour.

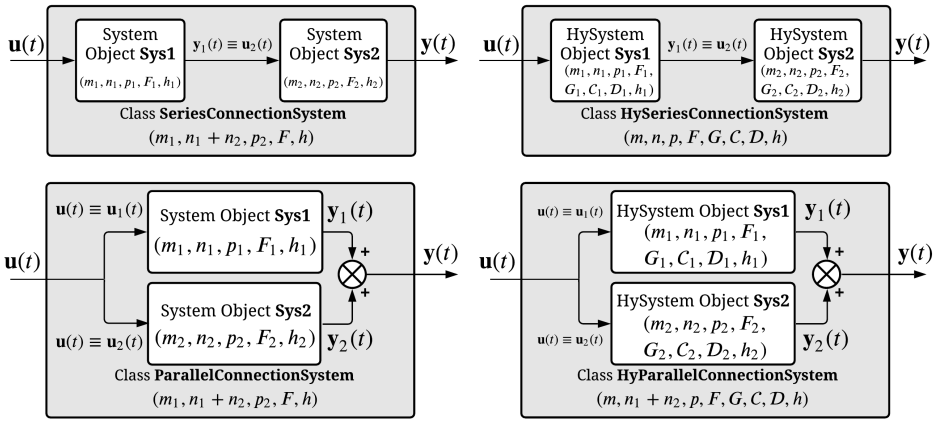


Figure 5.2: Series and parallel connections for general-purpose systems with structure (2.1) and hybrid systems as in (2.7).

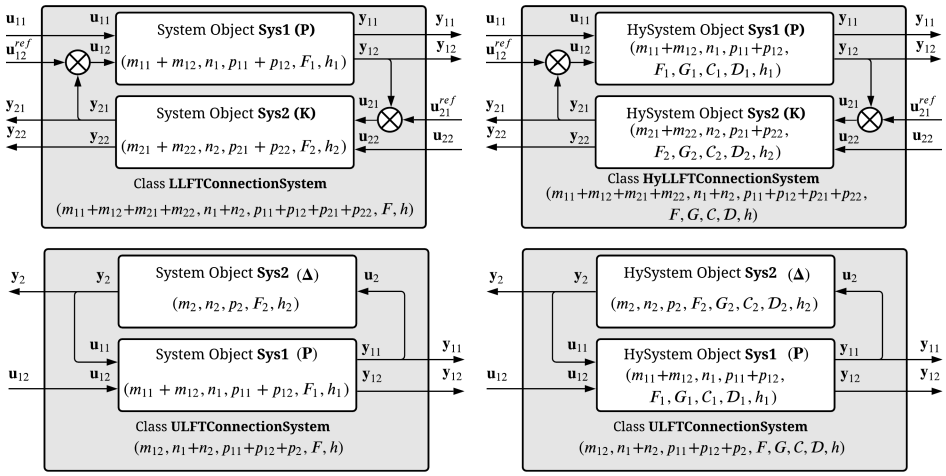


Figure 5.3: Upper (ULFT) and lower (LLFT) linear fractional transformation interconnections for general-purpose nonlinear and hybrid systems, with the ability to impose external reference signals.

## 5.3 System linearization. Equilibrium point computation

The current section presents an approach to compute the equilibrium points for an arbitrary family of nonlinear systems in an automated manner, which will be then used to linearize such systems around said equilibrium points, with direct applicability for uncertainty modelling as a prerequisite for $\mu$-synthesis, initially presented in the journal paper [Șuș+21].

Given a nonlinear system as in (2.1), which may also include interconnections of systems, an operating point is usually desired with some of the input, state, and output variables imposed. As such, a mechanism to automatically compute a partially imposed equilibrium point for an entire family of uncertain plants, relative to one which is considered nominal at the design phase, is proposed in this paragraph.

**Problem 3.** *Starting from the system definition with dimensions $m$, $n$, and $p$, consider the sets of indices, denoted $\mathcal{I}$, and prescribed values, denoted by $\mathcal{V}$, for the input, state, and output variables, respectively:*

$$\mathcal{I}_u = \left\{i_1^u, i_2^u, \ldots, i_{\overline{m}_u}^u\right\},\ \mathcal{V}_u = \left\{\overline{u}\left(i\right) \mid i \in \mathcal{I}_u\right\},\ 0 \leq \overline{m}_u \leq m; \tag{5.1a}$$

$$\mathcal{I}_x = \left\{i_1^x, i_2^x, \ldots, i_{\overline{n}_x}^x\right\},\ \mathcal{V}_x\ = \left\{\overline{x}\left(i\right) \mid i \in \mathcal{I}_x\right\},\ 0 \leq \overline{n}_x \leq n; \tag{5.1b}$$

$$\mathcal{I}_y = \left\{i_1^y, i_2^y, \ldots, i_{\overline{p}_y}^y\right\},\ \mathcal{V}_y = \left\{\overline{y}\left(i\right) \mid i \in \mathcal{I}_y\right\},\ 0 \leq \overline{p}_y \leq p, \tag{5.1c}$$

*along with their complementary sets of values for the indices, denoted by $\overline{\mathcal{I}}$, and the values, denoted $\overline{\mathcal{V}}$, to be computed through optimization by solving a system of equations:*

$$\overline{\mathcal{I}}_u \left\{i_1^u, i_2^u, \ldots, i_{\widetilde{m}_u}^u\right\}, \overline{\mathcal{V}}_u \left\{\widetilde{u}\left(i_1^u\right), \widetilde{u}\left(i_2^u\right), \ldots, \widetilde{u}\left(i_{\widetilde{m}_u}^u\right)\right\},\ 0 \leq \widetilde{m}_u \leq m; \tag{5.2a}$$

$$\overline{\mathcal{I}}_x \left\{i_1^x, i_2^x, \ldots, i_{\widetilde{n}_x}^x\right\},\ \overline{\mathcal{V}}_x \left\{\widetilde{x}\left(i_1^x\right), \widetilde{x}\left(i_2^x\right), \ldots, \widetilde{x}\left(i_{\widetilde{n}_x}^x\right)\right\}, 0 \leq \widetilde{n}_x \leq n; \tag{5.2b}$$

$$\overline{\mathcal{I}}_y \left\{i_1^y, i_2^y, \ldots, i_{\widetilde{p}_y}^y\right\},\ \overline{\mathcal{V}}_y \left\{\widetilde{y}\left(i_1^y\right), \widetilde{y}\left(i_2^y\right), \ldots, \widetilde{y}\left(i_{\widetilde{p}_y}^y\right)\right\}, 0 \leq \widetilde{p}_y \leq p, \tag{5.2c}$$

*with:*

$$\overline{m}_u + \widetilde{m}_u = m, \quad \mathcal{I}_u \cup \overline{\mathcal{I}}_u = \{1, 2, \ldots, m\}, \quad \mathcal{I}_u \cap \overline{\mathcal{I}}_u = \emptyset; \tag{5.3a}$$

$$\overline{n}_x + \widetilde{n}_x = n, \quad \mathcal{I}_x \cup \overline{\mathcal{I}}_x = \{1, 2, \ldots, n\}, \quad \mathcal{I}_x \cap \overline{\mathcal{I}}_x = \emptyset; \tag{5.3b}$$

$$\overline{p}_y + \widetilde{p}_y = p, \quad \mathcal{I}_y \cup \overline{\mathcal{I}}_y = \{1, 2, \ldots, p\}, \quad \mathcal{I}_y \cap \overline{\mathcal{I}}_y = \emptyset. \tag{5.3c}$$

*a set of permutation matrices $P_u \in \mathbb{R}^{m \times m}$, $P_x \in \mathbb{R}^{n \times n}$, $P_y \in \mathbb{R}^{p \times p}$ are*

*obtained after sorting the indices such as the following system of vector-valued equations needs to be solved:*

$$0 = F\left(P_x \cdot \begin{bmatrix}\overline{x}\\ \widetilde{x}\end{bmatrix}, P_u \cdot \begin{bmatrix}\overline{u}\\ \widetilde{u}\end{bmatrix}, \widetilde{t}\right); \tag{5.4a}$$

$$P_y \cdot \begin{bmatrix}\overline{y}\\ \widetilde{y}\end{bmatrix} = h\left(P_x \cdot \begin{bmatrix}\overline{x}\\ \widetilde{x}\end{bmatrix}, P_u \cdot \begin{bmatrix}\overline{u}\\ \widetilde{u}\end{bmatrix}, \widetilde{t}\right). \tag{5.4b}$$

*The system* (5.4) *becomes equivalent to directly solving a system of equations of the form* $0 = \mathcal{F}(z)$ *in the vector-valued unknown:*

$$z = \begin{pmatrix}\widetilde{x}^\top & \widetilde{u}^\top & \widetilde{y}^\top & \widetilde{t}\end{pmatrix}^\top \in \mathbb{R}^{\widetilde{n}_x+\widetilde{m}_u+\widetilde{p}_y+1}. \tag{5.5}$$

**Remark 2.** *If the dynamical system is time-invariant or if the required time value is known a priori, then the time variable can be removed from the solver or it can be imposed to a certain value* $\overline{t}$ *in the same manner as the for the other signals. Moreover, the method is flexible and allows imposing and solving only the subsystem* (5.4a) *if the output variables coincide with the states.*

The unknown variables from Equation (5.5) can be initialized to random values or a rough estimate for the entire family of uncertain plants can be obtained with the simulation to a step response of the nominal plant at the required amplitudes. All systems in the uncertain physical plant set will be found in the same mathematical vicinity. After solving the preferred algebraic system configuration from Equation (5.4), the desired equilibrium point $\left(\overline{u}, \overline{x}, \overline{y}, \overline{t}\right)$ can be reconstructed using the inverse permutation matrices $P_u^{-1}$, $P_x^{-1}$, $P_y^{-1}$ and the notations from Equations (5.1) and (5.2). The method `findEqPoint` from class `System` forms and solves the system (5.4) and computes the desired equilibrium point for its predefined dynamical system based on the specifications from Equations (5.1) and (5.2) given in the software structure `eqOpts`.

After acquiring the desired equilibrium point, the system linearization can be easily deduced through numeric differentiation methods. The most straightforward method is to compute the first-order Jacobian matrices of the functions $F$ and $h$ with respect to the state and input signals

$x$ and $u$, respectively:

$$A = \left.\frac{\partial F}{\partial x}\right|_{(x_0,u_0,t_0)}; \; B = \left.\frac{\partial F}{\partial u}\right|_{(x_0,u_0,t_0)}; \; C = \left.\frac{\partial h}{\partial x}\right|_{(x_0,u_0,t_0)}; \; D = \left.\frac{\partial h}{\partial u}\right|_{(x_0,u_0,t_0)}. \tag{5.6}$$

The method `linearize` computes the matrices from Equation (5.6) with a first-order derivative approximation and also the output equilibrium value $y_0 = h(x_0, u_0, t_0)$:

$$A_{\overline{1,n},i} \approx \frac{F(x_0 + \Delta x_0^i, u_0, t_0) - F(x_0, u_0, t_0)}{\Delta x}; \tag{5.7}$$

$$B_{\overline{1,m},j} \approx \frac{F\left(x_0, u_0 + \Delta u_0^j, t_0\right) - F(x_0, u_0, t_0)}{\Delta u}, \tag{5.8}$$

following that the output matrices $C$ and $D$ to be computed in a similar manner by replacing $F$ with $h$ in the above formulas, with notations:

$$\Delta x_0^i = \begin{bmatrix} 0 & \cdots & 0 & \Delta x & 0 & \cdots & 0 \end{bmatrix}^\top; \tag{5.9}$$

$$\Delta u_0^j = \begin{bmatrix} 0 & \cdots & 0 & \Delta u & 0 & \cdots & 0 \end{bmatrix}^\top, \tag{5.10}$$

for the disturbance vectors corresponding to the state with the index $i \in \overline{1,n}$ or input with index $j \in \overline{1,m}$. The optimal unit perturbations are, according to [GW08], $\Delta x = \varepsilon \times (1 + \|x_0\|_2)$ and $\Delta u = \varepsilon \times (1 + \|u_0\|_2)$, $\varepsilon = 10^{-5}$ using double precision. Obviously, when linearizing the system, the static amplification of the initial nonlinear system is not accounted in the procedure, but will not be relevant in the actual control design process and implementation due to the consideration of only Lipschitz function-based systems and, as such, it will be correctly compensated.

## 5.4 Conclusions

The framework provided in this section will be used as an intermediary step in the development of other results presented throughout the book, along with using various of its features to develop the experiments and case studies provided in Chapter 11.

# 6. Uncertainty modelling aspects

## 6.1 Motivation and contributions

The framework from this chapter is based on the paper [Șuș+23], with extensions proposed in [ȘMD23b], presenting the developed results in increased levels of generality and illustrated on different case studies, emphasizing different phenomena. This section presents an alternative nonconvex approach to fit single-input and single-output transfer function models on magnitude frequency-based response measurements, with additional constraints such as upper boundness, stability, minimum phase and validity with respect to provided data. The proposed solution presents an improvement over the established Log-Chebyshev convex fit which is used as a well-placed starting point and refines the optimization to become less conservative and feasible in cases where (near) singularities are present and limit its sole application. As such, it provides advantages in cases such as in $\mu$-synthesis where the uncertainty model should have a low order to reduce conservativeness of the structured singular value approximation. A continuation of this research direction addressing descriptor SISO systems through convex Chebyshev frequency-domain fitting was recently reported in [Mar+24]. This extends the framework from regular to descriptor state-space systems while retaining a convex formulation; however, descriptor-system uncertainty bounds are not pursued further in the present chapter.

## 6.2 Proposed approach

The main limitation of $\mathcal{H}_\infty$ and $\mu$–synthesis consists in the dimension of the resulting controller, because the optimization problem (3.43) involves solving a set of $\mathcal{H}_\infty$ control problems of increasing order, and each return a controller having the same order as the process. As such, if the uncertainty block $\mathbf{\Delta}$ has a large dimension, the resulting controller

will be of high order and will present implementation difficulties. Consider the lemma from [PDB93] as a main motivation for the next section.

**Lemma 1.** *If* $\Delta = \mathbb{C}^{n\times n}$ *(*$n_s = 0$, $n_f = 1$, $m_1 = n$*), then* $\mu_\Delta(M) = \overline{\sigma}(M)$.

The main focus will now consist in finding a suitable uncertainty weighting function $U_\theta(s)$ for SISO models such that the set $\mathbf{\Delta}$ will contain a single full block (i.e. $n_s$=0 and $n_f$=1). Denote the uncertainty model:

$$U_\theta(s) = k \cdot \frac{b_m s^m + \cdots + b_1 s + b_0}{s^n + a_{n-1}s^{n-1} + \cdots + a_1 s + a_0} = \frac{\beta(s)}{\alpha(s)}, \tag{6.1}$$

having the number of poles $n$ and the number of zeros $m$ as hyperparameters, with the unknowns vector:

$$\theta_n^m \equiv \theta = \begin{pmatrix} k & b_m & \dots & b_0 & a_{n-1} & \dots & a_0 \end{pmatrix}^\top \in \mathbb{R}^{1+m+n}. \tag{6.2}$$

A theoretically redundant gain term $k$ is considered in the structure to have an optimization dimension accounting for a complete magnitude response scaling, which cannot be easily conveyed through the individual terms $b_i$. Further denote by:

$$M_\theta(\omega) = |U_\theta(j\omega)|^2, \quad M^\star(\omega) = |\ell(j\omega)|^2, \tag{6.3}$$

with $\ell(\omega)$ as the maximum achieved value of the uncertainty at a given frequency $\omega$, while $M_\theta(\omega)$ can be expressed as follows:

$$M_\theta(\omega) = k^2 \frac{\left(\sum_{i=0}^{\lfloor \frac{m}{2} \rfloor} b_{2i}(-1)^i \omega^{2i}\right)^2 + \left(\sum_{i=0}^{\lfloor \frac{m}{2} \rfloor} b_{2i+1}(-1)^i \omega^{2i+1}\right)^2}{\left(\sum_{i=0}^{\lfloor \frac{n}{2} \rfloor} a_{2i}(-1)^i \omega^{2i}\right)^2 + \left(\sum_{i=0}^{\lfloor \frac{n}{2} \rfloor} a_{2i+1}(-1)^i \omega^{2i+1}\right)^2}, \tag{6.4}$$

where $a_n = 1$, with the auxiliary notation for even and odd sums to be later used: $M_\theta(\omega) = k^2 \left( \left(\Sigma_\beta^e\right)^2 + \left(\Sigma_\beta^o\right)^2 \right) \Big/ \left( (\Sigma_\alpha^e)^2 + (\Sigma_\alpha^o)^2 \right)$.

Define the cost functional $L : \mathbb{R}^{1+m+n} \to \mathbb{R}_+$:

$$L(\theta) = \sum_{\omega \in \Omega} \left( |M_\theta(\omega) - M^\star(\omega)| \right), \tag{6.5}$$

where $\Omega$ is the frequency set used to obtain the upper bounds $\ell(\omega)$. The functional is not differentiable in the current form, but it can be differentiable if the absolute value is neglected or by considering subgradient methods. The gradient of the cost functional with the absolute value function is given by:

$$\nabla_\theta L = \left( \frac{\partial L}{\partial k} \quad \frac{\partial L}{\partial b_i}\Big|_{0 \le i \le m} \quad \frac{\partial L}{\partial a_i}\Big|_{0 \le i \le n-1} \right), \tag{6.6}$$

with proceeding terms:

$$\frac{\partial L}{\partial k} = \sum_{\omega \in \Omega} \operatorname{sign}\left(M_\theta(\omega) - M^\star(\omega)\right) \frac{2}{k} M_\theta(\omega); \tag{6.7}$$

$$\frac{\partial L}{\partial b_i} = \sum_{\omega \in \Omega} \operatorname{sign}\left(M_\theta(\omega) - M^\star(\omega)\right) \frac{2 M_\theta(\omega) \varepsilon_i \omega^i \sum_\beta^x}{|\beta(j\omega)^2|}; \tag{6.8}$$

$$\frac{\partial L}{\partial a_i} = -\sum_{\omega \in \Omega} \operatorname{sign}\left(M_\theta(\omega) - M^\star(\omega)\right) \frac{2 M_\theta(\omega) \varepsilon_i \omega^i \sum_\alpha^x}{|\alpha(j\omega)^2|}, \tag{6.9}$$

while the gradient by discarding the theoretically-optional absolute value (replaced by a positivity constraint) remains the same as above sans the sign function term. The coefficients $\varepsilon_i$ take values $\varepsilon_i = 1$ if $i \equiv 0, 1 \pmod 4$, and $\varepsilon_i = -1$, otherwise.

Next, three sets of constraints should be imposed: (i) the upper bound constraints $C_b(\theta)$; (ii) the stability and minimum phase constraints $C_s(\theta)$; (iii) the model validity constraints $C_v(\theta)$. The differentiable upper bound constraint $C_b : \mathbb{R}^{1+m+n} \to \mathbb{R}^{|\Omega|}$ is imposed in order to ensure that the model $U_\theta$ represents an upper bound of the frequency measurements, i.e. $|U_\theta(j\omega)| \ge |\ell(\omega)|$ for each $\omega \in \Omega$:

$$C_b(\theta) = \Big( M_\theta(\omega) - M^\star(\omega) \Big)_{\omega \in \Omega} \succeq 0. \tag{6.10}$$

These constraints also allow to solve the problem of minimizing $L(\theta)$ from (6.5) without the non-differentiable absolute value function. Additionally, the Jacobian of the constraints vector $C_b(\theta)$ can be expressed as

follows, each term $C_b^\omega$ corresponding to a particular constraint $M_\theta(\omega) - M^\star(\omega) \geq 0$, $\omega \in \Omega$:

$$\frac{\partial C_b^\omega(\theta)}{\partial k} = \frac{2}{k} M_\theta(\omega),\ \omega \in \Omega; \tag{6.11}$$

$$\frac{\partial C_b^\omega(\theta)}{\partial b_i} = \frac{2M_\theta(\omega)\varepsilon_i \omega^i \sum_\beta^x}{|\beta(j\omega)^2|},\ \omega \in \Omega; \tag{6.12}$$

$$\frac{\partial C_b^\omega(\theta)}{\partial a_i} = -\frac{2M_\theta(\omega)\varepsilon_i \omega^i \sum_\alpha^x}{|\alpha(j\omega)^2|},\ \omega \in \Omega. \tag{6.13}$$

The next set of constraints are called the stability constraints and consist of two parts: imposing the model $U_\theta(s)$ to be stable, i.e. the roots of $\alpha$ are in the left half-plane, and of minimum phase, i.e. the roots of $\beta$ are in the left half-plane. For both conditions we can use the Routh-Hurwitz criterion to formulate the vector function $C_s : \mathbb{R}^{1+m+n} \to \mathbb{R}^{m+n}$.

**Definition 8.** *Given a real polynomial $P$ of degree $n > 0$:*

$$P(s) = \lambda_0 s^n + \lambda_1 s^{n-1} + \cdots + \lambda_{n-1} s + \lambda_n,\ \lambda_0 \neq 0, \tag{6.14}$$

*define its Hurwitz matrix as:*

$$\mathcal{H}(P) = \begin{pmatrix} \lambda_1 & \lambda_3 & \lambda_5 & \cdots & \cdots & \cdots & 0 & 0 & 0 \\ \lambda_0 & \lambda_2 & \lambda_4 & & & & \vdots & \vdots & \vdots \\ 0 & \lambda_1 & \lambda_3 & & & & \vdots & \vdots & \vdots \\ \vdots & \lambda_0 & \lambda_2 & \ddots & & & 0 & \vdots & \vdots \\ \vdots & 0 & \lambda_1 & & & \ddots & \lambda_{n-1} & 0 & \vdots \\ \vdots & \vdots & 0 & & & & \lambda_{n-3} & \lambda_{n-1} & 0 \\ 0 & 0 & 0 & \cdots & \cdots & \cdots & \lambda_{n-4} & \lambda_{n-2} & \lambda_n \end{pmatrix}. \tag{6.15}$$

*Additionally, define the Routh-Hurwitz inequality applied to $P$:*

$$\mathcal{RH}(P) = \begin{pmatrix} \det \mathcal{H}(P)_{\substack{1\leq i\leq 1\\ 1\leq j\leq 1}} \\ \det \mathcal{H}(P)_{\substack{1\leq i\leq 2\\ 1\leq j\leq 2}} \\ \vdots \\ \det \mathcal{H}(P)_{\substack{1\leq i\leq deg(P)\\ 1\leq j\leq deg(P)}} \end{pmatrix} \succeq 0, \tag{6.16}$$

where "$\succeq$" denotes the operator "$\geq$" applied element-wise. As such, the minimum phase condition can be written as $\mathcal{RH}(\beta) \succeq 0$, with the stability condition given by $\mathcal{RH}(\alpha)\succeq 0$, resulting an expression of the stability constraints vector:

$$C_s(\theta) = \begin{pmatrix} \mathcal{RH}(\beta) \\ \mathcal{RH}(\alpha) \end{pmatrix} \succeq 0. \tag{6.17}$$

Each involved determinant is a differentiable function with respect to its parameters. Last but not least, we must ensure that the uncertainty model $U_\theta(s)$ is valid. Consider the lemma from [Poo+94]:

**Lemma 2.** *Given three complex matrices $W_\Delta$, $W_1$ and $W_2$ with appropriate dimensions, the equation $W_\Delta = W_1 \Delta W_2$ has a solution $\Delta$ with $\overline{\sigma}(\Delta) \leq 1$ if and only if:*

$$\begin{pmatrix} W_1 W_1^\star & W_\Delta \\ W_\Delta^\star & W_2^\star W_2 \end{pmatrix} \geq 0. \tag{6.18}$$

Based on the frequency measurements $\ell(\omega)$, $\omega \in \Omega$, of the uncertainty for a SISO system, $U_\theta(s)$, the model is valid if and only if the equation $\ell(\omega) = U_\theta(j\omega)\Delta$ has a solution $\Delta$ with $\overline{\sigma}(\Delta) \leq 1$, for each $\omega \in \Omega$. As such, the following set of LMIs must be integrated as additional constraints in order to guarantee that the uncertainty model is valid with respect to the data:

$$\begin{pmatrix} M_\theta(\omega) & \ell(\omega) \\ \ell(\omega)^\star & 1 \end{pmatrix} \geq 0, \quad \forall \omega \in \Omega. \tag{6.19}$$

The above LMIs can be rewritten in a differentiable way by imposing the

trace and the determinant positive. Thus, relation (6.19) equivalates to:

$$1 + M_\theta(\omega) \geq 0 \quad \text{and} \quad M_\theta(\omega) - M^\star(\omega) \geq 0, \tag{6.20}$$

which are both satisfied by the constraints already imposed through $C_b(\theta)$. As such, the additional set of constraints $C_v(\theta)$ can be encompassed into the set $C_b(s)$.

## 6.3 Optimization problem and numeric solution

As detailed, the resulting optimization problem can be formulated as the following classical nonlinear minimization:

**Problem 4.** *Let the nonlinear minimization problem with unknown variable $\theta \in \mathbb{R}^{n_\theta}$, loss function $L : \mathbb{R}^{n_\theta} \to \mathbb{R}_+$, set of nonlinear constraints $C : \mathbb{R}^{n_\theta} \to \mathbb{R}^{n_C}$ and bounds of the optimization variable $\underline{\theta}$ and $\overline{\theta}$:*

$$\min L(\theta) \quad s.t. \quad \begin{cases} C(\theta) \succeq 0; \\ \underline{\theta} \preceq \theta \preceq \overline{\theta}. \end{cases} \tag{6.21}$$

A well-established solution to Problem 4 is implemented in the `fmincon` routine from the Global Optimization Toolbox [Mat22], also used for this paper, and is based on the interior-point or trust-region reflective algorithms of [BGN00; Glo98], which also use the gradients of the objective and constraint multivariable functions. As described in [Lew07; Cla90], such a minimization problem converges if the subgradient method is applied, case in which the sign function has been considered:

$$\text{sign}\,(x) = \begin{cases} -1, x < 0; \\ \ \ 1, x \geq 0, \end{cases} \tag{6.22}$$

which ensures continuity from the right for the gradient (6.6).

Due to a nonconvex optimization procedure being principally unable to guarantee the global extremum nature of a found point $\theta^\star$, instead of a randomized variable initialization, a well-placed guess $\theta^m_{n,0} \equiv \theta_0$ based on the SDP optimization (3.37) will be considered as a starting point for the minimization of (6.5) to limit the search in a relevant neighbourhood of the desired optimum. Furthermore, the optimum pole-zero structure of the transfer function must be obtained in a formal manner. The previous two points can be gathered into a separate optimization problem

which leads to an ideal starting point $\theta_0$.

**Problem 5.** *The recommended initial point $\theta_0$ and its pole-zero configuration $(n, m)$ for the uncertainty model can be computed by solving the following discrete optimization problem, using the objective (6.5) and auxiliary SDP subproblems (3.37):*

$$\begin{aligned}(n^\star, m^\star) = \arg \min_{(n,m)\in\mathbb{N}^2} & L\left(\theta_{n,0}^m\right) + \lambda \cdot n \\ s.t. \quad & \theta_{n,0}^m = \arg\min_\theta \mathcal{S}_\gamma\left(\theta_n^m\right), \ \lambda > 0. \end{aligned} \tag{6.23}$$

An efficient manner to solve Problem 5 is to use a lower triangular rook search method on the matrix with entries $(n, m)$ of dimensions limited up to a maximum accepted order $N \in \mathbb{N}_+$.

The SDP solution of [BV04] is based on the assumption that the optimized transfer function does not contain singularities on or near the imaginary axis, as it otherwise leads to infeasible outcomes. In this case, the interior-point algorithm employed from [BGN00] presents the advantage that it allows to bring the optimization variable $\theta$ into the feasibility range even though the optimal initial point $\theta_0$ may start infeasible.

Adapting the nonlinear minimization (6.21) with the defined objective and constraints from Section 6.2, along with the initial point algorithm of (6.23), we obtain the proposed nonconvex uncertainty model optimization problem in the variable $\theta \in \mathcal{D}$.

**Problem 6.** *The least conservative in the sense of (6.5) SISO transfer function $U_\theta(s)$ with uncertainty sizes $n_s = 0, n_f = 1$ as in (3.34), transformation $\mathcal{T}$ from Table 3.1, based on magnitude measurements $\ell(j\omega)$ from (3.36), with structure and initial point $\theta_0$, to be used in robust synthesis can be obtained by solving:*

$$\min_\theta L(\theta) \quad s.t. \tag{6.24}$$

$$\begin{cases} C(\theta) & = \left(C_{bv}(\theta)^\top \quad C_s(\theta)^\top\right)^\top \succeq 0; \\ \theta_{n^\star,0}^{m^\star} & = \arg\min_\theta \mathcal{S}_\gamma\left(\theta_n^m\right); \\ (n^\star, m^\star) & = \arg\min_{(n,m)\in\mathbb{N}^2} L\left(\theta_{n,0}^m\right) + \lambda \cdot n, \end{cases}$$

*with auxiliary gradients $\nabla_\theta L(\theta)$, $\nabla_\theta C(\theta)$, and denoting by $C_{bv}(\theta) \equiv C_b(\theta)$ due to the $C_v(\theta)$ condition being already included in the constraint $C_b(\theta)$.*

**Remark 3.** *The framework lends itself to analytical differentiation, as*

*many terms in the gradients directly depend on reusing terms of the form* $M_\theta(\omega)$, $\omega \in \Omega$, *and sums* $\Sigma_\beta^e, \Sigma_\beta^o, \Sigma_\alpha^e, \Sigma_\alpha^o$, *being straightforward to be computed programmatically. As such, algorithmic differentiation techniques as presented in [GW08] have been employed in the implementation of Problem 6 alongside the functions from [Mat22].*

## 6.4 Conclusions

The present section proposed a different approach to model transfer function constraints, with imposed stability, minimum phase and validity properties, and least conservative in an $\ell_1$-norm sense. It aids in several corner cases obtained in practice, such as in using measurements from highly-resonant mechanical systems, or situations when the performances imposed through the loop-shaping weighting functions are strict.

# 7. Nonlinear cascade control using robust dynamical path planning

## 7.1 Motivation and contributions

This section presents an application of robust control synthesis, viewed as a dynamical path planning algorithm alongside a primary nonlinear control technique used to guarantee global asymptotic stability of the process. The results developed for passivity-based control, described in papers [MȘD21; Mih+22d; Mih+22c; Mih+22e; MȘD23a; MȘD23b; MȘD25] are briefly recalled, with emphasis on the robust control aspects of the analysis. In addition, an nonlinear robust synthesis based on $\mathcal{L}_2$-gain specifications has been further extended in [Mih+25].

The focus will be on input-affine systems as defined in (2.3), with the particularized affine structure of the nonlinear functions, $g_k(x) = A_k x + b_k$, $k = \overline{0, m}$, with $A_k \in \mathbb{R}^{n\times n}$ and $b_k \in \mathbb{R}^n$:

$$(\Sigma^a): \begin{cases} \dot{x} &= g_0(x) + \sum_{i=1}^{m} g_i(x) \cdot u; \\ y &= C \cdot x. \end{cases} \tag{7.1}$$

## 7.2 Passivity-based control background

Assume the notion of dissipative systems with respect to a supply rate, according to [Kha15], based on the following definition.

**Definition 9.** *The system $\Sigma^a$ described in (7.1) is said to be dissipative with respect to the supply rate $\omega : \mathbb{R}^n \times \mathbb{R}^m \to \mathbb{R}$ if there exists a storage function $S : \mathbb{R}^n \to \mathbb{R}_+$ of class $C^1$ such that:*

$$\frac{\partial S(x)}{\partial x} f(x,u) \leq \omega(x,u), \quad \forall\, (x,u) \in \mathbb{R}^n \times \mathbb{R}^m. \tag{7.2}$$

Assume that the supply-rate can be described as $\omega(x,u) = u^\top h(x)$, with $h : \mathbb{R}^n \to \mathbb{R}^m$. The vectors $u$ and $y = h(x)$ are called port variables.

The critical difficulty to prove the passivity is characterized by a suitable choice of the storage function. To design a passivity based controller (PBC), the following extended system can be considered [Sch82]:

$$(\Sigma_e) : \begin{cases} \dot{x} &= f(x,u); \\ \dot{u} &= u_d, \end{cases} \tag{7.3}$$

where $u_d \in \mathbb{R}^m$ is the new input vector and $\widetilde{x} = [x^\top \ u^\top]^\top \in \mathbb{R}^{n+m}$ is the new state vector. A new passivity concept was introduced by [KKS19] using a storage function similar with the Lyapunov candidate function constructed using Krasovskii's method presented in [Kha15].

**Definition 10.** *Let $h_K : \mathbb{R}^n \times \mathbb{R}^m \to \mathbb{R}^m$ be the output port variable function. The nonlinear system $\Sigma$ is said to be Krasovskii passive if its extended system $\Sigma_e$ is dissipative with respect to the supply rate:*

$$\omega_K(\widetilde{x}, u_d) = u_d^\top h_K(\widetilde{x}),$$

*with a storage function:*

$$S_K(\widetilde{x}) = \frac{1}{2}||f(x,u)||_Q^2, \quad \forall\, \widetilde{x} \equiv (x,u) \in \mathbb{R}^n \times \mathbb{R}^m, \quad Q = Q^\top \geq 0.$$

A sufficient set of conditions for a system to be Krasovskii passive is presented in the following theorem. For simplicity, for a symmetric and positive semidefinite matrix $Q \in \mathbb{R}^{n\times n}$ consider the shorthand notation:

$$Q_{g_k}(x) = Q\frac{\partial g_k(x)}{\partial x} + \frac{\partial g_k^\top(x)}{\partial x}Q, \ \ k = \overline{0,m}. \tag{7.4}$$

**Theorem 1.** *The system $(\Sigma)$ is Krasovskii passive with the supply-rate $\omega_K(\widetilde{x}, u_d) = u_d^\top h_K(\widetilde{x})$, where the port variable $h_K$ can be expressed as:*

$$h_K(x,u) = [g_1^\top(x) \dots g_m^\top(x)] \cdot Q \cdot f(x,u) \tag{7.5}$$

*and with the storage function:*

$$S_K(\widetilde{x}) \equiv S_K(x,u) = \frac{1}{2}||f(x,u)||_Q^2, \tag{7.6}$$

*if there exists a matrix* $Q \in \mathbb{R}^{n\times n}$, $Q = Q^\top \geq 0$, *that satisfies:*

$$Q(\widetilde{x}) \equiv Q_{g_0}(x) + \sum_{k=1}^{m} Q_{g_k}(x)u_k \leq 0, \quad \forall\ \widetilde{x} \equiv (x,u) \in \mathbb{R}^n \times \mathbb{R}^m. \tag{7.7}$$

The now necessary and sufficient conditions indicated in the above theorem are an extension of the necessary and sufficient conditions for a system to be differential passive [Sch13], which assert that $Q_{g_0}(x) \leq 0$ and $Q_{g_k}(x) = 0$, for each $x \in \mathbb{R}^n$. These necessary and sufficient conditions were extended in [KKS19] to be sufficient conditions to Krasovskii passivity.

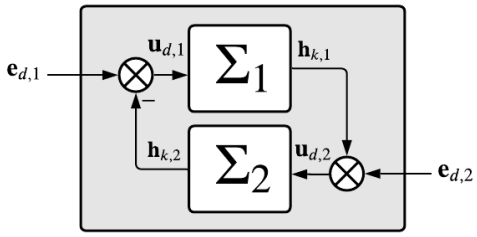


Figure 7.1: Passivity interconnection of systems $\Sigma_1$ and $\Sigma_2$.

The LFT connection of two Krasovskii passive systems also forms a Krasovskii passive system. Denote two such systems $\Sigma_1$, $\Sigma_2$ given by:

$$(\Sigma_j) : \dot{x}_j = f(x_j, u_j),\ j \in \{1,2\}, \tag{7.8}$$

having the extended systems $\Sigma_{e,1}$ and $\Sigma_{e,2}$ with states $\widetilde{x}_j \equiv (x_j, u_j)$, which are Krasovskii passive with respect to the supply rates $\omega_{K,j}(\widetilde{x}_j, u_{d,j}) = u_{d,j}^\top h_{K,j}(\widetilde{x}_j)$ and storage functions $S_{K,j}(\widetilde{x}_j)$. The connection of systems $\Sigma_{e,j}$ can be written as:

$$(\Sigma_i) : \quad \begin{bmatrix} u_{d,1} \\ u_{d,2} \end{bmatrix} = \begin{bmatrix} 0 & -1 \\ 1 & 0 \end{bmatrix} \begin{bmatrix} h_{K,1} \\ h_{K,2} \end{bmatrix} + \begin{bmatrix} e_{d_1} \\ e_{d_2} \end{bmatrix}, \tag{7.9}$$

where $e_1, e_2 \in \mathbb{R}^m$ are external inputs and $e_{d,j} = \dot{e}_j$ are their derivatives. The extended system state can be expressed as:

$$\widetilde{x} = [\widetilde{x}_1^\top + [0_n\ e_1^\top] \quad \widetilde{x}_2 + [0_n\ e_2^\top]]^\top. \tag{7.10}$$

**Lemma 3.** *The closed-loop system $\Sigma_i$ is Krasovskii passive with respect to the supply-rate:*

$$\omega_{K,i}(\widetilde{x}, e_{d_1}, e_{d_2}) = e_{d_1}^\top h_{K,1}(\widetilde{x}_1) + e_{d_2}^\top h_{K,2}(\widetilde{x}_2), \tag{7.11}$$

*and storage function:*

$$S_{K,i}(\widetilde{x}) = S_{K,1}(\widetilde{x}_1) + S_{K,2}(\widetilde{x}_2). \tag{7.12}$$

Thus, a procedure to design a first-order type Krasovskii passivity-based controller (KPBC) results. Define:

$$(\Sigma_c): \ y_c(t) = \dot{x}_c(t) = K_1(K_2 x_c - u_c(t)) \equiv f_c(x_c, u_c), \tag{7.13}$$

where $x_c \in \mathbb{R}^{n_c}$ is the state vector, $u_c$ and $y_c$ are the input and output vectors, while matrices $K_1, K_2 \in \mathbb{R}^{n_c \times n_c}$ must be symmetric and negative definite, along with symmetric and positive definite, respectively.

**Lemma 4.** *The controller $\Sigma_c$ is Krasovskii passive with respect to the supply-rate $\omega_{K,c}(y_c, u_c) = y_c^\top u_c$ and storage function $S_{K,c} = \frac{1}{2}||x_c||_{K_2}^2$.*

Now, consider the interconnection of systems $\Sigma_e$ and $\Sigma_c$:

$$\begin{bmatrix} u_d \\ u_c \end{bmatrix} = \begin{bmatrix} 0 & -1 \\ 1 & 0 \end{bmatrix} \begin{bmatrix} h_K \\ y_c \end{bmatrix} + \begin{bmatrix} 0 \\ \bar{u} \end{bmatrix}, \tag{7.14}$$

where $\bar{u}$ is the external input. The following theorem gives the sufficient condition such that the above interconnection is Krasovskii passive.

**Theorem 2.** *Consider the extended system $(\Sigma_e)$ which satisfies the conditions of Theorem 1 for a symmetric and positive definite matrix $Q \in \mathbb{R}^{n \times n}$ with at least one equilibrium isolated point $(x^*, u^*)$. Also, consider the controller given by $(\Sigma_c)$ with the states $x_c = u^* - u$ and the interconnection given by (7.14). The closed-loop system is dissipative with respect to the supply rate $\omega_o(u_d, \bar{u}) = u_d^\top \bar{u}$ with the storage function:*

$$S_o(x, u, x_c) = \frac{1}{2}||f(x, u)||_Q^2 + \frac{1}{2}||x_c||_{K_2}^2. \tag{7.15}$$

## 7.3 Proposed approach

The previous results are further used to develop a unified approach to design KPB controllers for a class of input-affine nonlinear

systems, which was particularized to families of DC-DC converters in paper [MŞD21], and exemplified in the case study from Section 11.6.2, using Theorem 1 as a main motivation.

Considering that $\frac{\partial g_k(x)}{\partial x} = A_k,\ \forall k = \overline{0,m}$, and, using Theorem 1, the necessary and sufficient condition for a system $\Sigma_a$ to be Krasovskii passive can be written as:

$$QA_0 + A_0^\top Q + \sum_{i=1}^{m} \left(QA_i + A_i^\top Q\right) u_i \leq 0,\ \forall u = [u_1, u_2, \ldots, u_m]^\top \in \mathbb{R}^m. \tag{7.16}$$

Due to the physical constraints of the process, the command vector is bounded: $u \in [u_1^l, u_1^u] \times [u_2^l, u_2^u] \times \cdots \times [u_m^l, u_m^u]$. Given that the space spanned by the values of the command signal describes a polytope, the problem (7.16) can be formulated as a union of LMI problems, one for each vertex of the polytope. Using this remark, the necessary and sufficient conditions for a quasi-linear affine input-affine system $\Sigma_a$ to be Krasovskii passive are presented in the following theorem.

**Theorem 3.** *The system $(\Sigma_a)$ is Krasovskii passive with the supply-rate $\omega_K(x,u) = u^\top h_K(x)$, where the port variable $h_K$ can be expressed as:*

$$h_K(x,u) = [x^\top A_1^\top + b_1^\top \ldots x^\top A_m^\top + b_m^\top] \cdot Q \cdot \dot{x}, \tag{7.17}$$

*and with the storage function: $S_K(x) = \frac{1}{2}\|\dot{x}\|_Q^2$ if and only if there exists a symmetrical matrix $Q = Q^\top \geq 0 \in \mathbb{R}^{n\times n}$ which satisfies the conditions:*

$$QA_0 + A_0^\top Q + \sum_{i=1}^{m} \left(\left(QA_i + A_i^\top Q\right) e_i u_i^l + \left(QA_i + A_i^\top Q\right)(1-e_i) u_i^u\right) \leq 0, \tag{7.18}$$

*for each binary word $e = \begin{pmatrix} e_1 & e_2 & \ldots & e_m \end{pmatrix}^\top \in \mathbb{Z}_2^m$.*

*Proof.* Taking the Lie derivative of $S_K$ along the vector field of $(\Sigma_a)$:

$$\frac{\partial S_K(x)}{\partial x} f(x,u) = \dot{x}^\top \cdot \left(QA_0 + A_0^\top Q + \sum_{i=1}^{m} \left(QA_i + A_i^\top Q\right) u_i\right) \cdot \dot{x} + u^\top h_K(x).$$

Now, in order to impose the desired behaviour, we need the inequality:

$$\frac{\partial S_K(x)}{\partial x} f(x,u) \leq u^\top h_K(x)$$

to be true for each state trajectory $x \in \mathbb{R}^n$ and for each input trajectory $u \in \mathbb{R}^m$, which is equivalent with the following LMIs:

$$QA_0 + A_0^\top Q + \sum_{i=1}^{m} \left(QA_i + A_i^\top Q\right) u_i \leq 0$$

to have a common solution for each command signal $u \in [u_1^l, u_1^u] \times [u_2^l, u_2^u] \times \cdots \times [u_m^l, u_m^u]$, which is a polytope problem and can be solved in its vertices only, and the proof is complete. □

After the output port-variable is computed as in the previous theorem, a KPBC having the form (7.13) is computed such that the closed-loop system is Krasosvkii passive. This property ensures asymptotic stability. As such, the closed-loop system will follow an input trajectory $u^\star$. However, to give a trajectory according to the desired reference for the output $y^\star$, another component, i.e. trajectory path planning, is needed. For this component, a robust controller $K_{\text{rob}}$ is used, configured in the cascade structure presented in Figure 7.2.

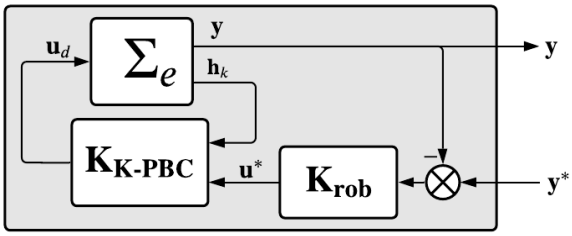


Figure 7.2: Proposed closed-loop cascade control structure which employs a low level KPB controller and high level robust controller path-planning.

The robust controller which computes the input trajectory for the KPBC is designed for a linearized model of the system around a forced equilibrium point $\widetilde{x}^\star = \left(x^{\star,\top}\ u^{\star,\top}\right)$. The LTI model of the linearized plant of the input-affine quasi-linear system $(\Sigma_a)$ can be computed as:

$$A = \left.\frac{\partial f(x,u)}{\partial x}\right|_{\widetilde{x}=\widetilde{x}^\star} = A_0 + \sum_{k=1}^{m} A_i u_i^\star; \tag{7.19}$$

$$B = \left.\frac{\partial f(x,u)}{\partial u}\right|_{\widetilde{x}=\widetilde{x}^\star} = \sum_{k=1}^{m} \left(A_i x^\star + b_i\right), \tag{7.20}$$

followed by a similar extension to the output matrices $C$ and $D$. Now, the linearized plant can be represented as:

$$(\Sigma_{a,lin}): \quad \begin{cases} \dot{\Delta x}(t) = A \cdot \Delta x(t) + B \cdot \Delta u(t); \\ \Delta y(t) = C \cdot \Delta x(t) + D \cdot \Delta u(t), \end{cases} \tag{7.21}$$

which coincides with the form (2.5). Thus, uncertain modelling techniques as proposed in Chapter 6 can be applied to obtain an uncertainty block $\mathbf{\Delta}$ as in (3.29), the uncertain process model $G$ and, finally, to prepare the augmented plant $P$ for robust controller synthesis. Figure 7.3 encompasses all these steps. After the mixed sensitivity loop-shaping $\mu$-synthesis control problem 3.43 is solved, the order reduction for the resulting high-order controller is applied.

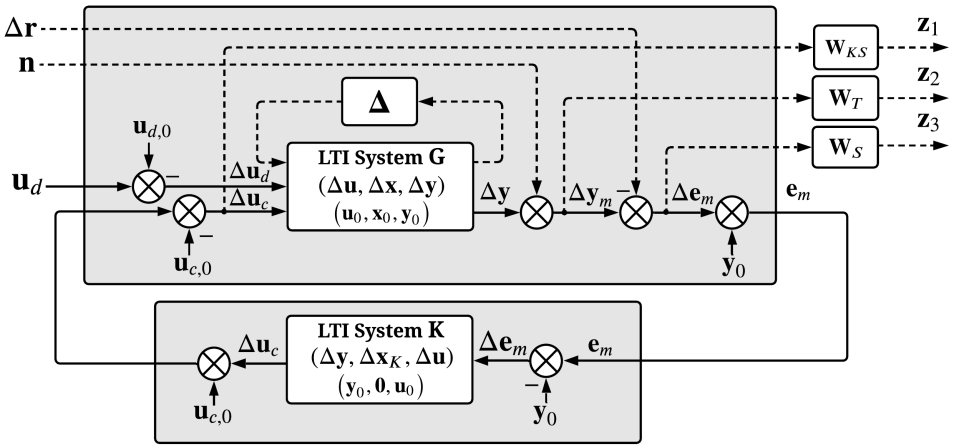


Figure 7.3: Robust regulator synthesis diagram for the linearized Krasovskii passive system (7.21) using the closed-loop shaping method.

To implement the proposed improvements and control structure from this section, an extension of the class diagram previously presented in Figure 5.1 is illustrated in Figure 7.4. Class `ExtendedDcDcConverter` implements the input-affine system (7.3), extended with the port variable $h_K(x,u)$ from (7.5). In a similar manner, class `KrasovskiiPassivityBasedController` implements the KPBC system as described in (7.13). An auxiliary class which provides an interface between the plant $\Sigma_e$ with KPBC $K_{KPBC}$ in the connection (7.14) and robust controller $K_{rob}$ is implemented in `KPBCWrapper`, as in the left part of Figure 7.2.

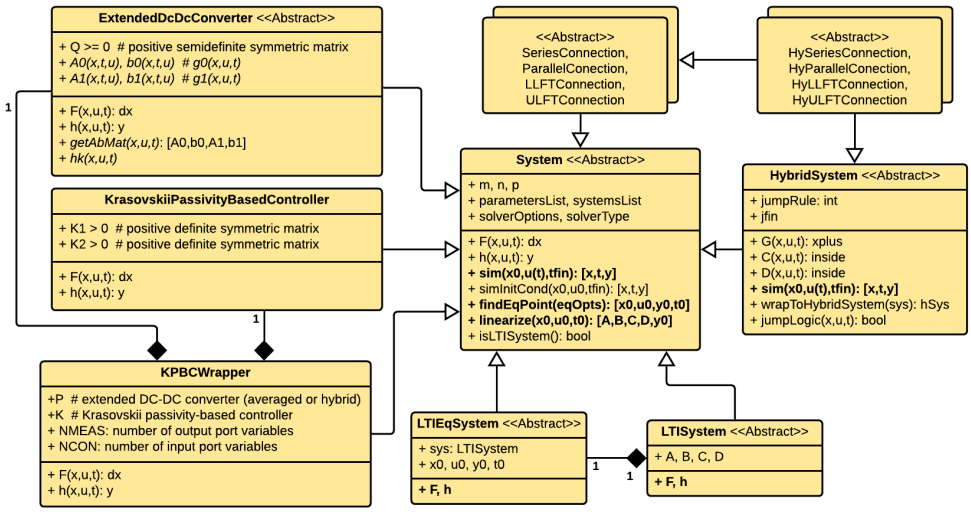


Figure 7.4: Extended class diagram to account for passivity-based control law design and simulation.

The KPBC and $\mu$-synthesis controllers are decoupled, can be used individually to control the quasi-linear affine plant, but are used to gather the benefits of both approaches, as the KPBC ensures asymptotic stability of the nonlinear plant, while the $\mu$-synthesis controller is used for the RS and RP properties around the operating point. A final LLFT connection, implemented by means of class `LLFTConnection`, as in Figure 7.2, gives the proposed closed-loop system.

For the Model-in-the-Loop component of the toolbox, an auxiliary functionality was created to specify various input signals using a predefined set of atomic operations, such as step signals, ramps, sine waves and interpolated lookup tables, on desired input channels, as necessary for multi-input systems, based on function handles, cell arrays and flexible low-level signal definitions.

## 7.4 Conclusions

The results presented in this section propose an application of the robust control synthesis framework in an extended context for nonlinear systems, by gathering the advantages of both passivity-based control laws applied for the operating point of a nonlinear system, along with the flexibility of imposing performance metrics given by robust regulators.

# 8. Sampling and discretization

This chapter is based on results published in papers [Șuș+22a], [Șuș+22b], [ȘMD23c], in increasing order of generality. It proposes optimization-based approaches to select the sampling periods for classes of LTI regulators in single-rate systems, such as 1DOF and 2DOF structures, along with cascaded multi-rate control structures, to account for practical implementation. Starting from the Shannon-Nyquist sampling theorem, which proposes the minimum required sampling frequency for completely recovering the original analog signal from its discrete samples, the scope of the sampling process, viewed from a control perspective, is to ensure asymptotic stability of the closed-loop system, with the smallest possible degradation of the initially-proposed performance indices as possible according to a set of well-picked criteria. As such, a configurable optimization-based approach is proposed, solved with the mixed-integer artificial bee colony (MI-ABC) algorithm, for selecting the sampling periods by specifying the emphasis between closed-loop fidelity and ease of implementation, with intuitive visualization methods. A direct application of the performance-based heuristics developed in this chapter is presented in [ȘNM25].

## 8.1 Motivation and contributions

The current section proposes a method to formulate optimization problems having as solution the quasi-optimal value of the sampling period in order to eliminate the *ad hoc* rules presented in literature. The main contributions are:

(i) the description of the functionals which encompass both open/closed-loop fidelity of the control system, quantization implementation difficulty, and stability preservation of the closed-loop system;

(ii) the construction of the functional necessary for minimization in the single-loop control systems irrespective of the structure of the LTI controller;
(iii) a straightforward extension to the multi-rate case materialized through the form of cascade control structures;
(iv) the illustration of numeric examples with detailed discussions on the selection of the hyperparameter sets.

Compared to the conference paper [Șuș+22a], with improvements provided for a worst-case execution time analysis in the article [Șuș+22b], important improvements and modifications are:

(a) the optimization problem is posed in a multi-rate context, with the direct applicability in MIMO cascade control structures, with the possibility to particularize the structure for single loop control structures for (SISO) cases;
(b) the proposed functionals are extended to the multi-input and multi-output case by quantifying the magnitude using the singular values of the system;
(c) a mixed-integer artificial bee colony algorithm is designed and implemented for solving the described non-convex optimization problems instead of using a simple linesearch algorithm;
(d) one and two-dimensional representations of the global functional are portrayed, with intuitive means of distinguishing clusters of solutions, which reveal the non-convex nature of the resulting optimization problem and marks the differences towards available approaches.

### 8.1.1 $z$- and $\delta$-plane modelling comparison

The classical shift operator $z$ for implementing the numeric controllers will be considered, due to the advantage of being widely used in the literature and being familiar to many engineers, but with the major problem of quantization phenomena which arise due to the finite number of bits used for the dynamic range. On the other hand, the $\delta$-operator, closer to the derivative operator [MG90] has the great advantage of emphasizing the link between continuous and discrete systems. Moreover, this operator tries to overcome the quantization difficulties. However, the current section will underline that even for the $\delta$-operator with its superior behaviour, the quantization problem remains relevant. This fact,

together with the popularity of the shift operator, motivates the choice for considering the $\mathcal{Z}$ transform for implementing the multi-rate control system detailed in the subsequent writing.

A numeric example is used to illustrate that the quantization problems appear in both $z$-operator and $\delta$-operator frameworks. Consider the continuous-time controller:

$$K(s) = \frac{s - 1.5}{s(s + 0.5)} = \frac{s + 1 - a_{11}}{s^2 + (3 - a_{11})s + 5 - 2a_{11}}, \tag{8.1}$$

where $a_{11} \in \mathbb{R}$ will be a parameter having the nominal value $a_{11,0} = 2.5$, and its influence will be studied during the quantization procedure.

Using the forward Euler discretization method, along with a sampling rate $T = 1$ $[s]$, the resulting numeric controller can be expressed based on the $z$-operator as follows:

$$K(z) = \frac{z - a_{11}}{z^2 + (1 - a_{11})z + 3 - a_{11}}. \tag{8.2}$$

If the $\Delta$ transform is used instead of the classical $\mathcal{Z}$ transform, with the aforementioned $\delta$-operator, the link between $z$ and $\delta$ can be written as:

$$\delta = \frac{z - 1}{T}, \tag{8.3}$$

leading to a transfer function having the same expression as the continuous-time representation of the controller:

$$K(\delta) = \frac{\delta + 1 - a_{11}}{\delta^2 + (3 - a_{11})\delta + 5 - 2a_{11}}. \tag{8.4}$$

Considering a variation of $a_{11}$ around the nominal value $a_{11,0}$, Figure 8.1 illustrates that both the $z$ and $\delta$-based operator implementations present quantization difficulties, which justifies the quantization difficulty to be an important factor in the optimization of the sampling rate of the numeric controller, irrespective of the modelling method.

A different compromise also arises when using the difference operator versus its shift equivalent, such that the dynamic range of the regulator coefficients considerably extends with the $\delta$ framework, due to the poles belonging to the disk $\mathcal{C}\left(-\frac{1}{T}, \frac{1}{T}\right)$ instead of a limited range for the $z$ framework, with acceptable poles in $\mathcal{C}\left(0, 1\right)$, but with many bits necessary to be allocated to the fractional number part.

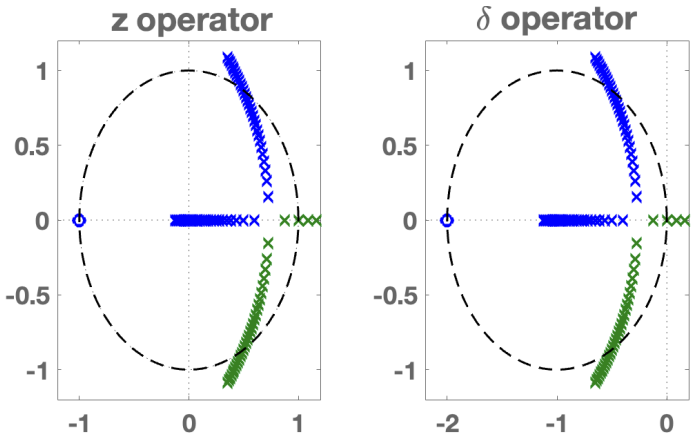


Figure 8.1: Root locus method applied for the quantization effect of the coefficient $a_{11}$ in Equations (8.2) and (8.4).

## 8.2 Proposed method

### 8.2.1 General framework

In this subsection, we will provide and justify the use of three mathematical functionals depending on the sampling periods $\mathcal{T}$ of numeric controllers $K_T(z)$, as a means of measuring various performance indices with theoretical and practical relevance, alike, along with means of implementing them in a numerically-sound manner. All functionals will be defined over the set of admissible sampling times involved in the control structures presented in the above subsection, with the mention that the set $\mathcal{T}$ will be a singleton $T$ for the single-loop case and a set with two elements $(T, k)$ for the cascade control strategy. As such, the admissible domain can be defined as $\mathcal{D} \subset (0, \infty)$ for the single loop case and $\mathcal{D} \subset (0, \infty) \times \mathbb{Z}_+$ for cascade control.

In order to measure the similarity between a continuous-time LTI system $G(s)$ and a discrete-time system $G_{\mathcal{T}}(z)$ over the frequency range $\Omega$, the classical mean square error can be used to measure the difference between the maximum singular values of the reference continuous-time systems and the obtained discrete-time systems. As such, the resulting functional can be defined as $S_G^{\Omega} : \mathcal{D} \to (0, \infty)$:

$$\mathcal{S}_G^{\Omega}(\mathcal{T}) = \int_{\Omega} \left(\overline{\sigma}\left(G(j\omega)\right) - \overline{\sigma}\left(G_T\left(e^{j\omega T}\right)\right)\right)^2 \mathrm{d}\omega, \tag{8.5}$$

where $\overline{\sigma}(\cdot)$ is the maximum singular value, while $\Omega$ is the frequency range where the similarity is measured. Considering that the available frequency domain is $\Omega = (0, \omega_N)$, where $\omega_N$ is the Nyquist-Shannon frequency regarding to the smallest sampling period from $\mathcal{T}$, the similarity functional becomes $S_G : \mathcal{D} \to (0, \infty)$:

$$\mathcal{S}_G(\mathcal{T}) = \int_{0^+}^{\omega_N^-} \left(\overline{\sigma}\left(G(j\omega)\right) - \overline{\sigma}\left(G_T\left(e^{j\omega T}\right)\right)\right)^2 \mathrm{d}\omega. \tag{8.6}$$

**Remark 4.** *There are several alternatives in defining the similarity of two LTI systems, with particular interest for closed-loop connections, such as the normalized dissimilarity function metric, described in [WYH08], the standard $\nu$-gap metric, with its limitations exposed in [HS93], or the improved Vinnicombe $\nu$-gap metric [Vin93], described as:*

$$\delta(G_1, G_2) = \max\left(\overline{\delta}\left(G_1, G_2\right), \overline{\delta}\left(G_2, G_1\right)\right), \tag{8.7}$$

*with:*

$$\overline{\delta}(G_1, G_2) = \inf_{Q \in H_\infty} \left\| \begin{pmatrix} M_1 \\ N_1 \end{pmatrix} - \begin{pmatrix} M_2 \\ N_2 \end{pmatrix} Q \right\|_\infty, \tag{8.8}$$

*where for the reference systems $G_1$ and $G_2$, their right normalized coprime factorizations will be considered: $G_1 = N_1 M_1^{-1}$ and $G_2 = N_2 M_2^{-1}$, which in context of the proposed sampling rate optimization problem, the differences should be computed with the subsystems applied in $G_1 \equiv K(s) \mapsto j\omega$ and $G_2 \equiv K_T(z) \mapsto e^{j\omega T}$, respectively.*

When sampling LTI controllers, the following remarks can be made by studying the pole-zero behaviour and, also, by taking into consideration the mapping (4.3):

- integrator and derivative terms, along with the rest of the singularities placed on the unit circle $\mathcal{C}(0, 1)$ do not matter in deciding the practical sampling time, as they are invariant relative to the stability boundary;
- poles and zeros from the imaginary axis in the $s$-domain are maintained on the unit circle in the $z$-domain irrespective of the sampling period $T > 0$.
- unstable poles and zeros tend decreasingly to the unit circle's circumference, i.e. $|p| \searrow 1$ and $|z| \searrow 1$ as $T \searrow 0$; this aspect re-

garding the poles is relevant when sampling systems, as controllers generally do not employ unstable poles in their structure, only in the exceptional cases of non-strongly stabilizable systems, as mentioned in Section 9.2.2.5;

- stable poles and zeros tend increasingly to the unit circle's circumference, i.e. $|p| \nearrow 1$ and $|z| \nearrow 1$ as $T \searrow 0$, requiring additional decimal or binary digits for an accurate representation;

- the steady-state quantization error $\varepsilon_Q$ increases as $T \searrow 0$, where the quantizer $Q$ is described by input precision $\delta_e$, state precision $\delta_x$ and output precision $\delta_u$, as proved in Section 9.2, Theorems 4 and 5, this quantization error can be bounded as follows:

$$\|\varepsilon_Q\|_\infty \leq \frac{1}{1-\rho(\Phi)} f(\delta_e, \delta_x, \delta_u), \tag{8.9}$$

where $\rho(\Phi)$ denotes the spectral radius of the closed-loop state matrix: $\Phi = \hat{A} - \hat{B}\left(I + \hat{D}\right)^{-1}\hat{C}$, based on the series interconnection between the controller and the process model matrices denoted $\left(\hat{A}, \hat{B}, \hat{C}, \hat{D}\right)$, while $f(\delta_e, \delta_x, \delta_u)$ is a function which depends on the structure of the system and of the quantizer $Q$; therefore, the guaranteed steady state error is proportional to $\frac{1}{1-\rho(\Phi)}$;

As the sampling time decreases, the implemented singularities $p, z \in \mathbb{C}\backslash\mathcal{C}(0,1)$ of the system $G$ tend to $\mathcal{C}(0,1)$, which implies that an increasing number of decimal values become necessary to properly represent the controller coefficients and, thus, its singularities. As such, another functional $\mathcal{I}_G(\mathcal{T}) : \mathcal{D} \to (0, \infty)$ will be defined to account for the quantization implementation difficulty of the LTI system $G_\mathcal{T}(z)$ as:

$$\mathcal{I}_G(\mathcal{T}) = \frac{1}{\min\left\{\left||\lambda| - 1\right|,\ \lambda \in \mathcal{P}(G_T) \cup \mathcal{Z}(G_T)\right\}}, \tag{8.10}$$

with $\mathcal{P}(\cdot)$ and $\mathcal{Z}(\cdot)$ denoting the pole and zero sets of their input argument, respectively, excluding singularities from the set $\mathcal{C}(0,1)$.

Alongside the previous implementability quantization functional, an execution time cost functional $\mathcal{W}(T) : \mathcal{D} \to (0, \infty)$ becomes necessary to limit the decrease of $T \searrow 0$ which would ideally lead the similarity

functional costs to zero:

$$\mathcal{W}(T) = \frac{1}{T}. \tag{8.11}$$

A concluding functional with global effect, $\mathcal{J}_{\text{stab}(G)} : \mathcal{D} \to \{0, \infty\}$, will define the feasibility domain of the optimization problem, because it accepts or rejects a specific sampling period value, due to the possibility to destabilize a continuous system through discretization, thus indicating the feasible searching area. It induces an infinitely-valued constant when the closed-loop numeric system becomes unstable, and otherwise, defaults to no penalization:

$$\mathcal{J}_{\text{stab}(G)}(\mathcal{T}) = \begin{cases} +\infty, \text{ if } G_T \text{ has unstable poles;} \\ 0, \text{ otherwise.} \end{cases} \tag{8.12}$$

### 8.2.2 1DOF control structure

For the single-loop control structure presented in Figure 3.2, the variable $\mathcal{T}$ is a singleton $T$ and represents the sampling time used for implementing the controller $K(s)$. In order to find the suitable sampling time $T$, the following functionals will be considered:

(1) the similarity $\mathcal{S}_K^{\Omega}(T)$ between the continuous-time and the discrete-time representations of the controller $K(s)$ over the frequency range $\Omega = (0, \omega_N)$, along with the similarity $\mathcal{S}_{G_0}^{\Omega}(T)$ between the continuous and its discrete-time representation of the closed-loop system $G_0(s)$ as in (3.9), (3.11) over the same frequency range;

(2) the quantization implementation difficulty $\mathcal{I}_K(T)$ of the controller $K(s)$ along with the inverse of the sampling period $T$ in $\mathcal{W}(T)$, which manages to penalize the additional microprocessor load necessary to implement the same controller structure and prevents the attainment of a high-order discrete time delay $z^{-N}$, as $N = \left\lfloor \frac{\tau_m}{T} \right\rfloor$, for a given plant delay $\tau_m > 0$;

(3) the stability functional $\mathcal{J}_{\text{stab}(G_0)}(T)$ of the resulting numeric closed-loop system $G_{0,T}(z)$ from (3.11).

The first two terms from (1) are used to measure the fidelity between the desired system designed in the continuous-time domain and the resulting discrete-time system, considering the transient and steady-state

performance alterations. The next two terms from (2) encompass the implementation difficulty problem which implies that for a smaller $T$, the same number of software operations must be executed in a shorter time span and with a greater number of digits considered for quantization. As such, a trade-off between these two sets of performance indices must be established for the optimization problem. The last term (3) remains only a correction used to define the feasibility subdomain of $\mathcal{D}$.

Considering weights $c_1, c_2 \in \mathbb{R}_+$ for the fidelity measurement indices and $c_3, c_4 \in \mathbb{R}_+$ for the implementability indices, the final functional $\mathcal{J}^{\Omega} : \mathcal{D} \to \overline{\mathbb{R}}_+$, used to find the quasi-optimal sampling time can be defined as follows:

$$\mathcal{J}^{\Omega}(T) = c_1 \mathcal{S}_K^{\Omega}(T) + c_2 \mathcal{S}_{G_0}^{\Omega}(T) + c_3 \mathcal{I}_K(T) + c_4 \mathcal{W}_K(T) + \mathcal{J}_{\text{stab}(G_0)}(T). \tag{8.13}$$

**Remark 5.** *To numerically compute the integral terms from $\mathcal{J}^{\Omega}$, a discrete frequency set $\overline{\Omega} = \{\underline{\omega} = \omega_1 < \omega_2 < \cdots < \omega_N - \omega_\varepsilon = \overline{\omega}\}$ can be considered, with the similarity performance index approximated as follows:*

$$\mathcal{S}_G^{\overline{\Omega}}(T) \simeq \sum_{\omega \in \overline{\Omega}} \left(\overline{\sigma}\left(G(j\omega)\right) - \overline{\sigma}\left(G_T\left(e^{j\omega T}\right)\right)\right)^2 \Delta\omega, \tag{8.14}$$

*where $\omega_\varepsilon > 0$ is a predefined threshold used to avoid the prewarping phenomenon which appears in the magnitude response when $\omega \to \omega_N$.*

**Remark 6.** *Another issue for the implementation part consists in defining a value $\alpha_\infty$ sufficiently large such that the stability functional manages to keep the role of determining the feasibility subdomain of $\mathcal{D}$, leading to an approximation of the original performance index:*

$$\mathcal{J}_{stab(G)}^{\alpha_\infty}(T) = \begin{cases} +\alpha_\infty, \text{ if } G_T \text{ has unstable poles;} \\ 0, \text{ otherwise.} \end{cases} \tag{8.15}$$

As such, a numerically-implementable functional which encompasses all the functionals described above and manages to offer a trade-off between implementability and fidelity through coefficients $c_{\overline{1,4}}$ leads to the following non-convex optimization problem:

**Problem 7.** *Given an LTI plant model $G(s)$ of (2.4) with a specified continuous controller $K(s)$ as in (3.6), define an ordered pulsation set:*

$$\overline{\Omega} = (\underline{\omega} = \omega_1 < \omega_2 < \ldots < \omega_N - \omega_\varepsilon = \overline{\omega}) \subset (0, \infty). \tag{8.16}$$

*Then, the functional* $\mathcal{J}^{\overline{\Omega}} : \mathcal{D} \to \mathbb{R}_+$*:*

$$\mathcal{J}^{\overline{\Omega}}(T) = c_1 \mathcal{S}_K^{\overline{\Omega}}(T) + c_2 \mathcal{S}_{H_0}^{\overline{\Omega}}(T) + c_3 \mathcal{I}_K(T) + c_4 \mathcal{W}(T) + \mathcal{J}_{stab(H_0)}^{\alpha_\infty}(T), \quad (8.17)$$

*with weighting coefficients* $c_{\overline{1,4}} \in \mathbb{R}_+$ *leads to the following quasi-optimal sampling time optimization problem:*

$$\min_{T \in \mathcal{D}} \mathcal{J}^{\overline{\Omega}}(T). \quad (8.18)$$

### 8.2.3 2DOF control structure

In the case of the two-degrees-of-freedom control structure proposed in Figure 3.3, the following functionals will be considered to formulate the optimization problem to obtain the sampling rate $T$:

(1) two terms $\mathcal{S}_{K_{\text{in}}}^{\Omega}(T)$ and $\mathcal{S}_{K_{\text{ff}}}^{\Omega}(T)$ representing the similarity between the continuous-time and the discrete-time representations of the controllers $K_{\text{in}}(s)$ and $K_{\text{ff}}(s)$ from (3.12) and (3.13) over the frequency range $\Omega = (0, \omega_N)$;

(2) two terms $\mathcal{S}_{G_0^r}^{\Omega}(T)$ and $\mathcal{S}_{G_0^d}^{\Omega}(T)$ representing the similarity between the continuous-time (3.16) and discrete-time (3.18) representations of the resulting closed-loop systems $G_0^r(s)$ and $G_0^d(s)$ over the same frequency range;

(3) the quantization implementation difficulties $\mathcal{I}_{K_{\text{in}}}(T)$ and $\mathcal{I}_{K_{\text{ff}}}(T)$ of each controller along with the execution time functional $\mathcal{W}_K(T)$;

(4) the stability functional $\mathcal{J}_{\text{stab}(G_0^r)}(T)$ of the resulting numeric closed-loop system $G_{0,T}^r(z)$. A separate term for $G_0^d$ is redundant, as the internal stability of $G_0^r$ is equivalent to that of $G_0^d$.

The pairs of functionals from (1) and (2) are used to measure the fidelity between the components of the continuous-time designed system and the resulting components in the discrete-time domain, considering the transient and steady-state performance degradation. The next set of three terms from (3) manages to encompass the implementation difficulty arising in $K_{\text{in}}$ and $K_{\text{ff}}$. The last term (4) maintains its role as to encompass the feasibility subdomain of $\mathcal{D}$. As such, a trade-off between the terms (1)–(3) must be established by tacking into account the last feasibility term (4), resulting a non-convex optimization problem.

However, to increase the flexibility of the optimization problem, a set of weights $c_{\overline{1,7}} \in \mathbb{R}_+$ can be considered as follows: the weights $c_1$, $c_2$, $c_3$, $c_4$ are for the fidelity measurement indices, while weights $c_5$, $c_6$, $c_7$ are for the implementability indices, the final functional $\mathcal{J}^{\Omega} : \mathcal{D} \to \overline{\mathbb{R}}_+$ being:

$$\begin{aligned}\mathcal{J}^{\Omega}(T) = c_1\mathcal{S}^{\Omega}_{K_{\text{in}}}(T) + c_2\mathcal{S}^{\Omega}_{K_{\text{ff}}}(T) + c_3\mathcal{S}^{\Omega}_{G_0^r}(T) + c_4\mathcal{S}^{\Omega}_{G_0^d}(T) + \\ + c_5\mathcal{I}_{K_{\text{in}}}(T) + c_6\mathcal{I}_{K_{\text{ff}}}(T) + c_7\mathcal{W}(T) + \mathcal{J}_{\text{stab}(G_0^r)}(T).\end{aligned} \tag{8.19}$$

Moreover, considering the numeric approximations (8.14) and (8.15), the following numerically-implementable non-convex optimization problem follows:

**Problem 8.** *For an LTI plant model $G(s)$ with output disturbance dynamics $G_d(s)$ as in (3.15) included in a two-degrees-of-freedom control structure with the continuous-time inner controller $K_{in}(s)$ and feedforward controller $K_{ff}(s)$ as in Figure 3.3, define an ordered set of pulsations:*

$$\overline{\Omega} = (\underline{\omega} = \omega_1 < \omega_2 < \ldots < \omega_N - \omega_\varepsilon = \overline{\omega}) . \tag{8.20}$$

*Then, the functional $\mathcal{J}^{\overline{\Omega}} : \mathcal{D} \to \mathbb{R}_+$:*

$$\begin{aligned}\mathcal{J}^{\overline{\Omega}}(T) = c_1\mathcal{S}^{\overline{\Omega}}_{K_{in}}(T) + c_2\mathcal{S}^{\overline{\Omega}}_{K_{ff}}(T)c_3\mathcal{S}^{\overline{\Omega}}_{G_0^r}(T) + c_4\mathcal{S}^{\overline{\Omega}}_{G_0^d}(T) + \\ + c_5\mathcal{I}_{K_{in}}(T) + c_6\mathcal{I}_{K_{ff}}(T) + c_7\mathcal{W}(T) + \mathcal{J}^{\alpha_\infty}_{stab(G_0^r)}(T),\end{aligned} \tag{8.21}$$

*with weighting terms $c_{\overline{1,7}} \in \mathbb{R}_+$, leads to the following quasi-optimal sampling time optimization problem:*

$$\min_{T \in \mathcal{D}} \mathcal{J}^{\overline{\Omega}}(T) . \tag{8.22}$$

### 8.2.4 Cascade control structure

For the cascade control structure from Figure 3.4, the variable $\mathcal{T}$ contains the sampling time of the inner loop $T_{in} \equiv T$ and the integer factor $k$ which represents the proportionality factor between the sampling periods of the outer and the inner loop, respectively. To find the suitable such tuple $\mathcal{T} = (T, k)$, the following functionals will be considered in a similar manner to those defined for the single-loop and 2DOF cases:

(1) the similarities $\mathcal{S}^{\Omega}_{K_{in}}(T)$ and $\mathcal{S}^{\Omega}_{K_{out}}(T, k)$ between the continuous-time and the discrete-time representations of the controllers $K_{\text{in}}$ and

$K_{\text{out}}$ (3.19) involved in the proposed structure over the frequency range $\Omega = (0, \omega_N)$;

(2) the similarity functionals $\mathcal{S}^{\Omega}_{G_{0,\text{in}}}(T)$ and $\mathcal{S}^{\Omega}_{G_{0,\text{out}}}(T,k)$ between the continuous and the discrete representations of the inner and output closed-loop systems from (3.22) and (3.24), respectively, over $\Omega$;

(3) the quantization difficulty terms $\mathcal{I}_{K_{\text{in}}}(T)$ and $\mathcal{I}_{K_{\text{out}}}(T,k)$ of the controllers $K_{\text{in}}(s)$ and $K_{\text{out}}(s)$, respectively, along with the inverses of the inner sampling period $T$ and outer factor $k$, $\mathcal{W}(T)$ and $\mathcal{W}(k)$;

(4) the stability functionals of the resulting numeric closed-loop systems $\mathcal{J}_{\text{stab}(G_{0,\text{in}})}(T)$ and $\mathcal{J}_{\text{stab}(G_{0,\text{out}})}(T,k)$, with the closed-loop expressions obtained using formulas (3.22) and (3.24).

As mentioned in the previous two cases from Sections 8.2.2 and 8.2.3, the terms from (1) and (2) account for response fidelity between the desired systems designed in the continuous-time domain and the resulting discrete-time counterparts, considering the transient and steady-state performance degradation. The terms from (3) encompass the implementation difficulties, with the correction terms from (4) used to define the feasibility subdomain of $\mathcal{D}$.

Considering weights $c_{\overline{1,4}} \in \mathbb{R}_+$ for fidelity measurement indices and $c_{\overline{5,8}} \in \mathbb{R}_+$ for implementability metrics, a final functional $\mathcal{J}^{\Omega} : \mathcal{D} \to \overline{\mathbb{R}}_+$ which is used to find the quasi-optimal sampling time for the cascade control structure 3.4 can be defined as:

$$\begin{aligned}\mathcal{J}^{\Omega}(\mathcal{T}) = {} & c_1\mathcal{S}^{\Omega}_{K_{\text{in}}}(T) + c_2\mathcal{S}^{\Omega}_{K_{\text{out}}}(T,k) + c_3\mathcal{S}^{\Omega}_{G_{0,\text{in}}}(T) + \\ & + c_4\mathcal{S}^{\Omega}_{G_{0,\text{out}}}(T,k) + c_5\mathcal{I}_{K_{\text{in}}}(T) + c_6\mathcal{I}_{K_{\text{out}}}(T,k) + \\ & + c_7\mathcal{W}(T) + c_8\mathcal{W}(k) + \mathcal{J}_{\text{stab}(G_{0,\text{in}})}(T) + \mathcal{J}_{\text{stab}(G_{0,\text{out}})}(T,k).\end{aligned} \tag{8.23}$$

After taking into account the approximations (8.14), (8.15), the equivalent numerically-implementable optimization problem becomes:

**Problem 9.** *For an LTI plant model containing the inner faster dynamics $G_{in}(s)$ and the outer slower dynamics $G_{out}(s)$ with specified continuous-time controllers $K_{in}(s)$ and $K_{out}(s)$ as in (3.19), define an ordered pulsation set:*

$$\overline{\Omega} = (\underline{\omega} = \omega_1 < \omega_2 < \ldots < \omega_N - \omega_\varepsilon = \overline{\omega}). \tag{8.24}$$

*Then, the functional* $\mathcal{J}^{\overline{\Omega}} : \mathcal{D} \to \mathbb{R}_+$*:*

$$\begin{aligned}\mathcal{J}^{\overline{\Omega}}(\mathcal{T}) =& c_1 \mathcal{S}^{\overline{\Omega}}_{K_{in}}(T) + c_2 \mathcal{S}^{\overline{\Omega}}_{K_{out}}(\mathcal{T}) + c_3 \mathcal{S}^{\overline{\Omega}}_{G_{0,in}}(T) + \\ & c_4 \mathcal{S}^{\overline{\Omega}}_{G_{0,out}}(\mathcal{T}) + c_5 \mathcal{I}_{K_{in}}(T) + c_6 \mathcal{I}_{K_{out}}(\mathcal{T}) + \\ & c_7 \mathcal{W}(T) + c_8 \mathcal{W}(k) + \mathcal{J}^{\alpha_\infty}_{stab(G_{0,in})}(T) + \mathcal{J}^{\alpha_\infty}_{stab(G_{0,out})}(\mathcal{T}),\end{aligned} \tag{8.25}$$

*with weighting terms* $c_{\overline{1,8}} \in \mathbb{R}_+$*, leads to the following quasi-optimal sampling time optimization problem:*

$$\min_{\mathcal{T} \equiv (T,k) \in \mathcal{D}} \mathcal{J}^{\overline{\Omega}}(\mathcal{T}) \,. \tag{8.26}$$

**Remark 7.** *By retaining only the coefficients* $c_i > 0$*,* $i = \overline{1,4}$ *with the remaining values set to* $c_{\overline{5,8}} = 0$*, one obtains the sampling rate solution which models the behaviour of the continuous-time regulators in the best possible manner, while the opposite situation gives the largest possible magnitudes for* $T$ *and* $k$ *such that the closed-loop system remains stable, through expressions* (8.23) *and* (8.25) *seen as minimization problems with feasibility constraints* $\mathcal{J}_{stab(G_{0,in})}$ *and* $\mathcal{J}_{stab(G_{0,out})}$*. As a rule of thumb, experiments proved that selecting the coefficients by two orders of magnitude apart, a strong emphasis may be induced on the fidelity or implementability behaviours, while maintaining all coefficients* $c_{\overline{1,8}}$ *in the same range will provide a good trade-off between both qualities.*

## 8.3 Metaheuristic optimization solution

Furthermore, a metaheuristic approach is described to solve the optimization problems 7, 8 and 9 detailed in the previous section, which are non-convex due to their component behaviours. However, in order to emphasize the integer constraints imposed on the second variable, a solution for Problem 9 will be presented only, with Problems 7 and 8 seen as particular cases. As such, consider the following mixed domain:

$$\mathcal{D} = \left[\underline{T}, \overline{T}\right] \times \left\{\underline{k} \equiv 1, 2, \ldots, \overline{k}\right\}, \tag{8.27}$$

with the general multi-rate cascade case emphasized through Problem 9, whose solution is the optimal value of the sampling time $T^\star$ used for the inner loop and the optimal value of the proportionality factor between the outer loop's and inner loop's sampling period $k^\star$ according to the

prescribed importance of each functional given by the coefficients $c_{\overline{1,7}}$.

A means to find the near-optimal solution is using a meta-heuristic approach. For the purpose of this paper, we implemented a mixed-integer version of the artificial bee colony (ABC) optimization, starting from [KB07; Aka+21]. This algorithm mimics the behaviour of real honeybees, having three categories: employed, onlooker and scout bees. The numbers of employed bees and onlooker bees are the same and represent the swarm problem's dimension, denoted $\mathcal{N}$ in our case. The position of the $i$th employed bee at iteration $j$ is represented by $\mathbf{p}_i^{(j)} \in \mathcal{D}$.

The initial position of each employed bee is randomly selected from the feasible domain $\mathcal{D}$:

$$\mathbf{p}_i^{(0)} = \begin{pmatrix} \underline{T} + \phi_{i,1}^{(0)} \cdot (\overline{T} - \underline{T}) \\ \left\lceil \underline{k} + \phi_{i,2}^{(0)} \cdot (\overline{k} - \underline{k}) \right\rfloor \end{pmatrix} \in \mathcal{D}, \tag{8.28}$$

where $\lceil \cdot \rfloor$ is the round function and $\phi_{i,\overline{1,2}}^{(0)} \in [0,1]$ are random numbers. After such an initialization step is performed, a new possible position for each employed bee can be computed using the current location $\mathbf{p}_i^{(k)}$ and a randomly selected position $\mathbf{p}_{\mathbf{j}}^{(\mathbf{k})}$ using:

$$\overline{\mathbf{p}}_i^{(k)} = \begin{pmatrix} \texttt{sat}\left(\mathbf{p}_i^{(k)}[0] + \phi_{i,1}^{(k)}\left(\mathbf{p}_i^{(k)}[0] - \mathbf{p}_j^{(k)}[0]\right)\right) \\ \texttt{sat}\left(\left\lceil \mathbf{p}_i^{(k)}[1] + \phi_{i,2}^{(k)}\left(\mathbf{p}_i^{(k)}[1] - \mathbf{p}_j^{(k)}[1]\right)\right\rfloor\right) \end{pmatrix}, \tag{8.29}$$

where $\phi_{i,\overline{1,2}}^{(k)} \in [-1,1]^2$ are random numbers and $\texttt{sat}$ is the classical saturation function which maintains the position in the feasible domain $\mathcal{D}$. Based on the current position and on the next possible position, the next employed bee position is:

$$\mathbf{p}_i^{(k+1)} = \arg\min\left\{\mathcal{J}\left(\mathbf{p}_i^{(k)}\right), \mathcal{J}\left(\overline{\mathbf{p}}_i^{(k)}\right)\right\}. \tag{8.30}$$

If the next position coincides with the current position, the $i$th employed bee's abandonment counter increases, otherwise it is reset to zero.

Based on the information provided by all employed bees, the onlooker bees search another location using the fitness values $f(i)$ of the

positions $\mathbf{p}_i^k$ given by:

$$\log f(i) = -\frac{\mathcal{J}\left(\mathbf{p}_i^{(k)}\right)}{\frac{1}{N}\sum_j \mathcal{J}\left(\mathbf{p}_j^{(k)}\right)}, \tag{8.31}$$

which are then normalized in order to obtain a probability distribution:

$$\rho_i = \frac{f(i)}{\sum_j f(j)}. \tag{8.32}$$

This probability distribution is fed into a roulette wheel selection mechanism and, for each onlooker bee, a position $\mathbf{p}_i^{(k)}$ is selected. Using the same mechanism as in relation (8.30), the position of each onlooker bee is computed. If an onlooker bee finds a better solution than an employed bee, then they exchange their roles or, otherwise, the abandonment counter for the $i$th employed bee increases.

If the abandonment counter for a specific employed bee exceeds a predefined threshold, such an employed bee becomes a scout bee and a new initialization as in (8.28) is performed. Moreover, to avoid searching in an area of domain $\mathcal{D}$ where the cost function $\mathcal{J}$ indicates that the inner or the outer closed-loop system is unstable, the $i$th employed bee directly becomes scout bee if $\mathcal{J}\left(\mathbf{p}_i^{(k)}\right) \geq \alpha_\infty$.

After a cycle employed-onlooker-scout bee is performed, the best solution found in this stage is compered with the old best solution and, if no improvement is found, the NO_IMPROVE counter increases, otherwise it is reset. As stopping criteria we check if NO_IMPROVE counter exceeds a predefined threshold or a predefined maximum number of steps have been performed.

**Remark 8.** *To solve Problem 9, the same approach can be used by eliminating the second dimension and the non-convex continuous-domain problem can be solved using the classical ABC optimization technique.*

## 8.4 Conclusions

Several comparisons are performed relative to the well-established approaches for sampling rate selection based on a number of variations on the Shannon-Nyquist theorem, along with variations on the closed-loop bandwidth approach. Such examples are presented in sections 11.3 and

11.7.2, with emphasis on the construction of the proposed functionals and their practical implications.

The provided optimization problems become useful in cases where the preconditions of the Shannon-Nyquist sampling theorem are difficult to assess, such as when the traditional approach leads to unfeasible sampling times as of $T \ll$, which was found to be the case for the second example due to time delays, when it is unclear in distinguishing the relevant controller poles or the process poles are not entirely correlated to the regulator dynamics. It also allows to assess the possibility of considering a higher sampling period in the outer loop, fact not accounted for with the traditional approaches. The method permits to assess percentage improvements for a set of desired metrics, which can round up to an order of magnitude compared to classical recommended sampling rate values, while still maintaining acceptable performances in an industrial context.

A further extension of the method would be to formulate and solve a similar problem in an online manner and in real-time, which would prove to be useful in the case of LPV and LTV systems, alongside the domain of adaptive systems. In the context of rapid control prototyping, an additional analysis regarding the loss of controllability and observability of the physical process should be performed, along with further studying the convexity of the problem, as it is relevant in hardware-in-the-loop simulations and testing.

# 9. Quantization analysis

## 9.1 Transient response analysis

**Remark 9.** *For this section, the sampling period will be denoted $\tau$ instead of $T$, alongside the quantization step $q$, for a more compact notation. The two-dimensional optimization variable will be written as $\xi = (\tau, q) \in \mathbb{R}_+^2$. Regarding system frequency responses, for the continuous case, the transfer matrices will be implicitly evaluated at $j\omega$, i.e. $\{G, P, K\}|_{j\omega}$, while their discrete counterparts will be evaluated at $e^{j\omega\tau}$: $\left\{\widetilde{G}, \widetilde{P}, \widetilde{K}\right\}\Big|_{e^{j\omega\tau}}$.*

### 9.1.1 Motivation and contributions

The present results are published in the conference paper [ȘMD23a]. The inherent problem with continuous-time robust control synthesis is that it returns a controller which cannot directly be implemented on a numeric device. Discrete-time robust control synthesis does not fully solve this problem, as the sampling rate is considered as an input hyperparameter, without explicitly performing a selection, and the quantization of the controller coefficients is not encompassed in the synthesis procedure. The aim is to provide rigorous means to efficiently compute the sampling rate and quantization step for a given continuous regulator in order to maintain the RS and RP specifications guaranteed in the analog domain, assuming a constant rate and fixed-point arithmetic, using the structured singular value framework and global optimization techniques. The motivation of this section is given by the following problems related to discretization and quantization, starting from a satisfactory continuous-time designed controller, i.e. which fulfills RS and RP:

(1) the selection of the sampling rate and discretization method may lead to stability losses for initially stable open-loop process models,

in addition to destabilizing the closed-loop control system through an inadequate numeric regulator;

(2) discretization may lead to the loss of controllability for the process model [Kre99], [Liu+22], which is an inherent problem in the case of Hardware-in-the-Loop (HiL) simulators, where testing a control law on hardware mimicking the real process can lead to discrepancies between the properties of the continuous-time system and its discrete-time counterpart;

(3) quantization effects are usually studied for the nominal model, not on the entire uncertainty family.

The main contributions from this section are to:

(i) provide a joint optimization approach for the sampling rate and quantization step while ensuring RS and RP through the structured singular value framework;

(ii) present an approach to reuse the mathematical models of the augmented plant developed in the continuous domain to the discrete domain also, without affecting its conservativeness;

(iii) describe an approach to assert the quality of a sampling rate and quantization step pair through the sensitivity analysis of its vicinity in the searching space using the condition number.

### 9.1.2 Proposed method

The regulator $K$ can be synthesized in either the unstructured state-space form, as considered in [ZDG96], or using a fixed-structure forms, through the nonsmooth optimization approach of [AN17]. Either approach can be considered for the next section, as long it allows a (possibly sparse) state-space representation.

Consider a continuous-time generalized plant model $P$ as in (3.33), with its nominal process $G_n = (A, B_u, C_y, D_{yu})$ of (3.31) and uncertainty blocks $\Delta \in \mathbf{\Delta}$ having the structure of (3.29).

Recall the notations for the uncertain plant model $\mathcal{T}$ and $\mathcal{A}$ from (3.34) and (3.35). Furthermore, consider that the pair $(A, B_u)$ is stabilizable and the pair $(C_y, A)$ is detectable, assumptions necessary for the existence of a stabilizing controller $K$ [LY16]. As such, consider a stabilizing regulator $K = (A_K, B_K, C_K, D_K)$ with signal dimensions $(n_y, n_K, n_u)$, which further manages to fulfill the RS and RP specifications for $P$ considering the uncertainty dynamics $U$, blocks $\Delta \in \mathbf{\Delta}$ and specifications $W$.

The numeric regulator $\widetilde{K}$ is obtained through sampling with a fixed period $\tau \in \mathbb{R}_+$, followed by a discretization of $K$ and, finally, by a quantization of its coefficients with a fixed step $q \in \mathbb{R}_+$. Denoting $\xi = (\tau, q) \in \mathbb{R}_+^2$, we have:

$$\widetilde{K}_q = \mathcal{Q}\left\{\mathcal{D}\left\{K, \tau\right\}, q\right\} = \mathcal{Q}\left\{\widetilde{K}, q\right\}, \tag{9.1}$$

assuming an arbitrary discretization operator $\mathcal{D} : \mathcal{G} \to \mathcal{G}_D$ such as Tustin, forward Euler etc., and a quantization operator $\mathcal{Q} : \mathcal{G}_D \to \mathcal{G}_D$, which applies a quantization with step $q$ to each coefficient of $\widetilde{K}(z)$, leading to:

$$\widetilde{K}_q = \left(q\left\lfloor\frac{A_d}{q}\right\rceil, q\left\lfloor\frac{B_d}{q}\right\rceil, q\left\lfloor\frac{C_d}{q}\right\rceil, q\left\lfloor\frac{D_d}{q}\right\rceil\right), \tag{9.2}$$

described by the matrices $(A_d, B_d, C_d, D_d)$ obtained through $\mathcal{D}\left\{K, \tau\right\}$ of (9.1), and with the rounding operator $\lfloor\cdot\rceil$, applied element-wise to its matrix inputs.

To obtain the discrete-time uncertainty model may be unfeasible if the continuous-time model has been experimentally deduced [HSB02] or it can be deduced with the problem that it is not isomorphic to the continuous-time model, being computed in a different manner. An auxiliary result is that the discretization procedure with the period $\tau$ can also applied to $G_n \mapsto \widetilde{G}_n$, $U \mapsto \widetilde{U}$, $W \mapsto \widetilde{W}$, leading to the augmented plant $P \mapsto \widetilde{P}$ as in Figure 3.7–b), maintaining the mappings $\mathcal{T}$, $\mathcal{A}$ from (3.34), (3.35), possible according to the following lemma.

**Lemma 5.** *Given the continuous models $G_n$, $U$, $W$, $P$ and mappings $\mathcal{T}(\cdot,\cdot)$, $\mathcal{A}(\cdot,\cdot)$ from (3.34) and (3.35), the discrete augmented plant counterpart $\widetilde{P}$ can be computed based on the discretization of its individual components $\widetilde{G}_n$, $\widetilde{U}$, $\widetilde{W}$ through $\mathcal{D}\left\{\cdot, \tau\right\}$, $\tau > 0$. Moreover, the block $\boldsymbol{\Delta}$ is invariant from the continuous domain to the discrete domain. As such:*

$$\widetilde{G} = \mathcal{T}\left(\mathcal{D}\left\{G_n, \tau\right\}, \mathcal{D}\left\{U, \tau\right\}\right), \ \Delta \in \boldsymbol{\Delta}; \tag{9.3}$$

$$\widetilde{P} = \mathcal{D}\left\{P, \tau\right\} = \mathcal{A}\left(\widetilde{G}, \mathcal{D}\left\{W, \tau\right\}\right). \tag{9.4}$$

*Proof.* The operators $\mathcal{T}$ and $\mathcal{D}$ are not commutative, so the order of their application is relevant. If the nominal process $G_n$ and the uncertainties $U$ are discretized separately, then the physical significance of the signals presented in Figure 3.6–a) are also maintained for the case in Figure

3.6–b), thus resulting an isomorphic representation between $G$ and $\widetilde{G}$. Moreover, considering that $\mathbf{\Delta}$ contains only matrices from $\mathbb{C}^{k\times k}$, the block $\mathbf{\Delta}$ is invariant after applying $\mathcal{T}\circ\mathcal{D}$.

In a similar manner, the operators $\mathcal{A}$ and $\mathcal{D}$ are not commutative, and, to keep the physical significance of each signal involved in the augmentation step, the uncertain process $\widetilde{G}$ should be obtained separately from $\widetilde{W}$, the resulting discrete-time uncertain augmented plant being:

$$\widetilde{P} = \mathcal{A}\left(\mathcal{T}\left(\mathcal{D}\left\{G_n,\tau\right\},\mathcal{D}\left\{U,\tau\right\}\right),\mathcal{D}\left\{W,\tau\right\}\right). \tag{9.5}$$

□

With the previously-defined models $\widetilde{P}$ and $\widetilde{K}_q$, the evaluation of the structured singular value needs to be adapted for the discrete-time case in the following manner:

$$\mu_{\mathbf{\Delta}}(LLFT(\widetilde{P},\widetilde{K}_q)) = \sup_{\omega\in\Omega_N} \frac{1}{\min\limits_{\Delta\in\mathbf{\Delta}}\{\overline{\sigma}(\Delta), \det(I-\widetilde{M}_\omega\Delta)=0\}}, \tag{9.6}$$

with $\widetilde{M}_\omega = LLFT(\widetilde{P},\widetilde{K}_q)(e^{j\omega\tau})$ and domain $\Omega_N = [0,\omega_N)$, where $\omega_N = \pi/\tau$ is the Nyquist frequency for the period $\tau$.

Given that the augmented plant model $P$ encompasses the desired transient and steady-state specifications through the corresponding weighting function $W$, specifications ensured through the existence of $K$, a practical approach to obtain the sampling period $\tau$ and quantization step $q$, emphasizing the regulator's implementability on a numeric device, is by solving the following nonlinear optimization problem.

**Problem 10.** *Given a generalized plant model $P$ as in (3.33) with its corresponding regulator $K$, with the mechanisms to deduce the discrete-time equivalent $\widetilde{P}$ of (9.4) and $\widetilde{K}_q$ as in (9.1) and (9.2), the implementability optimization problem for computing the pair $\xi = (\tau, q) = (\xi_1, \xi_2)$ is defined as:*

$$\max_{\xi\in\mathbb{R}^2_+} \xi_1\cdot\xi_2 \quad s.t. \quad \mu_{\mathbf{\Delta}}(LLFT(\widetilde{P},\widetilde{K}_q)) < 1. \tag{9.7}$$

The expression (9.7) can be reformulated as a minimization problem without constraints using the interior point method, by employing a

logarithmic barrier term [Nes10] as $F_1 : \mathbb{R}_+^2 \to \overline{\mathbb{R}}$:

$$F_1(\xi) = -\xi_1 \cdot \xi_2 - \rho \ln\left(1 - \mu_\Delta(LLFT(\widetilde{P}, \widetilde{K}_q))\right), \ \rho > 0, \tag{9.8}$$

assuming $F_1(\xi) = \infty$ for $\xi$ where the logarithm is undefined.

The characteristics of the uncertainty weights $\widetilde{U}$ and performance filters $\widetilde{W}$ may be affected by the discretization process. To ensure that, through sampling and discretization, the above functional's solution does not lead to a controller $\widetilde{K}_q$ which fulfills the RS and RP properties for a "different" system, in case of high precision applications, where the hardware constraints of the numeric device are not the main shortcoming, a new optimization problem is proposed.

**Problem 11.** *Given a generalized plant model $P$ as in (3.33), its corresponding regulator $K$, with the mechanisms to deduce the discrete-time equivalent $\widetilde{P}$ from (9.4) and $\widetilde{K}_q$ as in (9.1), (9.2), the fidelity optimization problem for computing $\xi = (\tau, q)$ with minimum performance loss is defined as:*

$$\min_{\xi \in \mathbb{R}_+^2} \mathcal{I}(\xi) \quad s.t. \quad \mu_{\boldsymbol{\Delta}}(LLFT(\widetilde{P}, \widetilde{K}_q)) < 1, \tag{9.9}$$

*with the controller similarity integral defined over a frequency range $\Omega \subset [0, \omega_N]$ depending on the variable $\tau$:*

$$\mathcal{I}(\xi) = \int_\Omega \left|\overline{\sigma}(K) - \overline{\sigma}(\widetilde{K}_q)\right| \left(1 + \left\|\nabla^2 K\right\|\right) d\omega, \tag{9.10}$$

*with the Hessian of the controller's frequency response:*

$$\nabla^2 K(j\omega) = \frac{\partial^2}{\partial \omega^2}\left(K(j\omega)\right). \tag{9.11}$$

*Assuming a transfer matrix representation $[K_{ji}]_{\substack{1 \le i \le n_y \\ 1 \le j \le n_u}}$, for an arbitrary SISO component $K_{ji}(s) = \frac{\beta(s)}{\alpha(s)}$, it results that:*

$$\nabla^2 K(j\omega) = \left(\frac{\alpha\beta'' - 2\alpha'\beta' - \alpha''\beta}{\alpha^2} + \frac{2\beta\alpha'^2}{\alpha^3}\right)\Bigg|_{j\omega}. \tag{9.12}$$

*The expression (9.9) can be reformulated as a minimization problem without constraints using the interior point method, by employing a*

*logarithmic barrier term [Nes10] as* $F_2 : \mathbb{R}_+^2 \to \overline{\mathbb{R}}$*:*

$$F_2(\xi) = \mathcal{I}(\xi) - \rho \ln\Big(1 - \mu_{\Delta}(LLFT(\widetilde{P}, \widetilde{K}_q))\Big), \ \rho > 0, \tag{9.13}$$

*assuming* $F_2(\xi) = \infty$ *for* $\xi$ *where the logarithm is undefined.*

**Remark 10.** *In the frequency response of* $\widetilde{K}_q$*, as* $\omega$ *reaches the Nyquist frequency* $\omega_N$*, a prewarping phenomenon ensues in its magnitude and phase characteristics, which may be minimized by performing the integration up to a smaller upper limit. As such, the set* $\Omega$ *can be replaced in practice by* $\Omega \cap (0, \omega_N - \omega_\varepsilon]$*, for a prespecified threshold* $\omega_\varepsilon > 0$*.*

The procedure to sample and quantize the regulator by maintaining RS and RP in discrete-time domain, as a summary of the current section, is presented in Algorithm 1.

**Algorithm 1:** Optimal selection of sampling rate and quantization step for a continuous-time regulator $K$

**Input:** $K$, $G_n$, $U$, $W$, $\mathcal{T}$, $\mathcal{A}$, $\mathbf{\Delta}$, $F \in \{F_1, F_2\}$, $\Omega$, $\rho$
Discretization operators $\mathcal{D}_p\{\cdot, \tau\}$, $\mathcal{D}_c\{\cdot, \tau\}$.
{For the plant and controller models}
Solver algorithm $\xi_{k+1} = \Sigma(F, \xi_k)$.

**Output:** Optimum $\xi^\star = (\tau^\star, q^\star) \in \mathbb{R}_+^2$.

Initialize $\xi \leftarrow \xi_0 = (\tau_0, q_0) \in \mathbb{R}_+^2$.
**while** *stopping criterion is not satisfied* **do**
  $\widetilde{G}_n \leftarrow \mathcal{D}_c\{G_n, \xi_1\}$.
  $\widetilde{U} \leftarrow \mathcal{D}_c\{U, \xi_1\}$; $\widetilde{W} \leftarrow \mathcal{D}_c\{W, \xi_1\}$.
  $\widetilde{G} \leftarrow \mathcal{T}\left\{\widetilde{G}_n, \widetilde{U}\right\}$; $\widetilde{P} \leftarrow \mathcal{A}\left\{\widetilde{G}, \widetilde{W}\right\}$ {Lemma 5}.
  $\widetilde{K}_q \leftarrow \mathcal{Q}\{\mathcal{D}\{K, \xi_1\}, \xi_2\}$ {Eq. (9.1), (9.2)}.
  Compute $\mu_{\mathbf{\Delta}}\left(\mathrm{LLFT}\left(\widetilde{P}, \widetilde{K}_q\right)\right)$ approximation.
  Compute $F(\xi)$ {Eq. (9.8) or (9.13)}.
  Update $\xi \leftarrow \Sigma(F, \xi)$.
  Verify stopping criterion.
**end**

Without asserting on the continuity, differentiability and smoothness properties of $F_1$ and $F_2$, in particular to the peak structured singular

value logarithmic barrier term, consider the relative condition number [Hig02], denoting $F \in \{F_1, F_2\}$:

$$\kappa_F(\xi) = \lim_{\varepsilon \to 0} \sup_{\|\delta\xi\| \leq \varepsilon} \frac{\|F(\xi + \delta\xi) - F(\xi)\| / \|\delta\xi\|}{\|F(\xi)\| / \|\xi\|}, \tag{9.14}$$

along with the two-dimensional ellipse $\mathcal{E} : \mathbb{R}^2_+ \times \mathbb{R}^2_+ \to \mathbb{R}^2_+$:

$$\mathcal{E}(\xi, \delta\xi) = \left\{ x \in \mathbb{R}^2_+ \;\middle|\; \frac{|\xi_1 - x_1|^2}{\delta\xi_1^2} + \frac{|\xi_2 - x_2|^2}{\delta\xi_2^2} < 1 \right\}. \tag{9.15}$$

To assert the quality and, ultimately, validate the solutions obtained through optimization, a sufficiently high resilience of the condition number with respect to variations around a given nominal value is desired. As such, define for each feasible point $\xi = (\tau, q)$ a *least guaranteed sensitivity bound* $N_F : \mathbb{R}^2_+ \to \mathbb{R}$ for which the relative condition number $\kappa_F$ remains finite for all points in the encompassing ellipse:

$$N_F(\xi) = \inf_{\varepsilon > 0} \{\kappa_F(x) \in \mathbb{R} \mid \forall x \in \mathcal{E}(\xi, \delta\xi), \; \|\delta\xi\| < \varepsilon\}, \tag{9.16}$$

and otherwise, for unfeasible points, defined as zero.

### 9.1.3 Conclusions

The current analysis presented a set of mathematical tools to quantify the influence of a constant sampling rate and a fixed-point quantization scheme for the transient response of continuous-time uncertain plant models, by retaining the same modelling framework from the continuous to the discrete domain and maintaining the desired robust stability and performance according to the initially-provided specifications.

The selection of a smaller $(\tau, q)$ pair does not ensure better performance for the closed-loop system, as will be shown in section 11.4 with the aid of the sensitivity bound defined in (9.16). The dichotomic approach of the two proposed optimization problems allows a wide range of means to impose a compromise between fidelity and implementability based on the available hardware of the numeric regulator. A regularization term may be preferred for the fidelity problem to counteract solutions to extreme areas in the domain.

The proposed framework has also been successfully applied to the

robust controller synthesis for the class of singularly perturbed systems, as reported in [Şuş+24b], further illustrating its applicability beyond the examples considered in the present chapter.

## 9.2 Steady-state response analysis

The present results are published in the conference paper [ŞMD22]. This section proposes a set of theoretical results regarding the closed-loop control of continuous LTI physical processes using fixed-point discrete-time LTI regulators, interfaced using uniform data converters, by providing necessary and sufficient conditions to quantify the closed-loop stability up to a worst-case computable bound. Furthermore, in [Şuş+26], two other theoretical contributions are provided. On one hand, it presents a generalization of the previous worst-case bound for the quantization error using uniform fixed-point data encoding, without assumptions on the diagonalizability of the closed-loop state matrix. On the other hand, a set of design problems for the numeric regulator are formulated to compute a least conservative quantization error bound without affecting its desired transient response. Some approaches to solve said problems are described, with sufficient conditions provided by a simplified formulation.

**Remark 11.** *In this section, the symbol $\mathcal{R}$ is used as a label for sets of real numbers, while $\mathcal{F}$ denotes their fixed-point equivalent encodings. Similarly, real variables will be denoted $x$, $X$, while their fixed-point equivalents will become $\widetilde{x}$, $\widetilde{X}$. Denote $\lceil x \rceil_{\varepsilon>0} = \min\limits_{\varepsilon>0} \lceil x \cdot (1+\varepsilon) \rceil$.*

### 9.2.1 Motivation and contributions

The motivation for this paper was caused by the results developed in [PS03], where a set of conditions for limit cycle cancelling using describing functions is presented. Another case studied in [Pen+07] deals with the quantization error bound estimation and limit cycle cancellation for a particular structure of the controller. However, none of these papers treat the general LTI controller case in order to offer a tight upper quantization error bound.

The background of the developed analysis assumes a discretized plant model analyzed as necessary in rapid control prototyping (RCP) environments, with the scope of implementing the LTI control law in C/C++ source code production environments. The purpose of the study

is to provide general results as required in an RCP context, by deducing hard bounds for the controller signals, along with optimal selection of interfacing circuits which can guarantee the initially-designed continuous-time performances up to a predefined tolerance. The quantization problem is treated ad hoc for each individual control problem, but it is of general concern in cases where the regulators have high order.

Innovations concern:

(i) the fixed-point encoding of controller coefficients and interfacing circuits such that saturation operations will never occur during computations, where theoretically achievable;

(ii) obtaining of best approximation of the ideal discrete-time regulator based on the previously-designed word lengths, with the least influence on the transient response;

(iii) computation of an analytical solution for the worst-case steady-state bound of the limit cycles caused by quantization noise, in a unified manner, irrespective of the type of quantizer used, namely midtread and midriser.

### 9.2.2 Proposed method

Denote an ideal numeric controller $K(z)$ and its quantized correspondent $K_q(z)$, obtained using an arbitrary discretization method, in series with a nominal plant model $G(z)$, discretized through the zero-order hold method, in order to allow the interface with the numeric controller. Further results will be provided for $K_q(z)$, which retains the physical significance of $K(z)$, i.e. it has the same coefficient ranges, described with additional block sets, as in Definition 6, of:

- $n_u$ ADCs: $\mathcal{S}_e = (\mathcal{D}_u = [-R_u, R_u]^{n_u}, L_u, T_u) \mapsto Q_u$;
- $n_y$ DACs: $\mathcal{S}_u = (\mathcal{D}_y = [-R_y, R_y]^{n_y}, L_y, T_y) \mapsto Q_y$;
- $n_x + n_y$ quantizers for the state and output equations:

$$\mathcal{S}_x = \left(\mathcal{D}_x = [-R_x, R_x]^{n_x+n_y}, L_x, T_x\right) \mapsto Q_x,$$

with the configurable values $R_x > 0$, $L_x \in \mathbb{N}_+$ depending on the deployment microprocessor specifications.

**Definition 11.** *Let $K(z)$ be an ideal MIMO LTI controller with interface $(e, x_c, u)$, described in state-space form by:*

$$(K(z)) : \begin{cases} x_c[k{+}1] & = A_1 x_c[k] + B_1 e[k]; \\ u[k] & = C_1 x_c[k] + D_1 e[k]. \end{cases} \tag{9.17}$$

*A quantized controller $K_q(z)$ with quantizer structures $\mathcal{S}_e, \mathcal{S}_x, \mathcal{S}_u$ can be defined as:*

$$(K_q(z)) : \begin{cases} \overline{e}[k] & = Q_u\left(e[k]\right); \\ x_c[k{+}1] & = Q_x\left(A_1 x_c[k] + B_1 \overline{e}[k]\right); \\ \overline{u}[k] & = Q_x\left(C_1 x_c[k] + D_1 \overline{e}[k]\right); \\ u[k] & = Q_y\left(\overline{u}[k]\right). \end{cases} \tag{9.18}$$

Given $N_u = \max|\mathcal{D}_u| = R_u \in \mathbb{R}_+$, based on the $\mathcal{H}_\infty$ norm of the input-state and input-output subsystems, the following bounds hold:

$$H_x = \|(A_1, B_1,\ I, O)\|_\infty \in \overline{\mathbb{R}}_+; \tag{9.19}$$

$$H_y = \|(A_1, B_1, C_1, D_1)\|_\infty \in \overline{\mathbb{R}}_+. \tag{9.20}$$

Then, based on the definition of the $\mathcal{H}_\infty$ norm, the following dynamic range upper bounds, possibly infinite, will be obtained for the state and output signals, $x_c[k]$ and $u[k]$:

$$\sup_{k\geq 0} x_c[k] = N_x = H_x \cdot N_u \in \overline{\mathbb{R}}_+; \tag{9.21}$$

$$\sup_{k\geq 0} u[k] = N_y = H_y \cdot N_u \in \overline{\mathbb{R}}_+. \tag{9.22}$$

**Lemma 6.** *For a MIMO quantized LTI controller $K_q(z)$ having $H_x, H_y \in \mathbb{R}_+$, the state and output internal variables, encoded using fixed-point two's complement representation, will fit in a word length of size $L_x \in \mathbb{N}_+$ bits, defined as:*

$$L_x \geq L_u + \max\left(\lceil \log_2 H_x \rceil_{\varepsilon>0}, \lceil \log_2 H_y \rceil_{\varepsilon>0}, 0\right). \tag{9.23}$$

*Proof.* The word length $L_u$ encompasses the input domain $\mathcal{D}_u$ mapped to $\mathcal{D}^{\mathcal{F}}(L_u)$ after encoding, with bound $\widetilde{N}_u \leq 2^{L_u - 1}$. Using (9.21), the

upper bound $\widetilde{N}_x$ of the encoded state variable becomes:

$$\widetilde{N}_x = H_x \cdot \widetilde{N}_u \leq H_x \cdot 2^{L_u - 1},$$

while $\widetilde{N}_x$ must be covered by a word length $L_x$, implying:

$$H_x < \frac{2^{L_x - 1}}{2^{L_u - 1}} = 2^{L_x - L_u}. \tag{9.24}$$

In an analogous manner, the bound (9.22) leads to:

$$H_y < \frac{2^{L_x - 1}}{2^{L_u - 1}} = 2^{L_x - L_u}. \tag{9.25}$$

Gathering relations (9.24), (9.25), and considering $L_x \geq L_u$, the constraint for $L_x$ can be formulated as stated in (9.23).

□

**Lemma 7.** *Consider a quantized controller $K_q(z)$ as in (9.18), with the signal word length $L_x$ subject to the conditions of Lemma 6. Then, the optimal quantization for matrices $(A_1, B_1, C_1, D_1)$ such that the internal computations do not enter saturation can be found as:*

$$(A_q, B_q, C_q, D_q) = Q_\delta \left(A_1, B_1, C_1, D_1\right), \tag{9.26}$$

*with $\delta = \frac{1}{2^d}$, $d = L_x - f - 1 > 0$ and the least upper bound:*

$$f = \left\lceil \log_2 \left( \max \left\{ |a_{ij}|, |b_{ij}|, |c_{ij}|, |d_{ij}| \right\} \right) \right\rceil_{\varepsilon > 0}. \tag{9.27}$$

*Proof.* The objective is to compute the optimal scaling which obtains the best achievable precision while also allowing the largest controller coefficient to fit into the required word length $L_x$. As such, consider a partition of $L_x$ into its sign, dynamic range and decimal bits, respectively, $L_x = 1 + f + d$. The dynamic range bits $f$ must allow:

$$\inf_{\varepsilon > 0} \left\{ (1 + \varepsilon) \cdot \max \left\{ |a_{ij}|, |b_{ij}|, |c_{ij}|, |d_{ij}| \right\} \right\} < 2^f, \tag{9.28}$$

providing the remaining $d$ bits for extra decimal places.

□

In the following discussion, an augmented plant model is proposed, which accounts for the quantization noise caused by the input, state and

output quantizer functions $Q_u$, $Q_x$ and $Q_y$. First, it can be seen that a midtread quantizer function can be written based on the following uncertainty bounds:

$$Q_\delta^{mt}(x) = \delta \cdot \left( \left( \frac{x}{\delta} + \frac{1}{2} \right) - \left\{ \frac{x}{\delta} + \frac{1}{2} \right\} \right) = x + u_\delta(x) \cdot \delta, \tag{9.29}$$

where $u_\delta(x) = \frac{1}{2} - \left\{ \frac{x}{\delta} + \frac{1}{2} \right\} \in \left[ -\frac{1}{2}, \frac{1}{2} \right), \forall x \in \mathbb{R}$. In a similar manner, the midriser quantizer can be written as:

$$Q_\delta^{mr}(x) = \delta \cdot \left( \frac{x}{\delta} - \left\{ \frac{x}{\delta} \right\} + \frac{1}{2} \right) = x + v_\delta(x) \cdot \delta, \tag{9.30}$$

where $v_\delta(x) = \frac{1}{2} - \left\{ \frac{x}{\delta} \right\} \in \left( -\frac{1}{2}, \frac{1}{2} \right], \forall x \in \mathbb{R}$. As such, irrespective of the fields $T_u$, $T_x$, $T_y$, $K_q(z)$ from (9.18) with $(A_1, B_1, C_1, D_1)$ can be rewritten in a unified manner as:

$$(K_q(z)) : \begin{cases} \overline{e}[k] & = Q_u\left(e[k]\right) = e[k] + \gamma[k]; \\ x_c[k+1] & = A_1 x_c[k] + B_1\left(e[k] + \gamma[k]\right) + \alpha[k]; \\ \overline{u}[k] & = C_1 x_c[k] + D_1\left(e[k] + \gamma[k]\right) + \beta[k]; \\ u[k] & = Q_y\left(\overline{u}[k]\right) = \overline{u}[k] + \rho[k], \end{cases} \tag{9.31}$$

which remains in LTI form, having additional disturbance inputs:

- $\gamma[k] \in [-\delta_e/2, \delta_e/2]^{n_u}$ for the ADC quantization;
- $\eta[k] \in [-\delta_u/2, \delta_u/2]^{n_y}$ for the DAC quantization;
- $\alpha[k] \in [-\delta_x/2, \delta_x/2]^{n_x}$ and $\beta[k] \in [-\delta_x/2, \delta_x/2]^{n_y}$ for the state and output computation quantization, respectively.

Additionally, consider the ideal discretized plant:

$$(G(z)) : \begin{cases} x[k+1] & = A_2 x[k] + B_2 u[k]; \\ y[k] & = C_2 x[k] + D_2 u[k]. \end{cases} \tag{9.32}$$

As such, the open-loop system with input $e[k]$ from $K_q(z)$ and

output $y[k]$ from $G(z)$, with state vector $x_s = \begin{pmatrix} x_c^\top & x^\top \end{pmatrix}^\top$ can be written:

$$(L(z)) : \left(\begin{array}{cc|cccc|c} A_1 & O & B_1 & I & O & O & B_1 \\ B_2C_1 & A_2 & B_2D_1 & O & B_2 & B_2 & B_2D_1 \\ \hline D_2C_1 & C_2 & D_2D_1 & O & D_2 & D_2 & D_2D_1 \end{array}\right). \tag{9.33}$$

For such an open-loop system interconnection, consider the following auxiliary notations:

$$D_s{=}D_2D_1;\ \widehat{D}{=}\left(I + D_s\right)^{-1};\ \widehat{C}{=}\begin{pmatrix} D_2C_1 & C_2 \end{pmatrix};\ H{=}D_2;$$
$$\widehat{B}{=}\begin{pmatrix} B_1 \\ B_2D_1 \end{pmatrix};\ F{=}\begin{pmatrix} I \\ O \end{pmatrix};\ V{=}\begin{pmatrix} O \\ B_2 \end{pmatrix};\ M{=}-\widehat{B}\widehat{D};$$
$$\Phi{=}\begin{pmatrix} A_1 & O \\ B_2C_1 & A_2 \end{pmatrix} - \widehat{B}\widehat{D}\widehat{C} = \widehat{A}{-}\widehat{B}\widehat{D}\widehat{C};\ R{=}V{-}\widehat{B}\widehat{D}H.$$

#### 9.2.2.1 Quantization bound: diagonalizable $\Phi$

The following theorem generalizes the results presented in [PS03] and [Pen+07] by obtaining a worst-case bound for the steady-state limit cycles arising from LTI processes driven by fixed-point LTI regulators. It also assumes in the proof, without a loss of generality, that the reference signal is the origin of the measurements vector, i.e. $r \equiv 0$. To prove the result, an assumption must be performed on the structure of the closed-loop state matrix $\Phi$, namely it must be diagonalizale.

**Theorem 4.** *For an open-loop system $L(z)$ consisting of a quantized stabilizing numeric controller $K_q(z)$, with steps $\delta_e, \delta_x, \delta_u > 0$, in series with an ideal discretized process $G(z)$, then the worst-case deviation of $y_q[k]$ from the ideal closed-loop steady-state measurement $y[k]$ achievable by*

*$K(z)$ without quantization errors is:*

$$\sup_{k>k_\varepsilon} \|y_q[k] - y[k]\| \leq \tag{9.34}$$
$$\left\|\widehat{D}\widehat{C}P\right\| \frac{1}{1-\rho(\Phi)} \left\|P^{-1}R\right\| \left(\frac{\delta_x}{2} + \frac{\delta_u}{2}\right) +$$
$$\left\|\widehat{D}\widehat{C}P\right\| \frac{1}{1-\rho(\Phi)} \left(\left\|P^{-1}F\right\| \frac{\delta_x}{2} + \left\|P^{-1}M\right\| \frac{\delta_u}{2}\right) +$$
$$\left\|\widehat{D}H\right\| \left(\frac{\delta_x}{2} + \frac{\delta_u}{2}\right) + \left\|\widehat{D}D_s\right\| \frac{\delta_e}{2} \equiv \varepsilon_G\left(K_q, P, F\right),$$

*where the matrix $P$ diagonalizes $\Phi$, i.e. $\Phi = P{\cdot}J_\Phi{\cdot}P^{-1}$, $J_\phi = diag\left(\lambda_1, \ldots, \lambda_{n_\ell}\right)$, in the complex number field.*

*Proof.* Starting from the definition of the output equation and, applying $e[k] = -y[k]$, we obtain:

$$y_q[k] = \widehat{C}x_s[k] - D_s\left(y_q[k] + \gamma[k]\right) + H\left(\beta[k] + \eta[k]\right),$$

which, after separating $y_q[k]$, becomes:

$$y_q[k] = \widehat{D}\left(\widehat{C}x_s[k] + H\beta[k] + H\eta[k] - D_s\gamma[k]\right). \tag{9.35}$$

It must be noticed that this expression requires the invertibility of the matrix $(I + D_2D_1)$. On the other hand, the recurrent state equation can be written as:

$$x_s[k{+}1] = \widehat{A}x_s[k] + \widehat{B}\left(u[k] + \gamma[k]\right) + F\alpha[k] + V\left(\beta[k] + \eta[k]\right),$$

and with $e[k] = -y[k]$, along with $y[k]$ from (9.35), becomes:

$$x_s[k] = \Phi^k x_s[0] + S_k\left(\Phi, R, \beta + \eta\right) + S_k\left(\Phi, F, \alpha\right) + S_k\left(\Phi, M, \gamma\right), \tag{9.36}$$

with sums $S_k$ obtained based on matrices $X, Y$ and array $v$:

$$S_k\left(X, Y, v\right) = \sum_{i=0}^{k-1} X^i Y v[i]. \tag{9.37}$$

Assuming a closed-loop stable system, i.e. $\rho\left(\Phi\right) < 1$, with distinct poles, then the Jordan canonical form $J_\Phi$ of the state matrix $\Phi$ is a diagonal

matrix. As such, there exists a nonsingular matrix $P$ such that $\Phi = P \cdot J_\Phi \cdot P^{-1}$, resulting:

$$\begin{aligned}
\|S_k(\Phi, Y, v)\|_\infty &= \left\| P \cdot \sum_{i=1}^{k-1} J_\phi^i P^{-1} Y v[i] \right\|_\infty \leq \\
&\leq \|P\|_\infty \cdot \sum_{i=0}^{k-1} \left\|J_\Phi^i\right\|_\infty \cdot \left\|P^{-1}Y\right\|_\infty \cdot \|v[i]\|_\infty = \\
&= \|P\|_\infty \cdot \left\|P^{-1}Y\right\|_\infty \cdot \sum_{i=0}^{k-1} \rho(\Phi)^i \cdot \|v[i]\|_\infty ,
\end{aligned}$$

while, denoting $M_Y = \|P\|_\infty \cdot \|P^{-1}Y\|_\infty$ and $k \to \infty$:

$$\lim_{k\to\infty} \|S_k(\Phi, Y, v)\|_\infty \leq M_Y \cdot \frac{1}{1-\rho(\Phi)} \cdot \sup_{v[k]} \|v[k]\|_\infty . \tag{9.38}$$

To conclude the proof, the expression of the steady-state maximum deviation between the output $y_{K_q}[k]$ from (9.35) with state $x_s[k]$ replaced by (9.36), and its ideal counterpart $y[k] = \widehat{D}\widehat{C}\Phi^k x_s[0]$, due to $\alpha = \beta = \gamma = \eta \equiv 0$, and we have:

$$\begin{aligned}
\|\varepsilon_Q[k]\|_\infty = \|y_q[k] - y[k]\|_\infty \leq \sup_{\alpha,\beta,\gamma,\eta} \Big( &\left\|\widehat{D}\widehat{C}S_k(\Phi, R, \beta{+}\eta)\right\|_\infty \\
+ \left\|\widehat{D}\widehat{C}S_k(\Phi, F, \alpha)\right\|_\infty &+ \left\|\widehat{D}\widehat{C}S_k(\Phi, K, \gamma)\right\|_\infty + \\
+ \left\|\widehat{D}H(\beta[k]{+}\eta[k])\right\|_\infty &+ \left\|\widehat{D}D_s\gamma[k]\right\|_\infty \Big) ,
\end{aligned} \tag{9.39}$$

which, by transitioning to $k \to \infty$ and applying (9.38), will reduce to the initial statement (9.34), considering the worst-case values for the quantization noise effects, i.e. $\frac{1}{2} \times (\delta_e, \delta_x, \delta_u)$.

□

**Remark 12.** *The previous theorem shows that the worst-case deviation caused by quantization effects is directly-affected by the spectral radius of the closed-loop state matrix $\Phi$, i.e. in terms of the inverse of the distance between the closed-loop poles and the discrete-time stability bound given by the unit circle.*

Based on the previous results, a throughout closed-loop analysis in the case of a quantized controller implementation $K_q(z)$ can be per-

formed by selecting the minimum necessary word length for signal storage $L_x$, based on the $\mathcal{H}_\infty$ bounds (9.19), (9.20) and Lemma 6, followed by an optimal quantization of the controller matrices using Lemma 7, which affects the transient response of the initially-designed open-loop system, while Theorem 4 provides a worst-case bound on the steady-state deviation of the system output, all gathered in an equivalent LTI closed-loop control structure.

#### 9.2.2.2 Quantization bound: non-diagonalizable $\Phi$

If the assumption on the diagonalizability of matrix $\Phi$ is discarded, a generalized version of Theorem 4 becomes:

**Theorem 5.** *For an open-loop system $L(z)$ consisting of a quantized stabilizing numeric controller $K_q(z)$, with steps $\delta_e, \delta_x, \delta_u > 0$, in series with an ideal discretized process $G(z)$, then the worst-case deviation of $y_q[k]$ from the ideal closed-loop steady-state measurement $y[k]$ achievable by $K(z)$ without quantization errors is:*

$$\begin{aligned}
&\sup_{k>k_\varepsilon} \|y_q[k] - y[k]\| \leq \qquad (9.40)\\
&\sum_{i=1}^{N} \frac{1}{(1-\rho(\Phi))^i} \left\|\widehat{D}\widehat{C}P\right\| \left\|P^{-1}R\right\| \left(\frac{\delta_x}{2} + \frac{\delta_u}{2}\right) +\\
&\sum_{i=1}^{N} \frac{1}{(1-\rho(\Phi))^i} \left\|\widehat{D}\widehat{C}P\right\| \left(\left\|P^{-1}F\right\| \frac{\delta_x}{2} + \left\|P^{-1}M\right\| \frac{\delta_u}{2}\right) +\\
&\left\|\widehat{D}H\right\| \left(\frac{\delta_x}{2} + \frac{\delta_u}{2}\right) + \left\|\widehat{D}D_s\right\| \frac{\delta_e}{2} \equiv \varepsilon_G\left(K_q, P, F\right),
\end{aligned}$$

*where the matrix $P$ transforms $\Phi$ into its Jordan canonical form, i.e. $\Phi = P \cdot J_\Phi \cdot P^{-1}$ in the complex number field and $N$ is the maximum dimension of a Jordan cell from $J_\Phi$.*

*Proof.* In a similar manner to the proof of Theorem 4, we have:

$$y_q[k] = \widehat{D}\left(\widehat{C}x_s[k] + H\beta[k] + H\eta[k] - D_s\gamma[k]\right), \text{ and:} \qquad (9.41)$$

$$x_s[k] = \Phi^k x_s[0] + S_k\left(\Phi, R, \beta+\eta\right) + S_k\left(\Phi, F, \alpha\right) + S_k\left(\Phi, M, \gamma\right), \qquad (9.42)$$

where $S_k(X, Y, v)$ is a shorthand notation for:

$$S_k(X, Y, v) = \sum_{i=0}^{k-1} X^i Y v[i]. \tag{9.43}$$

The main problem will be to find a suitable upper bound for the norm of $S_k$ in the non-diagonalizable case. Consider $J_\Phi = \text{diag}(J_{N_1}(\lambda_1), \ldots, J_{N_s}(\lambda_s))$, with $N = \max\{N_1, \ldots, N_s\}$, and $J_{N_t}(\lambda_t)$ is the Jordan cell of size $N_t$ corresponding to the eigenvalue $\lambda_t$, and $P$ the similarity matrix, and we have:

$$\|S_k(\Phi, Y, v)\| \leq M_Y \sum_{i=0}^{k-1} \left\|J_\Phi^i\right\| \cdot \|v[i]\|, \tag{9.44}$$

where $M_Y = \|P\| \cdot \|P^{-1}Y\|$. For each Jordan cell we have:

$$\|J_{N_t}^m(\lambda_t)\| \leq \sum_{j=0}^{N_t-1} |\lambda_t|^{m-j} \binom{m}{j} \leq \sum_{j=0}^{N_t-1} \rho(\Phi)^{m-j} \binom{m}{j}.$$

Therefore, considering the maximum dimension of the Jordan cells from $J_\Phi$ and the convergence of the well-known power series with its derivatives, we obtain:

$$\lim_{k\to\infty} \|S_k(\Phi, Y, v)\| \leq M_Y \cdot \sum_{i=1}^{N} \frac{1}{(1-\rho(\Phi))^i} \cdot \sup_{v[k]} \|v[k]\|. \tag{9.45}$$

Moreover, the ideal counterpart of $y_q[k]$ is $y[k] = \widehat{D}\widehat{C}\Phi^k x_s[0]$, due to $\alpha = \beta = \gamma = \eta \equiv \mathbf{0}$, and we have:

$$\begin{aligned} \|y_q[k] - y[k]\| \leq \sup_{\alpha,\beta,\gamma,\eta} \Big( & \left\|\widehat{D}\widehat{C}S_k(\Phi, R, \beta{+}\eta)\right\| + \\ & \left\|\widehat{D}\widehat{C}S_k(\Phi, F, \alpha)\right\| + \left\|\widehat{D}\widehat{C}S_k(\Phi, K, \gamma)\right\| + \\ & \left\|\widehat{D}H(\beta[k]{+}\eta[k])\right\| + \left\|\widehat{D}D_s\gamma[k]\right\| \Big), \end{aligned} \tag{9.46}$$

which, by transitioning to $k{\to}\infty$ and applying (9.45), will reduce to the initial statement (9.40), considering the worst-case values for the quantization resolutions, i.e. $\frac{1}{2} \times (\delta_e, \delta_x, \delta_u)$. □

**Remark 13.** *In a similar light to the pole-placement algorithm of [KNV85],*

*with the technical limitation that the multiplicity of the closed-loop poles cannot exceed the rank of the input matrix $B_2$, it may become desirable in this case to design the control system such that the closed-loop state matrix $\Phi$ is diagonalizable (which is not equivalent to forcing poles to have multiplicity one) in order to apply the framework of Theorem 4 instead of 5, which is less conservative, brings additional degrees-of-freedom to the transformation matrix $P$, as will be proved in Lemma 8, and will also lead to a simplified optimization problem as demonstrated in the following section.*

**Remark 14.** *Although the assumption of a DAC circuit at the regulator output implies the zero-order hold discretization method, Theorems 4 and 5 are valid for any closed-loop stable control system, provided that the considered models are consistent with their practical implementations. A similar adaptation can be made for first-order hold circuits.*

#### 9.2.2.3 Tracking error minimization design

There are several available degrees-of-freedom in the quantization error bounds $\varepsilon_G(K_q, P)$ (9.34), (9.40), such as the selection of discretization method for regulator $K_q$ and possibility to apply a similarity transformation to its state-space representation and coordinate change $P$ for the Jordan canonical form of $\Phi$.

In case of the discretization method, its selection is usually preferable for the provided transient response of the regulator [Yep+10; ŞMD23a] and, as such, will not be the main focus of this section and we assume that $K_q$ provides the desired transient response.

The remainder of the design necessity is to propose an adequate scaling of the regulator matrices $(A_1, B_1, C_1, D_1)$ and find the similarity matrix $P$ to guarantee a least conservative bound to (9.34) and (9.40).

Starting from a fixed quantized regulator $K_q$ from (9.31), denote its similarity transformation through a matrix $T \in \mathrm{GL}_{n_c}(\mathbb{C})$ as a new regulator $K_{q,T}$ with invariant input-output response:

$$K_q = \left(\begin{array}{c|c} A_1 & B_1 \\ \hline C_1 & D_1 \end{array}\right) \overset{T}{\sim} \left(\begin{array}{c|c} T^{-1}A_1T & T^{-1}B_1 \\ \hline C_1T & D_1 \end{array}\right) \equiv K_{q,T}. \tag{9.47}$$

As such, the following optimization problem arises in terms of possible similarity matrices for the Jordan form of $\Phi$, forming the set $\mathcal{P}$, and of possible controller coordinate transformations, forming the set $\mathcal{T}$.

**Problem 12.** *Given a discrete-time controller $K_q$, the least conservative upper bound of the closed-loop quantization error is the solution of the following optimization problem:*

$$\mathcal{Q} = \min_{T \in \mathcal{T}} \min_{P \in \mathcal{P}} \varepsilon_G(K_{q,T}, P, F). \tag{9.48}$$

While the first set is given by $\mathcal{T} = \mathrm{GL}_{n_c}(\mathbb{C})$, the second set should be properly characterized. For the diagonalizable case, the following result will be considered.

**Lemma 8.** *For a diagonalizable closed-loop state matrix $\Phi$, the set of similarity matrices $P \in GL_{n_\ell}(\mathbb{C})$ can be obtained starting from an a given similarity matrix $P_0$ left multiplied by an arbitrary nonsingular block diagonal matrix having the same structure as $J_\Phi$.*

*Proof.* Let $\Lambda(\Phi) = \{\lambda_1, \lambda_2, \ldots, \lambda_s\}$ with the algebraic multiplicities $m_1, m_2, \ldots, m_s$. Then, for each eigenspace we have $\dim V_{\lambda_i} = m_i$, so we have:

$$V_{\lambda_i} = \mathrm{Span}\{p_1^{(i)}, \ldots, p_{m_i}^{(i)}\},$$

which can be used to construct the initial matrix $P_0$:

$$P_0 = \left[ p_1^{(1)} \quad \ldots \quad p_{m_1}^{(1)} | \ldots | p_1^{(s)} \quad \ldots \quad p_{m_s}^{(s)} \right].$$

Moreover, all algebraic bases of $V_{\lambda_i}$ can be characterized as $\{Q_i p_1^{(i)}, \ldots, Q_i p_{m_i}^{(i)}\}$, with matrices $Q_i \in \mathrm{GL}_{m_i}(\mathbb{C})$, and the conclusion follows. □

**Corollary 1.** *For the particular case of having $\Phi$ with all eigenvalues distinct complex numbers, the similarity matrices can be characterized as a product between an arbitrary diagonal matrix $D_\alpha$, $\alpha \in \mathbb{R}_+^{n_\ell}$, and a similarity matrix $P_0$.*

According to Corollary 1, a diagonal matrix $D_\alpha$ is a good choice for considering an additional scaling factor for minimizing the upper bound $\varepsilon_G(K_q, P_0, F)$ from Theorems 4 and 5, $\alpha \in \mathbb{R}_+^{n_\ell}$ representing $n_\ell$ degrees-of-freedom for the optimization problem. We consider the shorthand notation for the similarity matrix $P_\alpha = D_\alpha P_0$, $\alpha \in \mathbb{R}_+^{n_\ell}$, where $P_0 = P_\alpha|_{\alpha=\mathbf{1}}$. In a similar manner, a diagonal transformation $D_\xi$, $\xi \in \mathbb{R}_+^{n_c}$ of the initial regulator $K_q$ will be considered, resulting the set of regulators $K_{q,D_\xi} \equiv K_\xi$, its initial form being $K_q = K_\xi|_{\xi=\mathbf{1}}$.

To consider the worst-case steady-state guaranteeable bound (9.34) in the context of an optimization problem with vector variables, define the cost functional $\mathcal{J}: \mathbb{R}_+^{n_c} \times \mathbb{R}_+^{n_\ell} \to \mathbb{R}_+$, $\mathcal{J}(\xi, \alpha) = \varepsilon_G(K_\xi, P_\alpha, F)$. The hypothesis is that a change in $K_q$ implies a change in the state matrix $\Phi$ which, in turn, leads to a different similarity matrix $P$. This sequentiality assumption to select a regulator $K_q$, based upon which the matrix $P$ will be further computed, leads to the following minimization problem.

**Problem 13.** *Given a discrete quantized controller $K_q$ and a similarity matrix $P_0$, a least conservative upper bound of the closed-loop quantization error is the solution of the following optimization problem:*

$$\mathcal{Q} = \min_{\xi \in \mathbb{R}_+^{n_c}} \min_{\alpha \in \mathbb{R}_+^{n_\ell}} \mathcal{J}(\xi, \alpha) = \varepsilon_G(K_\xi, P_\alpha, F). \tag{9.49}$$

Starting from a diagonal matrix $D_\xi \in \mathbb{R}^{n_c \times n_c}$, an extended diagonal matrix $\overline{D}_\xi$ will also be defined as:

$$\overline{D}_\xi = \begin{pmatrix} D_\xi & O \\ O & I \end{pmatrix} \in \mathbb{R}^{n_\ell \times n_\ell}. \tag{9.50}$$

**Lemma 9.** *The diagonal scalings of the controller $K_q$ and similarity matrix $P_0$ can be formulated as a single diagonal scaling applied to $P_0$ and an auxiliary diagonal scaling of $F$:*

$$\varepsilon_G(K_\xi, P_\alpha, F) = \varepsilon_G\left(K_q, \left(\overline{D}_\xi^2 D_\alpha\right) P_0, \overline{D}_\xi F\right). \tag{9.51}$$

*Proof.* The coordinate transformation $D_\xi$ to $K_q$ implies:

$$\begin{aligned} \Phi \overset{D_\xi}{\sim} & \begin{pmatrix} D_\xi^{-1} A_1 D_\xi & O \\ B_2 C_1 D_\xi & A_2 \end{pmatrix} - \begin{pmatrix} D_\xi^{-1} B_1 \\ B_2 D_1 \end{pmatrix} \hat{D} \begin{pmatrix} D_2 C_1 D_\xi & C_2 \end{pmatrix} = \\ & = \overline{D}_\xi^{-1} \Phi \overline{D}_\xi, \end{aligned}$$

while considering the diagonal scaling $D_\alpha$ of $P_0$, we have:

$$\Phi = \left(\overline{D}_\xi D_\alpha P_0\right) J_\Phi\left(P_0^{-1} D_\alpha^{-1} \overline{D}_\xi^{-1}\right). \tag{9.52}$$

Additionally, the scaling through $D_\xi$ can be represented in a similar manner as a left multiplication by $\overline{D}_\xi^{-1}$ for the terms $R$ and $M$, and a

right multiplication by $\overline{D}_\xi$ for the term $\widehat{C}$ in (9.34) and (9.40). As such, considering the structure of $\varepsilon_G(K_q, P, F)$, one can easily obtain that:

$$\varepsilon_G\left(K_\xi, P_\alpha, F\right) = \varepsilon_G\left(K_q, \left(\overline{D}_\xi^2 D_\alpha\right) P_0, \overline{D}_\xi F\right), \tag{9.53}$$

which concludes the proof.

□

The main problem of introducing the controller's coordinate transformation consists in the possibility of obtaining a scaling matrix $D_\xi \to O$ or $D_\xi \to \infty I$ to minimize the upper bound of the steady-state quantization error. Let $\mathcal{N}_{x_c} = \|(A_1, B_1, I, O)\|$ and $\mathcal{N}_u = \|(A_1, B_1, C_1, D_1)\|$ denote the $\mathcal{H}_\infty$ norms of the regulator $K_q$ state and output signals, respectively, assumed finite. However, considering Lemma 6, a maximum admissible regulator state signal norm $\overline{\mathcal{N}}_{x_c}$, also depending on the ADCs' and DACs' dynamic range should be imposed. Given that $\mathcal{N}_u$ is invariant to similarity transformations $D_\xi$, an upper bound $\overline{\mathcal{N}}_{x_c} = \texttt{nextpow2}(\mathcal{N}_u)$ can be considered as a nonredundant starting point. As such, a similar optimization problem with $\mathcal{H}_\infty$-norm constraints can be formulated:

**Problem 14.** *Given a discrete quantized controller $K_q$, with a maximum allowed $\mathcal{H}_\infty$-norm $\overline{\mathcal{N}}_{x_c}$ for its state signal, and a similarity matrix $P_0$, a least conservative upper bound of the closed-loop steady-state quantization error is the solution of the optimization problem:*

$$\begin{aligned} \mathcal{Q} = \min_{(\xi,\alpha)\in\mathbb{R}_+^{n_c}\times\mathbb{R}_+^{n_\ell}} \mathcal{J}\left(\xi, \alpha\right) &= \varepsilon_G\left(K_q, \left(\overline{D}_\xi^2 D_\alpha\right) P_0, \overline{D}_\xi F\right) \\ s.t. \ \left\|\left(D_\xi^{-1} A_1 D_\xi, D_\xi^{-1} B_1, I, O\right)\right\| &< \overline{\mathcal{N}}_{x_c}. \end{aligned} \tag{9.54}$$

**Remark 15.** *For the case of having $\Phi$ non-diagonalizable, the scaling factor of the similarity matrix $P_0$, due to the lack of the homogeneity which occurs in the the case of forming the chain of associate vectors which generate the structure of the corresponding Jordan cell, still remains diagonal, partitioned as:*

$$D_\alpha = diag(\alpha_1 I_{N_1}, \alpha_2 I_{N_2}, \ldots, \alpha_s I_{N_s}), \tag{9.55}$$

*where $N_i$ are the sizes of the Jordan cells of $J_\Phi$, according to the notations used in Theorem 5, resulting a set of $s$ DOFs instead of the $n_\ell$ DOFs from the diagonal case of Theorem 4.*

#### 9.2.2.4 Numeric implementation aspects

The resulting optimization Problems 12–14 are not convex by nature. With the following convention for the sign function:

$$\operatorname{sign}(x) = \begin{cases} -1, x < 0; \\ 1, x \geq 0, \end{cases} \tag{9.56}$$

the partial derivative of the matrix $\infty$-norm $\|\cdot\|$ is:

$$\frac{\partial \|X\|}{\partial x_{ij}} = \operatorname{sign}(x_{ij})\delta_{kj}, \quad X \in \mathbb{R}^{n\times n} = [x_{ij}]_{i,j=\overline{1,n}}, \tag{9.57}$$

where $\delta_{kj}$ is the Kronecker delta function, with $k$ being the row for which the maximum is achieved. As such, the functional $\mathcal{J}(\xi, \alpha)$ is differentiable, but its Jacobian is not continuous, being right-continuous only. As described in [Lew07] and [Cla90], such a minimization problem converges if the subgradient method is applied.

The experiments have been performed using the `fmincon` routine from MATLAB, version R2022a, using several hyperparameter configurations and algorithms. From our findings, the sequential quadratic programming (`sqp`) algorithm works best, followed by the `interior-point` method, with its inherent advantage that it works for large-scale problems, but it halts at solutions with coarser tolerances and also tends to move away from the best found value in order to satisfy the first-order optimality conditions, and followed by the `active-set` algorithm which stalls prematurely for identical hyperparameters. The `trust-region-reflective` algorithm does not cover the constraint specified in (9.54).

The nonconvexity of the optimization problem can lead to a premature stopping of the algorithm into a local minimum point. A possible trick which can be used to reduce the possibility of early stopping is given in the next remark.

**Remark 16.** *Starting from a given similarity matrix $P_0$, each permutation matrix $\Pi$ leads to a new similarity matrix $\Pi P_0$ which can locally generate a new subset of similarity matrices of $\mathcal{P}$ and, considering that:*

$$\varepsilon_G(K_\xi, P_\alpha) = \varepsilon_G\left(K_q, \left(\overline{D}_\xi^2 D_\alpha \Pi\right) \cdot P_0, \overline{D}_\xi F\right), \tag{9.58}$$

*a maximum prescribed number of function evaluations can be used to find*

*the best possible local decreasing direction.*

#### 9.2.2.5 Practical implications

In the context of RCP, simulating the quantized numeric regulator $K_q(z)$ from (9.18) is covered in MiL testing. While this approach does provide the qualitative behaviour of the closed-loop system, a more accurate simulation in this case would be to fully use the fixed-point encoding in all computations involved in $K(z)$, more similar to a Software-in-the-Loop (SiL) simulation. As such, the controller computations will be transposed into the more realistic computer units instead of using signals truncated to the specified quantizer steps. A new controller model is thus proposed, denoted $K^{\mathcal{F}}(z)$, which adapts the functionality from (9.18) by replacing its continuous domains $\mathcal{D}$ with their integer counterparts $\mathcal{D}^{\mathcal{F}}$ from (4.8). The interrupt service routine (ISR) pseudocode for $K^{\mathcal{F}}(z)$ presented in Algorithm 2. The state-space matrices deduced in Lemma 7 must be scaled through left binary shifting with the value $d$, which guarantees the resolution $\delta = \frac{1}{2^d}$ in absolute units, as:

$$\widetilde{A} \leftarrow \lfloor A \ll d \rceil \, ; \; \widetilde{B} \leftarrow \lfloor B \ll d \rceil \, ; \; \widetilde{C} \leftarrow \lfloor C \ll d \rceil \, ; \; \widetilde{D} \leftarrow \lfloor D \ll d \rceil \, , \tag{9.59}$$

where $\lfloor \cdot \rceil$ denotes either truncation or rounding to the nearest integer, as supported by the hardware through $T_x$ from $\mathcal{S}_x$.

By design, unstructured robust controllers obtained through $\mathcal{H}_2$/$\mathcal{H}_\infty$/$\mu$-synthesis for strongly stabilizable systems do not employ integrator singularities and are inherently stable. As such, the dynamic ranges of the input, state and output signals for $K_q(z)$ and $K^{\mathcal{F}}(z)$, encompassing the hardware constraints of selecting the word lengths $L_u$, $L_x$ and $L_y$, along with the estimated worst-case bounds due to the system dynamics as in (9.19) and (9.20), with the established convention can be deduced as in Table 9.1. In particular cases of fixed-structure regulators or controllers computed for non-strongly stabilizable systems, which may contain integrator terms, extra caution must be made to ensure the nominal behaviour. In such cases, one possible approach would be to separate the regulator dynamics into a finite-norm component $\overline{K}_\infty(z)$, covered by the proposed theory, along with the accumulative or possibly-unstable dynamics described by $K_\infty(z)$, having infinite $\mathcal{H}_\infty$ norm, which would be implemented alongside saturation and anti-windup logic:

$$K(z) = \overline{K}_\infty(z) + K_\infty(z). \tag{9.60}$$

**Algorithm 2:** $K^{\mathcal{F}}(z)$ state-space ISR model

**Input:** Scaled matrices (9.59), $d$ from Lemma 7, $\widetilde{u}[k]$.
**Output:** $\widetilde{y}[k]$.

1 Read and encode $\widetilde{u}[k]$ from ADC {according to $\mathcal{S}_e$}
2 Compute extended output $\widetilde{Y}[k] = \widetilde{C}\widetilde{x}[k] + \widetilde{D}\widetilde{u}[k]$
3 Compute $\widetilde{y}[k] \leftarrow \left\lfloor \widetilde{Y}[k] \gg d \right\rceil$ {according to $\mathcal{S}_x$}
4 Compute extended state $\widetilde{X}[k+1] = \widetilde{A}\widetilde{x}[k] + \widetilde{B}\widetilde{u}[k]$
5 Compute $\widetilde{x}[k] \leftarrow \left\lfloor \widetilde{X}[k] \gg d \right\rceil$ {according to $\mathcal{S}_x$}
6 Delay state vector: $\widetilde{x}[k] \leftarrow \widetilde{x}[k+1]$
7 Decode and write $\widetilde{y}[k]$ to DAC {according to $\mathcal{S}_u$}

**Remark 17.** *An additional design constraint for $L_x$ is that the resulting coefficient resolution $\frac{1}{2^d}$ from Lemma 7 must be negligible enough as to not affect the stabilizing property of the controller $K_q$.*

**Remark 18.** *The matrix $\widehat{D}^{-1} = (I + D_2 D_1)$ necessary in Theorems 4 and 5 is invertible, because an open-loop system is fundamentally designed such that $-1 \notin \Lambda(D_2 D_1)$, by imposing a non-zero roll-off, i.e. $D_2 D_1 = O$, or a small constant matrix transfer with $\max|\Lambda(D_2 D_1)| \ll 1$. Similarly, the expansions (9.38) and (9.45) with powers of the stable state matrix $\Phi$ will always converge by design, ensuring finite quantization noise.*

Table 9.1: Dynamic ranges using absolute measurement units (for $K_q$) and fixed-point scaled equivalents (for $K^{\mathcal{F}}$): binary and real domain hardware constraints (HWC) versus estimated (EST) ranges.

| *Signal* | HWC $K_q$ | HWC $K^{\mathcal{F}}$ | EST $K_q$ | EST $K^{\mathcal{F}}$ |
|---|---|---|---|---|
| $\sup u_{k\geq 0}[k]$ | $R_u$ | $2^{L_u-1}$ | $R_u$ | $2^{L_u-1}$ |
| $\sup x_{k\geq 0}[k]$ | $R_u \cdot 2^{L_x-L_u}$ | $2^{L_x-1}$ | $H_x \cdot R_u$ | $\lceil H_x \cdot 2^{L_u-1} \rceil$ |
| $\sup y_{k\geq 0}[k]$ | $R_y$ | $2^{L_y-1}$ | $H_y \cdot R_u$ | $\lceil H_y \cdot 2^{L_u-1} \rceil$ |

### 9.2.3 Conclusions

The presented unified approach is useful in high-precision servo systems by providing guaranteed tolerances on the expected precision, by studying the quantization effects for the worst-case scenario, the entire analysis encompassing LTI systems only, in addition to providing theoretical means to determine the numeric bounds of the regulator signals and to quantize its coefficients for an optimal transient response.

To illustrate the proposed results, two numeric examples are considered in sections 11.5 and 11.6.3, showing the implications of directly applying the mathematical framework, along with additionally performing the tracking error optimization.

Part of the material presented in this chapter was further refined after the completion of the doctoral thesis. In particular, improvements regarding the state-space balancing framework and its theoretical guarantees are discussed in [Şuş+26], where a more general formulation and corrected derivations are provided. The present chapter retains the original exposition for consistency with the thesis context.

## 9.3 Quantized control systems using the hybrid framework

This brief section extends the `System` and `HybridSystem` software interfaces from Chapter 5 to allow the Model-in-the-Loop and Software-in-the-Loop simulation of discrete-time quantized regulators, as presented in Chapters 8 and 9, along with the possibility to simulate the closed-loop control system viewed as a hybrid model with continuous dynamics given by the process, along with discrete dynamics provided by the regulator.

Starting from an ideal discrete-time regulator with sampling rate $T > 0$, presented in state-space form (9.18), its quantized equivalent is described as in (9.17), according to Figure 3.1. Furthermore, its coefficients must also be quantized for practical implementation on a microcontroller device using, for example, the uniform encoding approach from (9.26).

Let the ideal state-space matrices be $(A_1, B_1, C_1, D_1)$, and their quantized counterparts be $(A_q, B_q, C_q, D_q)$. Then, the regulator becomes:

$$(K_q(z)) : \begin{cases} \overline{e}[k] & = Q_u\left(e[k]\right); \\ x_c[k{+}1] & = Q_x\left(A_q x_c[k] + B_q \overline{e}[k]\right); \\ \overline{u}[k] & = Q_x\left(C_q x_c[k] + D_q \overline{e}[k]\right); \\ u[k] & = Q_y\left(\overline{u}[k]\right), \end{cases} \tag{9.61}$$

with interface $(u_c, x_c, y_c) \equiv (e, x, u)$, required by the closed-loop structure from Figure 3.2.

The quantized discrete-time regulator (9.61) with dimensions $(n_y, n_c, n_u)$ can be described using the hybrid system framework (2.7) with input/state/output $(v, z, w) \equiv \left(e, \left[x_c^\top, e^\top, \tau\right]^\top, u\right)$ of dimensionality $(n_y, n_c + n_u + 1, n_u)$:

$$(\Sigma_q) : \begin{cases} \dot{z} & = F\left(z, v, t\right), \ (z, v, t) \in \mathcal{C}; \\ z^+ & = G\left(z, v, t\right), \ (z, v, t) \in \mathcal{D}; \\ w & = h\left(z, v, t\right). \end{cases} \tag{9.62}$$

The flow dynamics are described by:

$$F(z, v, t) = \begin{bmatrix} \mathbf{0}_{n_c} \\ \mathbf{0}_{n_y} \\ 1 \end{bmatrix}, \tag{9.63}$$

meaning an integration on the auxiliary time variable $\tau \in [0, T)$, with no updates on the regulator states $x_c$ or regarding the new input reading $e$. The jump map is described by:

$$G(z, v, t) = \begin{bmatrix} Q_x\left(A_q x_c(t - \Delta t) + B_q \overline{e}(t - \Delta t)\right) \\ Q_e\left(e(t)\right) \\ 0 \end{bmatrix}, \tag{9.64}$$

which denotes that the numeric state is computed using the previously stored states and inputs $x_c(t - \Delta t)$ and $\overline{e}(t - \Delta t)$, while the current input is read and quantized according to the input ADC hardware $Q_e$, respectively. The auxiliary time state $\tau$ is reset to zero at each jump. The jump dynamics must be performed after a sampling period has passed, i.e. $\tau = T + \varepsilon$, with $\varepsilon > 0$ the tolerance of the selected `ode` solver and its settings.

The flow domain can simply be described by:

$$\mathcal{C}(z, v, t) = 1, \tag{9.65}$$

meaning that the flow map is continuously executed, and only preempted

when a jump is necessary. The jump domain is described by:

$$\mathcal{D}(z, v, t) = \begin{cases} 0, & \text{if } \tau < T; \\ 1, & \text{otherwise,} \end{cases} \tag{9.66}$$

triggered when a multiple of the sampling rate $kT$ has passed, as would ideally be the behaviour in the regulator's definition (9.61). In the end, the output map of the hybrid system is described through:

$$h(z, v, t) = Q_u \left( C_q x_c(t - \Delta t) + D_q \overline{e}(t - \Delta t) \right), \tag{9.67}$$

being computed based on the current state $x_c[k]$, instead of the future $x_c[k+1]$ one, and current input $\overline{e}[k]$.

As such, a new extension is provided for such quantized systems with synchronous trigger dynamics by inheriting the `HybridSystem` class from Chapter 5, named `QuantizedSystem`. It implements the hybrid dynamics described in expressions (9.62)–(9.67), accounting for the auxiliary regulator state and input values $x_c(t - \Delta t)$ and $\overline{e}(t - \Delta t)$. An approach useful for Model-in-the-Loop simulation tests and validation is to use the previously-mentioned model, with real-valued signals and regulator coefficients, while an alternative approach useful for Software-in-the-Loop simulation would be to replace all signals with their fixed-point counterparts defined on $\mathcal{D}^{\mathcal{F}}(L)$ from (4.8), and system matrices scaled using (9.59). Both signal and coefficient can be accounted for uniform fixed-point encodings, such as the midtread and midriser quantizers, or other configurable approaches, such as floating-point or logarithmic quantizer circuits. Then, the hybrid model would model the microcontroller ISR pseudocode from Algorithm 2, with variable ranges anticipated as in Table 9.1 using the $\mathcal{H}_\infty$ norm bounds from Lemma 6. An important feature specific to this class is that it implements a private method `get_sys_ICs`, called implicitly when executing the `sim` and `simInitCond` methods, to apply the required quantization functions to the state and input signals in a transparent manner for the user, thus excluding the risk of signal inconsistency. Such a verification is performed recursively for all the subsystems chained through series, parallel, LLFT and ULLFT connections.

Using the regulator hybrid model described in this section ($\Sigma_q$), along with the continuous-time process models ($\Sigma$) from Chapter 2, definitions 2.1–2.7, then the numeric 1DOF control structure from Figure

3.2 can be treated in a unified manner as a `HybridLLFTConnection` class instance, described by (2.14), implemented in Figure 5.1:

$$\Sigma_0^h = LLFT\left(\Sigma, \Sigma_q\right). \tag{9.68}$$

Such hybrid closed-loop models can then be employed for realistic validations of the control system performance specifications as defined in Section 3.3 through classical performance indices or through the LSDP, by studying the transient and steady-state behaviours after the artifacts introduced by the sampled, discretized, and then quantized regulators $K_q(z)$ and $K^{\mathcal{F}}(z)$, analyzed in Chapters 8 and 9.

# 10. Execution time analysis

The current section proposes an estimation of the worst-case execution time (WCET) for LTI-based controllers. The WCET analysis can be seen as a verification step before automatic code generation, a computational model being provided. The proposed computational model encompasses state-space structures, infinite-impulse response (IIR) and finite-impulse response (FIR) filter models for the controller implementation, along with additional relevant phenomena being discussed, such as saturation, signal scaling and anti-windup techniques, which usually accompany the classical mathematical expressions.

## 10.1 Motivation and contributions

This section is based on the results first presented in the papers [Șuș+22c; Șuș+22b] and proposes an analysis of the execution time framing of the microcontroller operations into the specified sampling rate for 1DOF and 2DOF control structures. The main contributions are to:

(i) provide the user with an end-to-end computational model which can be used in two possible contexts: (1) to analyze the execution time of a numeric controller to be deployed in a production environment or (2) to analyze the execution time of a process simulation to be deployed in a Hardware-in-the-Loop simulation environment. Additionally, as a byproduct of the modelling necessary for the previous points, (3) it also provides the minimal and necessary interface to be implemented in a code generation software module;

(ii) provide a worst-case execution time analysis for state-space regulator structures, and for infinite impulse response or finite impulse response controller topologies, offering an upper bound estimation of the time span necessary to perform all the operations involved in the numeric implementation;

(iii) offer an exhaustive analysis which can be further performed in an automatic manner and integrated in the toolbox from Chapter 5.

## 10.2 Execution time model of LTI-based control laws

The necessary mathematical operations to fully implement an LTI-based control law are formally defined. Besides the LTI control law, the classical saturation and anti-windup nonlinearities will be considered, which are usually related to said LTI laws. The unary and binary mathematical operators defined in Table 10.1 and gathered in the operations alphabet $\mathbf{O} = \{\mathbf{n}, \mathbf{a}, \mathbf{m}, \mathbf{s}, \mathbf{w}, \mathbf{l}\}$, are considered with real operands and must be accounted for into a microprocessor-based environment.

Table 10.1: Formal operators necessary in LTI-based control laws.

| # | *Operator* $p_i$ | *Domain* | *Definition* |
|---|---|---|---|
| 1 | Add | $\mathbf{a} : \mathbb{R}^2 \to \mathbb{R}$ | $\mathbf{a}(x_1, x_2) = x_1 + x_2$ |
| 2 | Multiply | $\mathbf{m} : \mathbb{R}^2 \to \mathbb{R}$ | $\mathbf{m}(g, x) = g \cdot x$ |
| 3 | Saturate | $\mathbf{s}_{\underline{x},\overline{x}} : \mathbb{R} \to \mathbb{R}$ | $\mathbf{s}_{\underline{x},\overline{x}}(x) = \begin{cases} \underline{x}, & \text{if } x < \underline{x}; \\ x, & \text{if } \underline{x} \leq x \leq \overline{x}; \\ \overline{x}, & \text{if } \overline{x} < x, \end{cases}$ |
| 4 | Anti-windup | $\mathbf{w}_{\underline{x},\overline{x}} : \mathbb{R} \to \mathbb{R}$ | various [ÅH00; SFN18; TT09] |
| 5 | Load/Store | $\mathbf{l}(x) : \mathbb{R} \to \mathbb{R}$ | $\mathbf{l}(x) = x$ |
| 6 | Null | $\mathbf{n}(x) : \mathbb{R} \to \mathbb{R}$ | $\mathbf{n}(x) = 0$ |

**Remark 19.** *The operation* $\mathbf{a}$ *and* $\mathbf{l}$ *are bilinear,* $\mathbf{m}$ *is homogenous with respect to its arguments,* $\mathbf{s}$ *is a classical nonlinearity,* $\mathbf{w}$ *is used to compensate an infinite accumulation for integrator terms in the regulator dynamics, while* $\mathbf{n}$ *is used to model delays.*

As such, the process of computing a command signal $y[k]$ as in Figure 3.1 implies a finite and formal computational finite sequence $\mathbf{Sc} \in \mathbf{O}^N$, where all terms are mathematical operations as in Table 10.1, i.e. $\mathbf{Sc}[i] = p_i \in \mathbf{O}$, $i = \overline{1, N}$, where $N$ depends on the structure of the controller $K(z)$. Moreover, to additionally specify a set of practical hardware

specifications and constraints $\mathbf{H}$ and to uniformly describe the problem, the finite sequence can be now extended to a full sequence $\mathbf{Sc}^{K,\mathbf{H}} \in \mathbf{O}^{\infty}$:

$$\mathbf{Sc}^{K,\mathbf{H}} = (p_1, p_2, \ldots, p_N, \mathbf{n}, \mathbf{n}, \ldots)\,,\ p_i \in \mathbf{O}. \tag{10.1}$$

Starting from an array $\mathbf{Sc}^{K,\mathbf{H}}$ of operations as (10.1), a general-purpose instruction set model follows. Assume a Random-Access Machine (RAM) computational model as in [Cor+09], with deterministic operations.

**Definition 12.** *The hardware constraints and specification set* $\mathbf{H}$ *encompasses metadata which imply extra operations or different approaches to the standard operations performed on the controller signals and implementation specific information, with various outcomes on the total execution time, frequently found in practice being:*

*(1) reading reference signals* $r[k]$ *and plant measurements* $y[k]$*, all input signal reading steps may imply preprocessing constraints in terms of sensor delays, impulse counters or data type conversions – this equates to adding* $p_i \in \{\mathbf{n}, \mathbf{l}\}$ *steps;*

*(2) scaling operations for the input and output signals imposed by the operating point used for plant linearization:* $\Delta u[k] = u[k] - u_0$ *and* $y[k] = y_0 + \Delta y[k]$*, which equates to augmenting the sequence set with* $p_i \in \{\mathbf{a}, \mathbf{s}, \mathbf{l}\}$ *items;*

*(3) input and output signals scaling operations, i.e.* $u_s[k] = a_u \cdot u[k] + b_u$ *and* $y_s[k] = a_y \cdot y[k] + b_y$*, useful especially for sensor and adapter signals, and extend the operations with* $p_i \in \{\mathbf{a}, \mathbf{m}, \mathbf{s}, \mathbf{l}\}$*;*

*(4) starting from the variable base word length* $L$ *of the microcontroller arithmetic registers which allows operations to be executed in a single clock tick, each variable's type and size should be adequately adapted for* $2 \times L$*,* $4 \times L$ *etc., which complicates the adding and multiplication routines with additional* $p_i \in \{\mathbf{a}, \mathbf{m}, \mathbf{l}\}$ *steps;*

*(5) controller gain scheduling verifications and updates based on the value of the input signal* $u[k]$*, leading to extra* $p_i \in \{\mathbf{l}\}$*;*

*(6) underflow and overflow checks for involved signals, implying saturations* $p_i \in \{\mathbf{s}\}$*;*

(7) *availability of DMA modules, MAC instructions, circular buffers in opposition to linear buffering, or output bypassing, which has the advantage of discarding* $p_i \in \{\mathbf{l}\}$ *operations.*

Such specifications will be quantified by scaling factors $c_{1,2}>0$ as used in (4.9)–(4.11) to the base duration of the RISC machine model operations.

Therefore, a set of instructions $\mathbf{Sc}^{K,\mathbf{H}}$ can be manually designed or automatically deduced. For manual modelling, the control engineer needs to find this set for each control law, while for automatic mode, an RCP tool can already deduce this set. Such an RCP tool generally deals with the code generation for different environments. Now, the sequence of operations generator procedures can be seen as a functional:

$$\mathbf{\Gamma_c} : \mathcal{G}_D \times \mathbf{H} \rightarrow \mathbf{O}^{\infty},\ \mathbf{\Gamma_c}\,(K, \mathbf{H}) = \mathbf{Sc}^{K,\mathbf{H}}. \tag{10.2}$$

Table 10.2: Base assembly operations $a_i \in \mathbf{A}$ for a RAM model used for LTI-based control systems.

| # | *Operator* $a_i$ | *Abbreviation* | *Part of operation from* $\mathbf{O}$ |
|---|---|---|---|
| 1 | No operation | `NOP` | $\mathbf{n}$ |
| 2 | Memory fetch | `MF` | $\mathbf{l}$ |
| 3 | Memory store | `MS` | $\mathbf{l}$ |
| 4 | Add | `ADD` | $\mathbf{a}$ |
| 5 | Multiply | `MUL` | $\mathbf{m}$ |
| 6 | Binary shift | `SH` | $\mathbf{m}$ |
| 7 | Jump | `JMP` | $\mathbf{s}, \mathbf{w}, \mathbf{l}$ |
| 8 | Compare | `CMP` | $\mathbf{s}, \mathbf{w}, \mathbf{l}$ |

To implement operations $p_i \in \mathbf{O}$ from Table 10.1, the atomic assembly instructions $\mathbf{A} = \{\texttt{NOP}, \texttt{MF}, \texttt{MS}, \texttt{ADD}, \texttt{MUL}, \texttt{SH}, \texttt{JMP}, \texttt{CMP}\}$ from Table 10.2 will represent the building blocks. They cover arithmetical operations, conditional jumps for saturations and the anti-windup of integrator terms, forced and imposed delays through data acquisition hardware and access to memory devices. For each arbitrary atomic assembly operation $a_i \in \mathbf{A}$, the RISC machine assumption is that each instruction takes a fixed clock tick value $T_{clk} > 0$. The number of variants of obtaining the

necessary assembly instructions is not unique and it further depends on the structure of $\mathbf{H}$. As such, a new mathematical operator responsible with the generation of a computer-equivalent set of instructions given by the functional $\mathbf{Sp} \in \mathbf{A}^{\infty}$ is:

$$\mathbf{\Gamma_p} : \mathcal{G}_D \times \mathbf{H} \to \mathbf{A}^{\infty},\ \mathbf{\Gamma_p}\left(K, \mathbf{H}\right) = \mathbf{Sp}^{K,\mathbf{H}}, \tag{10.3}$$

which results in an infinite sequence of atomic software instructions, but with a finite number of them being different to `NOP`, located at the start of the sequence, which implement the linear controller formula:

$$\mathbf{Sp}^{K,\mathbf{H}} = \left(a_1, \ldots, a_M, \texttt{NOP}, \texttt{NOP}, \ldots\right),\ a_i \in \mathbf{A}. \tag{10.4}$$

The set $\mathbf{Sc}$ thus contains abstract mathematical operations $p_i \in \mathbf{O}$, and each such operation $p_i$ will be practically implemented using equivalent $a_{i,j} \in \mathbf{A}$ steps, $j = \overline{1, k_i}$, as in the mapping:

$$p_i \mapsto \left(a_{i,1}, a_{i,2}, \cdots, a_{i,k_i}\right),\ \forall i = \overline{1, N}, \tag{10.5}$$

the number of relevant atomic operations being $M = \sum k_i$.

**Remark 20.** *According to the study of Section 4.3.1, additional facilities can be employed in the assembly instruction implementation depending on the hardware architecture, such as SIMP for* `MF`*,* `MS`*,* `ADD`*,* `MUL`*,* `SH`*,* `CMP`*, MAC for instructions* `ADD`*,* `MUL`*, and SIMD for* `ADD`*,* `MUL`*,* `SH`*.*

Figure 10.1 gathers the sequences and functionals $\mathbf{Sc}^{K,\mathbf{H}}$, $\mathbf{\Gamma_c}$, $\mathbf{Sp}^{K,\mathbf{H}}$ and $\mathbf{\Gamma_p}$, and illustrates their connections in an RCP context. The mapping from $(K, \mathbf{H})$ to the set $\mathbf{Sc}^{K,\mathbf{H}}$ is usually performed for MiL simulations through an application $\mathbf{\Gamma_c}$, while the mapping $(K, \mathbf{H}) \mapsto \mathbf{Sp}^{K,\mathbf{H}}$ is done through SiL testing using an application $\mathbf{\Gamma_p}$. The master RCP program, having access to both $\mathbf{Sc}^{K,\mathbf{H}}$ and $\mathbf{Sp}^{K,\mathbf{H}}$, can subsequently perform a WCET analysis on the implementation of the digital regulator $K(z)$ in the production hardware context $\mathbf{H}$.

Figure 10.2 presents a sequence diagram with the timing constraints of a numeric controller $K$ with respect to other software threads from the microcontroller, with an illustration of the WCET of the controller interrupt service routine (ISR) thread. The main result of the section is gathered in the following theorem.

**Theorem 6.** *Given a numeric control law $K \in \mathcal{G}_D$, a specification set $\mathbf{H}$ and a code generation procedure by a pair $(\mathbf{\Gamma_c}, \mathbf{\Gamma_p})$, the worst-case*

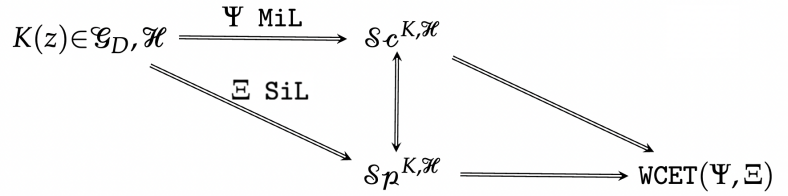


Figure 10.1: Rapid control prototyping relationship between the formal sets and functionals necessary to perform a worst-case execution time analysis for a regulator $K(z) \in \mathcal{G}_D$ in the production context $\mathbf{H}$.

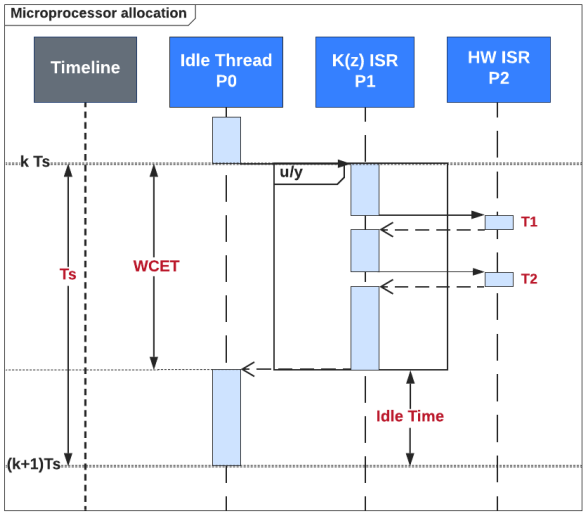


Figure 10.2: Sequence diagram illustrating the regulator $K(z)$ interrupt service routine execution among higher and lower priority threads for the duration of one sampling period $T_s$.

*execution time estimation can be computed as:*

$$WCET(\mathbf{\Gamma_c}, \mathbf{\Gamma_p}) = \left(\left|\mathbf{Sp}^{K,\mathbf{H}}\right| + \mathcal{O}(1)\right) \times T_{clk}, \tag{10.6}$$

*with the number of atomic assembly operations* $\left|\mathbf{Sp}^{K,\mathbf{H}}\right|$*, and* $\mathcal{O}(1)$ *accounts for context switching operations for uncorrelated software threads, independent to the input-output dimensions of* $K$*.*

*Proof.* According to the schematic representation from Figure 10.1, starting from the control law $K \in \mathcal{G}_D$ and the specification set $\mathbf{H}$, the set $\mathbf{Sc}^{K,\mathbf{H}}$ can be obtained via the MiL operator $\mathbf{\Gamma_c}$, resulting in $p_1, p_2, \ldots, p_N \in \mathbf{O}$. However, in order to measure each $p_i$, the set of atomic operations

must be attached via the SiL operator $\mathbf{\Gamma_p}$: $p_i \mapsto (a_{i,1}, a_{i,2}, \cdots, a_{i,N_i})$, each such atomic operation requiring exactly $T_{clk}$, leading to:

$$T_1 \equiv t\,(K) = \sum_{i=1}^{N}\sum_{l=1}^{N_i} t(a_{i,l}) = T_{clk} \cdot \sum_{i=1}^{N}\sum_{l=1}^{N_i} 1 = T_{clk} \times \left|\mathbf{Sp}^{K,\mathbf{H}}\right|, \quad (10.7)$$

where $t(\cdot)$ is the time necessary to execute a set of operations.

Additionally, a second term $T_2 = \sum_{\text{ISR}} \lambda$ accumulates ISR switching and stack handling operations handled by the scheduler, bounded by a processor-dependent constant $\lambda > 0$, modelled as $\mathcal{O}(1) \times T_{clk}$. As such, the worst-case execution time can now be written as:

$$\text{WCET}\,(\mathbf{\Gamma_c}, \mathbf{\Gamma_p}) = T_1 + T_2 = \left(\left|\mathbf{Sp}^{K,\mathbf{H}}\right| + \mathbf{O}(1)\right) \times T_{clk}, \quad (10.8)$$

which concludes the proof. □

**Remark 21.** *All possible delays caused by context switching to preemptive ISRs belonging to measurement data processing, with the cost of $\mathcal{O}(m)$, are included in the input processing step and do not remain unaccounted for in the execution time model of Theorem 10.6.*

Two additional performance qualifiers can be employed to globally assess the controller ISR implementation impact on the scheduling algorithm of the processor.

**Definition 13.** *The processor usage level qualifier relative to a fixed sampling period $T > 0$ of a discrete-time regulator $K(z) \in \mathcal{G}_D$, described in a relative manner, is defined by:*

$$\mathbf{U}\,(\mathbf{\Gamma_c}, \mathbf{\Gamma_p}, T) = \frac{WCET(\mathbf{\Gamma_c}, \mathbf{\Gamma_p})}{T} \times 100\ [\%]. \quad (10.9)$$

**Definition 14.** *The processor idle time qualifier with respect to a fixed sampling period $T > 0$ of a discrete-time regulator $K(z) \in \mathcal{G}_D$, described in absolute units, is defined by:*

$$\mathbf{I}\,(\mathbf{\Gamma_c}, \mathbf{\Gamma_p}, T) = \max\{0, T - WCET(\mathbf{\Gamma_c}, \mathbf{\Gamma_p})\}\ [s]. \quad (10.10)$$

## 10.3 Modelling duration of state-space realizations

Assume the state-space notation for a regulator $K(z)$ as in (3.7). The ISR model for such a regulator structure is based on the pseudocode

presented in Algorithm 2. Starting from the specifications from $\mathbf{H}$, each pseudocode line will have mandatory operations, along with optional operations, which will be accounted for into different constant weights $c_1$ and $c_2$. Further, Table 10.3 encompasses operations addressed in $\mathbf{H}$.

**Corollary 2.** *Based on Algorithm 2 and variations described in Table 10.3, a worst-case estimation for the number of operations can be written in terms of the base number of operations $g(n)$ corresponding to each line, scaled by weights $c_2$ and masked by coefficients $\varepsilon \in \{0, 1\}$ as:*

$$WCET(\mathbf{\Gamma_c}, \mathbf{\Gamma_p}) = \left( \mathcal{O}(1) + \sum_{Line\ i.j} c_2 \cdot (\varepsilon \cdot g_{i.j}(n)) \right) \times T_{clk}, \tag{10.11}$$

*where $\mathcal{O}(1)$ depends on the other higher-priority software threads and it is statistically modelled at deployment-level.*

The constructive proof follows using Theorem 6 by replacing the general-purpose sequence $\mathbf{Sp}^{K,\mathbf{H}}$ with its corresponding components from Table 10.3. Higher processor idle times $\mathbf{I}$ allow greater $\mathcal{O}(1)$ flexibility.

## 10.4 Modelling duration of FIR and IIR topologies

Consider a transfer matrix formulation of $G \in \mathcal{G}_D$ of (3.7), fully described by expressions of $m \times p$ SISO transfer functions $K_{ij} \in \mathcal{G}_D$:

$$(K(z)): \begin{pmatrix} Y_1 \\ Y_2 \\ \vdots \\ Y_p \end{pmatrix} = \begin{pmatrix} K_{11} & K_{12} & \cdots & K_{1m} \\ K_{21} & K_{22} & \cdots & K_{2m} \\ \vdots & \vdots & \ddots & \vdots \\ K_{p1} & K_{p2} & \cdots & K_{pm} \end{pmatrix} \cdot \begin{pmatrix} U_1 \\ U_2 \\ \vdots \\ U_m \end{pmatrix}. \tag{10.12}$$

Each element of the transfer matrix $K_{ij}$ can be modelled as an infinite-impulse response (IIR) filter or as a finite-impulse response (FIR) filter.

**Remark 22.** *Second-order sections are usually described with a gain term multiplied separately to the output of the transfer function as:*

$$H_2(z) = g \cdot \frac{b_2 z^2 + b_1 z + b_0}{z^2 + a_1 z + a_0},\ g \neq 0. \tag{10.13}$$

*To not further complicate the notations, the gain term $g$ will not be written, but will implicitly be considered in the execution time analysis.*

Table 10.3: State-space **Sp** WCET order of growth analysis for Algorithm 2 having $\Theta(g(n))$ with $c_1 \geq 0$ and $c_2 \geq 1$ as a function of $\mathbf{H}$.

| Line | Operation $[k]$ | $p_i \in \mathbf{O}$ | $a_i \in \mathbf{A} \mapsto g(n)$ | $\Theta(g(n))$ |
|---|---|---|---|---|
| 1.1 | Read $u$ | $\mathbf{l}$ | $m$ | $c_2 > 1$ |
| 1.2 | $u \leftarrow au + b$ | $\mathbf{l}, \mathbf{a}, \mathbf{m}$ | $2m$ | $c_2 > 1$ |
| 1.3 | Delay from $u$ | $\mathbf{n}$ | $m$ | $c_2 > 1$ |
| 1.4 | $\Delta u \leftarrow u - u_0$ | $\mathbf{l}, \mathbf{a}$ | $m$ | $c_2 > 1$ |
| 1.5 | Read $r$ | $\mathbf{l}$ | $m$ | $c_2 > 1$ |
| 1.6 | $u \leftarrow u - r$ | $\mathbf{l}, \mathbf{a}$ | $m$ | $c_2 > 1$ |
| 2.1 | $Cx$ | $\mathbf{l}, \mathbf{a}$ | $p(n-1)$ | $c_2 > 1$ |
| 2.2 | $Cx$ | $\mathbf{l}, \mathbf{m}$ | $pn$ | $c_2 > 1$ |
| 2.3 | $Du$ | $\mathbf{l}, \mathbf{a}$ | $p(m-1)$ | $c_2 > 1$ |
| 2.4 | $Du$ | $\mathbf{l}, \mathbf{m}$ | $pm$ | $c_2 > 1$ |
| 2.5 | $Cx + Du$ | $\mathbf{a}$ | $p$ | $c_2 > 1$ |
| 2.6 | $\mathbf{s}(y)$ | $\mathbf{l}, \mathbf{s}$ | $3p$ | $c_2 > 1$ |
| 2.7 | $\mathbf{w}(y)$ | $\mathbf{l}, \mathbf{w}$ | $4p$ | $c_2 > 1$ |
| 3.1 | $Ax$ | $\mathbf{l}, \mathbf{a}$ | $n(n-1)$ | $c_2 > 1$ |
| 3.2 | $Ax$ | $\mathbf{l}, \mathbf{m}$ | $n^2$ | $c_2 > 1$ |
| 3.3 | $Bu$ | $\mathbf{l}, \mathbf{a}$ | $n(m-1)$ | $c_2 > 1$ |
| 3.4 | $Bu$ | $\mathbf{l}, \mathbf{m}$ | $nm$ | $c_2 > 1$ |
| 3.5 | $Ax + Bu$ | $\mathbf{a}$ | $n$ | $c_2 \geq 1$ |
| 3.6 | $\mathbf{s}(x)$ | $\mathbf{l}, \mathbf{s}$ | $3n$ | $c_2 > 1$ |
| 3.7 | $\mathbf{w}(x)$ | $\mathbf{l}, \mathbf{w}$ | $4n$ | $c_2 > 1$ |
| 4.1 | $x[k] \leftarrow x[k+1]$ | $\mathbf{l}$ | $n$ | $c_2 > 1$ |
| 4.2 | $x \leftarrow \Delta x + x_0$ | $\mathbf{l}, \mathbf{a}$ | $n$ | $c_2 > 1$ |
| 4.3 | $x \leftarrow ax + b$ | $\mathbf{l}, \mathbf{a}, \mathbf{m}$ | $2n$ | $c_2 > 1$ |
| 5.1 | $y \leftarrow \Delta y + y_0$ | $\mathbf{l}, \mathbf{a}$ | $p$ | $c_2 > 1$ |
| 5.2 | $y \leftarrow ay + b$ | $\mathbf{l}, \mathbf{a}, \mathbf{m}$ | $2p$ | $c_2 > 1$ |
| 5.3 | Gain scheduling | $\mathbf{l}$ | $(\#K(z)) \times 2p$ | $c_2 > 1$ |
| 5.4 | Write $y$ | $\mathbf{l}$ | $p$ | $c_2 > 1$ |

Based on the definitions of the established IIR topologies illustrated in Table 4.1, Table 10.4 illustrates the minimum required arithmetical operations necessary for numeric implementation. As observed in the second column, all biquad topologies are based on four additions, five multiplications, and a different number of load and store operations.

Table 10.4: Minimum required arithmetical operations for each digital IIR biquadratic filter topology implementation described in Table 4.1.

| *IIR SOS Topology* | $\min \left\vert \mathbf{Sc}^{K,\mathbf{H}} \right\vert$ |
|---|---|
| Direct Form I (DFI) | 4**a**, 6**m**, 12**l** |
| Direct Form II (DFII) | 4**a**, 6**m**, 14**l** |
| Transposed Direct Form I (TDFI) | 4**a**, 6**m**, 14**l** |
| Transposed Direct Form II (TDFII) | 4**a**, 6**m**, 16**l** |

Based on the definitions of the established FIR topologies illustrated in Table 4.2, Table 10.5 illustrates the minimum required arithmetical operations necessary for numeric implementation. As observed in the second column, all FIR topologies are based on $N$ additions, and a different number of multiplication and load operations, depending on the definition.

Table 10.5: Minimum required arithmetical operations for each digital FIR filter topology implementation described in Table 4.2.

| *FIR topology* | $\min \left\vert \mathbf{Sc}^{K,\mathbf{H}} \right\vert$ |
|---|---|
| Direct Form | $N\mathbf{a}$, $(N{+}1)\,\mathbf{m}$, $(2N{+}2)\,\mathbf{l}$ |
| Direct Form Transposed | $N\mathbf{a}$, $(N{+}1)\,\mathbf{m}$, $(2N{+}2)\,\mathbf{l}$ |
| Symmetric | $N\mathbf{a}$, $\left(\lfloor \frac{N}{2} \rfloor {+}1\right)\mathbf{m}$, $\left(N{+}\lfloor \frac{N}{2} \rfloor {+}2\right)\mathbf{l}$ |
| Anti-symmetric | $N\mathbf{a}$, $\left(\lfloor \frac{N}{2} \rfloor {+}1\right)\mathbf{m}$, $\left(N{+}\lfloor \frac{N}{2} \rfloor {+}2\right)\mathbf{l}$ |

**Corollary 3.** *Given a MIMO regulator* $K \in \mathcal{G}_D^{p\times m}$ *as in* (10.12)*, where each component* $K_{ij}(z)$*,* $i \in \overline{1,p}, j \in \overline{1,m}$ *can be described as an IIR*

*filter* (4.15)*, with SOS terms as in Table 4.1 or a FIR filter* (4.18)*, with difference equations as in Table 4.2, the WCET can be computed as:*

$$WCET(\mathbf{\Gamma_c}, \mathbf{\Gamma_p}) = \left( \mathcal{O}(1) + \sum_{i=1}^{p} \sum_{j=1}^{m} \gamma_{ij} \cdot \min \left| \mathcal{S}_p^{H_{ij}, \mathcal{H}} \right| \right) \times T_{clk}, \quad (10.14)$$

*with coefficients* $\gamma_{ij} > 0$ *accounting for the hardware specifications set* $\mathbf{H}$ *from Definition 12, each assembly operation set* $\mathbf{Sp}^{K_{ij}, \mathbf{H}}$ *determined individually by the RCP application, given the microprocessor tick* $T_{clk} > 0$*, and* $\mathcal{O}(1)$ *depends only on the other higher-priority software threads.*

The proof immediately follows based on Theorem 6 by replacing the general-purpose sequence $\mathbf{Sp}^{K, \mathbf{H}}$ with its corresponding sum of subsystems $K_{ij}$ of the full MIMO regulator definition (10.12).

## 10.5 Conclusions

This section gathered a set of analysis and design tools to deduce a WCET estimation for LTI regulators through a formal language model which can be implemented in an RCP software tool. The execution time model is based on a deterministic, RISC architecture, where each operation is quantified with the same base clock tick duration and a higher-hierarchy is used to extend and adapt the base atomic operations in cases where there appear additional complications.

The theoretical results will be illustrated on an end-to-end design procedure for the case of a DC motor control problem in Section 11.7, starting from the 2DOF control design, followed by a choice of the quasi-optimal sampling rate and a worst-case execution time analysis, finalizing with with a detailed discussion.

# 11. Experiments, remarks, case studies

## 11.1 Fractional-order robust control benchmark example

A set of theoretical developments have been proposed in several conference and journal papers, from which the fractional-order (FO) regulator structures have been successfully integrated into the Robust Control Framework to be used with the $\mathcal{H}_\infty$ and $\mu$-synthesis procedures. The papers focus on different aspects on this subject, such as: performing the synthesis using a metaheuristic optimization approach with a Taylor series truncation in [Mih+21b], using nonsmooth optimization in [MȘD21], [Mih+22a], and [Mih+22b] for FO regulators of different structures, on integer and fractional-order uncertain plants alike, while several order-reduction techniques have been proposed for easier implementation of the synthesized controllers, while still maintaining robust stability and performance, in [Mih+23] and [MŞD23]. The following example described in this section is based on MIMO fractional-order PID and lead-lag compensator-based control of a benchmark mechanical system, first presented in [Mih+22a]. More recently, an end-to-end robust numerical implementation framework combining fractional-order robust control with sampling-rate and quantization design considerations has been reported in [MŞD24], further extending these developments toward practical deployment.

A comparative case study will be presented on a benchmark eight-order MIMO mass, spring, dashpot system, based on the articles 17 and 18 from [LGA11]. The system is LTI, with well-known and relatively complex dynamics modelled through the Euler-Lagrange equation:

$$\mathcal{M}\ddot{q}(t) + \mathcal{C}\dot{q}(t) + \mathcal{K}q(t) = \mathcal{T}u(t), \tag{11.1}$$

where $q(t) = [q_i]_{i\in\overline{1,4}}$ are the mechanical positions of the four masses, while matrices $\mathcal{M}, \mathcal{C}, \mathcal{K}, \mathcal{T}$ store the masses, frictions, elasticities of the

system, and the matrix to focus the two force inputs to the second and fourth masses' positions, respectively, given by:

$$\mathcal{M} = \begin{pmatrix} m_1 & 0 & 0 & 0 \\ 0 & m_2 & 0 & 0 \\ 0 & 0 & m_3 & 0 \\ 0 & 0 & & m_4 \end{pmatrix}; \quad \mathcal{T} = \begin{pmatrix} 0 & 0 \\ 1 & 0 \\ 0 & 0 \\ 0 & 1 \end{pmatrix}; \tag{11.2}$$

$$\mathcal{C} = \begin{pmatrix} c_1 + c_2 & -c_2 & 0 & 0 \\ -c_2 & c_2 + c_3 & -c_3 & 0 \\ 0 & -c_3 & c_3 + c_4 & -c_4 \\ 0 & 0 & -c_4 & c_4 \end{pmatrix}; \tag{11.3}$$

$$\mathcal{K} = \begin{pmatrix} k_1 + k_2 & -k_2 & 0 & 0 \\ -k_2 & k_2 + k_3 & -k_3 & 0 \\ 0 & -k_3 & k_3 + k_4 & -k_4 \\ 0 & 0 & -k_4 & k_4 \end{pmatrix}. \tag{11.4}$$

As such, the state-space model $G$ of the plant can be represented in the following manner, with the state defined as $x^\top = \begin{pmatrix} q^\top & \dot{q}^\top \end{pmatrix}$, the input $u^\top = \begin{pmatrix} f_1 & f_2 \end{pmatrix}$, and output $y^\top = \begin{pmatrix} x_2 & x_4 \end{pmatrix}$:

$$\left(\frac{\dot{x}(t)}{y(t)}\right) = \left(\begin{array}{cc|c} O_{4\times4} & I_{4\times4} & O_{4\times2} \\ -\mathcal{M}^{-1}\mathcal{K} & -\mathcal{M}^{-1}\mathcal{C} & \mathcal{M}^{-1}\mathcal{T} \\ \hline \mathcal{T}^\top & O_{2\times4} & O_{2\times2} \end{array}\right) \left(\frac{x(t)}{u(t)}\right). \tag{11.5}$$

To meaningfully illustrate the full capacity of the proposed method, the mechanical system will also be governed by parametric uncertainties, with values presented in Table 11.1. The singular values of the nominal plant, along with 100 Monte Carlo simulations sampled from the uncertainty set, are shown in Figure 11.1 (blue).

In order to impose the performance of the closed-loop system, i.e. the interconnection between the process $G$ and the controller $K$, the sensitivity function $S = (I + GK)^{-1}$ and the complementary sensitivity function $T = I - S$ will be weighted, obtaining an augmented plant $P$ having as performance inputs the reference signals $w^\top = \begin{pmatrix} r_1^\star & r_2^\star \end{pmatrix}$

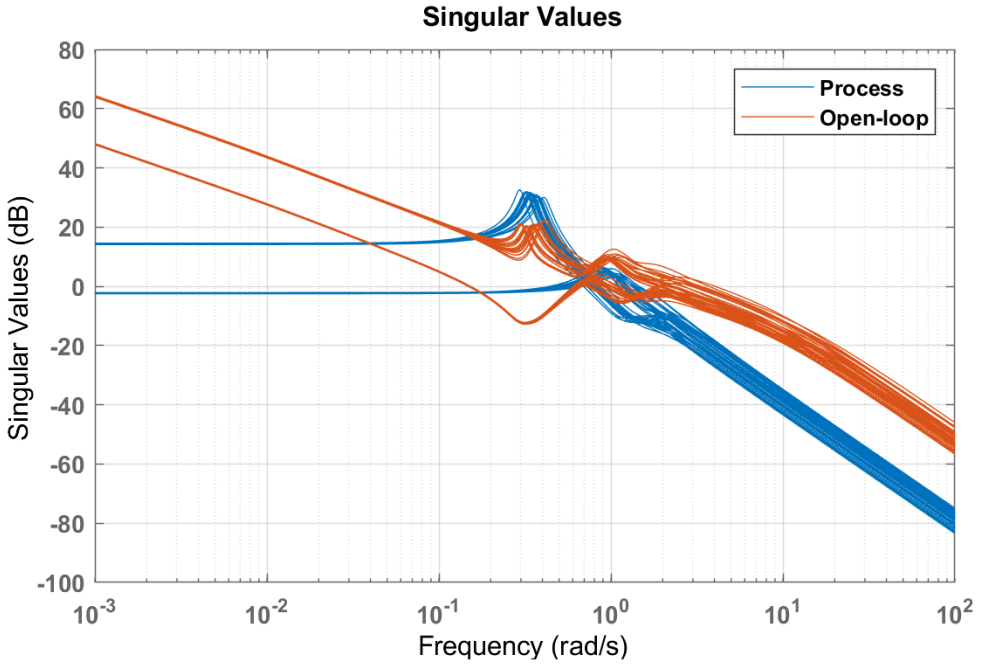


Figure 11.1: Singular value plot for the plant (11.5), values from Table 11.1 and for the open-loop control system $KG$.

Table 11.1: Mechanical parameters, nominal values and tolerances.

| *Param.* | *Nominal* | *Tol.* | *Param.* | *Nominal* | *Tol.* |
|---|---|---|---|---|---|
| $m_1$ | 1 [kg] | $\pm 10\%$ | $c_1$ | 0.4 [Ns/m] | $\pm 5\%$ |
| $m_2$ | 1 [kg] | $\pm 50\%$ | $c_2$ | 0.4 [Ns/m] | $\pm 5\%$ |
| $m_3$ | 1 [kg] | $\pm 50\%$ | $c_3$ | 0.4 [Ns/m] | $\pm 5\%$ |
| $m_4$ | 1 [kg] | $\pm 50\%$ | $c_4$ | 0.4 [Ns/m] | $\pm 5\%$ |
| $k_1$ | 1 [N/m] | $\pm 5\%$ | $k_2$ | 1 [N/m] | $\pm 5\%$ |
| $k_3$ | 1 [N/m] | $\pm 5\%$ | $k_4$ | 1 [N/m] | $\pm 5\%$ |

and as performance outputs $z^\top = \begin{pmatrix} z_{S,1} & z_{S,2} & z_{T,1} & z_{T,2} \end{pmatrix}$. The resulting problem is a mixed-sensitivity loop-shaping $\mu$-synthesis problem:

$$\begin{aligned} &\inf_{K\in\mathcal{K}} \sup_{\omega\in\mathbb{R}_+} \inf_{D\in\boldsymbol{D}} \overline{\sigma}\left(D(j\omega)\cdot LLFT(P,K)(j\omega)\cdot (D(j\omega))^{-1}\right) \\ &\text{s.t. } \left\| \begin{pmatrix} W_S S & W_T T \end{pmatrix} \right\|_\infty < 1, \end{aligned} \tag{11.6}$$

where the weighting functions are computed based on [Șuș+21]. For the purpose of this paper, weighting functions are considered to be diagonal, having the following parameters: maximum steady-state error $A_S = 0.01$, sensitivity peak amplitude $M_S = 2.4$, bandwidth $\omega_B = 0.15$ $[rad/s]$, complementary sensitivity peak amplitude $M_T = 2.4$, complementary bandwidth $\omega_{BT} = 6$ $[rad/s]$, maximum allowed high frequency amplitude $A_T = 0.01$, and roll-off $n_T = 2$, obtaining the diagonal filters:

$$W_S(s) = \begin{pmatrix} \frac{0.4167s+0.15}{s+0.0015} & 0 \\ 0 & \frac{0.4167s+0.15}{s+0.0015} \end{pmatrix}; \tag{11.7}$$

$$W_T(s) = \begin{pmatrix} 100\frac{(s+6)^2}{(s+92.95)^2} & 0 \\ 0 & 100\frac{(s+6)^2}{(s+92.95)^2} \end{pmatrix}. \tag{11.8}$$

As an illustrative example, the MIMO fractional-order controller has a diagonal structure, each component being a product between a FO-PID and a FO-lead-lag compensator:

$$K_{FO}^{(i,i)} = \left( K_P^{(i,i)} + \frac{K_I^{(i,i)}}{s^{\alpha_I^{(i,i)}}} + K_D s^{\alpha_D^{(i,i)}} \right) \frac{b_1^{(i,i)} s^{\beta_1^{(i,i)}} + 1}{a_1^{(i,i)} s^{\alpha_1^{(i,i)}} + 1}. \tag{11.9}$$

As can be noticed in Figure 11.1, the relevant frequency range is between $\omega_L = 10^{-2}$ $[rad/s]$ and $\omega_U = 10$ $[rad/s]$, which is used for the approximation of the fractional-order elements involved in the FO-controller, as well, along with an order of approximation equal to the number of decades of this range, i.e. $N = 3$. The `musyn` routine from MATLAB was used with the maximum number of iterations 20. The controller obtained after 6 $D$–$K$ iterations follows the upper bound $\mu_{\mathbf{\Delta}}(LLFT(P, K)) \leq 0.9298 < 1$, having the parameters presented in Table 11.2, with the open-loop response illustrated in Figure 11.1 (red), where the filter's frequency $\omega_\alpha$ is used as a free parameter, resulting $\omega_\alpha^{(1,1)} = 0.6669$ $[rad/s]$. The frequency performance, i.e. the sensitivity and the complementary sensitivity functions, are depicted in Figure 11.2 for the nominal plant along with 100 Monte Carlo simulations using the tolerances specified in Table 11.1, and it can be noticed that the imposed shapes are fulfilled.

Moreover, in order to compare the proposed method with previous research in this field, the metaheurisitc approach described in [Mih+21b] has also been used. For a fair comparison, the controller structure has

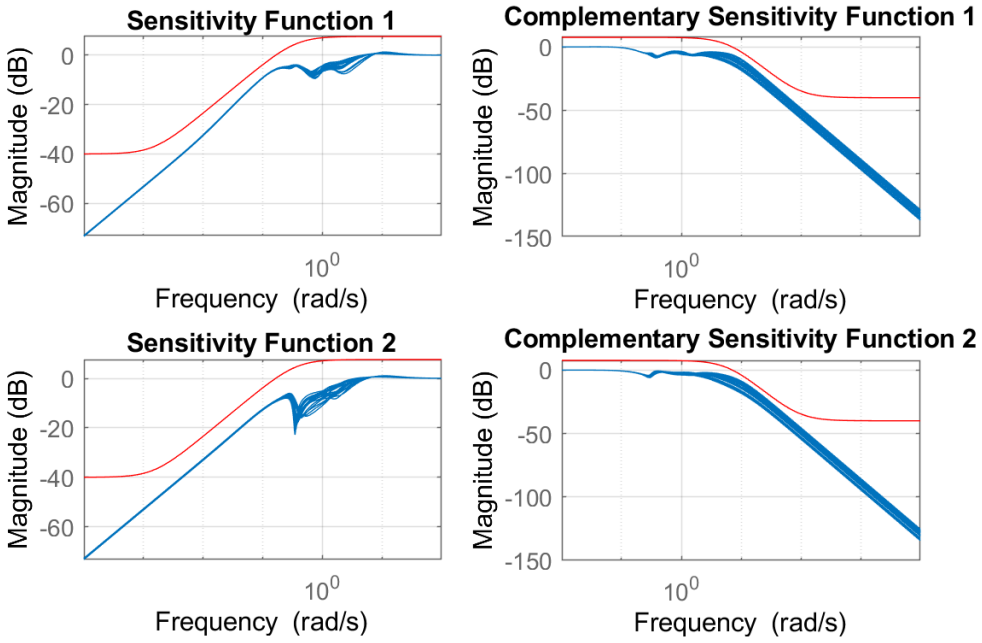


Figure 11.2: Sensitivity and closed-loop sensitivity functions for both nominal plant and 100 Monte Carlo simulations of uncertain plants, along with the imposed shapes in the augmentation step.

been maintained, with the algorithm hyperparameters: the swarm dimension 50, the maximum number of cycles with no improvements 10, the maximum number of D–K iterations 10, the maximum window length for assessing lack of progress 4, while the parameters for the cost functions are $\alpha_{ABC} = 1$ and $\beta_{ABC} = 10^5$. The parameters of the resulting con-

Table 11.2: Controller's parameters using the method of [Mih+22a].

| *Param.* | *Value* | *Param.* | *Value* | Param. | *Value* |
|---|---|---|---|---|---|
| $K_P^{(1,1)}$ | $-0.0491$ | $K_I^{(1,1)}$ | $-0.1515$ | $K_D^{(1,1)}$ | $-0.003$ |
| $\alpha_I^{(1,1)}$ | 1.6513 | $\alpha_D^{(1,1)}$ | 1.6335 | $b_1^{(1,1)}$ | 2.7223 |
| $\beta_1^{(1,1)}$ | 0.5724 | $\alpha_1^{(1,1)}$ | 0.0532 | $a_1^{(1,1)}$ | 0.2363 |
| $K_P^{(2,2)}$ | $-0.2226$ | $K_I^{(2,2)}$ | $-0.247$ | $K_D^{(2,2)}$ | $-0.0272$ |
| $\alpha_I^{(2,2)}$ | 1.009 | $\alpha_D^{(2,2)}$ | 0.9998 | $b_1^{(2,2)}$ | 6.8e-4 |
| $\beta_1^{(2,2)}$ | 0.9995 | $\alpha_1^{(2,2)}$ | 0.2473 | $a_1^{(2,2)}$ | 0.1105 |

troller are presented in Table 11.3, while the obtained structural singular value is $\mu_{\mathbf{\Delta}}(LLFT(P,K)) \leq 0.9998 < 1$.

Additionally, the same problem has been solved with an unstructurred controller using the `musyn` routine from MATLAB [Bal+22]. In this case, the $\mu$-synthesis problem converged with a resulting optimal state-space controller $K_{opt}$ of order 44 in 2 $D$–$K$ iterations, with the structural singular value $\mu_{\mathbf{\Delta}}(LLFT(P,K_{opt})) \leq 0.9473 < 1$.

In Figure 11.3, the structural singular values for these three experiments are presented. As noticeable, the upper bound of the structural singular value is less than 1 for all cases, which denotes that the resulting controllers guarantee both robust stability and performance. A comparison between the time-domain performance obtained with the three compared methods is depicted in Figure 11.4. It can be noticed that the overshoot is below 4[%], with comparable settling times, rise times and negligible steady-state errors, while the fixed-structure controllers present zero steady-state errors.

The proposed method concerns the controller step of a $D$–$K$ iteration. As such, the fractional order element can be integrated into the fixed-structure $\mathcal{H}_\infty$ control problem, resulting a controller which satisfies nominal stability and nominal performance. Using the `hinfstruct` routine from MATLAB, the following fixed-structure mixed-sensitivity loop shaping $\mathcal{H}_\infty$ control problem has been solved using the same structure of

Table 11.3: Controller's parameters using the method of [Mih+21b].

| *Param.* | *Value* | *Param.* | *Value* | *Param.* | *Value* |
|---|---|---|---|---|---|
| $K_P^{(1,1)}$ | $-0.0481$ | $K_I^{(1,1)}$ | $-0.105$ | $K_D^{(1,1)}$ | $-0.0646$ |
| $\alpha_I^{(1,1)}$ | 1.6 | $\alpha_D^{(1,1)}$ | 1.127 | $b_1^{(1,1)}$ | 2.1486 |
| $\beta_1^{(1,1)}$ | 0.6577 | $\alpha_1^{(1,1)}$ | 0.0499 | $a_1^{(1,1)}$ | 0.0691 |
| $K_P^{(2,2)}$ | $-0.0494$ | $K_I^{(2,2)}$ | $-0.2391$ | $K_D^{(2,2)}$ | $-0.0352$ |
| $\alpha_I^{(2,2)}$ | 1.0915 | $\alpha_D^{(2,2)}$ | 0.7769 | $b_1^{(2,2)}$ | 0.0647 |
| $\beta_1^{(2,2)}$ | 0.5750 | $\alpha_1^{(2,2)}$ | 0.0178 | $a_1^{(2,2)}$ | 0.164 |

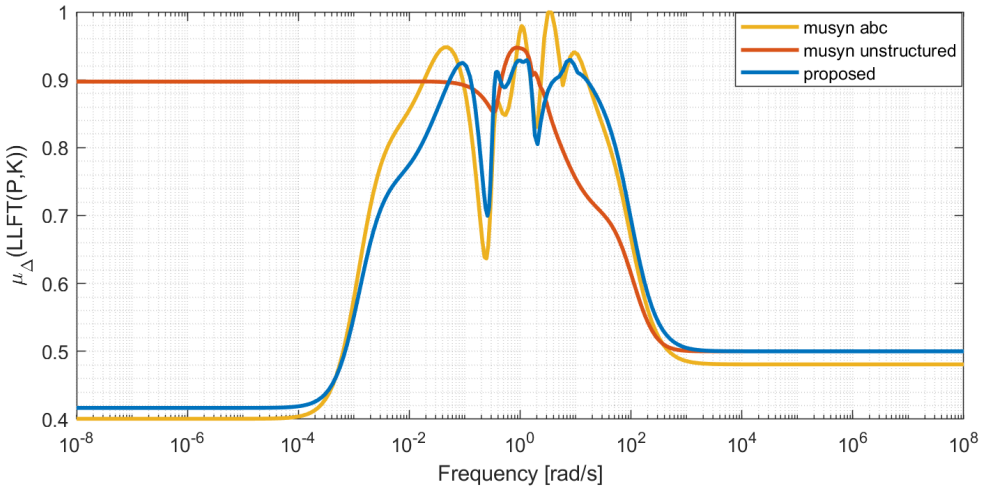


Figure 11.3: $\mu(j\omega)$ upper bound estimation magnitude characteristic for the three considered synthesis methods: optimized with the ABC method [Mih+21b], optimized through [PDB93], followed by the method of [Mih+22a].

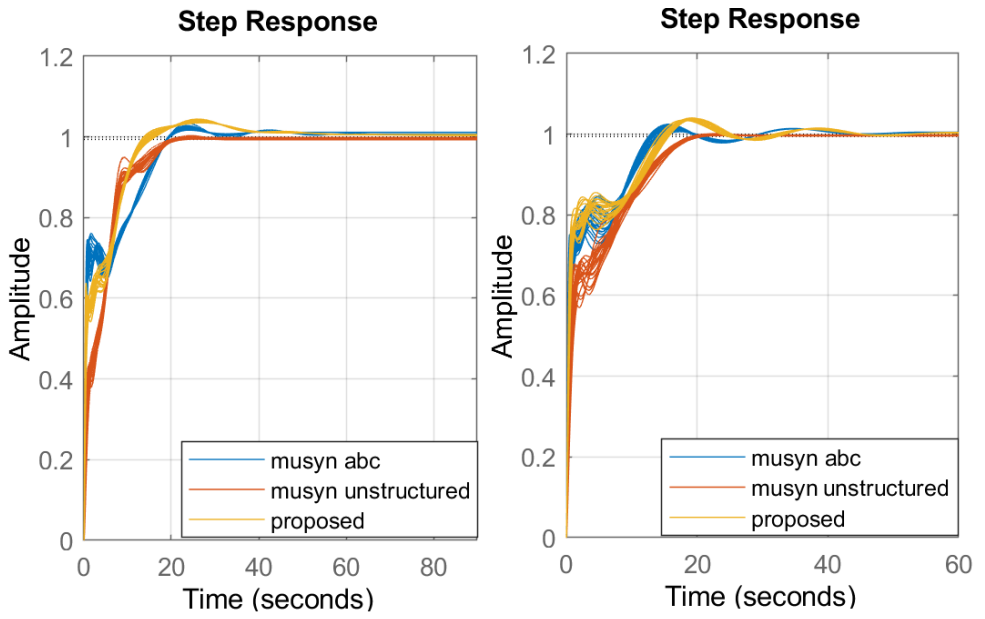


Figure 11.4: Time domain step response simulation of the mass, spring, dashpot uncertain plant for the three compared control methods.

the controller:

$$\begin{aligned} &\inf_{K\in\mathcal{K}} \sup_{\omega\in\mathbb{R}_+} \overline{\sigma}\left(LLFT(P,K)(j\omega)\right), \\ &\text{s.t. } \| \begin{pmatrix} W_S S & W_T T \end{pmatrix} \|_\infty < 1. \end{aligned} \tag{11.10}$$

The resulting parameters of the controller are presented in Table 11.4, having the $\mathcal{H}_\infty$ norm $\|LLFT(P,K)\|_\infty = 0.5541 < 1$. As such, the controller manages to fulfill nominal stability and performance. A comparison between the singular values of the resulting controllers is seen in Figure 11.5. It can be noticed that the controllers obtained with the ABC approach from [Mih+21b] and those obtained with the proposed method are quite similar.

The are two main improvements of the proposed method against the method presented in the previous work [Mih+21b]: (i) the proposed method offers the possibility to integrate the fractional-order element $s^\alpha$ into the Robust Control Framework using only the ORA approximation, while the previous method used an extra set of Taylor's first order approximations; (ii) the current method manages to write the approximation of the fractional element using only arithmetical operations which allows the use of nonsmooth optimization techniques [AN17], being faster than the metaheuristic ABC algorithm, which also required a more compact domain in order to find a solution in several hours.

Table 11.4: Controller's parameters using the `hinfstruct` method.

| *Param.* | *Value* | *Param.* | *Value* | *Param.* | *Value* |
|---|---|---|---|---|---|
| $K_P^{(1,1)}$ | $-0.0398$ | $K_I^{(1,1)}$ | $-0.2144$ | $K_D^{(1,1)}$ | $-5.34\text{e-}4$ |
| $\alpha_I^{(1,1)}$ | 1.7025 | $\alpha_D^{(1,1)}$ | 2 | $b_1^{(1,1)}$ | 3.0638 |
| $\beta_1^{(1,1)}$ | 1 | $\alpha_1^{(1,1)}$ | 0.4189 | $a_1^{(1,1)}$ | 0.468 |
| $K_P^{(2,2)}$ | 0.8394 | $K_I^{(2,2)}$ | $-1.6535$ | $K_D^{(2,2)}$ | $-0.3259$ |
| $\alpha_I^{(2,2)}$ | 1 | $\alpha_D^{(2,2)}$ | 0.7194 | $b_1^{(2,2)}$ | $9.58\text{e-}4$ |
| $\beta_1^{(2,2)}$ | 1 | $\alpha_1^{(2,2)}$ | 0.058 | $a_1^{(2,2)}$ | 1.7468 |

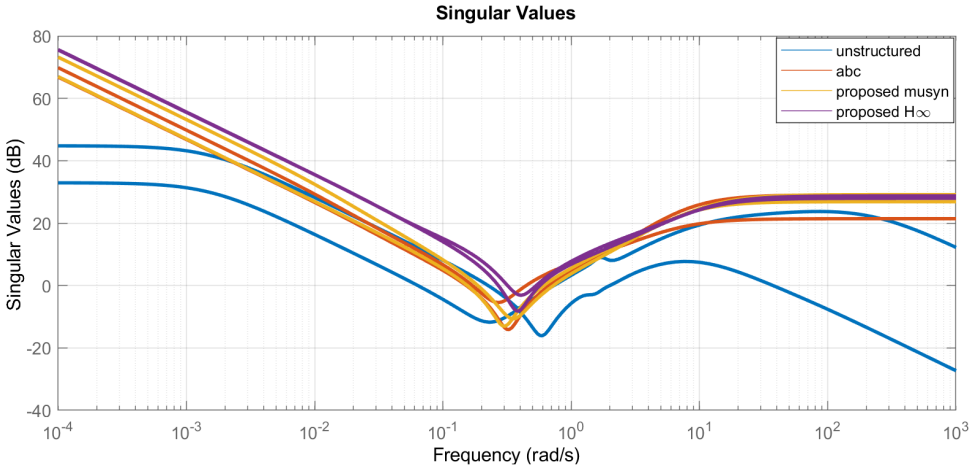


Figure 11.5: Singular values of the resulting controllers obtained with unstructured `musyn`, the metaheuristic approach from [Mih+21b], proposed method with `musyn`, and proposed method with `hinfstruct`, respectively.

## 11.2 Uncertainty modelling of mechanical systems

This section's examples emphasize contributions from Chapter 6.

### 11.2.1 Benchmark double resonance model

A first example is given by a simple benchmark transfer function which represents an envelope bound on the measurement points $\ell(j\omega)$ with added multiplicative noise, to illustrate one of the benefits of using the proposed nonconvex solution. Define such a function as the fourth order model with resonances:

$$U^{ref}(s) = \frac{5000}{(s^2 + 0.1s + 100)(s^2 + s + 400)}, \tag{11.11}$$

with a $\pm 10\%$ relative variation on each considered magnitude measurement sample in the frequency range $\Omega = [10^{-4}, 10^{4}]$, which has two damping factors: $\zeta_1 = 0.025$ and $\zeta_2 = 5{\times}10^{-3}$.

Using a Hankel singular values (HSV) plot to visualize the search domain of Problem 5, the obvious choice is to select the pole-zero excess as $e^\star = n^\star - m^\star = 4$ and no zeros, which leads to the optimization

structure $\theta = \begin{pmatrix} k & b_0 & a_3 & a_2 & a_1 & a_0 \end{pmatrix}^\top$:

$$U_\theta(s) = k \cdot \frac{b_0}{s^4 + a_3 s^3 + a_2 s^2 + a_1 s + a_0}. \tag{11.12}$$

The initial point $U_0$, which is the reference model using the convex optimization framework, used further in the proposed optimization will also constitute the means to compare the solution to another well-established method from the literature:

$$U_{\theta_0}(s) = \frac{5377.6}{(s^2 + 2.134{\times}10^{-7} s + 95.74)(s^2 + 0.4802 s + 408.5)}, \tag{11.13}$$

which is invalid with the data. The objective function $L(\theta)$ from (6.5) values in $[dB]$ computed for a complete configuration of pole-zero structures with order up to 10 is illustrated in Figure 11.6. The optimal configuration is obtained, based on $\lambda = 1000$, as $J(n^\star, m^\star) = J(4, 0) = 52.31\,[dB]$, surrounded by adjacent pairs $(n, m)$ of values in range $[53.94, 87.56]\,[dB]$.

The interior-point algorithm which performs the optimization allows to bring the variable $\theta$ into the feasible domain, i.e. $C(\theta) \succeq 0$, which, additionally, also leads to a smaller objective function value compared to its starting point $\theta_0$. This phenomenon can be seen in Figure 11.7. It shows optimization starting from an infeasible point (red) which converges towards a valid point (blue), with the best fit given the data and provided functional. Even after reaching feasibility, the loss functional managed to obtain a smaller value than in infeasible cases, so the method provided both feasibility and a better fit value.

After solving Problem 6, the vector of parameters becomes $\theta^\star = [1.03142 \quad 5.37758{\times}10^4 \quad 0.37298 \quad 488.487 \quad 37.3106 \quad 3.91147{\times}10^4]$, leading to a valid uncertainty model $U_{\theta^\star} \equiv U^\star$:

$$U^\star(s) = \frac{5546.6}{(s^2 + 2.358{\times}10^{-4} s + 100.9)(s^2 + 0.3727 s + 387.6)} \tag{11.14}$$

The comparison between the proposed fit and the established convex approach from [BV04] is shown in Figure 11.8. Due to the randomness introduced in the magnitude measurements, both transfer functions $U_{\theta_0}(s)$ and $U_{\theta^\star}(s)$ have slight differences based on the initial reference model from (11.11). This example shows that, even in a SISO case, because the inherent system presents a singularity in the case of the

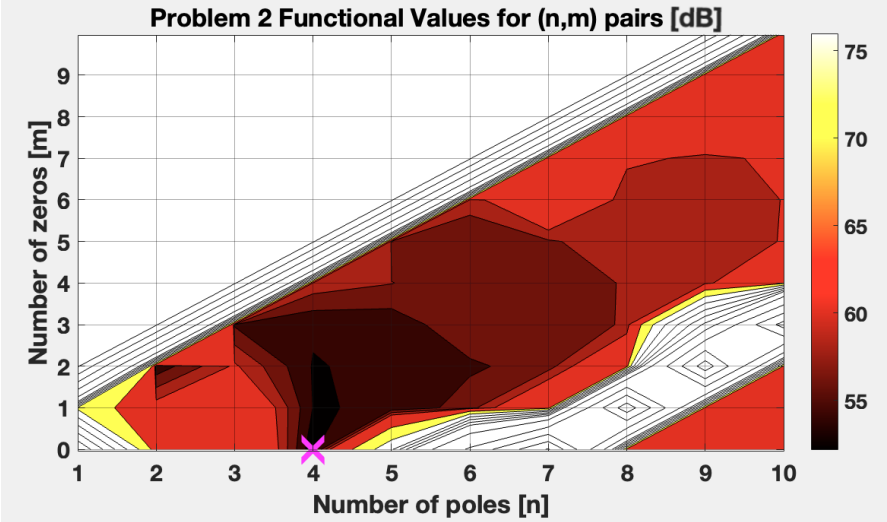


Figure 11.6: Two-dimensional initial point optimization Problem 5 applied for the benchmark case study of Section 11.2.1, with achieved optimum $(n^\star, m^\star) = (4, 0)$.

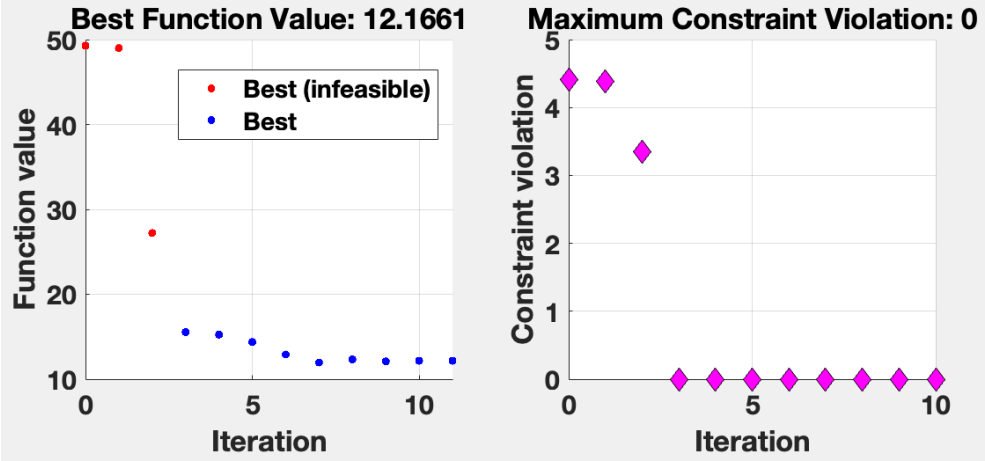


Figure 11.7: Number of iterations and achieved values for the objective and constraint function violation of Problem 6, for the case study of Section 11.2.1. The initial point $U_{\theta_0}(s)$ starts outside the feasible domain, as marked with red dots.

semidefinite programming solution, as poles on or near the imaginary axis are not supported by the method, the standard fitting approach may lead to potentially unsatisfactory results, as will be demonstrated

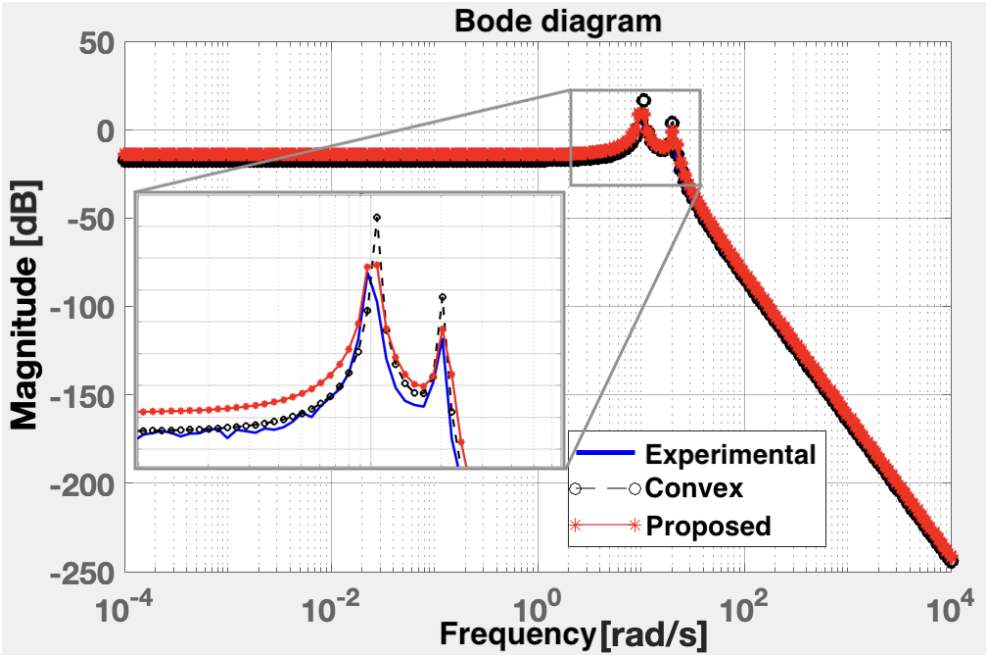


Figure 11.8: Magnitude response of the generated experimental points, alongside the proposed solution and the convex optimization alternative, which is invalid with respect to the data for the particular case study of Section 11.2.1.

for the next practical case study which illustrates such implications in a concrete robust control synthesis case.

### 11.2.2 Inverted pendulum modelling and control

The second case study focuses on an end-to-end robust control synthesis for an inverted pendulum-type mechanical system, with the particular structure known in the literature as Cubli, such as in [Gaj+12]. Other inverted pendulum structures can be found in [Stă+20], focusing on mechanical design aspects and LQR control. The analytical linearized model can be represented as the third order SISO state-space:

$$A = \begin{pmatrix} 0 & 1 & 0 \\ \frac{g(m_b\ell_b+m_w\ell)}{I_b+m_w\ell^2} & -\frac{C_b}{I_b+m_w\ell^2} & \frac{C_w}{I_b+m_w\ell^2} \\ -\frac{g(m_b\ell_b+m_w\ell)}{I_b+m_w\ell^2} & \frac{C_b}{I_b+m_w\ell^2} & -\frac{C_w\left(I_b+I_w+m_w\ell^2\right)}{I_w(I_b+m_w\ell^2)} \end{pmatrix};$$

$$B_u = \begin{pmatrix} 0 \\ -\frac{K_m}{I_b+m_w\ell^2} \\ \frac{K_m\left(I_b+I_w+m_w\ell^2\right)}{I_w(I_b+m_w\ell^2)} \end{pmatrix}; \quad C_y^\top = \begin{pmatrix} 1 \\ 0 \\ 0 \end{pmatrix}; \quad D_{yu} = 0, \tag{11.15}$$

with the corresponding transfer function:

$$H(s) = \frac{-\frac{K_m}{I_b+\ell^2 m_w}s}{s^3 + \alpha_2 s^2 + \alpha_1 s - \frac{C_w g(\ell_b m_b+\ell m_w)}{I_b+\ell^2 m_w}}, \tag{11.16}$$

where the remaining coefficients are written separately as:

$$\alpha_1 = \frac{\frac{C_w}{I_w}C_b - g(\ell_b m_b+\ell m_w)}{I_b+\ell^2 m_w}; \quad \alpha_2 = \frac{C_b+\frac{C_w}{I_w}I_b+C_w+\frac{C_w}{I_w}\ell^2 m_w}{I_b+\ell^2 m_w}.$$

The transfer function above highlights the derivative behavior of the system. An implicit integrator controller will be considered for this system during all discussions. Additionally, the fact that the system is unstable can also be deduced due to the presence of negative values in the denominator in (11.16). Such a system is governed by parametric uncertainties due to the practical difficulties of estimating the exact values of the mechanical parameters involved. A set of nominal values with variability ranges used for this study is presented in Table 11.5.

Table 11.5: Inverted pendulum parameters: nominal values, tolerances.

| *Param.* | *Val.* | *Tol.* | *Param.* | *Val.*$\times 10^3$ | *Tol.* |
|---|---|---|---|---|---|
| $\ell$ $[m]$ | 0.085 | $\pm 2\%$ | $C_b$ $\left[\frac{Nms}{rad}\right]$ | 1.02 | $\pm 20\%$ |
| $\ell_b$ $[m]$ | 0.075 | $\pm 2\%$ | $C_w$ $\left[\frac{Nms}{rad}\right]$ | 0.05 | $\pm 20\%$ |
| $m_b$ $[kg]$ | 0.419 | $\pm 20\%$ | $I_b$ $[kg\ m^2]$ | 3.34 | $\pm 20\%$ |
| $m_w$ $[kg]$ | 0.204 | $\pm 20\%$ | $I_w$ $[kg\ m^2]$ | 0.57 | $\pm 20\%$ |
| $g$ $\left[\frac{m}{s^2}\right]$ | 9.81 | – | $K_m$ $\left[\frac{Nm}{A}\right]$ | 10 | $\pm 20\%$ |

A mixed-sensitivity closed-loop shaping $\mu$-synthesis method will further be applied, using the well-known sensitivity function $S$ for steady-state performance, complementary sensitivity function $T$ for transient performance, along with the control effort $R = KS$ for limiting command

signal magnitudes. The weighting functions are structured as:

$$W_S(s) = \frac{0.5s + 7}{s + 0.007}; \quad W_{KS}(s) = \frac{10^{-7}s + 0.0001}{s + 0.01}; \\ W_T(s) = \frac{s^2 + 280s + 19600}{0.0001s^2 + 4.85s + 5.88{\times}10^4}, \tag{11.17}$$

focusing on a sensitivity bandwidth $\omega_B \geq 7$ $[rad/s]$, acceptable steady-state error $A \leq 10^{-3}$, a roll-off of at least $-40$ $[dB]$ active above the complementary sensitivity bandwidth of $\omega_{BT} \geq 140$ $[rad/s]$. As such, the augmented plant presents itself as:

$$P = \begin{bmatrix} W_S & 0 & 0 & 1 \\ -W_S G\frac{1}{s} & W_{KS} & W_T G\frac{1}{s} & -G\frac{1}{s} \end{bmatrix}^\top. \tag{11.18}$$

Starting from the analytical model (11.15) and uncertainty definitions from Table 11.5, there are several possible approaches to model the uncertain plant model $G$ using the structure from (3.34), which will be covered: (i) the direct approach, where each parameter will be considered using a separate block $\delta_i$ based on definition (3.29); (ii) the polytopic approach which considers the worst-case configurations of the state-space matrices involved in the model and can easily become conservative; (iii) the Log-Chebyshev SDP approach from (3.37) using magnitude measurements; (iv) the proposed nonconvex optimization approach.

Using approach (i), the plant $G$ from (3.34), part of (3.33), will have the resulting uncertainty-related signal dimensions $(n_d, n_v) = (58, 58)$. A reduced dimensionality can be obtained to $(48, 48)$ using the `simplify` routine, which applies the heuristics of [VL99] to reuse uncertainty blocks when redundant. With the scope of applying the $\mu$-synthesis procedure to $P$ with $G$ obtained using the above approach, a fundamental complication occurs, leading to the detectability loss of the augmented plant, property which is a precondition for the successful application of the $\mathcal{H}_\infty$ synthesis procedure, necessary in the $D$–$K$ iteration. As such, the SSV defaults to the value $\overline{\mu}_\Delta\left(\mathrm{LLFT}\left(P, K\right)\right) = +\infty$, and the approach becomes unfeasible, i.e. $K \in \emptyset$.

Using approach (ii), an uncertainty model with smaller dimension-

Table 11.6: Polytopic model parameters described in approach (ii) based on Table 11.5 and with the remark that $a_{31} = -a_{21}$ and $a_{32} = -a_{22}$.

| *Param.* | *Val.* | *Tol.* | *Param.* | *Val.* | *Tol.* |
|---|---|---|---|---|---|
| $a_{21}$ | 115 | $\pm 15\%$ | $a_{22}$ | $-0.199$ | $\pm 7.73\%$ |
| $100{\cdot}a_{23}$ | 0.976 | $\pm 7.73\%$ | $100{\cdot}a_{33}$ | $-9.75$ | $\pm 0.77\%$ |
| $b_2$ | $-6.21$ | $\pm 27.2\%$ | $b_3$ | 61.2 | $\pm 20.7\%$ |

ality can be obtained using a convex hull of vertices:

$$(G_n(s)) : \left(\begin{array}{c|c} A & B \\ \hline C & D \end{array}\right) = \left(\begin{array}{ccc|c} 0 & 1 & 0 & 0 \\ a_{21} & a_{22} & a_{23} & b_2 \\ a_{31} & a_{32} & a_{33} & b_3 \\ \hline 1 & 0 & 0 & 0 \end{array}\right), \tag{11.19}$$

$a_{ij} \in \left\{\underline{a_{ij}}, \overline{a_{ij}}\right\}$, $b_i \in \left\{\underline{b_i}, \overline{b_i}\right\}$, with each parameter of the model seen as a function of the Cubli parameters with tolerances from Table 11.5. The dimensionality becomes $(n_d, n_v) = (8, 8)$, finding that $a_{32} = -a_{22}$ and $a_{31} = -a_{21}$. The nominal values and tolerances of the polytopic model parameters $a_{ij}$, $b_i$ are illustrated in Table 11.6. This approach leads to a considerably lower dimensionality of the augmented plant, with the caveat of introducing conservativeness. In this case, the detectability issue is not present. After the $\mu$-synthesis, the least SSV is computed at $\overline{\mu}_{\Delta}\left(\mathrm{LLFT}\left(P, K\right)\right) = 976.0395 \gg 1$, leading to an unfeasible solution.

For the last two approaches, (iii) and (iv), we consider an input multiplicative normalized model for the uncertain plant, defined as $G = G\left(I + \Delta U\right) \in \mathcal{G}$, $\|\Delta\| \leq 1$, with $U(s)$ computed for (iii) using the Log-Chebyshev magnitude fit, which is also the initial point for the solution of (iv). The magnitude measurements $\ell(\omega)$, defined in (3.36), can thus be computed based on:

$$\ell\left(\omega\right) = \mathcal{T}^{-1}\left(G\left(\omega\right), G_n\left(\omega\right)\right) = \sup_{G_n \in G} \left|\frac{G\left(j\omega\right)}{G_n\left(j\omega\right)} - 1\right|, \ \|\Delta\| \leq 1, \tag{11.20}$$

for a discrete set of equally-spaced angular frequencies in logarithmic scale: $\Omega = \{\omega_1 < \omega_2 < \cdots < \omega_N\} \subset [10^{-3}, 10^{3}]$.

The solution $(n, m)$ to Problem 5 is given by the pair $(1, 1)$, which leads to an initial uncertainty fit $U_{\theta_0}(s)$, whereupon the solution $U^\star(s)$ to Problem 6 is based on. Their expressions are:

$$U_{\theta_0}(s) = 0.45824 \times \frac{s + 0.09807}{s + 0.04534},\ U^\star(s) = 0.45776 \times \frac{s + 0.1006}{s + 0.04883}.$$

with various trials for $\gamma(\omega) > 0$, $\omega \in \Omega$ for the SDP problem (3.37).

Proceeding with the developed uncertainty models, the augmented plant's dimensions are $(n_d, n_v) = (1, 1)$, while the $\mu$-synthesis procedure leads to a regulator $K_{\theta_0}$ of order 16 and SSV upper bound $\overline{\mu}_\Delta$ (LLFT $(P, K)$) $= 1.027 > 1$ in the case of $U_{\theta_0}$, which is close to the desired upper bound, but still remains unsatisfactory, compared to a regulator $K^\star$ of order 16, in the case of $U^\star$, with upper SSV of $\overline{\mu}_\Delta$ (LLFT $(P, K)) = 0.9799 < 1$.

To further assess the controller synthesis, we have verified through two order-reduction approaches using the balanced model reduction technique with additive and multiplicative errors that it does not accidentally lead to an upper SSV bound less than one for $K_{\theta_0}$, disproving this hypothesis. As such, the plant model with specified performance weights $W_S$, $W_R$, $W_T$ leads to an infeasible problem. On the other hand, the reduced-order regulator of order 6, for $K^\star$, remains within a 2% tolerance around the optimal solution. The reduced-order controllers are shown only, for brevity, which have similar frequency responses to the full 16th order ones. The reduced-order forms for $K_{\theta_0}$, $K^\star$, including the necessary integrator terms, are:

$$K^{red}_{\theta_0,6i}(s) = \frac{-1.621\times10^9\,(s + 37.52)\,(s + 10.54)}{s\,(s + 891.7)\,(s + 43.57)} \times \frac{(s + 2.779)\,(s^2 + 0.1651s + 0.009617)}{(s^2{+}0.01069s{+}3.134\times10^{-5})\,(s^2{+}691.7s{+}1.778\times10^5)}. \tag{11.21}$$

$$K^{\star,red}_{6i}(s) = \frac{-3.7935\times10^9\,(s + 39.09)\,(s + 10.44)}{s\,(s + 1169)\,(s + 45.89)} \times \frac{(s + 2.851)\,(s^2 + 0.1692s + 0.01018)}{(s^2{+}0.01187s{+}3.624\times10^{-5})\,(s^2{+}981.7s{+}2.916\times10^5)}. \tag{11.22}$$

The results of the previous discussion can be gathered in Figures 11.9, 11.10, and Table 11.7. Figure 11.9 shows the reduced conservative-

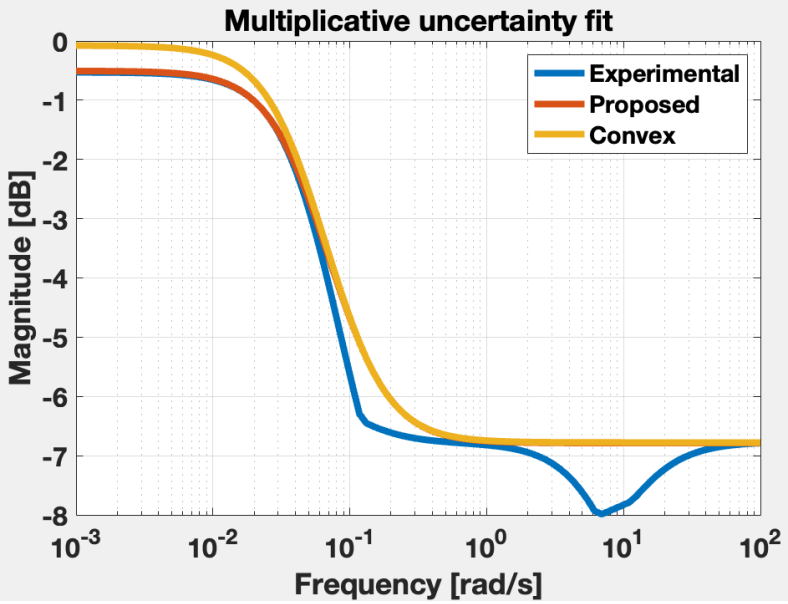


Figure 11.9: Multiplicative uncertainty fits for Cubli frequency response data based on analytical Monte Carlo samples for approaches (iii), (iv).

Table 11.7: $\mu$-synthesis results for various Cubli uncertainty models.

| Method | $D$–$K$ Iter. | Peak SSV | $K(s)$ | $(n_d, n_v)$ |
|---|---|---|---|---|
| `ureal` | 1 | $\infty$ | – | $(58, 58)$ |
| Polytopic | 3 | 976 | 9 | $(8, 8)$ |
| Convex | 9 | 1.03 | 17 (7) | $(1, 1)$ |
| **Proposed** | **9** | **0.98** | 17 (**7**) | $(\mathbf{1}, \mathbf{1})$ |

ness of $U^\star$ from the proposed method compared to the already-optimal initial point $U_{\theta_0}$, while their implications in the $\mu$-synthesis procedure can be visualized in Figure 11.10, showing the SSV frequency response, alongside the difficulty of the problem due to the lowpass behavior instead of a bandpass behaviour commonly-expected in various processes. Table 11.7 gathers all solutions with their orders and peak estimated SSVs, showing that only the proposed method leads to guaranteed robust stability and performance, and additionally $n_f = 1$.

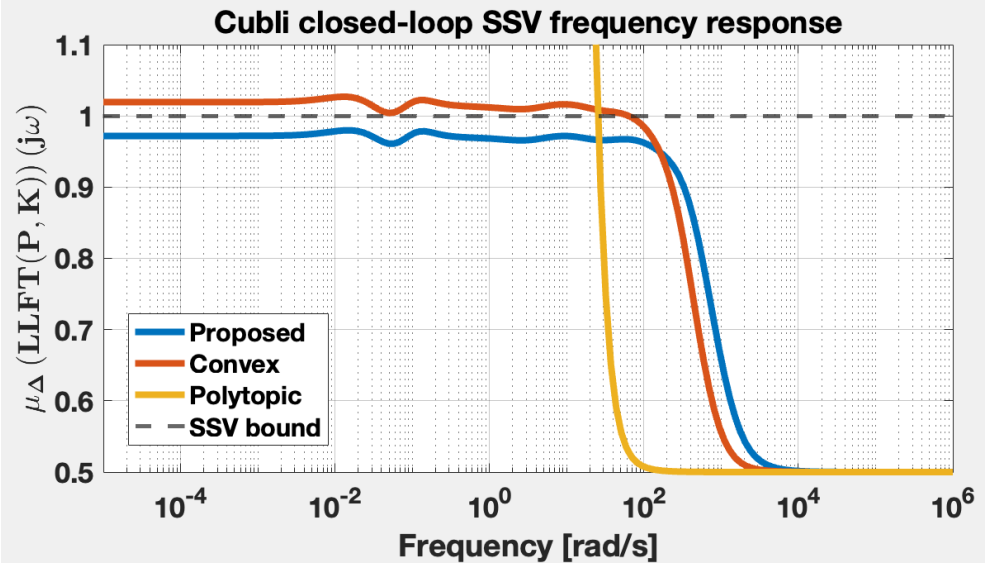


Figure 11.10: SSV frequency response plots using three of the compared regulator solutions, based on approaches (ii)–(iv) from Section 11.2.2.

## 11.3 Cascade control sampling time selection

Two case studies are proposed for the cascade sampling rate optimization of Chapter 8, Section 8.2.4. Each will emphasize a different phenomenon relative to sampling time selection: the first case will focus on the advantage of selecting a higher outer sampling rate compared to the inner loop, while the second example provides a better compromise relative to the established methods in the literature for maintaining desired performances while also not increasing the number of delays in the closed-loop system to an unfeasible extent.

### 11.3.1 Numeric benchmark problem

A first case study was elaborated based on a benchmark industrial process model of order four taken from [ÅH00], with the value of the coefficient $\alpha = 0.3$. This process has been split into two second-order

systems in series, to denote a faster inner part and a slower outer part:

$$G_{\text{out}}(s) = \frac{1}{(s+1)(\alpha s+1)}, \tag{11.23}$$

$$G_{\text{in}}(s) = \frac{1}{(\alpha^2 s+1)(\alpha^3 s+1)}. \tag{11.24}$$

A set of controllers have been designed using pole allocation and refined using the root locus method, leading to:

$$K_{\text{in}}(s) = \frac{1.0597(s+9.091)}{s}, \tag{11.25}$$

$$K_{\text{out}}(s) = \frac{27.989(s+3.03)(s+0.9091)}{s(s+26.32)}. \tag{11.26}$$

The searching range for the controller sampling rates is encompassed in the domain $\mathcal{D} = [10^{-6}, 1] \times \overline{1,6}$, with 1000 logarithmically-spaced points along the first dimension. Additionally, as the similarity functional (8.6) is based on frequency-response data, each particle corresponding to a fixed pair $\mathcal{T} = (T, k)$ will use a frequency set $\Omega(T) = [0.1, \pi/T]$, with 500 logarithmically-spaced points, $\omega_\varepsilon$ from Remark 5 selected to discard the last 3 points, and the range of the outer loop multiplier is selected as $k = \overline{1,10}$. The MI-ABC hyperparameters were $\beta = 10^5$, $\mathcal{N} = 200$ and a cost function improvement tolerance TOL $= 10^{-4}$. The two experiments' functional weights are presented in Table 11.8, where it can be seen that, for high fidelity, an optimal solution becomes $\mathcal{T}_1^\star = (0.012[s], 1)$, while by weighting the implementation penalty functionals more, an optimal solution becomes $\mathcal{T}_2^\star = (0.0419[s], 3)$.

Figures 11.11 and 11.12 illustrate the global extremum points for the approximated cost functional as in (8.25), with the contour plots denoting on the $(X, Y, Z)$-axes the variables $\left(\log_{10} T, k, -20\log_{10} \mathcal{J}^{\overline{\Omega}}(\mathcal{T})\right)$, which provide an intuitive view of the dynamics of the functional based on the input $\mathcal{T}$. The figures also illustrate the highly non-convex nature of the problem and the different influences the weighting parameters $c_{\overline{1,8}}$ have in the resulting contour plots. With this approach of viewing the cost functional, there are two easily distinguishable regions were the optimal values reside. The positions of said clusters give an approximate understanding of the available clusters possible for the values of $T$ and $k$, respectively, along with providing an intuition on the sensitivity of

Table 11.8: Benchmark problem hyperparameters for two optimization experiments with results: 1 – configured for high response fidelity; 2 – configured for practical implementation

| Item | Experiment 1 | Experiment 2 |
|---|---|---|
| $c_1$ | 1 | 1 |
| $c_2$ | 1 | 1 |
| $c_3$ | 10 | 2000 |
| $c_4$ | 20 | 2000 |
| $c_5$ | 1000 | 10 |
| $c_6$ | 5000 | 100 |
| $c_7$ | 10 | $10^4$ |
| $c_8$ | 10 | $5 \times 10^5$ |
| $\mathcal{T}^\star = (T^\star, k^\star)$ | $(0.012[s], 1)$ | $(0.0419[s], 3)$ |

the formulated problem as a function of its hyperparameters $c_{\overline{1,8}}$. The Z axis varies in the interval $[-247, -74]$ $[dB]$, with levels allocated in 4 $[dB]$ increments, denoting that the performance indices of the cascade control system illustrated through the considered functionals vary in a highly-non-convex manner as a function of the sampling rate.

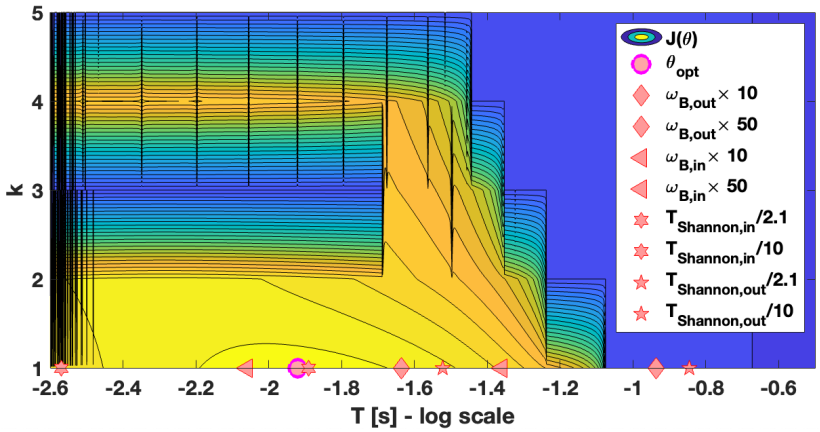


Figure 11.11: Benchmark control system with functional $\mathcal{J}$ calibrated for high response fidelity, resulting in the optimal solution $\mathcal{T} = (0.012[s], 1)$, alongside classical alternatives.

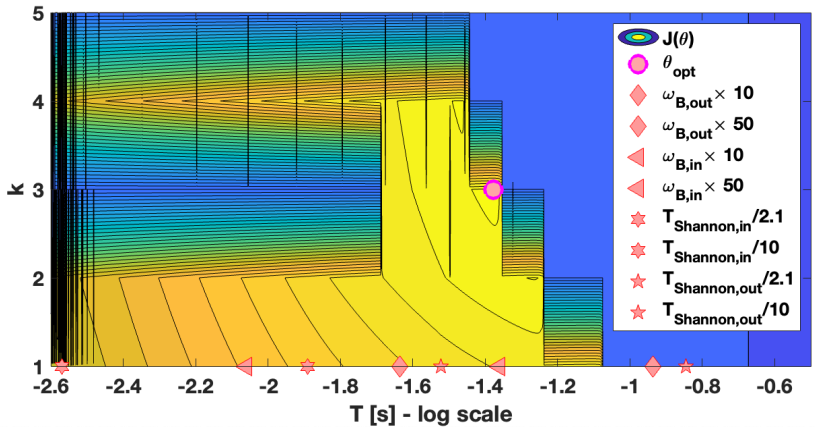


Figure 11.12: Benchmark control system with functional $\mathcal{J}$ calibrated for easier implementability, resulting in the optimal solution $\mathcal{T} = (0.0419[s], 3)$, alongside classical alternatives.

From the expressions of the process model dynamics, (11.23), (11.24), along their corresponding regulators (11.25), (11.26), the following relevant time dynamics can be gathered: pole time constants $\widehat{T}_{in,1}{=}\alpha^3{=}0.027[s]$, $\widehat{T}_{in,2}{=}\alpha^2{=}0.09[s]$, $\widehat{T}_{out,1}{=}\alpha{=}0.3[s]$, $\widehat{T}_{out,2}{=}1[s]$, closed-loop bandwidths: $\omega_{B,in}{=}14.4[rad/s]$, $\omega_{B,out}{=}5.42[rad/s]$. As such, the recommended alternatives for sampling time selection, as described in the monograph [MG90] are based on the theoretical and practical Nyquist-Shannon sampling approaches using the least time constant of the process, along with faster and slower multiples of the closed-loop bandwidth of the process. Among these values, we can select the range of the set:

$$\left(\frac{2\pi}{\omega_{B,out}{\times}10}, \frac{2\pi}{\omega_{B,out}{\times}50}, \frac{2\pi}{\omega_{B,in}{\times}10}, \frac{2\pi}{\omega_{B,in}{\times}50}, \frac{\widehat{T}_{in,1}}{2.1}, \frac{\widehat{T}_{in,1}}{10}, \frac{\widehat{T}_{out,1}}{2.1}, \frac{\widehat{T}_{out,1}}{10}\right)$$
$$= (115.9, 23.18, 43.63, 8.72, 12.85, 2.7, 142.8, 30)\ \ [ms], \tag{11.27}$$

values seen alongside the optimum suggestions, with the conclusion that the alternatives span a wide domain, with no straightforward manner to assess which approach is suitable for the problem at hand, and do not account for the possibility of a multi-rate cascade control system.

Figure 11.13 illustrates the differences between the fidelity solution $\mathcal{T}_1^\star$ and the lower implementability requirements solution $\mathcal{T}_2^\star$, materialized in the open- and closed-loop frequency responses of the outer control loop, a pole-zero plot of the different number of singularities

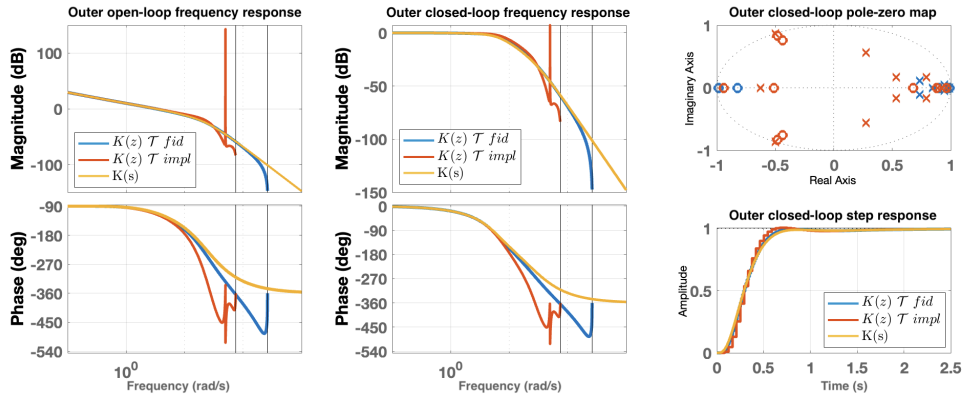


Figure 11.13: Benchmark control system analysis: outer subsystem frequency responses, with a pole-zero map of the closed-loop system, showing the influence of the external sampling rate factor $k_2^\star = 3$, and closed-loop step responses. The graphs illustrate the ideal continuous-time regulator case, along with the proposed quasi-optimal solutions of imposing high response fidelity compared to lower implementation requirements.

and their positioning in the complex plane, along with the similarity of the step responses. An additional resonance frequency occurs at the value $\omega_{res} = 50\ [rad/s]$ in the closed-loop system, along with regulator singularities as the 3rd complex roots of the regulator seen as function of the base sampling rate $T_2^\star = 0.0419\ [s]$ for the implementability optimum with $k^\star = 3$. For this case, the signal artifacts of using $K_{k_2^\star T_2^\star,out}(z) = K_{T_2^\star,out}(z^k)$ as in (3.23) for the implementability optimum $k^\star = 3$ are considered negligible by the optimization problem to gain additional execution time. The discretization of the regulators has been made using the Tustin method, along with the corresponding processes discretized using zero-order hold. The continuous-time inner closed-loop system has a phase margin $\gamma_k^i \approx 80[^\circ]$ and an ideal gain margin $m_k^i = \infty$, with its high fidelity and implementation-oriented discretized equivalents having $\gamma_k^{i1} = 75.8[^\circ]$, $\gamma_k^{i2} = 74.6[^\circ]$, respectively, along with $m_k^{i1} = 24.8\ [dB]$, $m_k^{i2} = 23.2\ [dB]$. In a similar manner, the values corresponding to the outer loop are: $\gamma_k^o \approx 69[^\circ]$, $\gamma_k^{o1} = 72[^\circ]$, $\gamma_k^{o2} = 70.6[^\circ]$, $m_k^o = 16.3\ [dB]$, $m_k^{o1} = 13.4\ [dB]$, $m_k^{o2} = 12.5\ [dB]$.

### 11.3.2 Temperature control system

The second case study involves the control of a temperature stability process as found in immersion lithography tools, with the series interconnection models described in [LZL17]. According to the control structure of Figure 3.4, the continuous-time plant has the following inner and outer dynamics:

$$G_{\text{in}}(s) = \frac{-1.3361}{11.834s + 1} e^{-11.63s}; \tag{11.28}$$

$$G_{\text{out}}(s) = \frac{1.0092(7.11s + 1)}{(116.71s + 1)(14.25s + 1)} e^{-35.75s}. \tag{11.29}$$

A pair of PI regulators have been designed using the root locus methodology, with the time delays replaced by first-order Padé approximants:

$$K_{\{\text{in,out}\}}(s) = K_{p,\{\text{in,out}\}} + \frac{K_{i,\{\text{in,out}\}}}{s}, \tag{11.30}$$

having $K_{p,\text{in}} = -0.37511$, $K_{i,\text{in}} = -0.030239$, $K_{p,\text{out}} = 1.2$, $K_{i,\text{out}} = 0.0082$.

Table 11.9: Temperature control system hyperparameters for two optimization experiments and their obtained results: 1 – configured for high response fidelity; 2 – configured for practical implementation

| Item | Experiment 1 | Experiment 2 |
|---|---|---|
| $c_1$ | 2000 | 1 |
| $c_2$ | 10000 | 1 |
| $c_3$ | 1 | 20 |
| $c_4$ | 1 | 20 |
| $c_5$ | 20000 | 1 |
| $c_6$ | 1000 | 1 |
| $c_7$ | 1 | 500 |
| $c_8$ | 1 | 200 |
| $\mathcal{T}^\star = (T^\star, k^\star)$ | $(2.887[s], 2)$ | $(13.219[s], 4)$ |

The sampling frequencies of the controllers are searched in the domain $\mathcal{D} = [10^{-2}, 100] \times \overline{1, 5}$, with 800 logarithmically-spaced points.

Additionally, as the similarity functionals (8.6) are based on frequency-response data, each particle corresponding to a fixed pair $(T, k)$ will use a frequency set $\Omega(T) = [0.001, \pi/T]$, with 500 logarithmically-spaced points, $\omega_\varepsilon$ from Remark 5 selected to discard the last 20 points, and the range of the outer loop multiplier is selected as $k = \overline{1, 20}$. The MI-ABC hyperparameters considered were $\beta = 10^5$, $\mathcal{N} = 200$ and a cost function improvement tolerance TOL$= 10^{-4}$. The hyperparameters for the two conducted experiments are presented in Table 11.9, where it can be seen that, for high fidelity emphasis, an optimal solution becomes $\mathcal{T}_1^\star = (2.887[s], 2)$, while by weighting for lower implementation requirements, an obtained optimal solution is $\mathcal{T}_2^\star = (13.219[s], 4)$. Figures 11.14 and 11.15 portray the global optimum points for the approximated functionals from (8.25), where the contours denote on the $(X, Y, Z)$-axes the variables $\left(\log_{10} T, k, -20 \log_{10} \mathcal{J}^{\overline{\Omega}}(\mathcal{T})\right)$, with the same purpose of obtaining higher readability as a function of $\mathcal{T} = (T, k)$. The figures also illustrate the highly-non-convex nature of the optimization problem and the influences the weighting parameters $c_{\overline{1,8}}$ have in the resulting plots.

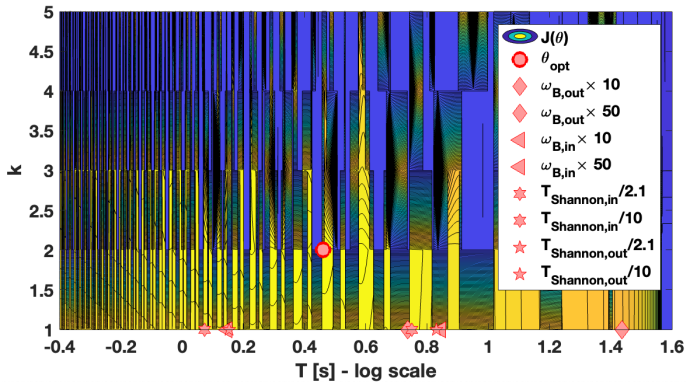


Figure 11.14: Heat exchanger control system with functional $\mathcal{J}$ calibrated for high response fidelity, resulting in the optimal solution $\mathcal{T} = (2.8876[s], 2)$, alongside classical alternatives.

Furthermore, the open-loop frequency responses of the inner and outer control loops are presented in Figure 11.16, with the closed-loop pole-zero maps adjacent to them. The closed-loop magnitude responses are plotted in Figure 11.17, with the corresponding closed-loop step responses portrayed in Figure 11.18. The discretizations were performed using the zero-order hold method for the process dynamics and with

Table 11.10: Inner and outer closed-loop performance metrics for the solutions from Table 11.9, compared to the ideal continuous-time case and to reference dynamics from the inner and outer loops using classical alternatives, such as the Shannon-Nyquist theorem (based on multiples $\omega_{SN}\times\{2.1, 5, 10\}$) and closed-loop bandwidth ($\omega_B\times\{10, 50\}$) [MG90].

| # | *Solution* | $T$ $[s]$ | $k$ | $\gamma_k^o$ $[^\circ]$ | $m_k^o$ | $t_r^o$ $[s]$ | $\sigma^o$ [%] | $N^o$ | $\gamma_k^i$ $[^\circ]$ | $m_k^i$ | $t_r^i$ $[s]$ | $\sigma^i$ [%] | $N^i$ |
|---|---|---|---|---|---|---|---|---|---|---|---|---|---|
| 1 | Ideal $K(s)$ | – | – | 59.88 | 2.54 | 94.77 | 8.26 | – | 63.89 | 3.27 | 24.18 | 1.35 | – |
| 2 | $T_{SN,in}/10$ | 1.1834 | 1 | 59.60 | 2.49 | 93.49 | 8.86 | 46 | 62.52 | 3.12 | 23.66 | 2.74 | 12 |
| 3 | $\omega_{B,in}\times 50$ | 1.4056 | 1 | 59.53 | 2.48 | 92.77 | 8.97 | 40 | 62.28 | 3.10 | 23.89 | 3.02 | 11 |
| 4 | $T_{SN,out}/10$ | 1.4249 | 1 | 59.52 | 2.48 | 92.61 | 8.99 | 40 | 62.24 | 3.09 | 24.22 | 3.05 | 11 |
| 5 | $(\mathbf{T}_1^\star, \mathbf{k}_1^\star)$ | **2.8877** | **2** | **59.05** | **2.43** | **89.51** | **9.74** | **24** | **60.45** | **2.91** | **23.10** | **5.19** | **7** |
| 6 | $\omega_{B,out}\times 50$ | 5.4636 | 1 | 58.22 | 2.34 | 92.88 | 11.13 | 15 | 57.56 | 2.71 | 21.85 | 9.11 | 5 |
| 7 | $T_{SN,in}/2.1$ | 5.6354 | 1 | 58.15 | 2.33 | 90.16 | 11.26 | 15 | 57.16 | 2.66 | 22.54 | 9.48 | 5 |
| 8 | $T_{SN,out}/2.1$ | 6.7853 | 1 | 57.81 | 2.30 | 88.20 | 11.86 | 13 | 56.67 | 2.73 | 20.35 | 10.57 | 4 |
| 9 | $\omega_{B,in}\times 10$ | 7.0282 | 1 | 57.72 | 2.29 | 91.36 | 12.00 | 13 | 56.56 | 2.75 | 28.11 | 10.68 | 4 |
| 10 | $(\mathbf{T}_2^\star, \mathbf{k}_2^\star)$ | **13.2194** | **4** | **56.28** | **2.16** | **92.53** | **14.06** | **12** | **49.30** | **2.33** | **13.21** | **21.14** | **3** |
| 11 | $\omega_{B,out}\times 10$ | 27.3182 | 1 | 51.56 | 1.87 | 81.95 | 23.58 | 8 | 44.67 | 3.86 | 27.31 | 23.77 | 3 |

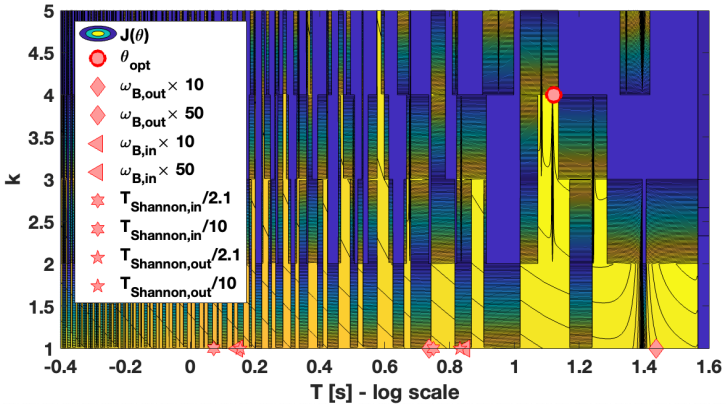


Figure 11.15: Heat exchanger control system with functional $\mathcal{J}$ calibrated for easier implementability, resulting in the optimal solution $\mathcal{T} = (13.21[s], 4)$, alongside classical alternatives.

the Tustin method for the regulators. Maintaining the notations from subsection 11.3.1, the resulting stability margins are: $\gamma_k^i = 63.89$ [°], $\gamma_k^{i1} = 60.45$ [°], $\gamma_k^{i2} = 49.30$ [°], $m_k^i = 10.29$ $[dB]$, $m_k^{i1} = 9.27$ $[dB]$, $m_k^{i2} = 7.34$ $[dB]$, $\gamma_k^o = 59.88$ [°], $\gamma_k^{o1} = 59.05$ [°], $\gamma_k^{o2} = 56.28$ [°], $m_k^o = 8.09$ $[dB]$, $m_k^{o1} = 7.71$ $[dB]$, $m_k^{o2} = 6.68$ $[dB]$. Depending on the imposed resolution levels of the colorbars (here the levels are configured for clusters of $2[dB]$), the 2D representations as in Figures 11.14 and 11.15 could be used to gather an intuition on the clusters of similarly-valued solutions $\mathcal{T}$.

To emphasize the results obtained with the proposed method, a comparison has been performed in Table 11.10 along sampling rates obtained by using the Shannon-Nyquist theorem on the poles of the continuous-time inner and outer dynamics of the plant models from (11.28) and (11.29), and also based on the closed-loop bandwidth of the system, as proposed in [MG90]. For this example, the faster subsystem has a physical time constant $\widehat{T}_{in,1} = 11.834[s]$, while the slower subsystem has the physical time constants $\widehat{T}_{out,1}$=14.25$[s]$ and $\widehat{T}_{out,2}$=116.71 $[s]$, $\widehat{T}_{out,1} \ll \widehat{T}_{out,2}$. Given that the sampling theorem (4.1) implies strict inequality, three relevant multiples of the Nyquist frequency will be considered: $\omega_{SN} \times 2.1$, $\omega_{SN} \times 5$ and $\omega_{SN} \times 10$, respectively, $\omega_{SN} \in \left\{ \frac{2\pi}{\widehat{T}_{in,1}}, \frac{2\pi}{\widehat{T}_{out,2}} \right\}$. Separately, in accordance to Figure 11.17, the bandwidths of the continuous-time inner and outer closed-loop systems can be deduced as $\omega_{B,in} \approx 0.0894$ $[rad/s]$, $\omega_{B,out} \approx 0.023$ $[rad/s]$, with a slow sampling response

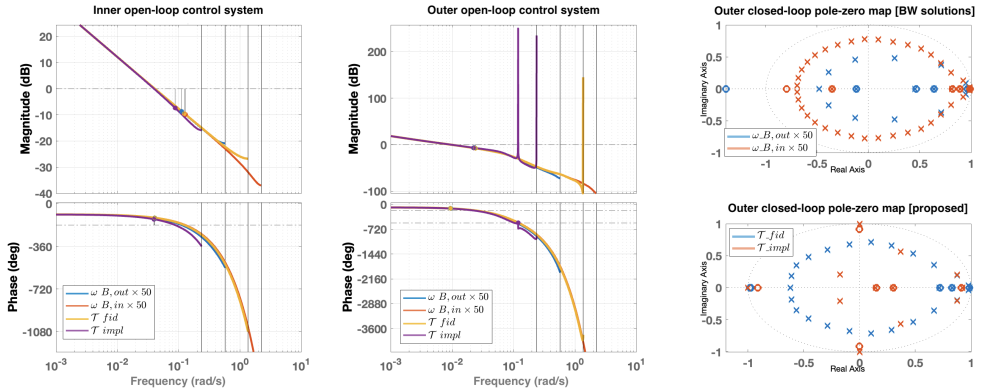


Figure 11.16: Heat exchanger control system: inner and outer open-loop frequency responses with emphasized stability margins for the two proposed quasi-optimal solutions, and two relevant comparisons using the system's bandwidth, along with their outer closed-loop pole-zero maps. The multi-rate factor $k_2^\star$=4 leads to a resonance peak $\omega_{res} = 0.119$ $[rad/s]$.

recommended at $\omega_B \times 10$ and a fast sampling response recommended at $\omega_B \times 50$ [MG90]. Gathering said alternatives for the selection of sampling period, we monitor a set of performance metrics for the closed-loop inner and outer systems, presented in Table 11.10. The studied performances include the phase and gain stability margins, $\gamma_k$ and $m_k$, rise time $t_r$, overshoot $\sigma$, and order of the numeric closed-loop system $N$, which is variable due to the time delays of the model. Inner-loop metrics will be denoted with the superscript $i$, while outer-loop performances will be distinguished with the superscript $o$. As noticeable, the solution which imposes response fidelity, $\mathcal{T}_1^\star$, converged between the Shannon $\omega_{SN,out} \times 10$ and bandwidth $\omega_{B,out} \times 50$ solutions, with a good compromise between imposed performance and closed-loop system order $N^o = 24 \in \overline{8, 46}$. On the other hand, the implementation-based solution, $\mathcal{T}_2^\star$, converged between the slow recommendations of the bandwidths based on the inner and outer dynamics, and illustrates the ability to actuate the closed-loop system with a 206.74 [%] improvement on the execution speed of the inner loop compared to the practical Shannon recommendation $\omega_{B,out} \times 10$ and 400 [%] less required overhead for the outer loop. The computed implementability optimum solution significantly improves the rise time of the inner control loop with the compromise of a higher overshoot, with the advantage of having $k_2^\star = 4 > 1$ that it maintains a low overshoot compared to $\omega_{B,out} \times 10$.

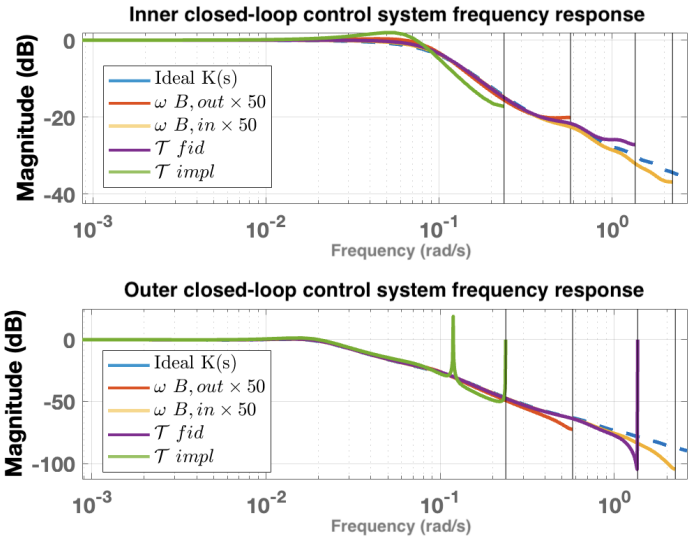


Figure 11.17: Heat exchanger control system: inner and outer closed-loop frequency magnitude responses for the proposed quasi-optimal solutions and two bandwidth-based alternatives.

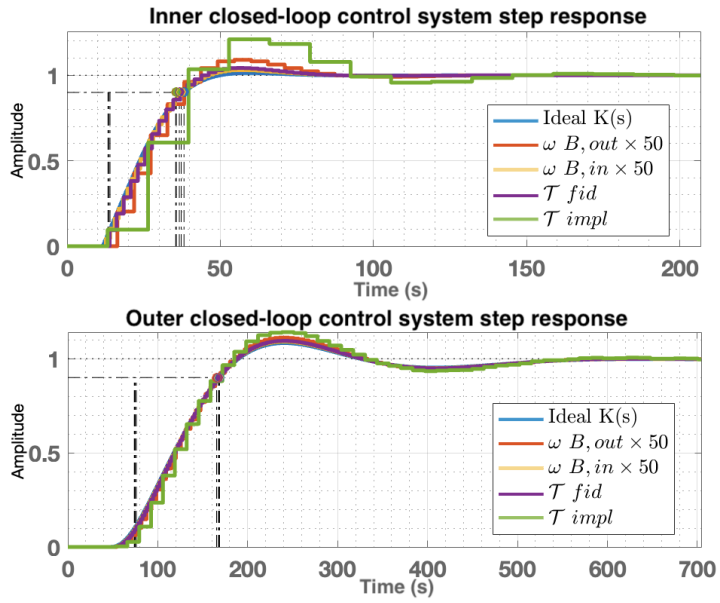


Figure 11.18: Heat exchanger control system: inner and outer closed-loop step responses with emphasized rise times for the proposed solutions and two bandwidth-based alternatives.

## 11.4 Sampling rate and quantization step joint optimization

The process selected to illustrate the results proposed in Chapter 9, Section 9.1, is gathered from the benchmark list of [ÅH00], namely a third order industrial process with a non-minimum phase zero and with added uncertainties, described using the notations (3.30) and (3.31) by:

$$G_n(s) = k_0 \frac{1-\alpha_0 s}{(s+1)^3}, \quad G(s) = k \frac{1-\alpha s}{(s+1)^3}, \tag{11.31}$$

with the nominal values $\alpha_0 = 0.1$ and $k_0 = 2$, alongside their tolerances $\texttt{tol}_\alpha = \pm 10$ [%] and $\texttt{tol}_k = \pm 5$ [%], respectively.

A continuous regulator $K$ is synthesized with the closed-loop shaping methodology [SP05] using the sensitivity $S$ with weighting function $W_S$, the complementary sensitivity $T$ with weight $W_T$, and the control effort $R = KS$ with weight $W_R$. Their expressions are:

$$W_S(s) = \frac{\frac{1}{M}s + \omega_B}{s + \omega_B A}, \; W_T(s) = \frac{s + \omega_{BT}}{A_T s + \omega_{BT} M_T}, \; W_R(s) = \frac{1}{A_R}, \tag{11.32}$$

with parameters $\omega_B = 1.5$ $[rad/s]$, $M = 2$, $A = 10^{-2}$, $\omega_{BT} = 15$ $[rad/s]$, $M_T = 2$, $A_T = 2$, $A_R = 10^5$.

The augmented continuous-time plant model, considering the above weighting functions gathered in the block structure $W = \begin{bmatrix} W_S & W_R & W_T \end{bmatrix}^\top$, can be written as:

$$P = \mathcal{A}(G, W) = \begin{bmatrix} W_S & 0 & 0 & 1 \\ -W_S G & W_R & W_T G & -G \end{bmatrix}^\top,$$

and, using the classical D-K iteration $\mu$-synthesis of [Bal+22], the resulting state-space regulator $K$ is shown in Equation (11.38).

Using the zero-order hold discretization method for the process (11.31), the following analytical expression results for an arbitrary $\tau > 0$:

$$\widetilde{G}_n(z) = \mathcal{D}\{G_n, \tau\} = \frac{k\left(b_1 z^{-1} + b_2 z^{-2} + b_3 z^{-3}\right)}{1 + a_1 z^{-1} + a_2 z^{-2} + a_3 z^{-3}}, \tag{11.33}$$

with notations $\gamma = e^{-\tau}$, $\delta = \tau\gamma$, $\lambda = \frac{\tau^2}{2}\gamma(1+\alpha)$ and coefficients:

$$b_1 = 1 - \gamma - \lambda - \delta; \tag{11.34}$$
$$b_2 = 2\gamma^2 + \gamma\left(-2 - \lambda - \delta\right) + \lambda + \delta; \tag{11.35}$$
$$b_3 = \gamma\left(-\gamma^2 + \gamma + \lambda - \delta\right); \tag{11.36}$$
$$a_1 = -3\gamma,\ a_2 = 3\gamma^2,\ a_3 = -\gamma^3. \tag{11.37}$$

The regulator $K(s) = (A_c, B_c, C_c, D_c{=}0)$, starting with matrix $A_c$:

$$\begin{pmatrix} -1.372 & 613.4 & 8.111 & -0.01228 & 7.242 & 0.2304 & -1.163 \\ -613.4 & -1234 & -198.3 & 0.2579 & -233.3 & -7.376 & 37.27 \\ -8.111 & -198.3 & -72.1 & 0.145 & -150.4 & -4.655 & 23.65 \\ -0.0129 & -0.42 & -0.2688 & -0.00613 & -12.27 & 0.5647 & -1.327 \\ 7.242 & 233.3 & 150.4 & 23.69 & -4357 & -483.1 & 1452 \\ -0.2303 & -7.373 & -4.651 & -0.8474 & 483 & -10.25 & 94.98 \\ 1.161 & 37.27 & 23.64 & 4.143 & -1452 & 95 & -2903 \end{pmatrix},$$

$$B_c^\top = \begin{pmatrix} 198.4 & 5564 & 512.1 & 0.9463 & -524.8 & 16.64 & -84.06 \end{pmatrix}; \tag{11.38}$$

$$C_c = \begin{pmatrix} -198.4 & 5564 & 512.1 & -0.5376 & 524.8 & 16.65 & -84.06 \end{pmatrix}.$$

The domain of definition for the optimization variable $\xi = (\tau, q)$ is $\mathcal{D} = [10^{-7}, 10^{-3}] \times [10^{-10}, 10^{-4}] \subset \mathbb{R}_+^2$, and an identical frequency domain has been used for the similarity integral of (9.10) for all $\xi \in \mathcal{D}$, namely $\overline{\omega_N} = 95[\%] \cdot \frac{2\pi}{\tau_{\max}} = 5969\ [rad/s]$, $\Omega = \left[\frac{\overline{\omega_N}}{10^4}, \overline{\omega_N}\right]$, sampled in linear scale. The auxiliary plant terms $U, W$ are discretized using zero-order hold, and the regulator $K$ is discretized using Tustin's method, for a better representation of its frequency response. Two optimal regulators are obtained, first with the solution $\xi_1^\star = (244.205, 24.4205) \times 10^{-6}$ by solving Problem 10, equivalent to the unconstrained functional (9.8), along with a solution $\xi_2^\star = (4.2739{\times}10^{-6}, 1.02448{\times}10^{-10})$ by solving Problem 11, equivalent to the unconstrained functional (9.13). The peak approximated SSVs resulted as $\mu_{\mathbf{\Delta}}|_{\xi_1^\star}$=0.9781<1 and $\mu_{\mathbf{\Delta}}|_{\xi_2^\star}$=0.9314<1, with $\mathcal{I}\left(\xi_2^\star\right) = 16.06 = 24.11[dB]$. To solve the problems, a global search algorithm [Ugr+07] was used, based on multiple instances of interior point nonlinear solvers [BGN00] with forward finite difference derivatives and LDL factorization-based solvers, and instance initializations performed using the scatter search algorithm [Glo98].

The previous results are illustrated in Figures 11.19, 11.20, 11.21, which show the two-dimensional plots of the cost functions from Problems 10 and 11, along with the SSV feasibility constraint for robustness. The implementability functional plot shows only the feasible areas, with the solution $\xi_1^\star$ found by the global solver, unobservable just by sampling the domain of definition with logarithmically-spaced points.

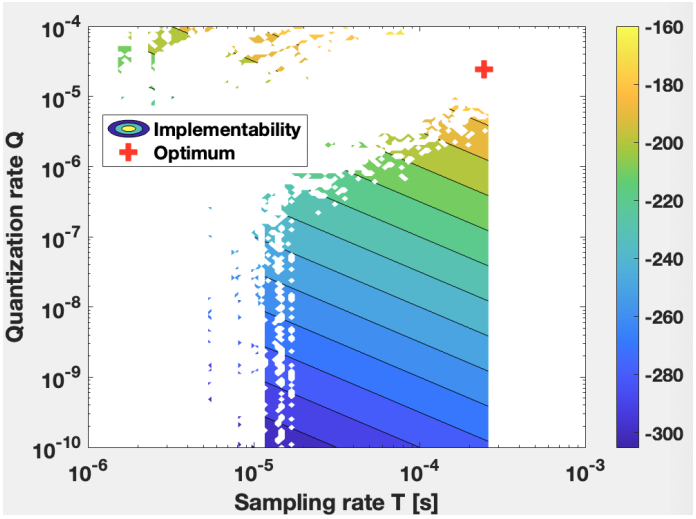


Figure 11.19: Feasible region contour plot illustration $[dB]$ of functional (9.7) for the example process (11.31) with optimum $\xi_1^\star = (244.205, 24.4205) \times 10^{-6}$.

**Remark 23.** *The authors of [Bal+22] warned about the synthesis of discrete-time regulators, which, for small sampling periods, the closed-loop poles tend to gather around $z = 1$ and lead to instability or loss of robust performance, with the recommendation of synthesizing the regulator in continuous-time. On the other hand, the experiment presented in this section via the results of Figure 11.21 showed that this problem remains valid even in case of sampling continuous regulators.*

**Remark 24.** *The fidelity problem solution $\xi_1^\star$, although found to be feasible, leads to numeric instability even when simulated with the standard IEEE 754 floating point with double precision arithmetic. Such difficulties appear in the case of the analytical expression deduced in (11.33), and also in the case of using the* `c2d` *function with the* `zoh` *method from MATLAB© for examples besides the nominal case. The coefficients of*

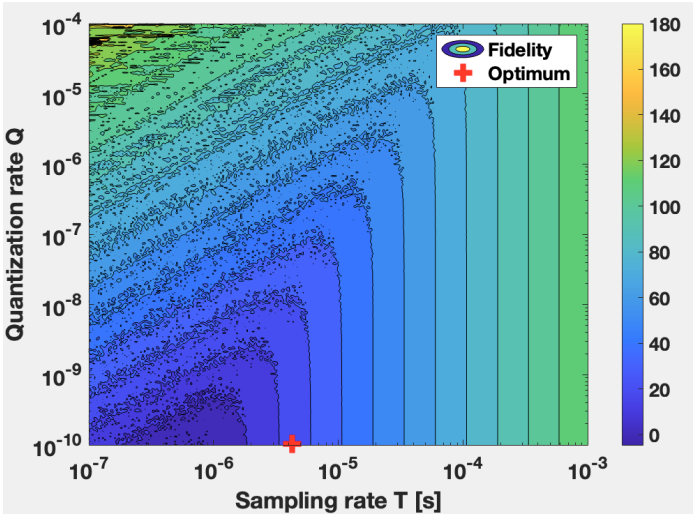


Figure 11.20: Functional (9.9) contour plot for the example process (11.31) with optimum $\xi_2^\star = (4.2739\times10^{-6}, 1.02448\times10^{-10})$.

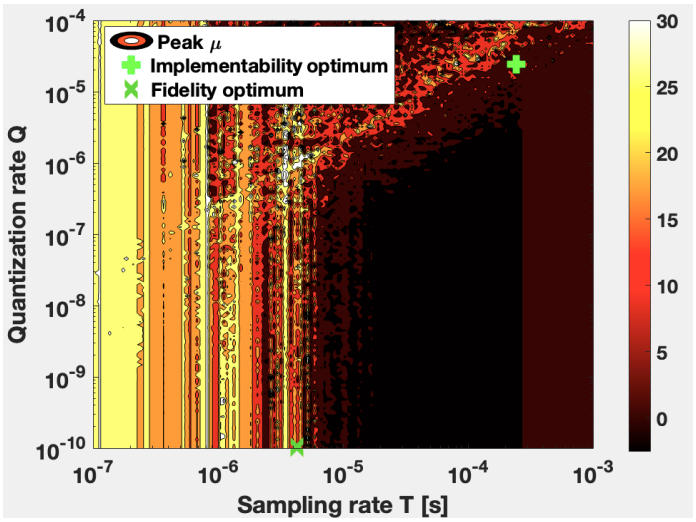


Figure 11.21: Peak structured singular value constraint $[dB]$ as function of $\xi \in \mathbb{R}^2_+$.

*the characteristic polynomial of* $\widetilde{G}_n$ *and corresponding poles are presented in Table 11.11, noting that both computations lead to complex conjugate poles and, additionally, the analytic formula leads to an unstable pole. As such, the simulations for the Monte Carlo experiments implying* $\xi_2^\star$ *required the use of additional balancing operations.*

*To further illustrate the numeric properties of solutions* $\xi_1^\star$ *and* $\xi_2^\star$*, a numeric approximation of the least guaranteed sensitivity bound* (9.16) *was deduced for both cases, using the more demanding function* $F_2$ *from* (9.13)*, for an objective comparison, with* 100 *Monte Carlo samples per experiment. For* $\xi_1^\star$*, a relative perturbation* $h_1 = 3.2{\times}10^{-6}$ *around* $\xi_1^\star$ *leads to* $N_{F_2}(\xi_1^\star) \approx 7.8535{\times}10^{-10}$*, and* $\kappa_{F_2}(x) \in [964.093, 7812.503]$*, for* $x{\in}\mathcal{E}(\xi_1^\star, h_1{\cdot}\xi_1^\star)$*, while a considerably smaller relative perturbation* $h_2 = 0.25{\times}10^{-15}$ *around* $\xi_2^\star$ *leads to* $N_{F_2}(\xi_2^\star) \approx 1.0685{\times}10^{-21}$ *and* $\kappa_{F_2}(x) \in [8.138, 84.705] \times 10^{17}$*, for* $x \in \mathcal{E}(\xi_2^\star, h_2{\cdot}\xi_2^\star)$*. A perturbation of* $h_1$ *is tolerable in practice due to stochastic numeric errors, being in the acceptable range for the least significant bit values for* $\tau$ *and* $q$*, while the case of* $\xi_2^\star$ *with a tolerance* $h_2$ *yields it unusable. This sensitivity analysis is directly reflected in the structured singular value plots from Figure 11.23, with relative deviations of* $10^{-6}$ *around the computed solutions, and a number of* 100 *Monte Carlo simulations, showing the ability to consistently maintain robust stability and performance criteria only for the case of* $\xi_1^\star$*, with* $\mu_\Delta\left(\widetilde{P}, \widetilde{K}_q\right) < 1$*, property not maintained around* $\xi_2^\star$*.*

Table 11.11: High numeric sensitivity of the characteristic polynomial of $\widetilde{G}_n$ for the solution $\xi_2^\star = (4.2739{\times}10^{-6}, 1.02448{\times}10^{-10})$.

| *Case* | *Parameter* | *Computed value* |
|---|---|---|
| 1 | Ideal $\hat{z}_{1,2,3}$ | $\mathbf{0.999995726091887 < 1}$ |
| 2 | Analytic $a_1$ | $-2.999987178275663$ |
| | Analytic $a_2$ | $2.999974356606124$ |
| | Analytic $a_3$ | $-0.999987178330461$ |
| 2 | Analytic $\hat{z}_1$ | $\mathbf{1.000005221571111 > 1}$ |
| | Analytic $\hat{z}_2$ | $0.999990978352276 + 0.000008223234706j$ |
| | Analytic $\hat{z}_3$ | $0.999990978352276 - 0.000008223234706j$ |
| 3 | `c2d` $a_1$ | $-2.999987178275662$ |
| | `c2d` $a_2$ | $2.999974356606122$ |
| | `c2d` $a_3$ | $-0.999987178330461$ |
| 3 | `c2d` $\hat{z}_1$ | $\mathbf{0.999995723377957 < 1}$ |
| | `c2d` $\hat{z}_2$ | $0.999995727448852 + 0.000000002350638j$ |
| | `c2d` $\hat{z}_3$ | $0.999995727448852 - 0.000000002350638j$ |

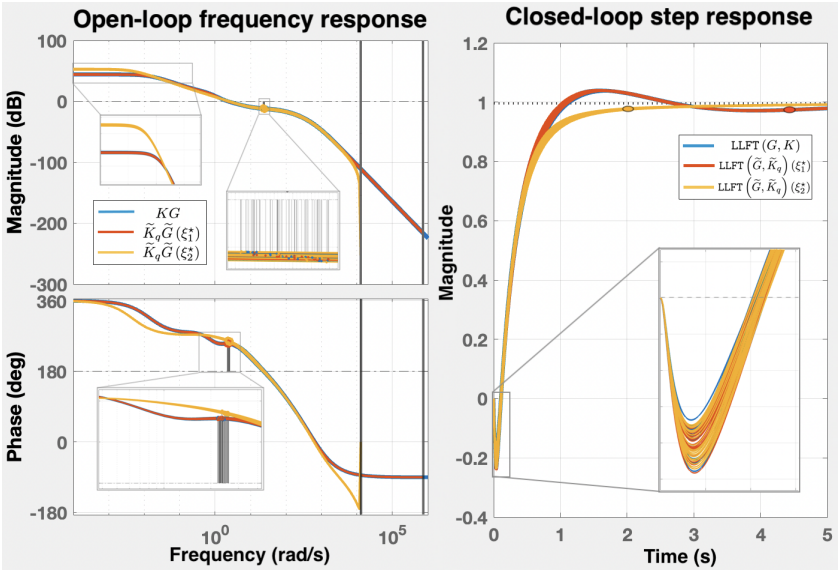


Figure 11.22: Open-loop frequency responses using the optimal discrete quantized regulators $\widetilde{K}_q$ based on $\xi_1^\star$ and $\xi_2^\star$, along with closed-loop step responses, compared to the initial continuous case $K$.

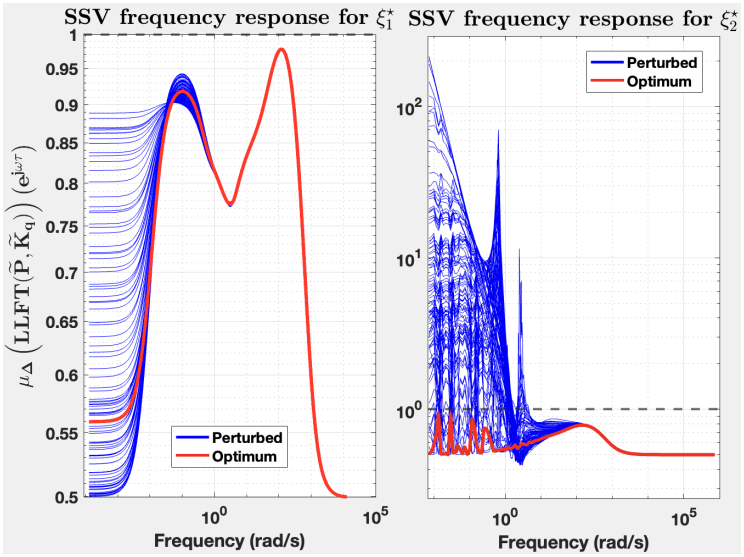


Figure 11.23: Structured singular value frequency plots for the two optimal solutions for $10^{-6}$ relative deviations: $\xi_1^\star$, shown to be insensitive; $\xi_2^\star$, shown to be sensitive by losing desired robust stability and performance.

## 11.5 Least conservative tracking error bound example

To illustrate the practical implications of the proposed results from Chapter 9, namely the optimization from Section 9.2.2.3, consider an academic example disseminated in [Şuş+24a]. It is characterized by an underdamped system with a pair of complex poles and a left half-plane zero to be controlled, with the desire to compute the least conservative quantization error bound given an arbitrary hardware configuration. The continuous-time model is:

$$(G(s)): \left(\begin{array}{c|c} A & B \\ \hline C & D \end{array}\right) = \left(\begin{array}{cc|c} -0.2 & -0.5 & 1 \\ 0.5 & 0 & 0 \\ \hline 0.1 & 1 & 0 \end{array}\right), \tag{11.39}$$

with singularities $\hat{s}_{1,2} = -0.1 \pm 0.4899j$ and $\mathring{s}_1 = -5$. The process is further discretized using the zero-order hold method and a sampling rate $T = 0.1[s]$, leading to an ideal numeric representation $G(z) = (A_2, B_2, C_2, D_2)$, as required in (9.32):

$$(G(z)): \left(\begin{array}{c|c} A_2 & B_2 \\ \hline C_2 & D_2 \end{array}\right) = \left(\begin{array}{cc|c} 0.979 & -0.04948 & 0.09897 \\ 0.04948 & 0.9988 & 0.002483 \\ \hline 0.1 & 1 & 0 \end{array}\right). \tag{11.40}$$

A set of closed-loop performance metrics are be imposed through the weighting functions:

$$W_S(s) = \frac{0.5s + 0.1}{s + 0.001}, \quad W_T(s) = \frac{s + 0.2}{0.01s + 0.4}, \quad W_R(s) = 1, \tag{11.41}$$

focusing on a sensitivity bandwidth $\omega_B = 0.1$[rad/s], peak sensitivity amplitude $M = 2$ and allowable steady-state error coefficient $A = 10^{-2}$. The regulator has been obtained through a $\mathcal{H}_\infty$ synthesis, tuned using the above loop-shaping for an overdamped response, with resulting continuous-time state-space representation:

$$(K(s)): \left(\begin{array}{ccc|c} -0.001 & 0.05579 & -6.35\times10^{-5} & 0.3432 \\ 0.05579 & -146 & 14.29 & -9.623 \\ 6.384\times10^{-5} & -14.29 & -0.00019 & -0.01085 \\ \hline 0.3432 & -9.623 & 0.01085 & 0 \end{array}\right) \tag{11.42}$$

and corresponding numeric regulator $K(z) = (A_1, B_1, C_1, D_1)$, using the Tustin discretization method:

$$(K(z)): \left(\begin{array}{ccc|c} 0.9999017 & -0.000633 & 0.0004463 & 0.107559 \\ -0.000633 & -0.773041 & -0.162164 & 0.345551 \\ -0.000446 & 0.1621641 & 0.8841128 & 0.243469 \\ \hline 0.1075598 & 0.3455512 & -0.243469 & 0.531996 \end{array}\right). \quad (11.43)$$

The default $\mathcal{H}_\infty$ norms of the input-state and input-output dynamics of $K(z)$ are $\mathcal{N}_{x_c} = \|(A_1, B_1, I, O)\| = 1085.3$ and $\mathcal{N}_u = \|(A_1, B_1, C_1, D_1)\| = 117.7$, respectively. Keeping in mind that $\mathcal{N}_u$ is invariant to similarity transformations (9.47), it adds no benefit to constrain $\mathcal{N}_{x_c} < 2^7 = 128$. Considering $\overline{\mathcal{N}}_{x_c} = 512$, then the minimum number of bits in the signal word length becomes $L_{x_c} = \log_2(512) + \max\{L_{ADC}, L_{DAC}\}$. Consider a standard configuration of $L_{ADC} = 12$, $L_{DAC} = 13$, in the supported range $e[k], u[k] \in [-5, 5]\,[V]$, leading to $L_{x_c} = 22$, without including the sign bit. As such, the working resolutions become $\delta_e = 2.441 \times 10^{-3}$, $\delta_x = 1.192 \times 10^{-6}$, $\delta_u = 1.22 \times 10^{-3}$. The default tracking error bound computed using (9.34) and the `eig` routine, without solving Problem 14, is $\mathcal{Q}_0 = 12.685 \times 10^{-3}$, with a corresponding similarity matrix:

$$P_0 = \begin{pmatrix} 0.0003 & 0.6448 & 0.6448 & -0.8051 & -0.0674 \\ 0.9949 & p_{22} & \overline{p}_{22} & -0.0100 & -0.0808 \\ -0.0987 & p_{32} & \overline{p}_{32} & 0.5404 & 0.9687 \\ -0.0210 & p_{42} & \overline{p}_{42} & 0.1184 & 0.2076 \\ 0.0001 & p_{52} & \overline{p}_{52} & -0.2135 & -0.0868 \end{pmatrix}, \quad (11.44)$$

with $p_{22} = -0.0224 + 0.0001j$, $p_{32} = 0.1037 + 0.6244j$, $p_{42} = 0.2890 + 0.0926j$, $p_{52} = 0.0355 - 0.2996j$.

Performing the optimization (9.54) with the observations from Section 9.2.2.4, the least guaranteeable tracking error becomes $\mathcal{Q}^\star = 0.924 \times 10^{-3}$ for a solution $(\xi^\star, \alpha^\star) \in \mathbb{R}^{n_c} \times \mathbb{R}^{n_\ell}$:

$$\xi^{\star\top} = \begin{pmatrix} 12.1729 & 8.6178 & 7.6911 \end{pmatrix}; \quad (11.45)$$

$$\alpha^{\star\top} = \begin{pmatrix} 7.5078 & 8.6092 & 7.7229 & 8.3333 & 3.3261 \end{pmatrix}, \quad (11.46)$$

which provides an improvement factor of $\mathcal{Q}_0/\mathcal{Q}^\star = 13.99$ beyond the

default value as deduced strictly by the theory developed in [ŞMD22]. The admissible range for the state signal becomes $\mathcal{N}_{x_c}^{\star} = 89.15 < \overline{\mathcal{N}}_{x_c}$, denoting a feasible solution. Thus, the regulator representation which guarantees this bound is $K_{\xi^{\star}}$, with a corresponding coordinate matrix $P_{\alpha^{\star}}$, up to a permutation $\Pi$ of its columns.

To further assess the tightness of $\mathcal{Q}^{\star}$, consider a series of experiments using $N = 500$ Monte Carlo simulations, with step reference signals varying in the range $r \in [0.5, 1.5]$, midriser quantizers for the ADC and DAC blocks, and midtread for the internal computations, respectively, along with a simulation time $t_{\text{sim}}$ large enough for the system output to stabilize under the prescribed $\mathcal{Q}^{\star}$ deviation. The computed closed-loop settling time is $t_s = 15.6[s]$, considering the $\pm 2\%$ convention. Assuming a dominant closed-loop pole with real part $\text{Re}\{\hat{s}_0\} = -\frac{4}{t_s}$, the necessary time frame for simulation such that the output signal's dominant oscillating mode is attenuated in the range of the quantization error is computed:

$$t_{\text{sim}} > \frac{t_s}{4} \ln\left(\frac{1}{\mathcal{Q}^{\star}}\right) = 27.32[s]. \tag{11.47}$$

Considering $t_{\text{sim}} = 120[s]$, the Monte Carlo simulations lead to a coverage $[0, 13.43]\,[\%]$ for $\mathcal{Q}_0$, with maximum at $r = 1.0128$ and $[0, 99.82]\,[\%]$ for $\mathcal{Q}^{\star}$, with maximum achieved for $r = 1.2323$, respectively. Additionally, the reference signal values for which the maximum coverage is attained are not unique. The results described in this section can be summarized through the illustration of Figure 11.24. This shows that the refined bound can become significantly lower than the default value and is also achievable in practice, so it cannot be further decreased. The command signal $u[k]$ is initially stochastic, but after a specific index $k > k_{\varepsilon} \in \mathbb{N}_{+}$, it converges either to a constant value or to a limit cycle trajectory.

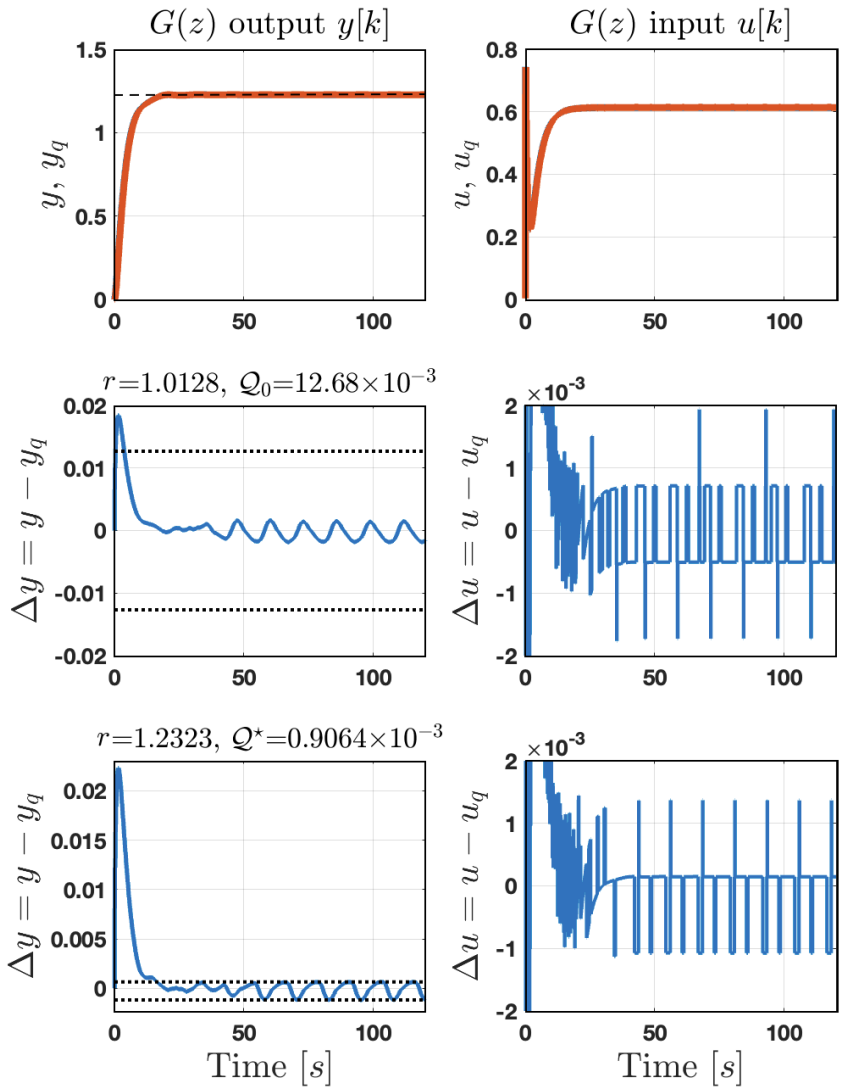


Figure 11.24: Closed-loop simulations of the quantized control system, where the first column involves output signals $y, y_q, \Delta y = y - y_q$ and the second column involves input signals $u, u_q, \Delta u = u - u_q$. The first row shows the closed-loop step response for an arbitrary step reference, the second row illustrates the default application of Theorem 4 with a conservative bound $\mathcal{Q}_0$ and best achieved tightness of 13.43[%], while the third row shows the obtained improvements by solving Problem 14, with the bound $\mathcal{Q}^\star$ covered up to 99.82[%].

## 11.6 SEPIC modelling, control and implementation

This section gathers results from multiple studies performed along the papers [Șuș+21; MȘD21; Șuș+22a; ȘMD22], and Chapters 5, 6, 7 and 9, starting with the proposal of hybrid and averaged state-space models, proceeding with a single full block uncertainty modelling as in [Șuș+21; Șuș+23] and further robust control synthesis step, followed by a Krasovskii passivity-based controller and robust controller cascade design as in [MȘD21], concluding with some practical aspects regarding the robust controller implementation, with the focus on steady-state quantization analysis, based on [ȘMD22]. Other modelling contributions for DC-to-DC converters, passivity-based control and renewable energy optimization have been presented in [MȘD19], [Mih+20], [Mih+21a].

### 11.6.1 Mathematical modelling

The non-ideal DC-to-DC single-ended primary-inductor converter (SEPIC) is presented in Figure 11.25, where each component is described:

- $S_1$, $S_2$: switching devices;
- $L_1$, $L_2$: converter inductors;
- $C_{in}$, $C_1$, $C_2$: converter capacitors;
- $R$: (variable) output load resistance;
- $E$: external source voltage;
- $r_{L_1}$, $r_{L_2}$: resistances associated with the inductors;
- $r_{C_{in}}$, $r_{C_1}$, $r_{C_2}$: capacitors parasitic resistances;
- $r_{DS_1}$, $r_{DS_2}$: resistances for the switching devices' $ON$ state;
- $V_{F_{1,2}}$: constant voltage drops for the conducting phases of $S_{1,2}$;
- $\mu \in [0, 1]$: normalized duty cycle for $S_1$, complementary to $S_2$.

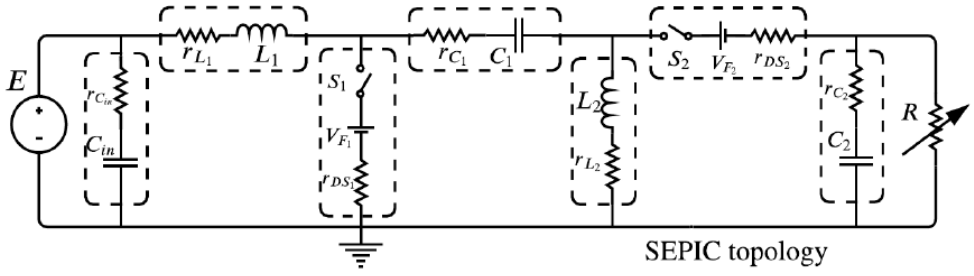


Figure 11.25: SEPIC circuit topology.

Although $S_2$ is typically a diode, it is preferable to use two encapsulated transistors for $S_1$ and $S_2$. When working in continuous conduction mode, the converter will have an $ON$ state, corresponding to $S_1$ being on and $S_2$ off, along with a complementary $OFF$ state.

Given that it has 5 active elements, a state vector will be considered $x = (v_{C_{in}}, i_{L_1}, v_{C_1}, i_{L_2}, v_{C_2})$. The corresponding LTI models, for a constant load resistance $R$, for the $ON/OFF$ states will be presented with the external voltage seen as a disturbance input $u = E$, the voltage drops $V_{F_1}$ and $V_{F_2}$ as constant DC inputs, and the load resistor voltage $v_R$ as measured output:

$$\begin{cases} \dot{x} = A_{ON} \cdot x + \begin{pmatrix} B_{ON} & B_{V,ON} \end{pmatrix} \begin{pmatrix} E & V_{F_1} & V_{F_2} \end{pmatrix}^\top; \\ y = C_{ON} \cdot x + \begin{pmatrix} D_{ON} & D_{V,ON} \end{pmatrix} \begin{pmatrix} E & V_{F_1} & V_{F_2} \end{pmatrix}^\top, \end{cases} \tag{11.48}$$

$$\begin{cases} \dot{x} = A_{OFF} \cdot x + \begin{pmatrix} B_{OFF} & B_{V,OFF} \end{pmatrix} \begin{pmatrix} E & V_{F_1} & V_{F_2} \end{pmatrix}^\top; \\ y = C_{OFF} \cdot x + \begin{pmatrix} D_{OFF} & D_{V,OFF} \end{pmatrix} \begin{pmatrix} E & V_{F_1} & V_{F_2} \end{pmatrix}^\top. \end{cases} \tag{11.49}$$

The control variable is the duty cycle of the switching devices $\mu \in [0, 1]$. Using a convex combination of the $ON$ and $OFF$ equation systems from (11.48) and (11.49), an averaged state-space nonlinear model of the process is obtained close to the hybrid model's behavior given a sufficiently high PWM frequency:

$$\dot{x} = \mu \cdot x_{ON} + (1 - \mu) \cdot x_{OFF} \equiv F\left(x, [E, R, \mu]^\top, t\right). \tag{11.50}$$

As such, an affine nonlinear system, with respect to $\mu$, with the state function $F$ above can be implemented by inheriting the class `System` of the toolbox. The disturbances affecting the system are the voltage source $E$ and variable output load $R$, stochastic by nature, along with uncertainties of its components due to manufacturing tolerances, relevant on inductors and capacitors. As the toolbox allows using the output capacitor voltage or output load voltage with minor modifications, the resistor voltage was considered as measurement variable due to its corresponding practical control use cases. By inheriting the class `UncertainPlantFactory`, a set of tolerances can be imposed on all relevant circuit parameters and, also, an LTI uncertain set can be automatically computed with the

provided mechanisms. According to the mechanism from Section 5.3, only the steady-state values of $\overline{E}$, $\overline{R}$, $\overline{u}_R$ will be imposed, part of the full operating point $(\overline{u},\overline{x},\overline{y}) = \left(\left[\overline{E},\overline{R},\overline{\mu}\right]^\top, \left[\overline{v}_{C_{in}},\overline{i}_{L_1},\overline{v}_{C_1},\overline{i}_{L_2},\overline{v}_{C_2}\right]^\top, \overline{v}_R\right)$.

The SEPIC converter state-space model for the *ON* state of switch $S_1$, as structured in (11.48), is:

$$\left(\begin{array}{ccccc|c|cc} -\frac{1}{r_{C_{in}}C_{in}} & 0 & 0 & 0 & 0 & \frac{1}{r_{C_{in}}C_{in}} & 0 & 0 \\ \frac{1}{L_1} & -\frac{r_{i,1}}{L_1} & 0 & \frac{r_{DS_2}}{L_1} & 0 & 0 & -\frac{1}{L_1} & 0 \\ 0 & 0 & 0 & \frac{1}{C_1} & 0 & 0 & 0 & 0 \\ 0 & -\frac{r_{DS_1}}{L_2} & -\frac{1}{L_2} & -\frac{r_{i,2}}{L_2} & 0 & 0 & \frac{1}{L_2} & 0 \\ 0 & 0 & 0 & 0 & -\frac{1}{(R+r_{C_2})C_2} & 0 & 0 & 0 \\ \hline 0 & 0 & 0 & 0 & \frac{R}{R+r_{C_2}} & 0 & 0 & 0 \end{array}\right), \tag{11.51}$$

with $r_{i,1} = r_{C_{in}} + r_{L_1} + r_{DS_1}$, $r_{i,2} = r_{DS_1} + r_{C_1} + r_{L_2}$, while for the *OFF* state of the switch $S_1$, according to (11.49), is:

$$\left(\begin{array}{ccccc|c|cc} -\frac{1}{r_{C_{in}}C_{in}} & 0 & 0 & 0 & 0 & \frac{1}{r_{C_{in}}C_{in}} & 0 & 0 \\ \frac{1}{L_1} & -\frac{r_{i,3}}{L_1} & -\frac{1}{L_1} & \frac{r_{i,5}}{L_1} & -\frac{1}{L_1} & 0 & 0 & -\frac{1}{L_1} \\ 0 & \frac{1}{C_1} & 0 & 0 & 0 & 0 & 0 & 0 \\ 0 & \frac{r_{i,5}}{L_2} & 0 & -\frac{r_{i,4}}{L_2} & \frac{1}{L_2} & 0 & 0 & \frac{1}{L_2} \\ 0 & \frac{R}{R_{i,6}C_2} & 0 & -\frac{R}{R_{i,6}C_2} & -\frac{1}{R_{i,6}C_2} & 0 & 0 & 0 \\ \hline 0 & \frac{r_C R}{R+r_C} & 0 & -\frac{r_C R}{R+r_C} & \frac{R}{R_{i,6}} & 0 & 0 & 0 \end{array}\right), \tag{11.52}$$

and notations $r_{i,3} = r_{L_1} + r_{C_1} + r_{DS_1} + r_{C_2} + r_{C_{in}}$, $r_{i,4} = r_{DS_2} + r_{C_2} + r_{L_2}$, $r_{i,5} = r_{DS_2} + r_{C_2}$, $R_{i,6} = R + r_{C_2}$.

Starting from the SEPIC physical circuit interface:

$$(u,x,y) = \left(\left[E,R,\mu\right]^\top \left[v_{C_{in}},i_{L_1},v_{C_1},i_{L_2},v_{C_2}\right]^\top, v_R\right), \tag{11.53}$$

it can then be extended to the hybrid framework interface of (2.7), written with the flow dynamics described by the map $F$:

$$\begin{bmatrix}\dot{x}\\ \dot{q}\\ \dot{\tau}\end{bmatrix} = \begin{bmatrix}(1-q)\left(A_{ON}x+\overline{B}_{ON}u\right)+q\left(A_{OFF}x+\overline{B}_{OFF}u\right)\\ 0\\ 1\end{bmatrix}, \tag{11.54}$$

with hybrid state, input and time vector $\left(z^\top = \begin{bmatrix} x^\top & q & \tau \end{bmatrix}^\top \quad u \quad t\right)^\top \in \mathcal{C}$, along with jump dynamics given by the map $G$:

$$\begin{bmatrix} x^+ \\ q^+ \\ \tau^+ \end{bmatrix} = \begin{bmatrix} x \\ \begin{cases} 1, & \text{if } q == 0 \\ 0, & \text{if } q == 1 \end{cases} \\ \begin{cases} \tau, & \text{if } q == 0 \\ 0, & \text{if} q \ == 1 \end{cases} \end{bmatrix}, (x, u, t) \in \mathcal{D}, \tag{11.55}$$

followed by the flow domain $\mathcal{C}$, defined as:

$$\begin{aligned} \mathcal{C}(z, u, t) = \{&((q == 0) \wedge (\tau \leq \mu \cdot T_{PWM})) \vee \\ &((q == 1) \wedge (\tau > \mu \cdot T_{PWM}))\}, \end{aligned} \tag{11.56}$$

the jump domain $\mathcal{D}$, defined as:

$$\mathcal{D}(z, u, t) = \{((q == 0) \wedge (\tau > \mu \cdot T_{PWM})) \vee ((q == 1) \wedge (\tau > T_{PWM}))\}, \tag{11.57}$$

and concluding with the output map $y = h(z, u, t) = v_R$.

### 11.6.2 Passivity-based control and path-planning design

A detailed design and analysis steps of the proposed Krasovskii passivity-based design with robust path-planning method from Chapter 7 and toolbox workflow for the SEPIC is further presented. The nominal values of the SEPIC converter parameters used for this set of numeric simulations are presented in Table 11.12, along with their tolerances.

Firstly, we proceed to obtain the robust controller used for path-planning, using the closed-loop shaping methodology. As such, we need to linearize the averaged state-space system (11.50) according to (5.4) and (7.19). Let a desired input/state/output operating point specification be to have the output signal $y_0(t) = 400$ $[V]$, with a nominal external voltage source $E_0 = 300$ $[V]$ and load input $R_0 = 80$ $[\Omega]$. An initial guess for the state equilibrium values was $\overline{x}_0 = [300 \quad 10 \quad 300 \quad -10 \quad 400]^\top$, followed by $\overline{\mu}_0 = 0.55$ for the duty cycle control input. Through numeric computation by solving Problem 3, the nominal equilibrium point follows:

$$(\overline{u}, \overline{x}, \overline{y}) = ([300, 80, 0.578], [300, 6.87, 297.72, -5, 400], 400). \tag{11.58}$$

| *Param.* | *Val.* | *Tol.* | *Param.* | *Val.* | *Tol.* |
|---|---|---|---|---|---|
| $L_1$ | 2.57 [mH] | $\pm 20\%$ | $L_2$ | 1.71[mH] | $\pm 20\%$ |
| $r_{L_1}$ | 130 [m$\Omega$] | $\pm 10\%$ | $r_{L_2}$ | 110 [m$\Omega$] | $\pm 10\%$ |
| $r_{DS_1}$ | 0.01 [$\Omega$] | $\pm 10\%$ | $r_{DS_2}$ | 80 [m$\Omega$] | $\pm 10\%$ |
| $C_1$ | 4.7 [$\mu$F] | $\pm 20\%$ | $C_2$ | 3.57 [$\mu$F] | $\pm 20\%$ |
| $r_{C_1}$ | 270 [m$\Omega$] | $\pm 10\%$ | $r_{C_2}$ | 350 [m$\Omega$] | $\pm 10\%$ |
| $C_{in}$ | 3.57 [$\mu$F] | $\pm 20\%$ | $r_{C_{in}}$ | 270 [m$\Omega$] | $\pm 10\%$ |
| $V_{F_1}$ | 0.2 [V] | $\pm 10\%$ | $V_{F_2}$ | 0.62 [V] | $\pm 10\%$ |

Table 11.12: SEPIC parameter values and tolerances.

After calling the `linearize()` routine for the plant model (11.50), performing (5.6), the uncertainty model needs to be computed. An input multiplicative uncertainty model, according to the framework from Chapter 6 was fitted, i.e. $G = G_n\,(1 + \Delta U)$, with $||\Delta||_\infty \leq 1$. This model has been automatically computed from input $u_3 \equiv \mu$ to output $y_1 \equiv v_R$, with the additional tolerances $E \in [290, 310]$ $[V]$ and $R \in [75, 85]$ $[\Omega]$, based on $N = 1000$ Monte Carlo simulations. An extensive frequency range for the converter is $\Omega = [\underline{\omega} = 10^{-2}, \overline{\omega} = 10^8]$, with 300 equally distributed samples in logarithmic scale. As performed in [Șuș+21], a particle swarm optimization algorithm was employed with hyperparameters: swarm size of 1000, initial swarm span of $10^4$, minimum neighbors fraction of 0.9, and inertia range of $[0.1, 1.1]$, resulting in:

$$U(s) = K\frac{s^2 + 2\zeta_z\omega_{n_z}s + \omega_{n_z}^2}{s^2 + 2\zeta_p\omega_{n_p}s + \omega_{n_p}^2} = 0.53201 \times \frac{s^2 + 1289s + 4.623{\times}10^5}{s^2 + 158.6s + 6.286{\times}10^7}. \tag{11.59}$$

The linearized SEPIC plant family is comprised of fourth-order stable systems, in minimal form, with four zeros, three of which are of nonminimum phase, corresponding to the control path. The nominal MISO transfer matrix model from $u \equiv [\Delta R, \Delta E, \Delta\mu]^\top$ to $y \equiv \Delta v_R$ is:

$$G_n(s) = \frac{s{+}8{\times}10^5}{\alpha(s)} \begin{bmatrix} 5.925{\times}10^7(s^2{+}162.5s{+}7.202{\times}10^7) \\ 0.021779(s + 346.5)(s^2 + 179.7s + 5.637{\times}10^7) \\ 4.1368(-s{+}2.304{\times}10^4)(s^2{-}717.4s{+}5.145{\times}10^7) \end{bmatrix}, \tag{11.60}$$

where $\alpha(s) = (s^2{+}2673s{+}3.749{\times}10^7)(s^2{+}1339s{+}6.493{\times}10^7)$.

A main purpose for the controller synthesis was to highly penalize the control effort near the system resonance, as the obtained controllers would be difficult to implement in practice otherwise, requiring high sampling frequencies, i.e., $f_e > 24$ [kHz]. As such, the sensitivity, complementary sensitivity and control effort loop-shaping filters are:

$$W_S(s) = \frac{0.5s + 200}{s + 2}; \quad W_{KS}(s) = \frac{100s + 346.5}{s + 346.5};$$
$$W_T(s) = \frac{s^2 + 4000s + 4{\times}10^6}{10^{-4}s^2 + 56.57s + 8{\times}10^6}, \tag{11.61}$$

with an imposed sensitivity bandwidth of at least $\omega_B = 200$ [rad/s], admissible steady state error of maximum $A = 10^{-2}$, allowed sensitivity peak at $M = 2$. A relatively low bandwidth was imposed to compensate the SEPIC converter resonance and presence of multiple nonminimum phase zeros. The complementary sensitivity bandwidth must be faster than $\omega_{BT} = 2000$ [rad/s], forcing a high frequency attenuation of at least $A_T = 10^{-4}$ with a roll-off order $n = 2$, with an allowed peak of $M_T = 2$. The control effort weighting function imposes all frequencies with magnitude less than 1, with a further penalization of maximum 0.1 above $\omega \approx 1000$ [rad/s], due to the resonant peak at $\omega_{peak} \approx 9000$ [rad/s].

From the direct application of the $\mu$-synthesis procedure for the augmented plant with uncertainties, a controller of order $n = 19$ is obtained. This procedure is followed by a balanced order reduction operation, with the smallest-order controller which manages to ensure all imposed performance specifications, with a peak value $\mu_{\mathbf{\Delta}}(\texttt{LLFT}(P, K)) \leq 0.901513 < 1$, being of order $n = 3$:

$$\left(K_{\text{rob}}^{\text{SEPIC}}(s)\right) : \left(\begin{array}{ccc|c} -1.997 & 3.056 & 3.227 & -0.5018 \\ -3.057 & -2197 & -6118 & -0.3838 \\ 3.225 & 6118 & -10160 & 0.4055 \\ \hline -0.5018 & 0.3838 & 0.4055 & 0 \end{array}\right). \tag{11.62}$$

In this case, the control system has very large stability margins, with a phase margin $\gamma_k \approx 80[^\circ]$ and gain margin of $m_k^{dB} \approx 19$ [dB]. Additionally, as specified by the $n = 2$ and $A_T = 10^{-4}$ parameters of the complementary sensitivity weight, $W_T$, the closed-loop control system mitigates stochastic sensor noise signals with a spectrum spanning from

$\omega_{BT} > 2000$ [rad/s], using an initial roll-off of $-40$ [dB/dec], followed by an attenuation of at least four orders of magnitude. In practice, the attenuation does not saturate at the prescribed value, as the system supports a further $-20$ [dB/dec] roll-off afterwards.

The SEPIC converter is a highly-nonlinear plant with respect to the command signal $\mu(t)$, and there are use cases where the operating point may be dynamic, along with being generally affected by a diverse set of perturbations. Besides the previously-mentioned advantages of the already designed robust controller, it will be used as an auxiliary path-planning component along with the K-PBC block used to guarantee asymptotic stability for the entire domain of operation for the converter.

To design the K-PBC, one needs to construct the output port-variable $h_K(x,u)$ such that the SEPIC converter is Krasovskii passive. The LMI problem presented in Claim 3 from [MŞD21], based on Theorem 3, having the bounds of the load resistance $R \in [10, 1000]$ [$\Omega$], has been solved, with a possible solution from the feasibility cone:

$$Q = 10^{-3} \times \begin{pmatrix} 0.000714 & 0 & 0 & 0 & 0 \\ 0 & 0.514 & 0 & 0 & 0 \\ 0 & 0 & 0.00094 & 0 & 0 \\ 0 & 0 & 0 & 0.342 & 0 \\ 0 & 0 & 0 & 0 & 0.000714 \end{pmatrix}, \quad (11.63)$$

from which the output port-variable has the form 7.17, with $m = 1$. After this supplementary output is designed, the K-PBC has the form:

$$(\Sigma_{\text{K-PBC}}): \quad \begin{cases} \dot{x}_c = K_1(K_2(x_c - \mu^\star) - h_K(x)); \\ y_c = x_c, \end{cases} \quad (11.64)$$

with two inputs: the output port-variable $h_K(x)$ of the extended $(\Sigma_{\text{SEPIC}})$ and the desired input trajectory $\mu^\star$, while the output is the actual value of the duty-cycle $\mu(t) \equiv y_c(t)$. The parameters of the controller (11.64) are $K_1 = 3\times10^{-5}$ and $K_2 = 1\times10^{8}$.

Figures 11.26 and 11.27 illustrate time domain simulations of the SEPIC in closed-loop configuration using the proposed structure of cascaded K-PBC with $\mu$-synthesis path-planning $K_{\text{rob}}^{\text{SEPIC}}$ at various operating points, along with different types of disturbances applied. The former compares the response of the proposed closed-loop system compared to

its robust controller only counterpart, while the latter figure illustrates the RS and RP properties of the proposed method for a set of 50 Monte Carlo simulations sampled from the tolerance set of Table 11.12.

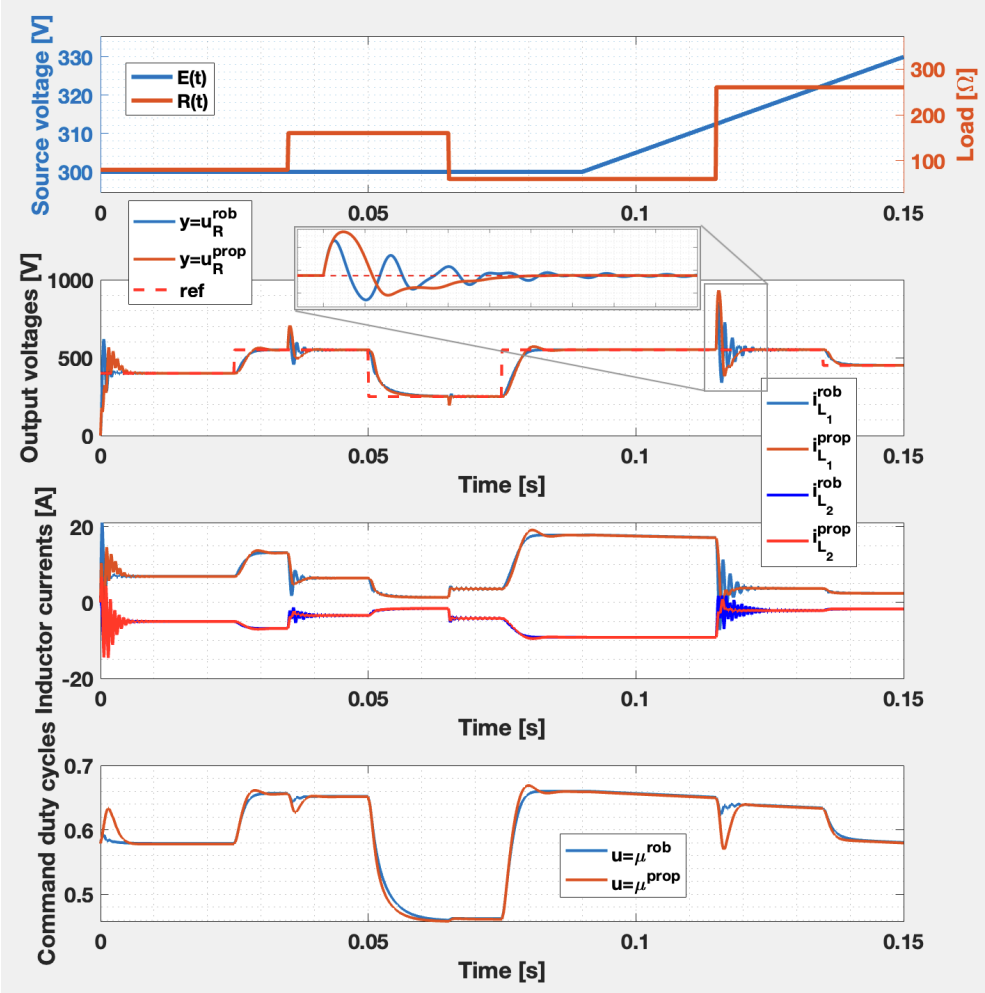


Figure 11.26: SEPIC averaged state-space closed-loop simulations using the robust controller $K_{\text{rob}}^{\text{SEPIC}}$ designed using loop-shaping with (11.61) versus the proposed cascade control structure from Figure 7.2: (i) time-varying disturbance inputs E(t) and R(t); (ii) output voltages $v_R(t)$; (iii) inductor currents $i_{L_1}(t)$ and $i_{L_2}(t)$; (iv) command signals $\mu(t)$.

Both experiments start from zero initial conditions to emphasize the behaviour to sudden jumps in the dynamics, followed by a succession of disturbances applied at the converter inputs, such as:

- a sequence of load resistance steps:
  - from $R(t_1^-{=}0.035_-) = \ 80[\Omega]$ to $R(t_1^+{=}0.035_+) = 160[\Omega]$;
  - from $R(t_2^-{=}0.065_+) = 160[\Omega]$ to $R(t_2^+{=}0.065_+) = \ 60[\Omega]$;
  - from $R(t_3^-{=}0.115_+) = \ 60[\Omega]$ to $R(t_3^+{=}0.115_+) = 260[\Omega]$.
- a ramp disturbance on the external source voltage from $E(t < 0.090) \equiv 300$ [V], starting at $t_4 = 0.090$ [s] with an increasing slope of 500 and saturated at 50 [V];
- a sequence of output reference steps:
  - from $u_R^*(t_5^-{=}0.025_-) = 400[\text{V}]$ to $u_R^*(t_5^+{=}0.025_+) = 550[\text{V}]$;
  - from $u_R^*(t_6^-{=}0.050_-) = 550[\text{V}]$ to $u_R^*(t_6^+{=}0.050_+) = 250[\text{V}]$;
  - from $u_R^*(t_7^-{=}0.075_-) = 250[\text{V}]$ to $u_R^*(t_7^+{=}0.075_+) = 550[\text{V}]$;
  - from $u_R^*(t_8^-{=}0.135_-) = 550[\text{V}]$ to $u_R^*(t_8^+{=}0.135_+) = 450[\text{V}]$.

As noticeable in Figure 11.26, the proposed method not only tracks the desired voltage reference at all operating points, but it also considerably improves transits caused by changes in the disturbance signals compared to using $K_{\text{rob}}^{\text{SEPIC}}$ only, such as for the moments $t \in \{0, t_1, t_2, t_3\}$, with smaller overshoots and more damped oscillations. A compromise is that it adds insignificant overshoots when reference changes occur, such as at time $t_6$. The steady-state performance is unaffected by the addition of the K-PBC subsystem, irrespective of arbitrary step and ramp disturbances appearing on $E(t)$ or $R(t)$ alike.

In addition to the previous results, Figure 11.27 shows the robustness of the method when subjected to the parametric uncertainties inherent to the SEPIC converter circuit, in which all the dynamic and steady-state performance indicators remain fundamentally unchanged even after $\pm 20\%$ variations of the circuit's main component values.

The main advantage brought by the cascade structure in favor of the robust controller only is that it now guarantees the asymptotic stability for the closed-loop system, irrespective of the operating point, property guaranteed only in the vicinity of the equilibrium point (11.58) otherwise. Further advantages of the K-PBC can be harvested by performing an optimization-based tuning on its parameters, i.e. $K_1$, $K_2$ and a scaling of the positive definite matrix $\alpha \cdot Q$, $\alpha > 0$, by still maintaing its trajectory on the feasibility cone, with such an application performed for closed-loop sensitivity minimization in the journal paper [Mih+22e].

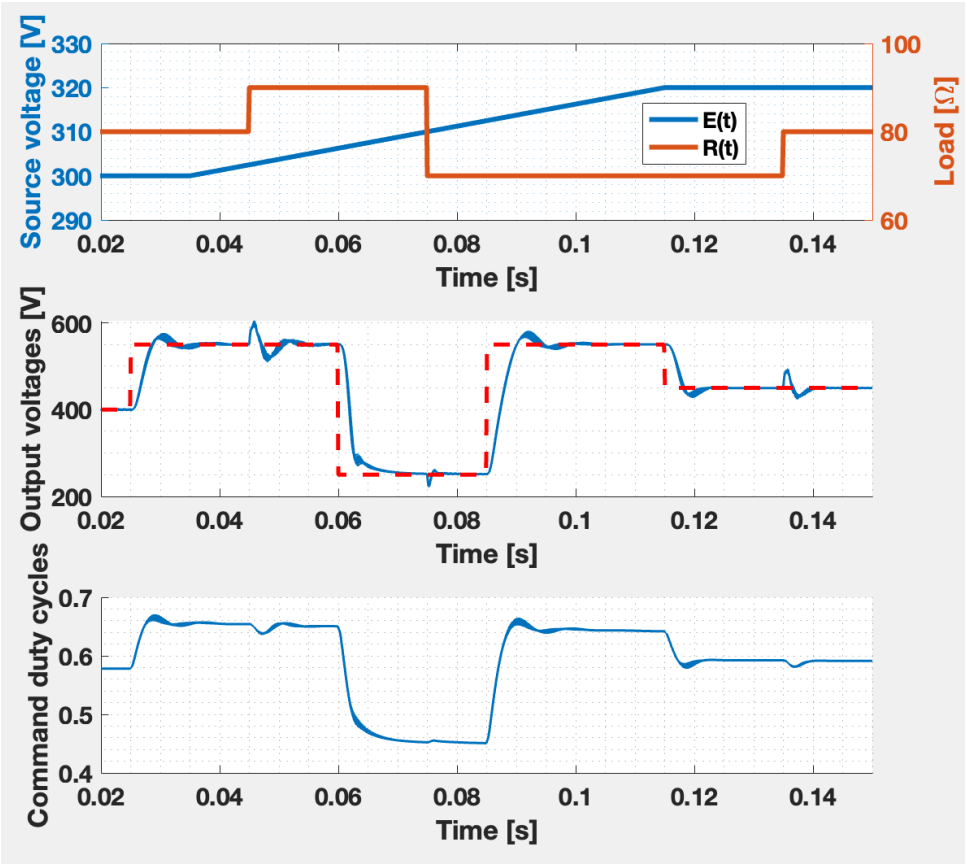


Figure 11.27: SEPIC-averaged state-space closed-loop simulations the proposed cascade control structure from Figure 7.2, illustrating 50 Monte Carlo simulations by sampling plant models from the tolerance set of Table 11.12: (i) time-varying disturbance inputs E(t) and R(t); (ii) output voltages $v_R(t)$; (iii) command signals $\mu(t)$.

### 11.6.3 Steady-state quantization analysis

An illustration of the steady-state analysis from Section 9.2 will proceed in this subsection, applied in the context of the SEPIC circuit, namely the straightforward application of Theorem 4 of Section 9.2.2.1, without the design problem of Section 9.2.2.1.

The ranges for the hardware devices $\mathcal{D}$ can be deduced based on a convenient interface between the controller and plant: $\mu = \mu_0 + \Delta\mu \in [0, 1]$, with $\mu_0 = 0.5788$, and, as such, $\mathcal{D}_y$ has $R_y = 0.5$, and an expected variation for the output $\Delta y$ in the range $\mathcal{D}_u$ with $R_u = 100$.

Starting from the regulator (11.62), by selecting a sampling frequency $f_s = 24\ [kHz]$, a Tustin discretization, and a Gramian-based balancing, the ideal numeric controller $K(z)$ becomes:

$$(K(z)): \left(\begin{array}{ccc|c} 0.9999 & -1.336\times10^{-4} & -9.691\times10^{-5} & 0.003239 \\ 1.336\times10^{-4} & 0.8883 & -0.1986 & -0.002599 \\ -9.691\times10^{-5} & 0.1986 & 0.6297 & 0.001887 \\ \hline 0.003239 & 0.002599 & 0.001887 & 4.496\times10^{-6} \end{array}\right). \tag{11.65}$$

The state and output bounds from relations (9.19) and (9.20) are:

$$N_x = \|(A, B,\ I, O)\|_\infty \cdot R_u = 38.8962 \cdot 100 = 3889.62; \tag{11.66}$$

$$N_y = \|(A, B, C, D)\|_\infty \cdot R_u = 0.12603 \cdot 100 = 12.603. \tag{11.67}$$

The base 2 logarithm applied to the previous bounds leads to $\log_2 R_u \approx 6.64$, $\log_2 H_x \approx 5.28$, $\log_2 N_x \approx 11.92$ and $\log_2 H_y \approx -2.98$, $\log_2 N_y \approx 3.65$. The application of Lemma 6 leads to:

$$L_x \geq L_u + \max\left(\lceil \log_2 H_x \rceil_{\varepsilon>0}, \lceil \log_2 H_y \rceil_{\varepsilon>0}, 0\right) = L_u + 6, \tag{11.68}$$

which denotes that 6 additional bits are necessary to completely host the state and output signals compared to a specified input precision $L_u$.

For an illustrative set of values for the ADC converter word lengths $L_u \in [15, 24]$, accounting for the sign bit, the internal variables $x_c[k]$ and $u[k]$ must be encoded in minimum $L_x = \max\{15, 24\} + 6 = 30$ bits, which fit into standard 32-bit microprocessor word lengths. Thus, according to Lemma 7, the optimal configuration adapted to such hardware specifications requires $L_x = 30,\ f = 0,\ M = 0.9999,\ d = 29$, having a worst-case of $x_{margin} = 0$ unused bits allocated for states, $y_{margin} = 8$ unused bits for outputs, and a coefficient resolution $\varepsilon_G(K_q, P, F) = 1.862 \times 10^{-9}$. Thus, an equivalent fixed-point regulator $K^{\mathcal{F}}(z)$ will be obtained through a coefficient scaling by (9.59):

$$\left(K^{\mathcal{F}}(z)\right): \left(\begin{array}{ccc|c} 8387910 & -1121 & -813 & 27171 \\ 1121 & 7451329 & -1666298 & -21799 \\ -813 & 1666298 & 5282413 & 15826 \\ \hline 27171 & 21799 & 15826 & 38 \end{array}\right). \tag{11.69}$$

Computing the quantization noise bounds based on Theorem 4 for $L_u \in \overline{15,24}$ and $L_y \in \overline{15,24}$, we obtain the steady-state deviations $\varepsilon_G(K_q, P, F) \in [5.0302 \times 10^{-4}, 0.2575]$. This results in relative errors valued between $[0.0001, 0.0644]$ [%] compared to the nominal voltage $y_0 = 400$ [$V$]. The quantization step for the states and outputs will become $\delta_x = \delta_u \times 2^{L_u - L_x}$, because the additional bits are valued as extra decimal digits in the number constructions. The transform matrices for the Jordan canonical form of $\Phi$ contribute with values $\|P\|_\infty = 2.6$ and $\|P^{-1}\|_\infty = 3.848$, obtained with the implicit factorization from MATLAB's `eig` function.

To demonstrate the previous results, a set of numeric simulations were illustrated in Figure 11.28, with $G(s)$ discretized using zero-order hold, and three use-cases: using an ideal regulator $K(z)$ with the IEEE-754 arithmetic, which ensures asymptotic stability, a MiL-based quantized regulator $K_q(z)$ with matrices $(A, B, C, D)$, followed by a SiL-based quantized regulator $K^{\mathcal{F}}(z)$. The simulations have been performed using the framework developed in Section 9.3. The values used are $L_u = L_y \in \{15, 24\}$. The results show tight bounds for the steady-state deviations, which become even stricter in cases where limit cycles are caused by deviations of several least significant bits from an ideal command.

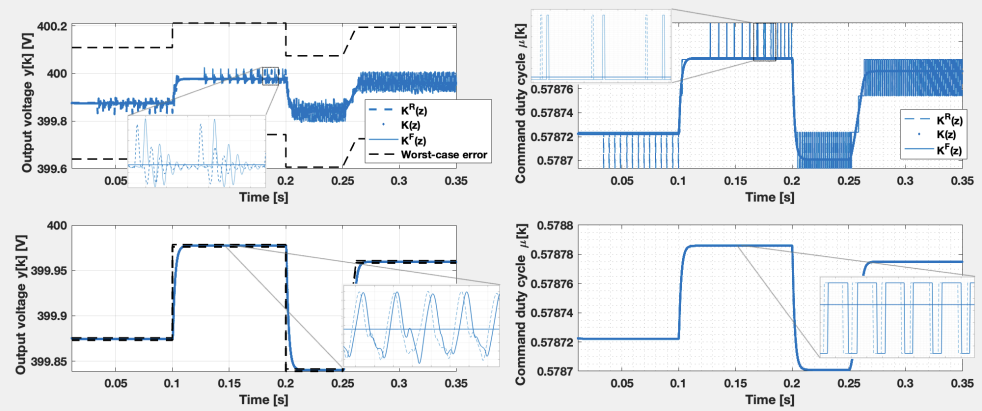


Figure 11.28: Numeric simulations for the SEPIC quantized closed-loop using regulators $K$, $K_q$, $K^{\mathcal{F}}$ for ADC/DAC resolutions $L_u$=$L_y$=$\{15, 24\}$, and quantizers $T_u$=$T_x$=$T_y$=`midtread`, with the framing of the steady-state limit cycle bounds deduced with Theorem 4; each row denotes an independent experiment.

## 11.7 DC motor 2DOF control design and implementation

This case study illustrates the proposed results from Section 8.2.3 and Chapter 10 on a direct current motor servo control example, and will encompass the following key points: process description, control performance specifications, continuous-time controller design, regulator discretization methods, sampling time optimization, controller structure selection, concluding with a WCET analysis.

### 11.7.1 Process model and controller synthesis

Consider a brushed direct-current motor (DCM) position control system. Figure 11.29 shows the closed-loop structure, being a particular case of 3.3, emphasizing both the process model and the 2DOF regulator structure. The motor process has a control input represented by the source voltage $V_a$ $[V]$, along with the disturbance load torque $T_d$ $[Nm]$, and the angular position $\theta$ $[rad]$ as output. As noticeable from the transfer functions, the DC motor model has a third order, with nominal component values listed in Table 11.13.

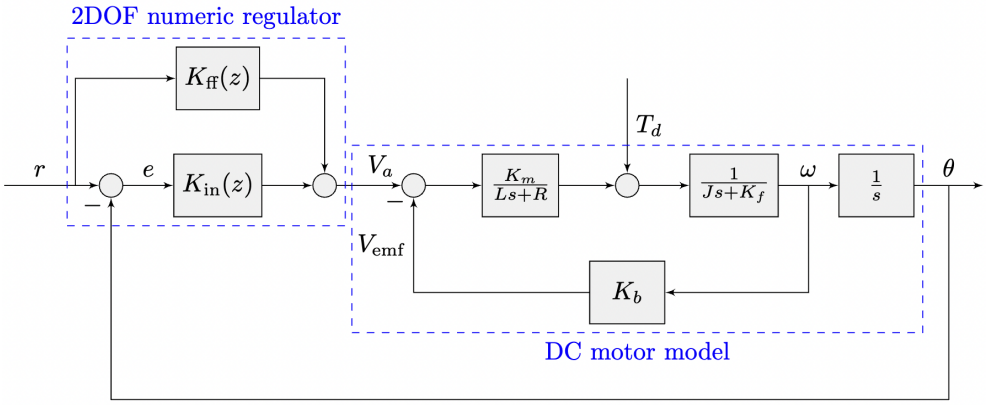


Figure 11.29: 2DOF position control structure for the DC motor system.

The process model from its two inputs to the angular position output is described by:

$$\Theta(s) = \frac{1}{s} \cdot \frac{G_L(s)}{1 + G_r(s)G_L(s)G_a(s)} \cdot T_d(s) + \frac{1}{s} \cdot \frac{G_a(s)G_L(s)}{1 + G_r(s)G_L(s)G_a(s)} \cdot V_a(s), \tag{11.70}$$

Table 11.13: DC motor physical parameters.

| Parameter | Value | Parameter | Value |
|---|---|---|---|
| $R$ | 2 $[\Omega]$ | $L$ | 0.5 $[H]$ |
| $K_m$ | 0.1 $[Nm{\cdot}A/V^2]$ | $K_f$ | 0.2 $[Nm]$ |
| $J$ | 0.02 $[kg{\cdot}m^2/s^2]$ | $K_b$ | 0.1 $[V{\cdot}s/\text{rad}]$ |

having the armature transfer function $G_a$, along with the load component $G_L$ and the reverse loop term $G_r$ which denotes the back-electromotive voltage constant $K_b$:

$$G_a(s) = \frac{K_m}{Ls + R}, \quad G_L(s) = \frac{1}{Js + K_f}, \quad G_r(s) = K_b. \tag{11.71}$$

The 2DOF controller components have the PID plus filter (PIDF) structure for $K_{\text{in}}$, while the integral term is canceled for the feedforward controller $K_{\text{ff}}$. This structure allows straightforward implementation in many industrial contexts as such PIDF regulators can be directly acquired and there are multiple validated approaches in the literature for their parameter tuning [OBO06; TA00]. They are defined as:

$$K_{\text{in}}(s) = \frac{U_{\text{in}}(s)}{R(s)} = K_P + K_I\frac{1}{s} + K_D\frac{s}{T_f s + 1}, \tag{11.72}$$

$$K_{\text{ff}}(s) = \frac{U_{\text{ff}}(s)}{R(s)} = \widetilde{b}\cdot K_P + \widetilde{c}\cdot K_D\frac{s}{T_f s + 1}, \tag{11.73}$$

with the feedforward parameters denoted $b$ and $c$, with $\widetilde{b} = -1 + b$ and $\widetilde{c} = -1 + c$. The command signal applicable to the motor input becomes:

$$U(s) = U_{\text{in}}(s) + U_{\text{ff}}(s) = K_{\text{in}}(s)E(s) + K_{\text{ff}}(s)R(s). \tag{11.74}$$

The closed-loop control specifications were selected as follows: a reference tracking settling time of $t_s \leq 1.5[s]$ with an overshoot $M_p \leq 0.05 \equiv 5[\%]$, with a fast rise time. Additionally, regarding the disturbance rejection specifications, a load torque of $1[Nm]$ must be rejected in less than $t_s^d \leq 1[s]$, i.e. its effect on the output measurement should become less than $0.1[rad]$ in the specified $t_s^d$, with a maximum allowed

disturbance of $y^d_{max} = 0.65[rad]$. The recommended approach in such designs [ÅH06] is to tune the inner PIDF controller $K_{\text{in}}$ to account for the disturbance rejection coefficients, as $K_{\text{ff}}$ does not influence that control loop, as written in the discrete-time counterpart expressions (11.83). The PIDF parameter tuning has been done using global optimization methods by encompassing the desired specifications. The first iteration which covered all disturbance rejection performances was accepted and halted the optimization procedure. Additionally, a further optimization as been performed on the 2DOF parameters $b$ and $c$, maintaining the halting procedure when the reference tracking requirements have been fulfilled. The outcomes of the regulator tuning is illustrated in Table 11.14, where, alongside the PIDF and additional PD synthesis, a separate 1DOF PIDF regulator has been also added, to account for servo behaviour only.

The closed-loop step responses for the reference tracking and disturbance rejection problems are portrayed in Figure 11.30, showing the effects of the three controller examples from Table 11.14, case in which the 2DOF structure is validated, as the obtained performance metrics are $t_s \approx 1.5[s]$, $M_p \approx 0[\%]$, rise time $t_r \approx 0.75[s]$ and steady-state error $\varepsilon_{ss} = 0$. As seen in the figure, the 2DOF structure ensures both the transient response performances and disturbance rejection behaviour, being the only regulator from the proposed triplet to cover both areas.

### 11.7.2 Sampling rate selection

For the PID discretizations, the forward Euler method has been considered for the integrator term, with approximation:

$$s \approx \frac{z-1}{T} = \frac{1-z^{-1}}{Tz^{-1}}, \tag{11.75}$$

Table 11.14: DCM 1DOF and 2DOF continuous controller coefficients.

| *PID structure* | $K_p$ | $K_i$ | $K_d$ | $T_f \times 10^3$ | $b$ | $c$ |
|---|---|---|---|---|---|---|
| 1DOF: servo | 21.06 | 8.757 | 7.7497 | 1.4717 | 1 | 1 |
| 1DOF: disturbance | 52.66 | 70.0560 | 7.7497 | 1.4717 | 1 | 1 |
| 2DOF | 52.66 | 70.0560 | 7.7497 | 1.4717 | 0.4 | 0.2 |

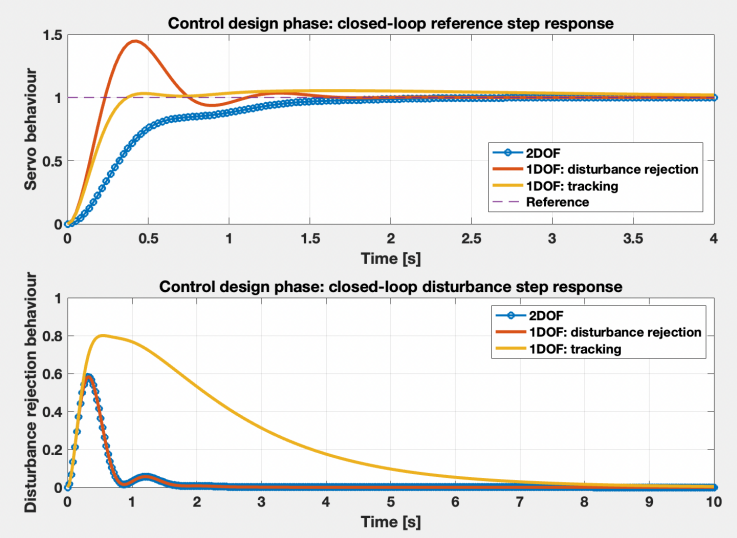


Figure 11.30: Continuous-time DCM control; step reference responses along with step disturbance rejections considering 1DOF regulators for servo tracking, disturbance rejection, and 2DOF for both performances.

while the derivative term was discretized using the backward Euler method:

$$s \approx \frac{z-1}{Tz} = \frac{1-z^{-1}}{T}, \tag{11.76}$$

leading to the expressions of $K_{\text{in}}$ and $K_{\text{ff}}$:

$$K_{\text{in}}(z) = K_P + \frac{K_I T}{z-1} + \frac{K_D}{T_f + \frac{Tz}{z-1}}, \tag{11.77}$$

$$K_{\text{ff}}(z) = \widetilde{b} \cdot K_P + \widetilde{c} \cdot \frac{K_D}{T_f + \frac{Tz}{z-1}}, \tag{11.78}$$

further used for the sampling time analysis.

Starting from the continuous-time open-loop model from (11.70), the discrete-time equivalent using the zero-order hold method becomes:

$$\Theta(z) = \mathcal{Z}\left\{\mathcal{L}^{-1}\left\{G_{\text{zoh},T}(s)G_{\text{aux}}(s)\right\}\right\} \cdot T_d(z) + \tag{11.79}$$

$$+ \mathcal{Z}\left\{\mathcal{L}^{-1}\left\{G_{\text{zoh},T}(s)G_a(s)G_{\text{aux}}(s)\right\}\right\} \cdot V_a(z), \tag{11.80}$$

with the auxiliary notations:

$$G_{\text{aux}}(s) = \frac{1}{s} \cdot \frac{G_L(s)}{1 + G_a(s)G_L(s)G_r(s)}, \tag{11.81}$$

$$\Theta(z) = G^{\text{op}}_{\text{dist}}(z) \cdot T_d(z) + G^{\text{op}}_{\text{servo}}(z) \cdot V_a(z). \tag{11.82}$$

The closed-loop system's expression thus becomes:

$$\Theta(z) = \frac{G^{\text{op}}_{\text{dist}}(z)}{1 + G^{\text{op}}_{\text{servo}}(z)K_{\text{in}}(z)} \cdot T_d(z) + \frac{G^{\text{op}}_{\text{servo}}(z)\left(K_{\text{ff}}(z) + K_{\text{in}}(z)\right)}{1 + G^{\text{op}}_{\text{servo}}(z)K_{\text{in}}(z)} \cdot R(z). \tag{11.83}$$

To solve the sampling period optimization Problem 8, two weighting sets $c_{\overline{1,7}}$ were considered in Table 11.15, corresponding to two distinct experiments, the first numeric column designating emphasis on the difficulty of implementation functionals, while the second numeric column coefficients focus mainly on open-loop and closed-loop fidelity. Using a general-purpose particle swarm optimization (PSO) implementation [KE95], the optimal implementability sampling period becomes $T_1^\star = 2.866 \times 10^{-3}$ $[s]$, while the fidelity sampling period is obtained at $T_2^\star = 1.260 \times 10^{-4}$ $[s] \ll T_1^\star$. To further extend the analysis, two extra sampling periods will be added to the comparison, the first representing the value obtained by applying the Shannon-Nyquist theorem (4.1), leading to a sampling period smaller than half the least time constant of the regulator, i.e. $T_3 < \frac{T_f}{2} \Rightarrow T_3 = 7.0081 \times 10^{-4}$ $[s]$, while the latter relevant value is considered as $T_4 = T_1\left(1 + 0.03\right) = 2.9520 \times 10^{-3}$, which represents a 3[%] disturbance increase on the implementability value, causing closed-loop instability. Figure 11.31 gathers all functionals and their weighted sums in its six subfigures, while also marking the positions of $T_1^\star$, $T_2^\star$, $T_3$. The open and closed-loop similarity functionals $\mathcal{S}^{\overline{\Omega}}_{K_{\text{in}}}$, $\mathcal{S}^{\overline{\Omega}}_{K_{\text{ff}}}$, $\mathcal{S}^{\overline{\Omega}}_{G_0^r}$, $\mathcal{S}^{\overline{\Omega}}_{G_0^d}$ are non-monotonic with respect to $T$, while the implementability functionals $\mathcal{I}_{K_{\text{in}}}$, $\mathcal{I}_{K_{\text{ff}}}$, $\mathcal{W}(T)$ are principally monotonically-decreasing. The existing exceptions are caused by numeric errors.

There are multiple approaches to implement the PID regulators. Both $K_{\text{in}}(z)$ and $K_{\text{ff}}(z)$ can be fully comprised of a biquadratic filter topology and, a first-order structure for $K_{\text{ff}}$, as in (4.15). The two main ones, given the simplicity of their structure, would be to implement it in parallel versus in series. For the inner regulator, the parallel topology,

Table 11.15: Functional weighting coefficients for the two considered experiments of the DCM case study: implementability of the controller versus fidelity compared to the continuous-time control counterpart.

| *Parameter* | *Implementability value* | *Fidelity value* |
|---|---|---|
| $c_1$ | 0.1 | 100 |
| $c_2$ | 0.1 | 100 |
| $c_3$ | 2000 | 1 |
| $c_4$ | 2000 | 1 |
| $c_5$ | 0.1 | 300 |
| $c_6$ | 0.1 | 100 |
| $c_7$ | 200 | 1 |
| $T^\star$ | $T_1^\star = 2.866 \times 10^{-3}\ [s]$ | $T_2^\star = 1.260 \times 10^{-4}\ [s]$ |

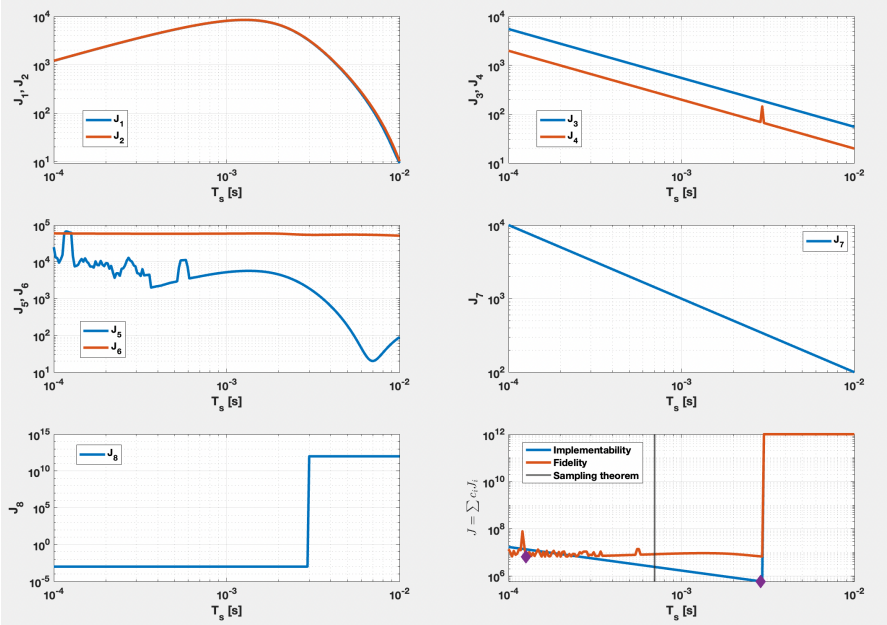


Figure 11.31: DCM 2DOF sampling rate functionals as specified in Problem 8 for both performed experiments. Besides the implementability and fidelity cases, a classical sampling theorem approach is also illustrated.

denoted with superscript $p$ can be split into three subsystems:

$$K_{\text{in}}^{p}(z) = H_{\text{in},1}(z) + H_{\text{in},2}(z) + H_{\text{in},3}(z) = K_P + \frac{K_I T}{z-1} + \frac{K_D(z-1)}{(T_f+T)z - T_f}, \tag{11.84}$$

while the series topology, denoted with the superscript $s$, is:

$$K_{\text{in}}^{s}(z) = \frac{b_2 z^2 + b_1 z + b_0}{z^2 + a_1 z + a_0} = g \cdot \frac{\widetilde{b}_2 z^2 + \widetilde{b}_1 z + \widetilde{b}_0}{a_2 z^2 + a_1 z + a_0}, \quad a_2 = 1. \tag{11.85}$$

where the equivalent normalized coefficients are obtained:

$$b_2 = \frac{K_P(T_f+T) + K_D}{T_f+T}; \;\; b_1 = \frac{-K_P(2T_f+T) + K_I T(T_f+T) - 2K_D}{T_f+T}; \tag{11.86}$$

$$b_0 = \frac{K_P T_f - K_I T T_f + K_D}{T_f+T}; \;\; a_1 = -\frac{2T_f+T}{T_f+T}; \;\; a_0 = \frac{T_f}{T_f+T}. \tag{11.87}$$

In the same manner, the parallel form of the feedforward regulator is:

$$K_{\text{ff}}^{p}(z) = \widetilde{b} H_{\text{ff},1}(z) + \widetilde{c} H_{\text{ff},2}(z) = \widetilde{b} \cdot K_P + \widetilde{c} \cdot \frac{K_D(z-1)}{(T_f+T)z - T_f}, \tag{11.88}$$

with a first-order series form of:

$$K_{\text{ff}}^{s}(z) = \frac{b_1 z + b_0}{z + a_0} = g \cdot \frac{\widetilde{b}_1 z + \widetilde{b}_0}{a_1 z + a_0}, \quad a_1 = 1. \tag{11.89}$$

and equivalent normalized coefficients:

$$b_1 = \frac{\widetilde{b} K_P(T_f+T) + \widetilde{c} K_D}{T_f+T}; \;\; b_0 = \frac{-\widetilde{b} K_P T_f - \widetilde{c} K_D}{T_f+T}; \;\; a_0 = \frac{-T_f}{T_f+T}. \tag{11.90}$$

### 11.7.3 Execution time analysis

After the discretization procedures (11.75) and (11.76), using the right-hand side notation for the coefficients in (11.85) and (11.89), the numeric values of the coefficients become as in Table 11.16, using the deduced sampling rates from Subsection 11.7.2, $T_1^{\star}$, $T_2^{\star}$, $T_3$, $T_4$. The gain coefficients $g \equiv b_2 = 5.3184815 \times 10^3$ for $K_{\text{in}}$ and $g \equiv b_1 = -4.244251 \times 10^3$ for $K_{\text{ff}}$, respectively, remain invariant in this set of experiments, while

the remaining non-unit coefficients vary with respect to $T$ and necessitate increasingly more decimals as the sampling rate tends towards zero.

Table 11.16: DCM case study discrete ideal controller coefficients.

| *Coefficient* | $T_1^\star$ | $T_2^\star$ | $T_3$ | $T_4$ |
|---|---|---|---|---|
| $\widetilde{b}_1$: $K_{\text{in}}(z)$ | $-1.980677$ | $-1.999150$ | $-1.995275$ | $-1.980097$ |
| $\widetilde{b}_0$: $K_{\text{in}}(z)$ | 0.980751 | 0.999150 | 0.995279 | 0.980175 |
| $a_1$: $K_{\text{in}}(z)$ | $-0.052546$ | $-1.914358$ | $-1.523809$ | 0.005877 |
| $a_0$: $K_{\text{in}}(z)$ | $-0.947453$ | 0.914358 | 0.523809 | $-1.005877$ |
| $\widetilde{b}_0$: $K_{\text{ff}}(z)$ | $-0.985500$ | $-0.999362$ | $-0.996454$ | $-0.985065$ |
| $a_0$: $K_{\text{ff}}(z)$ | 0.947453 | $-0.914358$ | $-0.523809$ | 1.005877 |

To account for the necessary word length analysis, two frequently-used configurations have been considered: the first case is to store the operands, i.e. coefficients and inputs, states, outputs into 16-bit registers, considered the standard length for the RISC machine hosting the 2DOF controller, followed by a set of 32-bit length registers, which will increase the working precision, but with added execution time overhead, as modelled in continuation. Given the dynamic range of the final filter gains $g$, this final multiplication will be considered separately. Thus, the set $\mathbf{H}$ for this case study will encompass the properties:

- clock tick $T_{clk}=\frac{1}{1[MHz]}=1[\mu s]$, obtainable on common microcontrollers by configuring the phase-locked loop to a low-power setting;
- implements the SOS terms using the DFII for $K_{\text{in}}$ and a series connection for the first-order term $K_{\text{ff}}$, denoted $y[k] = f\left(y[k-i], u[k-i]\right)$;
- two configurations for the operand word lengths: 16-bit and 32-bit;
- saturation on output command signals $y[k]$;
- anti-windup on the integrator of $K_{\text{in}}$ using back-calculation:

$$\mathbf{w}_{\underline{I},\overline{I}}\left(x[k+1]\right) = x[k] + \left[K_w \cdot \left(\mathbf{s}_{\underline{Y},\overline{Y}}(y[k]) - y[k]\right)\right] \cdot (K_i T) \cdot u[k],$$

  with additional parameters $K_w$, $\underline{I}$, $\overline{I}$ represented using 16-bit words;
- output measurement $\Theta$ computed as a sum of impulses, with a maximum expected frequency of $f_{max} = 80000$ impulses per $100[ms]$ time unit, and each such impulse triggers a hardware interrupt

with a 15 assembly operation stack commutation cost; the scaling is then performed using a multiplication with a 16-bit variable;
- $K_{\text{ff}}$ accepts reference $r$ inputs, while $K_{\text{in}}$ accepts errors $e = r - \Theta$.

Table 11.17: Operations of the implementation of the 2DOF structure for the DCM case study in the hypothesis of a base word length of $L = 16$ bits and two considered quantization levels for the controller coefficients: 16-bit and 32-bit lengths. Notation: $N_c = 120 \times 10^3 \times T$.

| $\#r_i$ | $p_i$ | $K_{\text{in}}^s$ | $K_{\text{in}}^p$ | $K_{\text{ff}}^s$ | $K_{\text{ff}}^p$ | $c_i$ 16 | $c_i$ 32 | *Observations for* $K, \mathbf{H}$ |
|---|---|---|---|---|---|---|---|---|
| 1 | **l** | 14 | 18 | 8 | 13 | 1 | 2 | $y[k]{=}f\left(y[k{-}i], u[k{-}i]\right)$ |
| 1 | **a** | 4 | 5 | 2 | 3 | 1 | 2 | $y[k]{=}f\left(y[k{-}i], u[k{-}i]\right)$ |
| 1 | **m** | 6 | 5 | 4 | 4 | 1 | 6 | $y[k]{=}f\left(y[k{-}i], u[k{-}i]\right)$ |
| 8 | **s** | 1 | 1 | 1 | 1 | 1 | 2 | $\mathbf{s}\left(y[k]\right)$ |
| 20 | **w** | 1 | 1 | 0 | 0 | 1 | 6 | Integrator anti-windup |
| $N_c$ | **a** | 1 | 1 | 0 | 0 | 1 | 1 | $\Theta[k]$ impulse counter |
| 1 | **m** | 1 | 1 | 0 | 0 | 1 | 6 | $\Theta[k]$ scaling |
| 1 | **a** | 1 | 1 | 0 | 0 | 1 | 2 | $e[k] = r[k] - \Theta[k]$ |
| 1 | **l** | 3 | 3 | 0 | 0 | 1 | 2 | $e[k] = r[k] - \Theta[k]$ |
| 1 | **l** | 2 | 2 | 1 | 1 | 1 | 2 | $y[k{-}i] \leftarrow y[k{-}i{-}1]$ |
| 1 | **l** | 2 | 2 | 1 | 1 | 1 | 2 | $u[k{-}i] \leftarrow u[k{-}i{-}1]$ |

The mathematical operations $p_i \in \mathbf{O}$, along with their assembly instruction correspondents (10.5) are detailed in Table 11.17, with an emphasis on each type of operation based on its physical significance, as written in the last column. The hyperparameters $\gamma_i$ in the case of standard 16-bit word lengths have been considered with the value 1, denoting that each base arithmetical operations costs only $T_{clk}$, while the values are scaled upwards for the case when the operands exceed the word length to 32 bits. The impulse counter assembly operation cost for $\Theta[k]$ has been computed as $80000 \times 0.1 \times 15 \times T$. Additionally, Table 11.18 totalizes the number of assembly operations based on the previous table's description, along with computing the worst-case execution times for the

Table 11.18: DCM case study WCET analysis in conditions of Table 11.17, emphasizing the number of assembly operations $\left|\mathbf{Sp}^{K,\mathbf{H}}\right|$ necessary to implement the 2DOF structure comprised of $K_{\text{in}}$, $K_{\text{ff}}$, along with processor usage levels for the three stable sampling rate values. The total cumulated WCET values in $[\mu s]$ are: $T_1^\star \rightarrow 2866$, $T_2^\star \rightarrow 126$, $T_3 \rightarrow 700.8$.

| | 16 $K_{\text{in}}^s$ | 16 $K_{\text{ff}}^s$ | 16 $K_{\text{in}}^p$ | 16 $K_{\text{ff}}^p$ | 32 $K_{\text{in}}^s$ | 32 $K_{\text{ff}}^s$ | 32 $K_{\text{in}}^p$ | 32 $K_{\text{ff}}^p$ |
|---|---|---|---|---|---|---|---|---|
| $\left\|\mathbf{Sp}^{K,\mathbf{H}}\right\|$ | 77 | 24 | 81 | 30 | 246 | 64 | 250 | 76 |
| $\left\|\mathbf{Sp}^{K,\mathbf{H}}\right\|$ | 101 | | 111 | | 310 | | 326 | |
| $\text{WCET}_1^\star$ | 429$[\mu s]$ | | 439$[\mu s]$ | | 638$[\mu s]$ | | 654$[\mu s]$ | |
| $\text{WCET}_2^\star$ | 101$[\mu s]$ | | 111$[\mu s]$ | | 310$[\mu s]$ | | 326$[\mu s]$ | |
| $\text{WCET}_3$ | 170$[\mu s]$ | | 180$[\mu s]$ | | 379$[\mu s]$ | | 395$[\mu s]$ | |
| $\mathbf{U}\left(T_1^\star\right)$ | 14.96[%] | | 15.31[%] | | 22.26[%] | | 22.81[%] | |
| $\mathbf{U}\left(T_2^\star\right)$ | 80.15[%] | | 88.09[%] | | 246.03[%] | | 258.73[%] | |
| $\mathbf{U}\left(T_3\right)$ | 24.25[%] | | 25.68[%] | | 54.08[%] | | 56.36[%] | |

three stable sampling rate values: $T_1^\star$–$T_3$. As seen from the table, the optimal sampling rate solution featuring implementability emphasis $T_1^\star$ occupies the microprocessor for less than 25[%] of its capability in either 16 or 32-bit quantizations alike, with the Shannon theorem approach $T_3$ following with sufficient headroom in the scheduler algorithm, while the fidelity-based approach in this case occupies the scheduler with small margins in the case of 16-bit quantizations, and exceeds the allowed time frame in the case of the 32-bit configuration.

Based exclusively on the previous WCET analysis, there are several feasible solutions. In order to decide between the three sampling rate and quantization pair configurations, further analysis is performed on the frequency response of the $K_{\text{in}}$ and $K_{\text{ff}}$ controllers, along with the closed-loop responses using said controllers. As such, Figures 11.32 and 11.33, respectively, gather the previously-said behaviours. In addition to the three sampling rates, for completeness, the fourth, unstable sampling rate $T_4$ is shared, along with the ideal continuous-time equivalent controllers in the frequency response plot. In both figures, columns one

and two expose the 32-bit and 16-bit quantization configurations, respectively, while the lines distinguish between the $K_{\text{in}}$, $K_{\text{ff}}$ controllers in the frequency response figure and reference step response compared to the step disturbance responses in the time-domain simulation, respectively. The main conclusion drawn from this final pair of Figures is that the considered 2DOF control scheme is sensitive to the coefficient quantization levels, such that for $T_2$ and $T_3$, the only acceptable solution would be to use the precise 32-bit configuration, with the exception of the implementability solution which manages to follow the imposed closed-loop transient response specifications with a reasonable degradation of the performances. The 16-bit quantization frequency responses for $K_{\text{in}}(z)$ drastically alter the integrator effect, which, in effect, disturbs the ability of the closed-loop motor system to track reference signals and to reject step-like load torque disturbances.

To conclude the case study, the acceptable solutions are to consider the implementability-based sampling rate optimum $T_1^{\star}$, with practically ideal behaviour if a 32-bit word length setup is acceptable, and with a small performance degradation if only the 16-bit standard word length is supported, depending also on other execution threads running in the microprocessor, not covered in this experiment.

Further extensions, as in using more complex controllers for both the tracking regulator and the feedforward component, considering cases such as fractional-order controllers or 2DOF robust control synthesis results can be treated in an analogous manner by splitting such control laws into their component second-order sections and applying the theory from Tables 10.4 and 10.5.

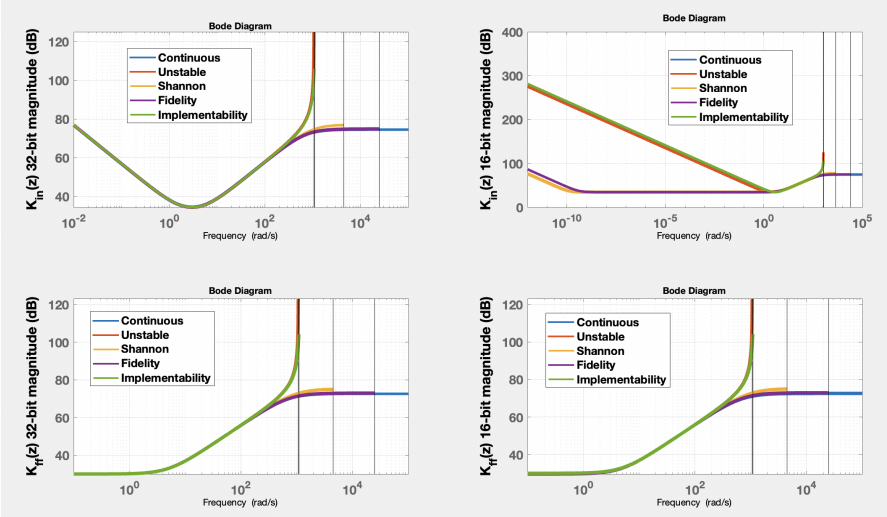


Figure 11.32: DCM study regulator frequency magnitude responses; the first line gathers the inner regulator $K_{\text{in}}(z)$ with 32-bit and 16-bit quantized regulator coefficients, while the second line gathers the feedforward controller $K_{\text{ff}}(z)$ in the same 32-bit and 16-bit configurations. For completeness, the continuous-time ideal regulators $K_{\text{in}}(s)$ and $K_{\text{ff}}(s)$ were also added alongside their discrete-time counterparts.

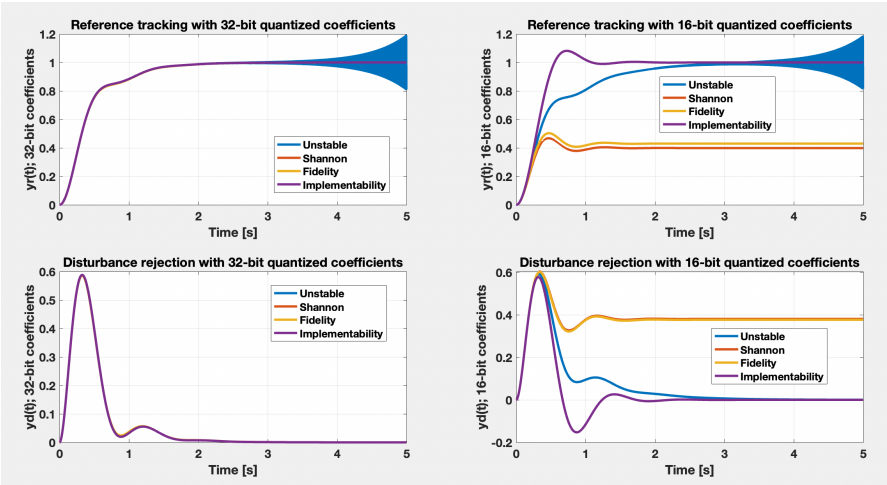


Figure 11.33: DCM closed-loop step responses using the proposed 2DOF structure; the first line gathers the reference tracking behaviour with 32-bit and 16-bit quantized regulator coefficients, while the second line gathers the disturbance rejection behaviour in the same configurations.

# CONCLUSIONS

## 12.1 Conclusions and discussions

This book presents several intermediate frameworks and methods for developing robust control synthesis and implementing the resulting regulators, through sampling rate, quantization step and worst-case execution time analyses. Said frameworks can be seen as self-sufficient solutions for specific control-oriented problems, or can be used together to provide an end-to-end design and validation framework. These approaches are shown to be effective in handling challenging cases where the performances imposed through the loop-shaping weighting functions are strict. The approaches presented in the book are shown to have practical implications and are illustrated through numerical examples, ranging from industrial processes with slow dynamics, such as temperature control systems with time delays, inverted pendulum type systems, highly-resonant mechanical systems, towards plants with fast dynamics, such as voltage converters and motor control applications. Several theoretical benchmark plants have also been used, to obtain a unitary comparison to other adequate methods in the literature. The monograph also proposes a unified approach for studying the effects of quantization in high-precision servo systems by providing guaranteed tolerances on the expected precision and studying the quantization effects for the worst-case scenario, with potential extensions for online and real-time applications.

For uncertain system modelling in the framework of LTI systems, this book provided a nonconvex optimization approach for SISO transfer function fitting, imposing the expected properties of stability, minimum phase and model validity. This approach can be extended to MIMO system modelling through individual input/output channel fitting, provided there are sufficient experimental data or an analytical nonlinear model of the system exists, although it introduces conservativeness. Using the notation (3.34), the premise for extending Problem 6 to MIMO systems is the fact that the transfer matrix $G \in \mathcal{G}$ can be written in various modalities based on the nominal plant $G_n$, individual uncertainty structures $\mathcal{T} \equiv [\mathcal{T}_{ij}]$ and SISO uncertainty blocks $U \equiv [U_{ij}]$ as in:

$$G = \begin{pmatrix} \mathcal{T}_{11}\left(G_n, U_{11}\right) & \cdots & \mathcal{T}_{1n_u}\left(G_n, U_{1n_u}\right) \\ \vdots & \ddots & \vdots \\ \mathcal{T}_{n_y1}\left(G_n, U_{n_y1}\right) & \cdots & \mathcal{T}_{n_yn_u}\left(G_n, U_{n_yn_u}\right) \end{pmatrix}. \tag{12.91}$$

This work opens perspectives for the implementation of a general purpose non-convex framework, on one hand for the extension of a least conservative approach for MIMO systems, and also to encompass nonlinear system measurements through data-driven approaches.

The presented robust control techniques can be used in wider context than the standard LTI framework, such as fractional-order regulator families, as exemplified in Section 11.1, or by employing gain scheduling techniques and more general adaptive control methods, while some of them are inherently designed in conjunction with nonlinear techniques, such as the robust path-planning controller designed in Chapter 7 cascaded with the Krasovskii passivity-based controller.

There are several results which can be gathered into a Rapid Control Prototyping software tool to receive a continuous-time model of a regulator $K(s)$ and return its discrete counterpart $K_q(z)$ such that it still ensures the proposed specifications for $K(s)$. Towards this goal, Problems 7, 8, 9 from Chapter 8, Lemmas 6, 7 and Theorems 4, 5 from Chapter 9, along with Theorem 6 and its Corollaries 2 and 3 from Chapter 10 can be solved and applied to gather a report on the ability to maintain the imposed specifications. On the other hand, besides the description of the numeric regulator, a different design problem can be proposed to gather the minimum required hardware specifications to maintain the imposed RS and RP conditions, the tracking error less than a prescribed tolerance $\mathcal{Q}$ and processor usage level less than 100[%] by an imposed margin `tol` $> 0$, leading to the combinatorial problem:

**Problem 15.** *Given a continuous-time regulator $K(s) \in \mathcal{G}$ synthesized for a continuous augmented plant model $P(s)$ with uncertainties according to a set of specifications imposed through LSDP, then the discrete-time regulator with minimum hardware requirements such that it maintains the robust stability and performance conditions, with an allowed steady-state tracking error $\mathcal{Q} > 0$ and such that the software implementation of the regulator is ensured by a processor with a guaranteed usage level, with an arbitrary cost function $J$, can be obtained by solving the optimization*

*problem:*

$$\underset{\tau,q,L_e,L_x,L_u>0}{\arg\max} \; J\left(\tau, q, L_e, L_x, L_u\right) \tag{12.92}$$

$$s.t. \quad \begin{cases} \mu_{\mathbf{\Delta}}(LLFT(\widetilde{P}, \widetilde{K}_q)) < 1; \\ \varepsilon_G\left(K_\xi, P_\alpha, F\right) < \mathcal{Q}; \\ \mathbf{U}\left(\mathbf{\Gamma_c}, \mathbf{\Gamma_p}, \tau\right) < 100 - \texttt{tol}\ [\%]. \end{cases}$$

## 12.2 Future research directions

The current concept of optimizing the sampling rate from Chapter 8 can be extended to linear time variant and linear parameter-varying systems, providing an online algorithm to suggest an optimal sampling rate depending on the current processor load. Furthermore, this concept can be linked with the idea of controllability or observability losses, as presented in [Kre99], to suggest the time-varying sampling rate that counters such phenomena by modelling them as additional constraints.

Regarding the applicability of the robust control framework, an extension or workaround for Lemma 5 from Chapter 9 would be to expand the modelling framework for discrete-time systems with uncertainties. The alternative of including parametric uncertainties with direct physical significance leads to transcendental functions, such as discrete poles $e^{\tau/T}$ for arbitrary time constants $T > 0$, which would currently require ad hoc solutions for each specific control problem.

To select the ideal sampling rate and quantization step pair in order to maintain robust stability and performance, Section 9.1 focused on two complementary optimization definitions, i.e. Problems 10 and 11. A real life application may use a cost functional encompassing both of them and a weighting term to impose the emphasis of one term over the other. For example, the sampling rate $\tau$ should be dictated by the operating frequency of the system whereas the quantization step $q$ should be determined by the data handling capability (memory, bandwidth) of the system. Having different units and different hardware architectures will offer different possibilities. Since the structure of objective functions (9.9) and (9.7) does not affect the overall approach, a natural generalization would better present the idea with an abstract objective function of the form $F(\xi)$, which can be configured based on several available implementation aspects.

In a similar manner, Problems 7–9 can be rewritten with performance constraints, such as a least required phase margin, to obtain the specifications of the most basic microcontroller that can deliver a certain set of performance criteria, including the cheapest possible hardware configuration. This problem can be considered independent to the coefficient quantization selection in case of slow processes where the precision of the computations can be sufficiently high, using 64-bit floating point computations for example, as to not impose regulator dynamics compromises, case in which the problem conceptually reduces to ensuring a good discretization of the continuous regulator definition.

Several generalizations can be studied for extended classes of systems, beyond the LTI framework, such as LTV and LPV models, along with control affine systems, which cover a wide range of physical process behaviours. Further studies will be focused on the inclusion of other classes of nonlinear systems into the robust control framework, with specific focus on output feedback linearization techniques using Lie derivatives or the Koopman operator, with example approaches specified in Section 2.3. A branch of control systems which is not exhaustively studied is that of the quantization sensitivity analysis of diffeomorphisms involved in such feedback linearization techniques.

In accordance with the context of the control systems domain described in Section 1.1, further goals would be to harness the advantages of data-driven approaches in order to combine them with well-established model-based frameworks. Among such advantages are the flexibility and ability to inherently validate the models directly using real data from the process.

# INDEX

# Index

# REFERENCES


[AMC23] A. Abdullah, F. Musolino, and P.S. Crovetti. "Limit-Cycle Free, Digitally-Controlled Boost Converter Based on DDPWM". In: *IEEE Access* 11 (2023), pp. 9403–9414. DOI: 10.1109/ACCESS.2023.3239883.

[Aka+21] B. Akay, D. Karaboga, B. Gorkemli, and E. Kaya. "A survey on the Artificial Bee Colony algorithm variants for binary, integer and mixed integer programming problems". In: *Applied Soft Computing, 106 107351, Elsevier B.V.* (2021), pp. 1568–4946. DOI: 10.1016/j.asoc.2021.107351.

[Apk11] P. Apkarian. "Nonsmooth $\mu$ synthesis". In: *International Journal of Robust and Nonlinear Control* 21.8 (2011), pp. 1493–1508. DOI: 10.1002/rnc.1644.

[AN17] P. Apkarian and D. Noll. "The $\mathcal{H}_\infty$ Control Problem is Solved". In: *Design and Validation of Aerospace Control Systems* (2017), pp. 1–11. DOI: 10.12762/2017.AL13-01.

[AM22] F. Assadian and K.R. Mallon. *Robust Control: Youla Parametrization Approach*. Wiley, 2022. ISBN: 978-1-119-50036-0.

[ÅH00] K.J. Åström and T. Hägglund. "Benchmark systems for PID control". In: *IFAC Digital Control: Past, Present and Future of PID Control*. 2000, pp. 165–166.

[ÅH06] K.J. Åström and T. Hägglund. *Advanced PID Control*. ISA-The Instr., Systems, and Automation Society. Research Triangle Park, 2006.

[ÅW02] K.J. Åström and B. Wittenmark. *Computer-Controlled Systems: Theory and Design*. Tsinghua University Press, Prentice Hall, 2002.

[Bal+22] G. Balas, R. Chiang, A. Packard, and M. Safonov. "Robust Control Toolbox$^{\text{TM}}$". In: *The MathWorks, Reference, Version 6.11.2 (R2022b)*. Natick, MA, USA, 2022. URL: https://www.mathworks.com/help/pdf_doc/robust/index.html.

[BPS09] G.J. Balas, A.K. Packard, and P.J. Seiler. "Uncertain Model Set Calculation from Frequency Domain Data". In: *Hof, P., Scherer, C., Heuberger, P. (Eds.) Model-Based Control:. Springer, Boston, MA* (2009), pp. 89–105. DOI: 10.1007/978-1-4419-0895-7_6.

[Ben+20] T. Bensic, T. Varga, M. Barukcic, and V.J. Stil. “Optimization Procedure for Computing Sampling Time for Induction Machine Parameter Estimation”. In: *Applied Sciences, vol. 10, 3222* (2020). DOI: 10.3390/app10093222.

[Bha17] S.P. Bhattacharyya. “Robust control under parametric uncertainty: An overview and recent results”. In: *Annual Reviews in Control* 44 (2017), pp. 45–77. DOI: 10.1016/j.arcontrol.2017.05.001.

[BCK95] S.P. Bhattacharyya, H. Chapellat, and L.H. Keel. *Robust Control: The Parametric Approach*. Prentice Hall PTR, 1995. ISBN: 0-13-781576-X.

[BMP02] A. Bicchi, A. Marigo, and B. Piccoli. “On the reachability of quantized control systems”. In: *IEEE Transactions on Automatic Control* 47.4 (2002), pp. 546–563. DOI: 10.1109/9.995034.

[BS16] C. Blackwell and M.K.S. Sastry. “Multivar - A MATLAB based MIMO Control System Design Application”. In: *8th International Conference on Computational Intelligence and Communication Networks*. Tehri, India, 2016. DOI: 10.1109/CICN.2016.69.

[BP20] J.J.Jr. Bongiorno and K. Park. *Design of Linear Multivariable Feedback Control Systems: The Wiener–Hopf Approach using Transforms and Spectral Factorization*. Springer, 2020. ISBN: 978-3-030-44355-9.

[BV04] S. Boyd and L. Vandenberghe. *Convex Optimization*. Cambridge University Press, 2004.

[BL00] R.W. Brockett and D. Liberzon. “Quantized feedback stabilization of linear systems”. In: *IEEE Transactions on Automatic Control, vol. 45, no. 7* (2000), pp. 1279–1289. DOI: 10.1109/9.867021.

[Bru+22] S.L. Brunton, M. Budišić, E. Kaiser, and J.N. Kutz. “Modern Koopman Theory for Dynamical Systems”. In: *SIAM Review* 64.2 (2022). DOI: 10.1137/21M1401243.

[Bur+06] J.V. Burke, D. Henrion, A.S. Lewis, and M.L. Overton. “HIFOO - A MATLAB Package for Fixed-order Controller Design and H-infinity Optimization”. In: *IFAC Symposium on Robust Control Design*. Toulouse, France, 2006. DOI: 10.3182/20060705-3-FR-2907.00059.

[BGN00] R. Byrd, J. Gilbert, and J. Nocedal. “A trust region method based on interior point techniques for nonlinear programming”. In: *Mathematical Programming* 89 (2000), pp. 149–185. DOI: 10.1007/PL00011391.

[Che+18] N. Chen, T. Wei, K. Shang, and R. Wang. “Digital controller based on delta operator for high-frequency DC-DC switching converters”. In: *IET Power Electronics* 11.7 (2018), pp. 1224–1230. DOI: 10.1049/iet-pel.2017.0556.

[CF11] T. Chen and B. Francis. *Optimal sampled-data control systems*. 2nd Edition. Springer, 2011. ISBN: 978-1447130390.

[CZJ21] X. Chi, Y. Zhang, and X. Jia. "Event-Triggered Predictive Control for Networked Systems Based on a Dual-Rate Sampling Switched Observer". In: *IEEE Access* 9 (2021), pp. 89580–89592. DOI: 10.1109/ACCESS.2021.3089360.

[Cla90] F.H. Clarke. *Optimization and Nonsmooth Analysis*. Philadelphia: Society for Industrial and Applied Mathematics (SIAM), 1990.

[Col04] R.D. Colgren. *Applications of Robust Control to Nonlinear Systems*. American Institute of Aeronautics and Astronautics, Inc., 2004.

[Col99] E.G. Collins. "A delta operator approach to discrete-time $H_\infty$ control". In: *International Journal of Control* 72.4 (1999), pp. 315–320. DOI: 10.1080/002071799221127.

[Cor+09] T.H. Cormen, C.E. Leiserson, R.L. Rivest, and C. Stein. *Introduction to Algorithms*. 3rd Edition. MIT Press, 2009.

[DRQ18] M.S. Darup, A. Redder, and D. Quevedo. "A fixed-point implementation of explicit MPC laws". In: *IEEE American Control Conference (ACC)*. Milwaukee, WI, USA, 2018, pp. 749–755. DOI: 10.23919/ACC.2018.8431781.

[Dat04] B.N. Datta. *Numerical methods for linear control: systems design and analysis*. San Diego, California, USA: Elsevier Academic Press, 2004.

[DR00] F. Dohnal and V. Rerucha. "Practical Aspects of Digital Control Systems Design – Sampling Period Choice". In: *IFAC Programmable Devices and Systems*. Ostrava, Czech Republic, 2000.

[Doy+89] J.C. Doyle, K. Glover, P.P. Khargonekar, and B.A. Francis. "State-Space Solutions to Standard $\mathbf{H}_2$ and $\mathbf{H}_\infty$ Control Problems". In: *IEEE Transactions on Automatic Control, Vol. 34, No. 8* (1989). DOI: 10.1109/9.29425.

[DȘK18] E.H. Dulf, M. Șușcă, and L. Kovács. "Novel Optimum Magnitude Based Fractional Order Controller Design Method". In: *IFAC-PapersOnLine, 3rd IFAC Conference on Advances in Proportional-Integral-Derivative Control PID 2018*. Vol. 51. 4. Ghent, Belgium, 2018, pp. 912–917. DOI: 10.1016/j.ifacol.2018.06.107.

[ER20] O.M. Escrig and J.-A. Romero-Pérez. "Regular quantisation with hysteresis: a new sampling strategy for event-based PID control systems". In: *IET Control Theory & Applications* 14.15 (2020), pp. 2163–2175. DOI: 10.1049/iet-cta.2020.0128.

[Ess20] G. Essl. "Topological IIR Filters Over Simplicial Topologies via Sheaves". In: *IEEE Signal Processing Letters* 27 (2020), pp. 1215–1219. DOI: 10.1109/LSP.2020.3005548.

[FY17] Y. Feng and M. Yagoubi. *Robust Control of Linear Descriptor Systems*. Studies in Systems, Decision and Control, vol. 102. Springer, 2017.

[Fer15] F. Ferrante. "On quantization and sporadic measurements in control systems: stability, stabilization, and observer design". PhD thesis. Stanford, CA: ISAE - Institut Supérieur de l'Aéronautique et de l'Espace, June 2015.

[FPW06] G.F. Franklin, J.D. Powell, and M.L. Workman. *Digital Control of Dynamic Systems*. 3rd Edition. Half Moon Bay, CA, USA: Ellis-Kagle Press, 2006.

[FX05] M. Fu and L. Xie. "The sector bound approach to quantized feedback control". In: *IEEE Transactions on Automatic Control* 50.11 (2005), pp. 1698–1711. DOI: 10.1109/TAC.2005.858689.

[GA94] P. Gahinet and P. Apkarian. "A Linear Matrix Inequality Approach to $\mathbf{H}_\infty$ Control". In: *International Journal of Robust and Nonlinear Control, Vol. 4* (1994), pp. 421–448. DOI: 10.1002/rnc.4590040403.

[GA13] P. Gahinet and P. Apkarian. "Automated Tuning of Gain-Scheduled Control Systems". In: *IEEE Conference of Decision and Control (CDC)*. Firenze, Italy, 2013. DOI: 10.1109/CDC.2013.6760297.

[Gaj+12] M. Gajamohan, M. Merz, I. Thommen, and R. D'Andrea. "The Cubli: cube that can jump up and balance". In: *IEEE/RSJ Int. Conference on Intelligent Robots and Systems*. Vilamoura-Algarve, Portugal, 2012. DOI: 10.1109/IROS.2012.6385896.

[GV68] A. Gelb and W.E.V. Velde. *Multiple-Input Describing Functions and Nonlinear System Design*. McGraw-Hill Book Company, 1968.

[Glo98] F. Glover. "A template for scatter search and path relinking". In: *Artificial Evolution, Lecture Notes in Computer Science*. Ed. by J.K. Hao, E. Lutton, E. Ronald, M. Schoenauer, and D. Snyers. Vol. 1363. Berlin, Heidelberg: Springer, 1998, pp. 1–51. DOI: 10.1007/BFb0026589.

[GST12] R. Goebel, R.G. Sanfelice, and A.R. Teel. *Hybrid Dynamical Systems: Modeling, Stability, and Robustness*. Princeton University Press: Princeton, NJ, USA, 2012.

[GW08] A. Griewank and A. Walther. *Evaluating Derivatives: Principles and Techniques of Algorithmic Differentiation*. 2nd Edition. Society for Industrial and Applied Mathematics SIAM, Philadelphia, 2008.

[Gu+19] P. Gu, Z. Zhou, S. Qu, C. Zhang, and B. Duan. "Influence Analysis and Optimization of Sampling Frequency on the Accuracy of Model and State-of-Charge Estimation for LiNCM Battery". In: *Energies, 12, 1205* (2019). DOI: 10.3390/en12071205.

[Gum+09] S. Gumussoy, D. Henrion, M. Millstone, and M.L. Overton. "Multiobjective Robust Control with HIFOO 2.0". In: *IFAC Proceedings Volumes, 6th IFAC Symposium on Robust Control Design*. Vol. 42. 6. Haifa, Israel, 2009, pp. 144–149. DOI: 10.3182/20090616-3-IL-2002.00025.

[GMO08] S. Gumussoy, M. Millstone, and M.L. Overton. "$H_\infty$ strong stabilization via HIFOO, a package for fixed-order controller design". In: *47th IEEE Conference on Decision and Control (CDC)*. Cancún, Mexico, 2008. DOI: 10.1109/CDC.2008.4738750.

[HJ99] J.W. Helton and M.R. James. *Extending $\mathbf{H}^\infty$ Control to Nonlinear Systems: Control of Nonlinear Systems to Achieve Performance Objectives*. Philadelphia: Society for Industrial and Applied Mathematics (SIAM), 1999.

[Hig02] N.J. Higham. *Accuracy and Stability of Numerical Algorithms*. 2nd Edition. Society for Industrial and Applied Mathematics SIAM, Philadelphia, 2002. ISBN: 0-89871-521-0.

[HSB02] H Hindi, C.Y. Seong, and S. Boyd. "Computing optimal uncertainty models from frequency domain data". In: *Proceedings of the 41st IEEE Conference on Decision and Control (CDC), vol. 3*. Las Vegas, NV, USA, 2002, pp. 2898–2905. DOI: 10.1109/CDC.2002.1184290.

[HI01] A. Horch and A.J. Isaksson. "Assessment of the sampling rate in control systems". In: *Control Engineering Practice* 9.5 (2001), pp. 533–544. DOI: 10.1016/S0967-0661(01)00015-6.

[HS93] G.C. Hsieh and M.G. Safonov. "Conservatism of the gap metric". In: *IEEE Transactions on Automatic Control* 38.4 (1993), pp. 594–598. DOI: 10.1109/9.250528.

[Hu+17] Z. Hu, F. Deng, X. Zhao, and H. Ren. "Quantized $H_\infty$ control for stochastic systems with packet losses". In: *36th Chinese Control Conference (CCC)*. Dalian, China, 2017, pp. 1838–1843. DOI: 10.23919/ChiCC.2017.8027620.

[IOW99] V. Ionescu, C. Oară, and M. Weiss. *Generalized Riccati Theory and Robust Control: A Popov Function Approach*. John Wiley & Sons Ltd., England, 1999.

[Isi94] A. Isidori. "$\mathbf{H}_\infty$ Control via Measurement Feedback for Affine Nonlinear Systems". In: *International Journal of Robust and Nonlinear Control* 4.4 (1994), pp. 553–574. DOI: 10.1002/rnc.4590040409.

[Isi95] A. Isidori. *Nonlinear Control Systems*. 3rd Edition. Springer, 1995.

[Jac+18] L. Jacobs et al. "A toolbox for robust control design: An illustrative case study". In: *IEEE 15th Int. Workshop on Advanced Motion Control (AMC)*. Tokyo, Japan, 2018. DOI: 10.1109/AMC.2019.8371058.

[JU21] T. Janus and B. Ulanicki. "Effects of Sampling on Stability and Performance of Electronically Controlled Pressure-Reducing Valves". In: *Journal of Water Resources Planning and Management* 147.3 (2021).

[KB07] D. Karaboga and B. Basturk. "Artifical Bee Colony (ABC) Optimization Algorithm for Solving Constrained Optimization Problems". In: *P. Melin et al. (Eds.): Foundations of Fuzzy Logic and Soft Computing, International Fuzzy Systems Association, LNAI 4529, Springer-Verlag Berlin* (2007).

[Kar13] A.S. Karimi. "Frequency-Domain Robust Control Toolbox". In: *52nd IEEE Conference on Decision and Control (CDC)*. Firenze, Italy, 2013. DOI: 10.1109/CDC.2013.6760460.

[KNV85] J. Kautsky, N.K. Nichols, and P. Van Dooren. "Robust pole assignment in linear state feedback". In: *International Journal of Control* 41.5 (1985). DOI: 10.1080/0020718508961188.

[KE95] J. Kennedy and R. Eberhart. "Particle Swarm Optimization". In: *IEEE International Conference on Neural Networks*. Vol. 4. Perth, WA, Australia, 1995, pp. 1942–1948.

[Kha15] H.K. Khalil. *Nonlinear Control*. Global Edition, 1st Edition. Pearson Education Limited, 2015.

[KRM22] I.-H. Khoo, H.C. Reddy, and G.S. Moschytz. "Structure-induced low-sensitivity design of sampled data and digital ladder filters using delta discrete-time operator". In: *International Journal of Circuit Theory and Applications* 50.6 (2022), pp. 2228–2251. DOI: 10.1002/cta.3248.

[KH22] J.H. Kim and T. Hagiwara. "The generalized $H_2$ controller synthesis problem of sampled-data systems". In: *Automatica, Vol. 142, 110400* (2022). DOI: 10.1016/j.automatica.2022.110400.

[KKS19] K.C. Kosaraju, Y. Kawano, and J.M.A. Scherpen. "Krasovskii's Passivity". In: *Proceeding of 11th IFAC Symposium on Nonlinear Control Systems NOLCOS*. Vol. 52. 16. Vienna, Austria, 2019, pp. 466–471. DOI: 10.1016/j.ifacol.2019.12.005.

[Kos+21] V. Kostina, Y. Peres, G. Ranade, and M. Sellke. "Stabilizing a System With an Unbounded Random Gain Using Only Finitely Many Bits". In: *IEEE Transactions on Information Theory, vol. 67, no. 4* (2021), pp. 2554–2561. DOI: 10.1109/TIT.2021.3053140.

[Kre99] G. Kreisselmeier. "On sampling without loss of observability/ controllability". In: *IEEE Transactions on Automatic Control, vol. 44, no. 5* (1999), pp. 1021–1025. DOI: 10.1109/9.763221.

[LaV06] S.M. LaValle. *Planning Algorithms*. Cambridge University Press, 2006. URL: http://planning.cs.uiuc.edu/.

[Lew07] A.S. Lewis. "Nonsmooth optimization and robust control". In: *Annual Reviews in Control* 31.2 (2007), pp. 167–177. DOI: doi:10.1016/j.arcontrol.2007.09.002.

[LXP08] F.L. Lewis, L. Xie, and D. Popa. *Optimal and Robust Estimation – With an Introduction to Stochastic Control Theory*. 2nd Edition. CRC Press, Taylor & Francis Group, 2008.

[LZL17] X. Li, Y. Zhao, and M. Lei. "High precision and stability temperature control system for the immersion liquid in immersion lithography". In: *Flow Measurement and Instrumentation* 53, Part B (2017), pp. 317–325. DOI: 10.1016/j.flowmeasinst.2016.08.014.

[Lin17] Q. Ling. “Bit Rate Conditions to Stabilize a Continuous-Time Scalar Linear System Based on Event Triggering”. In: *IEEE Transactions on Automatic Control, vol. 62, no. 8* (2017), pp. 4093–4100. DOI: 10.1109/TAC.2016.2618000.

[LK09a] K.-Z. Liu and H. Kobayashi. “Neo-robust control theory (part II)”. In: *2009 7th Asian Control Conference*. Hong Kong, China, 2009, pp. 808–813.

[LK09b] K.Z. Liu and H. Kobayashi. “Neo-Robust Control Theory (Part I) – Uncertainty Model and Robust Stability Analysis”. In: *7th Asian Control Conference* (2009), pp. 802–807.

[LS09] K.Z. Liu and B. Shirnen. “Neo-Robust Control Theory For Factorized Uncertainty”. In: *48th IEEE Conference on Decision and Control (CDC)*. Shanghai, China, 2009, pp. 650–655. DOI: 10.1109/CDC.2009.5400161.

[LY16] K.Z. Liu and Y. Yao. *Robust Control—Theory and Applications*. John Wiley & Sons, Singapore, 2016.

[Liu+22] W. Liu, J. Sun, G. Wang, F. Bullo, and J. Chen. “Resilient Control Under Quantization and Denial-of-Service: Codesigning a Deadbeat Controller and Transmission Protocol”. In: *IEEE Transactions on Automatic Control, vol. 67, no. 8* (2022), pp. 3879–3891. DOI: 10.1109/TAC.2021.3107145.

[Lju99] L. Ljung. *System Identification – Theory for the User*. 2nd Edition. Prentice Hall PTR, 1999.

[Lju20] L. Ljung. “System Identification Toolbox, Reference for MATLAB”. In: *The MathWorks, Inc.* Natick, MA, USA, 2020.

[Löf04] J. Löfberg. “YALMIP : A Toolbox for Modeling and Optimization in MATLAB”. In: *Proc. of the CACSD Conference*. Taipei, Taiwan, 2004.

[LGA11] L. Lublin, S. Grocott, and M. Athans. “$\mathcal{H}_2$ (LQG) and $\mathcal{H}_\infty$ Control”. In: *The Control Handbook: Control System Advanced Methods*. Ed. by W.S. Levine. Boca Raton, FL: CRC Press, Taylor & Francis Gr., 2011.

[LL09] J. Lunze and F.L. Lagarrigue. *Handbook of Hybrid Systems Control: Theory, Tools, Applications*. Cambridge University Press, UK, 2009.

[MLY22] J. Ma, W. Lan, and X. Yu. “Quantized feedback control of linear system with performance barrier”. In: *Int. Journal of Robust and Nonlinear Control* 32.12 (2022), pp. 7113–7131. DOI: 10.1002/rnc.6210.

[MOF20] M. Mae, W. Ohnishi, and H. Fujimoto. “MIMO multirate feedforward controller design with selection of input multiplicities and intersample behavior analysis”. In: *Mechatronics, 102442* 71 (2020). DOI: 10.1016/j.mechatronics.2020.102442.

[Man14] S. Mandra. “Comparison of Automatically Tuned Cascade Control Systems of Servo-Drives for Numerically Controlled Machine Tools”. In: *Electronika Ir Electrotechnika* 20.3 (2014). DOI: 10.5755/j01.eee.20.3.2788.

[Mar18] J. Marjanovic. "Low vs High Level Programming for FPGA". In: *7th International Beam Instrumentation Conference (IBIC)*. Shanghai, China, 2018. DOI: 10.18429/JACoW-IBIC2018-THOA01.

[Mar+24] I. Markiş, V. Mihaly, M. Şuşcă, and P. Dobra. "Convex Chebyshev Approximation for Descriptor Systems for Frequency Domain Data Fitting". In: *2024 28th International Conference on System Theory, Control and Computing (ICSTCC)*. 2024, pp. 368–373. DOI: 10.1109/ICSTCC62912.2024.10744712.

[Mat22] The MathWorks. "MATLAB". In: *Global Optimization Toolbox User's Guide*. Natick, MA, USA, 2022.

[MP11] R. Matušů and R. Prokop. "Graphical analysis of robust stability for systems with parametric uncertainty: an overview". In: *Transactions of the Institute of Measurement and Control* 33.2 (2011), pp. 274–290. DOI: 10.1177/0142331210361409.

[MŞY17] R. Matušů, B. Şenol, and C. Yeroğlu. "Linear systems with unstructured multiplicative uncertainty: Modeling and robust stability analysis". In: *PLoS ONE* 12.7 (2017). DOI: 10.1371/journal.pone.0181078.

[MG92] D. McFarlane and K. Glover. "A loop-shaping design procedure using H/sub infinity / synthesis". In: *IEEE Transactions on Automatic Control, vol. 37, no. 6* (1992), pp. 759–769. DOI: 10.1109/9.256330.

[MG90] R.H. Middleton and G.C. Goodwin. *Digital Control and Estimation. A Unified Approach*. Prentice Hall, 1990.

[Mih20] V. Mihaly. *General Purpose Linear Matrix Inequality Solver with Applications in Robust and Nonlinear Control*. Cluj-Napoca, Romania: Master's Thesis, Technical University of Cluj-Napoca, 2020.

[Mih+20] V. Mihaly, M. Stănese, M. Șușcă, and P. Dobra. "Interior Point Methods for Renewable Energy Management". In: *IEEE Int. Conf. on Automation, Quality and Testing, Robotics (AQTR)*. Cluj-Napoca, Romania, 2020, pp. 1–6. DOI: 10.1109/AQTR49680.2020.9129953.

[Mih+23] V. Mihaly, M. Şuşcă, I. Bîrs, and P. Dobra. "Reduced-Order Approximation of Fractional-Order Controllers by keeping Robust Stability and Robust Performance". In: *IEEE American Control Conference (ACC)*. San Diego, CA, USA, 2023. DOI: 10.23919/ACC55779.2023.10156398.

[MŞD21] V. Mihaly, M. Şuşcă, and P. Dobra. "Krasovskii Passivity and $\mu$-Synthesis Control Design for Quasi-Linear Affine Systems". In: *Energies, vol. 14(17), 5571* (2021). DOI: 10.3390/en14175571.

[MŞD23] V. Mihaly, M. Şuşcă, and P. Dobra. "Low-Order Representation of Robust Fractional-Order Controllers for Fractional-Order Interval Plants". In: *IEEE European Control Conference (ECC)*. Bucharest, Romania, 2023. DOI: 10.23919/ECC57647.2023.10178413.

[MŞD24] V. Mihaly, M. Şuşcă, and P. Dobra. “Robust numeric implementation of the fractional-order element”. In: *Journal of the Franklin Institute* 361.14 (2024), p. 107087. DOI: 10.1016/j.jfranklin.2024.107087.

[MȘD19] V. Mihaly, M. Șușcă, and P. Dobra. “Passivity-Based Controller for Nonideal DC-to-DC Boost Converter”. In: *2019 22nd International Conference on Control Systems and Computer Science (CSCS)*. Bucharest, Romania, 2019, pp. 30–35. DOI: 10.1109/CSCS.2019.00013.

[MȘD23a] V. Mihaly, M. Șușcă, and P. Dobra. “Exponential Rate for Bilinear Systems via Passivity-Based Controllers”. In: *IEEE Conference on Control Technology and Applications (CCTA)*. Bridgetown, Barbados, 2023.

[MȘD23b] V. Mihaly, M. Șușcă, and P. Dobra. “Maximizing the Exponential Decay Rate for Finite Dimensional Bilinear Systems using Passivity-Based Controllers”. In: *2023 62nd IEEE Conference on Decision and Control (CDC)*. Singapore, Singapore, 2023, pp. 5670–5675. DOI: 10.1109/CDC49753.2023.10383741.

[MȘD25] V. Mihaly, M. Șușcă, and P. Dobra. “Fixed-Structure Robust Feedback Linearization for Full Relative Degree Nonlinear Systems”. In: *IEEE/CAA Journal of Automatica Sinica* 12.10 (2025), pp. 2026–2039. DOI: 10.1109/JAS.2025.125354.

[MȘD21] V. Mihaly, M. Șușcă, and E.H. Dulf. “$\mu$-Synthesis FO-PID for Twin Rotor Aerodynamic System”. In: *Mathematics, 9(19), 2504* (2021). DOI: 10.3390/math9192504.

[Mih+22a] V. Mihaly, M. Şuşcă, E.H. Dulf, and P. Dobra. “Approximating the Fractional-Order Element for the Robust Control Framework”. In: *2022 IEEE American Control Conference (ACC)*. Atlanta, GA, USA, 2022, pp. 1151–1157. DOI: 10.23919/ACC53348.2022.9867658.

[Mih+22b] V. Mihaly, M. Şuşcă, E.H. Dulf, D. Morar, and Dobra P. “Fractional Order Robust Controller for Fractional-Order Interval Plants”. In: *IFAC-PapersOnLine, 10th IFAC Symposium on Robust Control Design ROCOND 2022*. Vol. 55. 25. Kyoto, Japan (Online), 2022, pp. 151–156.

[Mih+22c] V. Mihaly, M. Şuşcă, D. Morar, and P. Dobra. “Closed-Loop System Sensitivity Analysis for Passivity-Based Controller Parameters”. In: *2022 IEEE Int. Conf. on Automation, Quality and Testing, Robotics (AQTR)*. Cluj-Napoca, Romania, 2022, pp. 1–6. DOI: 10.1109/AQTR55203.2022.9802070.

[Mih+21a] V. Mihaly, M. Șușcă, D. Morar, and P. Dobra. “Extended Nonideal Passivity Based Controller for DC-DC Boost Converter”. In: *2021 25th International Conference on System Theory, Control and Computing (ICSTCC)*. Iași, Romania, 2021, pp. 46–51. DOI: 10.1109/ICSTCC52150.2021.9607248.

[Mih+21b] V. Mihaly, M. Șușcă, D. Morar, M. Stănese, and P. Dobra. “$\mu$-Synthesis for Fractional-Order Robust Controllers”. In: *Mathematics, 9(8), 911* (2021). DOI: 10.3390/math9080911.

[Mih+22d] V. Mihaly, M. Şuşcă, M. Morar, and P. Dobra. "Polytopic Robust Passivity Cascade Controller Design for Nonlinear Systems". In: *2022 IEEE European Control Conference (ECC)*. London, United Kingdom, 2022, pp. 2105–2110. DOI: 10.23919/ECC55457.2022.9838073.

[Mih+22e] V. Mihaly, M. Şuşcă, M. Morar, and P. Dobra. "Sensitivity Analysis of Krasovskii Passivity-Based Controllers". In: *Mathematics, 3750* 10.20 (2022). DOI: 10.3390/math10203750.

[Mih+25] V. Mihaly, M. Şuşcă, P. Pintea, and P. Dobra. "Robust Stabilization and $\mathcal{L}_2$-Gain Sensitivity Specification for Nonlinear Systems with Stable Zero Dynamics and Matched Uncertainties". In: *2025 European Control Conference (ECC)*. Thessaloniki, Greece, 2025, pp. 428–433. DOI: 10.23919/ECC65951.2025.11187081.

[Mor+22] D. Morar, V. Mihaly, M. Şuşcă, and M. Dobra. "LMI Conditions for CNC Cascade Controller Design - A State Feedback Approach". In: *2022 IEEE Int. Conf. on Automation, Quality and Testing, Robotics (AQTR)*. Cluj-Napoca, Romania, 2022, pp. 1–6. DOI: 10.1109/AQTR55203.2022.9801985.

[Mor+23] D. Morar, V. Mihaly, M. Şuşcă, and P. Dobra. "Cascade Control for Two-Axis Position Mechatronic Systems". In: *Fractal and Fractional, Applications of Fractional-Order Calculus in Robotics* 7.2, 122 (2023). DOI: 10.3390/fractalfract7020122.

[Mül00] P.C. Müller. "Descriptor systems: pros and cons of system modelling by differential-algebraic equations". In: *Mathematics and Computers in Simulation* (2000), pp. 273–279. DOI: 10.1016/S0378-4754(00)00213-5.

[Mur+89] K. Murakami, N. Irie, M. Kuga, and S. Tomita. "SIMP (single Instruction Stream/multiple Instruction Pipelining): A Novel High-speed Single-processor Architecture". In: *16th Annual International Symposium on Computer Architecture*. 1989, pp. 78–83. DOI: 10.1109/ISCA.1989.714527.

[Nes10] Y. Nesterov. *Lectures on Convex Optimization*. 2nd Edition. Springer, 2010.

[Ngh+12] T.X. Nghiem, G.J. Pappas, R. Alur, and A. Girard. "Time-triggered Implementations of Dynamic Controllers". In: *ACM Transactions on Embedded Computing Systems (TECS), 11(S2), Article 58* (2012).

[Oga95] K. Ogata. *Discrete-time control systems*. 2nd Edition. Englewood Cliffs, New Jersey 07632: Prentice-Hall International Inc., 1995.

[Oga10] K. Ogata. *Modern Control Engineering*. 5th Edition. Englewood Cliffs, New Jersey 07632: Prentice-Hall International Inc., 2010.

[Ost11] E. Ostertag. *Mono- and Multivariable Control and Estimation. Linear, Quadratic and LMI Methods*. Springer-Verlag Berlin Heidelberg, 2011.

[OBO06] J.J.E. Oviedo, T. Boelen, and P. van Overschee. “Robust advanced PID control (RaPID): PID tuning based on engineering specifications”. In: *IEEE Control Systems Magazine* 26.1 (2006), pp. 15–19. DOI: 10.1109/MCS.2006.1580148.

[PDB93] A. Packard, J. Doyle, and G. Balas. “Linear Multivariable Robust Control with a $\mu$ Perspective”. In: *Journal of Dynamic Systems, Measurement, and Control, 115* (1993), pp. 426–438. DOI: 10.1115/1.2899083.

[Pat+23] B. Patartics, P. Seiler, B. Takarics, and B. Vanek. “Worst Case Uncertainty Construction via Multifrequency Gain Maximization With Application to Flutter Control”. In: *IEEE Transactions on Control Systems Technology* 31.1 (2023), pp. 155–165. DOI: 10.1109/TCST.2022.3173044.

[PE14] D. Peaucelle and Y. Ebihara. “Robust stability analysis of discrete-time systems with parametric and switching uncertainties”. In: *IFAC Proceedings Volumes, Volume 47, Issue 3*. 2014, pp. 724–729. DOI: 10.3182/20140824-6-ZA-1003.00282.

[PZ15] C. Peng and J. Zhang. “Event-triggered output-feedback $\mathcal{H}_\infty$ control for networked control systems with time-varying sampling”. In: *IET Control Theory & Applications* 9.9 (2015), pp. 1384–1391. DOI: 10.1049/iet-cta.2014.0876.

[Pen+07] H. Peng, A. Prodic, E. Alarcon, and D. Maksimovic. “Modeling of Quantization Effects in Digitally Controlled DC–DC Converters”. In: *IEEE Trans. on Power Electronics, vol. 22, no. 1* (2007), pp. 208–215. DOI: 10.1109/TPEL.2006.886602.

[PS03] A.V. Peterchev and S.R. Sanders. “Quantization resolution and limit cycling in digitally controlled PWM converters”. In: *IEEE Transactions on Power Electronics, vol. 18, no. 1* (2003), pp. 301–308. DOI: 10.1109/TPEL.2002.807092.

[PSK18] P.H. Petkov, T.N. Slavov, and J.K. Kralev. *Design of Embedded Robust Control Systems Using MATLAB®/Simulink®*. IET CONTROL, ROBOTICS AND SENSORS SERIES 113. The Institution of Engineering and Technology (IET), 2018. ISBN: 978-1-78561-330-2.

[Pet+21] M.P. Petronijević, Č. Milosavljević, B. Veselić, B.P. Draženović, and S. Huseinbegović. “Robust cascade control of electrical drives using discrete-time chattering-free sliding mode controllers with output saturation”. In: *Electrical Engineering, 103:2181–2195* (2021). DOI: 10.1007/s00202-020-01198-x.

[Pod99] I. Podlubny. “Fractional-order systems and $PI^{\lambda}D^{\mu}$-controllers”. In: *IEEE Transactions on Automatic Control* 44.1 (1999). DOI: 10.1109/9.739144.

[Poo+94] K. Poolla, P. Khargonekar, A. Tikku, J. Krause, and K. Nagpal. “A time-domain approach to model validation”. In: *IEEE Transactions on Automatic Control* 39.5 (1994), pp. 951–959. DOI: 10.1109/9.284871.

[PM22] J.G. Proakis and D.G. Manolakis. *Digital Signal Processing: Principles, Algorithms and Applications*. 5th Edition. New Jersey 07458: Pearson, Prentice Hall, Upper Saddle River, 2022. ISBN: 9780137348657.

[SOK12] M. Sadeghpour, V. de Oliveira, and A. Karimi. "A Toolbox for Robust PID Controller Tuning Using Convex Optimization". In: *IFAC Proceedings Volumes, 2nd IFAC Conference on Advances in PID Control*. Vol. 45. 3. 2012, pp. 158–163. DOI: 10.3182/20120328-3-IT-3014.00027.

[SK14] A. Sadeghzadeh and A.S. Karimi. "Fixed-structure $\mathcal{H}_2$ controller design for polytopic systems via LMIs". In: *Optimal Control Applications and Methods* 36.6 (2014), pp. 794–809. DOI: 10.1002/oca.2132.

[Sal+12] A.J. Salim, N.R. Samsudin, S.I.M. Salim, and Y. Soo. "Multiply- accumulate instruction set extension in a soft-core RISC Processor". In: *10th IEEE International Conference on Semiconductor Electronics (ICSE)*. Kuala Lumpur, Malaysia, 2012, pp. 512–516. DOI: 10.1109/SMElec.2012.6417198.

[SCN13] R.G. Sanfelice, D.A. Copp, and P. Nanez. "Hybrid Equations (HyEQ) Toolbox v2.04–A Toolbox for Simulating Hybrid Systems in MATLAB/ Simulink®". In: *HSCC '13: Proceedings of the 16th international conference on Hybrid systems: computation and control*. 2013, pp. 101–106. DOI: 10.1145/2461328.2461346.

[SAK18] S.I.T. Sato, N. Araki, and Y. Konishi. "Two-loop Design for Dual-rate Cascade System". In: *IFAC PapersOnLine* 51.4 (2018), pp. 581–585. DOI: 10.1016/j.ifacol.2018.06.158.

[Sch82] A.J van der Schaft. "Observability and Controllability for Smooth Nonlinear Systems". In: *SIAM Journal on Control and Optimization* 20.3 (1982). DOI: 10.1137/0320026.

[Sch13] A.J van der Schaft. "On differential passivity". In: *Proceeding of the 9th IFAC Symposium on Nonlinear Control Systems*. Vol. 46. 23. Toulouse, France, 2013, pp. 21–25. DOI: 10.3182/20130904-3-FR-2041.00008.

[SFN18] L.R. da Silva, R.C.C. Flesch, and J.E. Normey-Rico. "Analysis of Anti-windup Techniques in PID Control of Processes with Measurement Noise". In: *IFAC-PapersOnLine*. Vol. 51. 4. 2018, pp. 948–953. DOI: 10.1016/j.ifacol.2018.06.100.

[ȘȘD18] F. Șimonca, M. Șușcă, and P. Dobra. "Optimization for CNC pathing". In: *2018 IEEE Int. Conf. on Automation, Quality and Testing, Robotics (AQTR)*. Cluj-Napoca, Romania, 2018, pp. 1–4. DOI: 10.1109/AQTR.2018.8402761.

[SVK16] R.P. Singh, A.K. Vashishtha, and R. Krishna. "32 Bit re-configurable RISC processor design and implementation for BETA ISA with inbuilt matrix multiplier". In: *Sixth International Symposium on Embedded Computing and System Design (ISED)*. Patna, India, 2016, pp. 112–116. DOI: 10.1109/ISED.2016.7977065.

[SP05] S. Skogestad and I. Postlethwaite. *Multivariable Feedback Control: Analysis and design*. 2nd Edition. John Wiley & Sons, 2005.

[Som+22] F. Somers et al. "Probabilistic gain, phase and disk margins with application to AOCS validation". In: *IFAC-PapersOnLine, 10th IFAC Symposium on Robust Control Design ROCOND*. Vol. 55. 25. Kyoto, Japan (Online), 2022, pp. 1–6. DOI: 10.1016/j.ifacol.2022.09.314.

[Son98] E. Sontag. *Mathematical Control Theory*. Springer, 1998.

[Spe+20] A. Sperilă, F.S. Tudor, B.D. Ciubotaru, and C. Oară. "$\mathbf{H}_\infty$ Control for Differential-Algebraic Systems". In: *IFAC World Congress*. Berlin, Germany, 2020. DOI: 10.1016/j.ifacol.2020.12.2577.

[Stă+20] M. Stănese, M. Şuşcă, V. Mihaly, and I. Naşcu. "Design and Control of a Self-Balancing Robot". In: *IEEE Int. Conf. on Automation, Quality and Testing, Robotics (AQTR)*. Cluj-Napoca, Romania, 2020, pp. 1–6. DOI: 10.1109/AQTR49680.2020.9129935.

[Șuș19] M. Șușcă. *Solving Algebraic Riccati Equations Using Proper Deflating Subspaces for $\mathcal{H}_2/\mathcal{H}_\infty$ Synthesis*. Cluj-Napoca, Romania: Master's Thesis, Technical University of Cluj-Napoca, 2019.

[ȘD16] M. Șușcă and P. Dobra. "Notch filter sensitivity analysis with root locus considering parameter uncertainty". In: *2016 20th International Conference on System Theory, Control and Computing (ICSTCC)*. Sinaia, Romania, 2016, pp. 387–391. DOI: 10.1109/ICSTCC.2016.7790696.

[Șuș+18] M. Șușcă, P. Dobra, C. Feștilă, and F. Șimonca. "General-purpose model of a three-phase asynchronous machine for simulation". In: *2018 IEEE Int. Conf. on Automation, Quality and Testing, Robotics (AQTR)*. Cluj-Napoca, Romania, 2018, pp. 1–6. DOI: 10.1109/AQTR.2018.8402749.

[ȘMD22] M. Șușcă, V. Mihaly, and P. Dobra. "Fixed-Point Uniform Quantization Analysis for Numerical Controllers". In: *2022 IEEE Conference on Decision and Control (CDC)*. Cancún, Mexico, 2022, pp. 3681–3686. DOI: 10.1109/CDC51059.2022.9993223.

[ȘMD23a] M. Șușcă, V. Mihaly, and P. Dobra. "Maintaining Robust Stability and Performance through Sampling and Quantization". In: *2023 IEEE American Control Conference (ACC)*. San Diego, CA, USA, 2023. DOI: 979-8-3503-2807-3.

[ȘMD23b] M. Șușcă, V. Mihaly, and P. Dobra. "Nonconvex Valid Uncertainty Modelling Approach for Robust Control Synthesis". In: *27th International Conference on System Theory, Control and Computing, Timișoara, Romania (ICSTCC)*. Timișoara, Romania, 2023.

[ȘMD23c] M. Șușcă, V. Mihaly, and P. Dobra. "Sampling Rate Selection for Multi-Loop Cascade Control Systems in an Optimal Manner". In: *IET Control Theory & Applications, Wiley* 17.8 (2023), pp. 1073–1087. DOI: 10.1049/cth2.12444.

[Şuş+26] M. Şuşcă, V. Mihaly, Zs. Lendek, I.-C. Morărescu, and P. Dobra. "Controller redesign to minimize uniform quantization errors in uncertain linear systems with fixed hardware constraints". In: *Nonlinear Analysis: Hybrid Systems* 60 (2026), p. 101683. DOI: 10.1016/j.nahs.2026.101683.

[Șuș+22a] M. Șușcă, V. Mihaly, D. Morar, and P. Dobra. "Quasi-Optimal Sampling Time Computation for LTI Controllers". In: *IFAC-PapersOnLine, Vol. 55, Issue 15, pp. 87-92, 6th IFAC Conference on Intelligent Control and Automation Sciences, ICONS*. Cluj-Napoca, Romania, 2022. DOI: 10.1016/j.ifacol.2018.06.107.

[Șuș+22b] M. Șușcă, V. Mihaly, D. Morar, and P. Dobra. "Sampling Rate Optimization and Execution Time Analysis for Two-Degrees-of-Freedom Control Systems". In: *Mathematics, 10(19), 3449* (2022). DOI: 10.3390/math10193449.

[Șuș+22c] M. Șușcă, V. Mihaly, D. Morar, and P. Dobra. "Worst-Case Execution Time Estimation for Numerical Controllers". In: *2022 IEEE Int. Conf. on Automation, Quality and Testing, Robotics (AQTR)*. Cluj-Napoca, Romania, 2022, pp. 1–6. DOI: 10.1109/AQTR55203.2022.9802027.

[Şuş+24a] M. Şuşcă, V. Mihaly, S.D. Sim, and P. Dobra. "Design of Linear Control Laws for Minimum Uniform Quantization Tracking Error". In: *2024 European Control Conference (ECC)*. Stockholm, Sweden, 2024, pp. 3624–3629. DOI: 10.23919/ECC64448.2024.10591232.

[Şuş+20] M. Şuşcă, V. Mihaly, M. Stănese, and P. Dobra. "Iterative Refinement Procedure for Solutions to Algebraic Riccati Equations". In: *IEEE Int. Conf. on Automation, Quality and Testing, Robotics (AQTR)*. Cluj-Napoca, Romania, 2020, pp. 1–5. DOI: 10.1109/AQTR49680.2020.9130027.

[Șuș+23] M. Șușcă, V. Mihaly, M. Stănese, and P. Dobra. "Uncertainty Modelling of Mechanical Systems with Derivative Behaviour for Robust Control Synthesis". In: *IEEE European Control Conference (ECC)*. Bucharest, Romania, 2023. DOI: 978-3-907144-09-1.

[Șuș+21] M. Șușcă, V. Mihaly, M. Stănese, D. Morar, and P. Dobra. "Unified CACSD Toolbox for Hybrid Simulation and Robust Controller Synthesis with Applications in DC-to-DC Power Converter Control". In: *Mathematics, 9(7), 731* (2021). DOI: 10.3390/math9070731.

[ŞNM25] M. Şuşcă, I. Naşcu, and V. Mihaly. "Robust Control of Rotary Tablet Press via Suboptimal Open-Loop Augmentation Scheme". In: *2025 29th International Conference on System Theory, Control and Computing (ICSTCC)*. Cluj-Napoca, Romania, 2025, pp. 253–259. DOI: 10.1109/ICSTCC66753.2025.11240454.

[Şuş+24b] M. Şuşcă et al. "Singularly Perturbed Systems Augmentation for Robust Synthesis". In: *2024 28th International Conference on System Theory, Control and Computing (ICSTCC)*. Sinaia, Romania, 2024, pp. 503–508. DOI: 10.1109/ICSTCC62912.2024.10744763.

[Swe+22] J. Swevers et al. “LCToolbox: Facilitating Optimal Linear Feedback Controller Design”. In: *IEEJ Journal of Industry Applications* 9.2 (2022), pp. 109–116. DOI: 10.1541/ieejjia.9.109.

[TA00] H. Taguchi and M. Araki. “Two-degree-of-freedom PID Controllers – Their Functions and Optimal Tuning –”. In: *IFAC Digital Control: Past. Present and Future of PID Control*. Terrassa, Spain, 2000. DOI: 10.1016/S1474-6670(17)38226-5.

[TJ19] L. Tan and J. Jiang. *Digital Signal Processing: Fundamentals and Applications*. Third Edition. Academic Press. Elsevier, 2019.

[TT09] S. Tarbouriech and M. Turner. “Anti-windup design: an overview of some recent advances and open problems”. In: *IET Control Theory & Applications* 3.1 (2009). DOI: 10.1049/iet-cta:20070435.

[TBL99] A.L. Tits, V. Balakrishnan, and L. Lee. “Robustness Under Bounded Uncertainty with Phase Information”. In: *IEEE Transactions on Automatic Control* 44.1 (1999). DOI: 10.1109/9.739067.

[TC17] E.S. Tognetti and T.R. Calliero. “Digital control and sampling period assignment of multiple plants in networked control systems”. In: *IET Control Theory & Applications* 11.17 (2017), pp. 3089–3096. DOI: 10.1049/iet-cta.2017.0151.

[TG07] L. Tomov and E. Garipov. “Choice of Sample Time in Digital PID Controllers”. In: *RECENT, vol. 8, no. 2(20)* (2007).

[TO15] S.F. Tudor and C. Oară. “$\mathcal{H}_\infty$ control problem for generalized discrete-time LTI systems”. In: *American Control Conference (ACC)*. Chicago, IL, USA, 2015, pp. 4640–4645. DOI: 10.1109/ACC.2015.7172060.

[Ugr+07] Z. Ugray et al. “Scatter Search and Local NLP Solvers: A Multistart Framework for Global Optimization”. In: *INFORMS Journal on Computing* 19.3 (2007), pp. 328–340. DOI: 10.1287/ijoc.1060.0175.

[VL99] A. Varga and G. Looye. “Symbolic and numerical software tools for LFT-based low order uncertainty modeling”. In: *Proceedings of the 1999 IEEE International Symposium on Computer Aided Control System Design*. Kohala Coast, Hawaii, USA, 1999, pp. 1–6. DOI: 10.1109/CACSD.1999.808615.

[VSP16] M. Verbandt, J. Swevers, and G. Pipeleers. “An LTI control toolbox–simplifying optimal feedback controller design”. In: *IEEE European Control Conference (ECC)*. Aalborg, Denmark, 2016. DOI: 10.1109/ecc.2016.7810586.

[Vin93] G. Vinnicombe. “Frequency domain uncertainty and the graph topology”. In: *IEEE Transactions on Automatic Control* 38.9 (1993), pp. 1371–1383. DOI: 10.1109/9.237648.

[Wan+16] D. Wang, T. Liu, X. Sun, and C. Zhong. “Discrete-time domain two-degree-of-freedom control design for integrating and unstable processes with time delay”. In: *ISA Transactions* 63 (2016), pp. 121–132. DOI: 10.1016/j.isatra.2016.03.017.

[Wan+21] P. Wang et al. “Unsupervised Network Quantization via Fixed-Point Factorization”. In: *IEEE Transactions on Neural Networks and Learning Systems* 32.6 (2021), pp. 2706–2720. DOI: 10.1109/TNNLS.2020.3007749.

[Wan+19] T. Wang, Y. Liu, X. Wang, and J. Li. “Robust sampling-based switching design for piecewise affine systems with application to DC–DC converters”. In: *IET Control Theory & Applications* 13 (9 2019), pp. 1404–1412. DOI: 10.1049/iet-cta.2018.5611.

[WYH08] M. Whorton, L. Yang, and R. Hall. *Similarity Metrics for Closed Loop Dynamic Systems*. Honolulu, Hawaii, 2008. DOI: 10.2514/6.2008-6624.

[WK08] B. Widrow and I. Kollár. *Quantization Noise: Roundoff Error in Digital Computation, Signal Processing, Control, and Communications*. Cambridge University Press, Cambridge, UK, 2008. ISBN: 9780521886710.

[Wil+08] R. Wilhelm et al. “The Worst-Case Execution Time Problem — Overview of Methods and Survey of Tools”. In: *ACM Transactions on Embedded Computing Systems* (2008), pp. 1–47. DOI: 10.1145/1347375.1347389.

[Xia+15] M. Xia, P.J. Antsaklis, Gupta V., and M.J. McCourt. “Determining Passivity Using Linearization for Systems With Feedthrough Terms”. In: *IEEE Transactions on Automatic Control* 60.9 (2015), pp. 2536–2541. DOI: 10.1109/TAC.2014.2383013.

[Xia+20] M. Xia, P. Gahinet, N. Abroug, C. Buhr, and E. Laroche. “Sector bounds in stability analysis and control design”. In: *International Journal of Robust and Nonlinear Control, vol. 30* (2020), pp. 7857–7882. DOI: 10.1002/rnc.5236.

[Xia+19] Y. Xiao, Y. Chen, K. Liu, Huang L., and X. Yang. “A Sampling Rate Selecting Algorithm for the Arbitrary Waveform Generator”. In: *IEEE Access* 7 (2019), pp. 83761–83770. DOI: 10.1109/ACCESS.2019.2922989.

[Xia+22] Y. Xiao, W. Mo, K. Liu, W. Zhao, and C. Hu. “Selecting the optimal sampling rate for the waveform generator with a variable clock”. In: *Digital Signal Processing, 103399* 123 (2022). ISSN: 1051-2004. DOI: 10.1016/j.dsp.2022.103399.

[Xu+22] T. Xu, Z. Duan, Z. Sun, and G. Chen. “A unified control method for consensus with various quantizers”. In: *Automatica* 110090, 136 (2022). DOI: 10.1016/j.automatica.2021.110090.

[XOG20] X. Xu, N. Ozay, and V. Gupta. “Passivity-based analysis of sampled and quantized control implementations”. In: *Automatica, Vol. 119, 109064* (2020). DOI: 10.1016/j.automatica.2020.109064.

[XZZ22] Y. Xu, Y. Zhang, and J.-F. Zhang. “A Pole Placement-Based Output Tracking Control Scheme by Finite-and-Quantized Output Feedback”. In: *IEEE Control Systems Letters* 6 (2022), pp. 3200–3205. DOI: 10.1109/LCSYS.2022.3184046.

[YY17] X. Yang and S. Yin. “Robust global identification and output estimation for LPV dual-rate systems subjected to random output time-delays”. In: *IEEE Transactions on Industrial Informatics* 13.6 (2017), pp. 2876–2885. DOI: 10.1109/TII.2017.2702754.

[Yep+10] A.G. Yepes et al. “Effects of Discretization Methods on the Performance of Resonant Controllers”. In: *IEEE Transactions on Power Electronics* 25.7 (2010), pp. 1692–1712. DOI: 10.1109/TPEL.2010.2041256.

[Yuk10] S. Yuksel. “Stochastic Stabilization of Noisy Linear Systems With Fixed-Rate Limited Feedback”. In: *IEEE Transactions on Automatic Control, vol. 55, no. 12* (2010), pp. 2847–2853. DOI: 10.1109/TAC.2010.2079510.

[Zam81] G. Zames. “Feedback and Optimal Sensitivity: Model Reference Transformations, Multiplicative Seminorms, and Approximate Inverses”. In: *IEEE Transactions on Automatic Control* 26.2 (1981). DOI: 10.1109/TAC.1981.1102603.

[ZK17] P.M. Zeugin and P. Keller. “Robust and optimal $\mathcal{H}_\infty$ control in LabVIEW”. In: *IEEE Conference on Control Technology and Applications (CCTA)*. Maui, HI, USA, 2017. DOI: 10.1109/CCTA.2017.8062753.

[Zha+22] Y. Zhang, J.-F. Zhang, X.-K. Liu, and Z. Liu. “Quantized-output feedback model reference control of discrete-time linear systems”. In: *Automatica* 110027, 137 (2022). DOI: 10.1016/j.automatica.2021.110027.

[ZDG96] K. Zhou, J.C. Doyle, and K. Glover. *Robust and Optimal Control*. Prentice Hall, Englewood Cliffs, New Jersey 07632, 1996.

[Zhu19] Q. Zhu. “Stabilization of Stochastic Nonlinear Delay Systems With Exogenous Disturbances and the Event-Triggered Feedback Control”. In: *IEEE Transactions on Automatic Control* 64.9 (2019), pp. 3764–3771. DOI: 10.1109/TAC.2018.2882067.